



The
University
Of
Sheffield.

The Role of Dystroglycan in Hearing and Hearing Loss

By:

Adam James Carlton

The University of Sheffield

Faculty of Science

Department of Biomedical Science

Acknowledgements

First and foremost, I'd like to thank both my supervisors Professor Steve Winder and Professor Walter Marcotti. I truly believe they have provided the perfect amount of support that allowed me to progress my project at a decent rate while also being able to incorporate my own ideas and theories along the way. This project did not always run smoothly, and with both of these excellent scientists in my corner I always knew that things would turn around and everything would make sense eventually.

I would also like to thank all members of the Winder/Asycough/Rainero and Marcotti labs for always being there to vent at and reminding me that there's always time for a coffee to think things over. Having genuine friends around me in both labs made the entire PhD much less daunting, and I honestly would have a lot more grey hairs showing if not for them. At the beginning of the PhD Ben Stevenson, Sarah Gratton, Stella Christou and Mona Nazemi all started with me at the same time, and you have felt like a second family from that point onwards. You are the best, and I'm so lucky to have had such great people around to keep my sane and ensure that I never felt alone. Special thanks also goes to Ellen Allwood and Iwona Smaczynska-de Rooij for being so kind and helpful while I was first finding my feet in the new lab; you both always make everything seem less scary. Also, special thanks to Jing-Yi Jeng and Anna Underhill for helping with the BAIAP2L2 experiments. I fully intend on annoying both lab groups with my continued presence; they have not escaped me yet.

I'd also like to thank my advisors Colby Eaton and Elena Rainero. Advisory meetings seemed so terrifying when we were first briefed for them, but you both made the process as productive and comfortable as possible. Your continued support throughout the entire PhD period has been crucial, and discussing things through with you both provided a great opportunity for me to take a step back and look at the project as a whole.

My family have been amazingly supportive over the course of this PhD, and humoured me while I talked their ears off about everything that's been happening around the lab recently. Visits from my mother, golfing with my father, and even working on my house with my partner's parents have all played their part in keeping me sane and happy. Last but certainly not least, I would like to thank my partner Rosie for always being there. The nature of lab work sometimes leads to bad moods and low energy, but you always find a way to cheer me up and give me someone to talk things through with. I couldn't have done this without you.

Abstract

The transduction of sound waves into electrical signals in the hair cells is entirely dependent on the stereociliary hair bundles that reside on their apical surface. These hair-like projections are organised into three or more rows in a staircase structure, with the height of each stereocilium being similar within each row. The current theory is that this height disparity between the rows is entirely established and maintained via the differential localisation of several actin effector proteins. Epidermal growth factor receptor pathway substrate 8 (EPS8) selectively localises to the tips of the tallest row of stereocilia, on the pillar side of the hair cell, with only small amounts of the protein detectable at the second tallest row. Conversely, EPS8 like protein 2 (EPS8L2) selectively localises to the shorter two rows of stereocilia. Each of these two interacts with a distinct complex of actin effector proteins and isoforms of the myosin-15 (MYO15) specialised motor protein, but the exact mechanism by which this differential localisation is established and maintained remains unknown.

Here, we investigate two proteins which were hypothesised to modulate the EPS8/EPS8L2 differential localisation axis. Dystroglycan, a specialised cell adhesion receptor best known for the role it plays in the pathogenesis of Duchenne's muscular dystrophy, was identified as a potential interactor of EPS8L2. The inverse bin-amphiphysin-rvs (I-BAR) family member BAR/IMD domain containing adaptor protein 2 like 2 (BAIAP2L2) was identified as a potential interactor of EPS8, and reported as important in hearing loss by the IMPC mutagenesis screen.

Dystroglycan expression could not be visualised within the organ of Corti with any of the antibodies at our disposal, and a hair cells specific knock-out of the protein did not result in elevated hearing thresholds. Single-cell whole-cell patch clamping experiments indicated that the basolateral profile of inner hair cells matured as normal. Conversely, the global knock-out of BAIAP2L2 resulted in deficits in hair cell mechanotransduction which became apparent at postnatal day 11 (P11). Hearing thresholds were significantly elevated at all ages tested and appeared to show a progressive phenotype reminiscent of a more severe version of the EPS8L2 knock-out. Scanning electron microscopy revealed that the shortest row of stereocilia had almost entirely degenerated by P54. Furthermore, immunostaining data indicated that EPS8 is not localised to the tips of the tallest stereocilia by BAIAP2L2 as originally hypothesised, and in fact BAIAP2L2 is dependent on the presence of EPS8 for proper localisation to the tips of the shorter two rows of stereocilia.

Table of Contents

Acknowledgments – ii

Abstract – iii

Table of Contents – iv

List of Figures – viii

List of Appendices – xii

Abbreviations – xiii

1. Main introduction – 1

1.1 The structure and mechanism of the mammalian inner ear – 1

1.2 Development and maintenance of the mechanotransduction machinery – 10

1.2.1 Structure of the stereocilia and the mechanotransduction apparatus –10

1.2.2 Development of the hair bundle, and the mechanisms responsible for the establishment and maintenance of the staircase architecture – 15

1.3 Ribbon synapses – 21

1.3.1 The structure and function of ribbon synapses in the cochlea – 21

1.3.2 Ribbon synapse molecular composition – 25

1.3.3 Ribbon synapse development and maturation – 28

1.4 The electrophysiological maturation of hair cells and their innervation – 31

1.4.1 Innervation of cochlear hair cells following birth – 31

1.4.2 Electrophysiological maturation of inner and outer hair cells in mice – 35

1.4.3 The use of mice in mammalian hearing research – 38

1.5 Dystroglycan and the dystrophin glycoprotein complex – 39

1.5.1 The dystrophin glycoprotein complex and the role it plays at the sarcolemma – 39

1.5.2 The role of dystroglycan in non-muscular tissues – 44

1.5.3 The role of dystroglycan in synapse formation and maintenance – 47

1.5.4 The possible functions of phosphorylated dystroglycan within the organ of Corti – 50

2. Materials and Methods – 52

- 2.1. Animal techniques – 52
 - 2.1.1. Ethical statement and animal strains – 52
 - 2.1.2. Tissue preparation – 53
 - 2.1.3. Whole-cell patch clamping and mechanotransduction – 54
 - 2.1.4. Auditory Brainstem Response (ABR) and Distortion Product Oto-Acoustic Emissions (DPOAE) recordings – 56
 - 2.1.5. Cochlea whole-mount immunofluorescence – 58
 - 2.1.6. Cryostat sample prep, sectioning and staining – 58
 - 2.1.7. Utricle twist-off – 60
 - 2.1.8. Genotyping – 61
- 2.2. Bacterial techniques – 61
 - 2.2.1. Creation of chemically competent bacteria – 61
 - 2.2.2. Plasmid purification – 62
 - 2.2.3. Bacterial transformation – 62
 - 2.2.4. Glutathione S-transferase (GST) protein purification – 62
- 2.3. Cell culture techniques – 63
 - 2.3.1. KM155, VOT-E36 and VOT-N33 cell culture methods – 63
 - 2.3.2. Electroporation – 65
 - 2.3.3. Cell immunofluorescence – 65
 - 2.3.4. Cell lysate collection – 66
- 2.4. Biochemistry and molecular biology techniques – 66
 - 2.4.1. SDS-PAGE – 66
 - 2.4.2. Coomassie staining – 67
 - 2.4.3. Western blot – 67
 - 2.4.4. Western blot membrane stripping – 68
 - 2.4.5. Silver staining – 68
 - 2.4.6. SPOT arrays – 69
 - 2.4.7. SPOT array stripping – 69
 - 2.4.8. DNA electrophoresis – 70
 - 2.4.9. Plasmid cloning – 70
 - 2.4.10. GST pull-down – 71
 - 2.4.11. Co-immunoprecipitation – 71
 - 2.4.12. Buffer exchange – 72
 - 2.4.13. Protein A IgG purification – 73

- 2.4.14. Antibody affinity purification – 73
- 2.4.15. mRNA extraction and DNase I treatment – 74
- 2.4.16. cDNA synthesis – 75
- 2.4.17. qPCR – 76
- 2.4.18. Statistical analysis – 76
- 3. Investigating the *in vitro* interaction of beta-dystroglycan and EPS8L2 – 77
 - 3.1. Introduction – 77
 - 3.2. Results – 78
 - 3.2.1. Investigating the binding site of EPS8L2 on the cytoplasmic region of β DG – 78
 - 3.2.2. Validating the VOT-N33 and E36 cell lines as sources of β DG and p β DG – 80
 - 3.2.3. Pull-down of β DG using the GST-fused SH3 domains of the EPS8 family – 83
 - 3.2.4. Creating mammalian expression vectors of the EPS8 family SH3 domains and using them for the co-immunoprecipitation of β DG – 87
 - 3.3. Discussion – 90
- 4. Investigating the expression and distribution of phosphorylated beta-dystroglycan in the cochlea using the Y890 phospho-specific antibody – 93
 - 4.1. Introduction – 93
 - 4.2. Results – 95
 - 4.2.1. The subcellular localisation of the 1709 signal within the cochlear hair cells – 95
 - 4.2.2. Affinity purification of 1709 and validation of the resulting fractions – 97
 - 4.2.3. Affinity purified 1709 signal within the organ of Corti – 99
 - 4.2.4. Investigating the possibility of pikachurin expression within the hair cell ribbon synapses – 102
 - 4.2.5. Attempted identification of the protein responsible for the depleted pY890 Ab stereocilia signal – 104
 - 4.3. Discussion – 107
- 5. Investigating the phenotype associated with the hair cell specific knock-out of dystroglycan – 109
 - 5.1. Introduction – 109

- 5.2. Results – 110
 - 5.2.1. Analysing the hearing thresholds and outer hair cell function of 1 month old DG knock-out mice – 110
 - 5.2.2. Analysing the hearing thresholds and outer hair cell function of 2 month old DG knock-out mice – 113
 - 5.2.3. Analysing the hearing thresholds of 6 month old DG knock-out mice – 116
 - 5.2.4. Investigating the quantity and alignment of ribbon synapses in the conditional DG knock-out – 117
 - 5.2.5. Investigating the maturation of inner hair cells in the DG knock-out mice – 119
- 5.3. Discussion – 126
- 6. Investigating the phenotype associated with the knock-out of BAIAP2L2, a protein that may be involved in the differential localisation of EPS8 and EPS8L2 – 129
 - 6.1. Introduction – 129
 - 6.2. Results – 131
 - 6.2.1. Investigating the severity and progression of hearing loss in BAIAP2L2 knock-out mice – 131
 - 6.2.2. Investigating mechanotransduction of P8-11 BAIAP2L2 knock-out outer hair cells – 142
 - 6.2.3. Investigating the maturation of BAIAP2L2 knock-out inner and outer hair cells – 149
 - 6.2.4. The impact of BAIAP2L2 knock-out on the morphology of the stereocilia bundle – 161
 - 6.2.5. The subcellular localisation of BAIAP2L2 within the hair cells – 165
 - 6.3. Discussion – 168
- 7. General discussion – 171

List of Figures

Figure 1.1 – Basic structure of the entire auditory system – 2

Figure 1.2 – Structure of the organ of Corti – 4

Figure 1.3 – Tonotopic organisation of the basilar membrane – 5

Figure 1.4 – The cell layers and channels of the stria vascularis – 9

Figure 1.5 – Structure and composition of the tip-links – 12

Figure 1.6 – Initial development of the hair bundle – 16

Figure 1.7 – Development and stabilisation of the row 1 complex – 19

Figure 1.8 – Gross morphology of the synaptic ribbon – 23

Figure 1.9 – The morphological development of synaptic ribbons throughout maturation – 30

Figure 1.10 – The development of hair cell innervation throughout the first two post-natal weeks – 33

Figure 1.11 – The development of the different currents within both inner and outer hair cells – 37

Figure 1.12 – Structure of the dystrophin glycoprotein complex – 40

Figure 1.13 – The extensive glycosylation of alpha-dystroglycan – 43

Figure 1.14 – The role of the DGC in the formation of proper ribbon synapses between photoreceptors and ON bipolar cells – 49

Figure 2.1 – Grid and chamber used for the immobilisation of cochlear sensory epithelia – 54

Figure 2.2 – Manual analysis of ABR hearing thresholds – 57

Figure 3.1 – The distinct binding site of EPS8L2 on the cytoplasmic tail of β DG – 79

Figure 3.2 – Visualisation of phosphorylated and non-phosphorylated dystroglycan expression in the VOT-N33 cell line – 81

Figure 3.3 – Visualisation of phosphorylated and non-phosphorylated dystroglycan expression in the VOT-E36 cell line – 82

Figure 3.4 – Western blot quantification of the ratio of β DG to p β DG in the VOT-N33 and E36 cell lines – 83

Figure 3.5 – Pull-down of β DG from the VOT-E36 cell line using the GST-fused SH3 domains of the EPS8 family – 85

Figure 3.6 – Pull-down of the purified cytoplasmic tail of β DG using the GST fused SH3 constructs – 86

Figure 3.7 – The creation and validation of the mammalian EPS8 SH3 expression constructs – 88

Figure 3.8 – Co-immunoprecipitation of β DG from the electroporated E36 lysates – 89

Figure 3.9 – Theoretical role of β DG at the shorter rows of stereocilia – 92

Figure 4.1 – Preliminary staining of the cochlea with β DG (Mandag2 monoclonal) and pY890 Ab (1709 polyclonal sera) – 94

Figure 4.2 – The specific localisation of pY890 Ab signal within the organ of Corti – 96

Figure 4.3 – Western blot and SPOT array validation of the AP pY890 Ab and depleted pY890 Ab fractions – 98

Figure 4.4 – Further validating the purified AP pY890 Ab fraction using sgRNA control and DG knock-out KM155 myoblasts – 99

Figure 4.5 – Staining P6-8 cochlea sections with affinity purified 1709 and the depleted IgG negative control – 101

Figure 4.6 – The expression of pikachurin within the mammalian cochlea – 103

Figure 4.7 – Investigating whether pikachurin interacts with DG in the organ of Corti – 104

Figure 4.8 – Collection of a stereocilia enriched lysate using the “twist-off” technique – 106

Figure 5.1 – DAG1 knock-out and control hearing thresholds in 1-month aged mice – 111

Figure 5.2 – The effect of dystroglycan knock-out on distortion product amplitude against stimulus volume for each frequency in 1 month old mice – 112

Figure 5.3 – DPOAE thresholds of 1 month old DAG1 knock-out and control mice – 113

Figure 5.4 – DAG1 knock-out and control hearing thresholds in 2-month aged mice – 114

Figure 5.5 – The effect of dystroglycan knock-out on distortion product amplitude against stimulus volume for each frequency in 2 month old mice – 115

Figure 5.6 – DPOAE thresholds of 2 month old DAG1 knock-out and control mice – 116

Figure 5.7 – DAG1 knock-out and control hearing thresholds in 6-month aged mice – 117

Figure 5.8 – The impact of DG deletion on the number and alignment of ribbon synapses in the cochlea – 118

Figure 5.9 – Analysing the expression of the BK and SK2 potassium channels in the control and knock-out mice – 120

Figure 5.10 – Investigating the current clamp responses of control and DG knock-out P17-24 inner hair cells – 122

Figure 5.11 – Current recordings from control and knock-out animals – 123

Figure 5.12 – Analysis of the control and knock-out current recordings – 124

Figure 5.13 – qPCR validation of the conditional post-natal deletion of dystroglycan – 125

Figure 6.1 – Domain organisation of the I-BAR protein family members – 130

Figure 6.2 – Hearing thresholds in P14 and P19-21 *BAIAP2L2*^{tm1b} homozygous knock-out and heterozygous control mice – 133

Figure 6.3 - Hearing thresholds in P48-61 and P104-115 *BAIAP2L2*^{tm1b} homozygote knock-out and heterozygous control mice – 135

Figure 6.4 – Hearing thresholds in P166-245 *BAIAP2L2*^{tm1b} homozygote knock-out and heterozygous control mice – 136

Figure 6.5 – The effect of *BAIAP2L2* knock-out on the latency and amplitude of ABR wave I – 138

Figure 6.6 - DPOAE thresholds in P19-22 and P48-61 *BAIAP2L2*^{tm1b} homozygote knock-out and heterozygous control mice – 140

Figure 6.7 - DPOAE thresholds in P48-61 and P105-115 *BAIAP2L2*^{tm1b} homozygote knock-out and heterozygous control mice – 141

Figure 6.8 – MET recordings from P8-9 *BAIAP2L2*^{tm1b} heterozygous and homozygous outer hair cells – 143

Figure 6.9 – The impact of *BAIAP2L2* mutation on the resting open probability of the MET channels in P8-9 mice – 144

Figure 6.10 – MET recordings from P11 *BAIAP2L2*^{tm1b} heterozygous and homozygous mice – 146

Figure 6.11 - The impact of *BAIAP2L2* mutation on the resting open probability of the MET channels in P11 mice – 147

- Figure 6.12 – Adaptation in the *BAIAP2L2*^{mb} homozygous and control mice – 148
- Figure 6.13 – Investigating the current clamp responses of heterozygous and homozygous *BAIAP2L2* P28-38 mice – 150
- Figure 6.14 – Investigating the voltage clamp current responses from heterozygous and homozygous *BAIAP2L2* P28-38 inner hair cells – 151
- Figure 6.15 – Analysis of the voltage clamp responses from heterozygous and homozygous *BAIAP2L2* P28-38 inner hair cells – 153
- Figure 6.16 - Investigating the current clamp voltage responses from heterozygous and homozygous *BAIAP2L2* P12 outer hair cells – 154
- Figure 6.17 – Preliminary investigation of the voltage clamp current responses from heterozygous and homozygous *BAIAP2L2* P12 outer hair cells – 156
- Figure 6.18 - Analysis of the voltage clamp responses from P12 heterozygous and homozygous *BAIAP2L2* outer hair cells – 157
- Figure 6.19 – Investigating the ribbon synapses and efferent innervation of *BAIAP2L2* knock-out hair cells – 159
- Figure 6.20 – Investigating the maturation of inner and outer hair cells in *BAIAP2L2* knock-out animals – 160
- Figure 6.21 – Hair bundle morphology in heterozygous and homozygous P10 *BAIAP2L2* mice – 162
- Figure 6.22 - Investigating the maturation of inner and outer hair cells in *BAIAP2L2* knock-out animals – 164
- Figure 6.23 – Hair bundle morphology in heterozygous and homozygous P245 *BAIAP2L2* mice – 165
- Figure 6.24 – The expression and localisation of *BAIAP2L2* in P4-113 wild-type hair bundles – 167
- Figure 6.25 – Investigating whether *BAIAP2L2* functions to localise EPS8 to the tallest row of stereocilia in outer hair cells – 168

List of Appendices

Appendix 2.1 – Antibodies Used – 224

Appendix 2.2 – PCR primers, reaction conditions and expected products – 226

Appendix 2.3 – Cell Lines Used – 228

Appendix 2.4 – Cellspot array of the cytoplasmic domain of β DG – 229

Abbreviations

γ INF	Gamma interferon
6J	C57BL/6J
6N	C57BL/6NTac
ABR	Auditory brainstem response
AChR	Acetylcholine receptor
α DG	Alpha dystroglycan
AZ	Active zone
BAIAP2L2	BAR/IMD Domain Containing Adaptor Protein 2 Like 2
β DG	Beta dystroglycan
BSA	Bovine serum albumin
<i>Cdh23^{ahl}</i>	Cadherin 23 repaired
Co-IP	Co-immunoprecipitation
DG	Dystroglycan
DGC	Dystrophin glycoprotein complex
DIC	Differential interference contrast
DMSO	Dimethyl sulfoxide
EDTA	Ethylenediaminetetraacetic acid
EGTA	Ethylene glycol tetraacetic acid
EP	Endocochlear potential
EPS8	Epidermal Growth Factor Receptor Pathway Substrate 8
EPS8L(X)	Epidermal Growth Factor Receptor Pathway Substrate 8-Like (1-3)
E(X)	Embryonic day
FCS	Foetal calf serum
GAP	GTPase activating protein
GNAi3	Inhibitory G-protein alpha 3
GPSM2	G-protein signalling modulator 2

GST	Glutathione S-transferase
HRP	Horse radish peroxidase
I-BAR	Inverse Bin/Amphiphysin/Rvs
I_{Ca}	Calcium current
I_K	Potassium current
I_{Na}	Sodium current
IHC	Inner hair cell
OHC	Outer hair cell
OTOG	Otogelin
MEM	Minimal essential media
MET	Mechano-electrical transduction
MYO15aL	Myosin 15a long isoform
MYO15aS	Myosin 15a short isoform
NMJ	Neuro-muscular junction
NrCAM	Neuronal cell adhesion molecule
p β DG	Phosphorylated beta-dystroglycan
PBS	Phospho-buffered saline
PFA	Paraformaldehyde
PTXa	Pertussis toxin subunit A
P(X)	Post-natal day
RIM	Rab3-interacting molecules
RIM-BP	RIM-binding protein
RRP	Readily releasable pool
SGN	Spiral ganglion neuron
SRP	Secondary releasable pool
SYT	Synaptotagmin
TAE	Tris-acetate EDTA

TECTA	Tectorin-A
TECTB	Tectorin-B
TMC	Trans-membrane channel-like protein
TMIE	Trans-membrane inner ear
WHRN	Whirlin

1 – Main introduction

Despite the importance of the auditory system in survival and communication, we still understand very little about how the system is set up and maintained. The hair cells of the organ of Corti, named due to the presence of the stereociliary hair bundles on their apical surface, are responsible for the transduction of acoustic information into electrical signals. The hair bundles, which possess a characteristic staircase morphology and contain the mechano-electrical transducer apparatus, are set up and maintained by the differential localisation of actin effector proteins across the different rows. An example of this system is the presence of EPS8 at the tips of the tallest row of stereocilia and EPS8L2 at the tips of the two subsequent shorter rows (Zampini *et al.* 2011, Furness *et al.* 2013). Knocking out either of these proteins ultimately results in hearing loss, the time-frame of which reflects the different roles of the two proteins in the morphogenesis and maintenance of the hair bundle. Exactly how the exquisite differential localisation of EPS8 and EPS8L2 is set up and maintained between the rows throughout life is unknown. Preliminary data has indicated that dystroglycan, a protein typically associated with muscular dystrophy, may interact with EPS8L2. Furthermore, new data has also shown that dystroglycan may also be present in the organ of Corti. Additional work on the role of dystroglycan in retinal synapses also alludes to the possibility that the protein may be functioning in a similar manner within the inner ear (Omori *et al.* 2012). Thus, the major aim of this project was to investigate if dystroglycan is functioning to correctly localise EPS8L2 in the mammalian cochlea, or facilitating normal synaptic development as it does in the retina.

1.1 – The structure and mechanism of the mammalian inner ear

The auditory system is an essential sensory tool for all animal species, and provides advantages in hunting, the avoidance of predators, communication and many other aspects necessary for survival and procreation. The auditory system can be sub-divided into three sections, the outer ear, the middle ear and the inner ear (**Figure 1.1**). The outer ear comprises the pinna and the ear canal, and functions to funnel the sound energy efficiently to the tympanic membrane that lies at the end of the canal. In the middle ear, sound energy strikes the tympanic membrane and induces vibrations in the three ossicles; the malleus, incus and stapes. These three bones, in turn, transfer the sound energy into the inner ear through the oval window. Due to the difference in surface area between the

tympanic membrane and the oval window, this effectively concentrates the energy into the inner ear. This system also prevents the majority of the sound waves from being simply reflected off the oval window due to the impedance difference between air and water, as the impedance of the tympanic membrane itself is close to that of air (Mason 2016). The sound energy enters the cochlea through the oval window, and the fluid displacement is permitted due to the presence of the flexible round window (**Figure 1.1**). The mammalian inner ear is composed of two major components: The vestibular system, which includes the vestibule and the semicircular canals, and the cochlea, which is the organ responsible for the transduction of sound and transmission of the information to the brain.

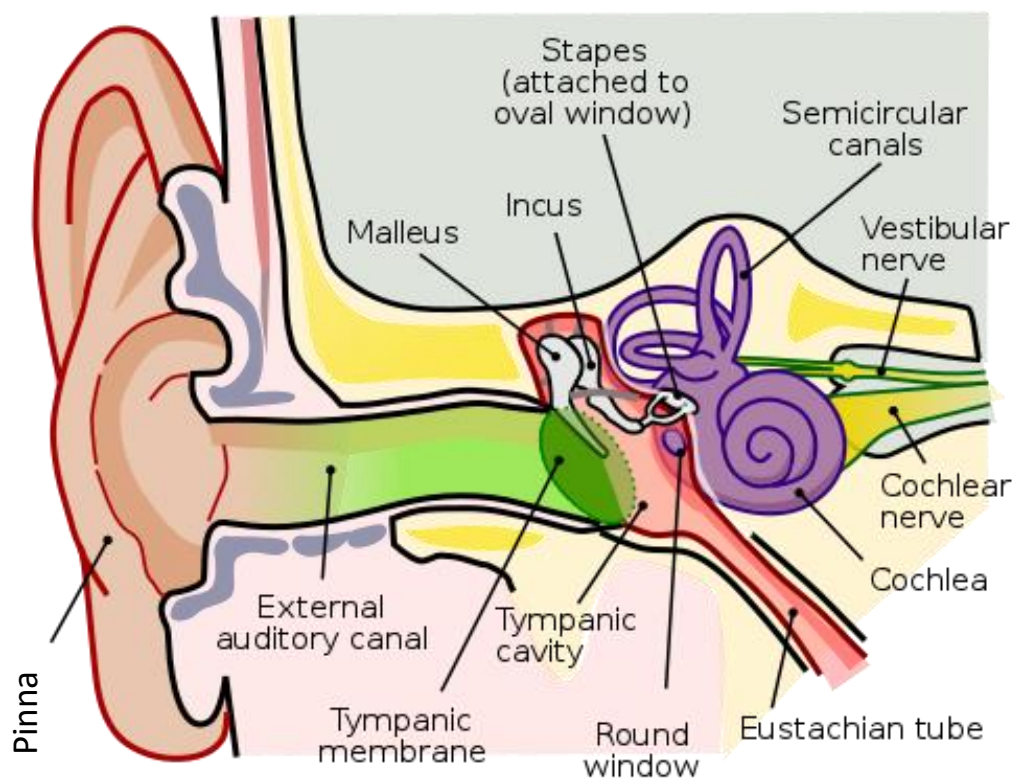


Figure 1.1 – Basic structure of the entire auditory system – The outer ear, comprising the pinna and the ear canal, functions to efficiently funnel sound to the tympanic membrane of the middle ear. The sound waves are transduced into mechanical vibrations of the ossicles in the middle ear, and the energy is concentrated into the inner ear comprising the cochlea of the auditory system and the vestibule of the vestibular system. Sound energy enters the cochlea through the oval window, and the displacement of fluid required to allow sound transmission is permitted by the round window, which prevents pressure build up. The pressure of the middle ear relative to the atmosphere is regulated by the Eustachian tube, to

maintain peak efficiency. Image adapted from commons.wikimedia.org/wiki/File:Anatomy_of_the_human_ear.svg.

The cochlea, which gained the name through the snail shell like appearance, is a coiled structure composed of three cavities: the scala media is positioned in the centre, scala vestibule at the top and scala tympani at the bottom (**Figure 1.2A**). The scala vestibule is separated from the scala media by Reissner's membrane, and the scala media is separated from the scala tympani by the reticular lamina which sits above the organ of Corti. The organ of Corti is positioned within the scala media atop of the basilar membrane, and contains the sound transducing hair cells. The mammalian cochlea possess three rows of outer hair cells, which are responsible for the amplification of sound energy, and a single row of inner hair cells, which are responsible for the detection of all conscious sound information. These extremely specialised hair cells possess apical hair-like projections termed stereocilia, which are capable of detecting deflections smaller than the diameter of a hydrogen atom (Rhode and Geisler 1967). The stereocilia of the outer hair cells come into direct contact with the tectorial membrane which is positioned above the organ of Corti (**Figure 1.2B**). As sound induces the basilar membrane to move up and down, it elicits a shearing motion between the tectorial membrane and the outer hair cell stereocilia bundles. This motion leads to the deflection of the stereocilliary hair bundle and opening of the mechano-electrical transducer (MET) channels, which modulate the hair cell receptor potential. The tectorial membrane is composed of collagen II, V, IX and XI, as well as the glycoproteins alpha tectorin (TECTA), beta tectorin (TECTB) and otogelin (OTOG) (Richardson *et al.* 2008). The membrane is organised as thick collagen bundles embedded in a tectorin matrix orientated towards the outer hair cells. The tips of the tallest row of outer hair cell stereocilia are physically linked to the tectorial membrane by stereocilin (Verpy *et al.* 2011). Stereocilin is localised to the tips of each stereocilium in the tallest row in a ring pattern, and can also be visualised in the stereocilia dents on the underside of the tectorial membrane. Stereocilin is not likely the only protein involved in the stereocilia and tectorial membrane link, and another likely candidate is caecam16, which was also detected at the tips of the outer hair cell stereocilia where it interacts with TECTA in the tectorial membrane (Zheng *et al.* 2011). The function of this contact between the outer hair cells and the tectorial membrane is to better translate movement of the organ of Corti into displacement of the stereocilia bundles. When this stereocilia contact or the tectorial

membrane itself is disrupted, the result is a severe decrease in hearing sensitivity (Legan *et al.* 2000).

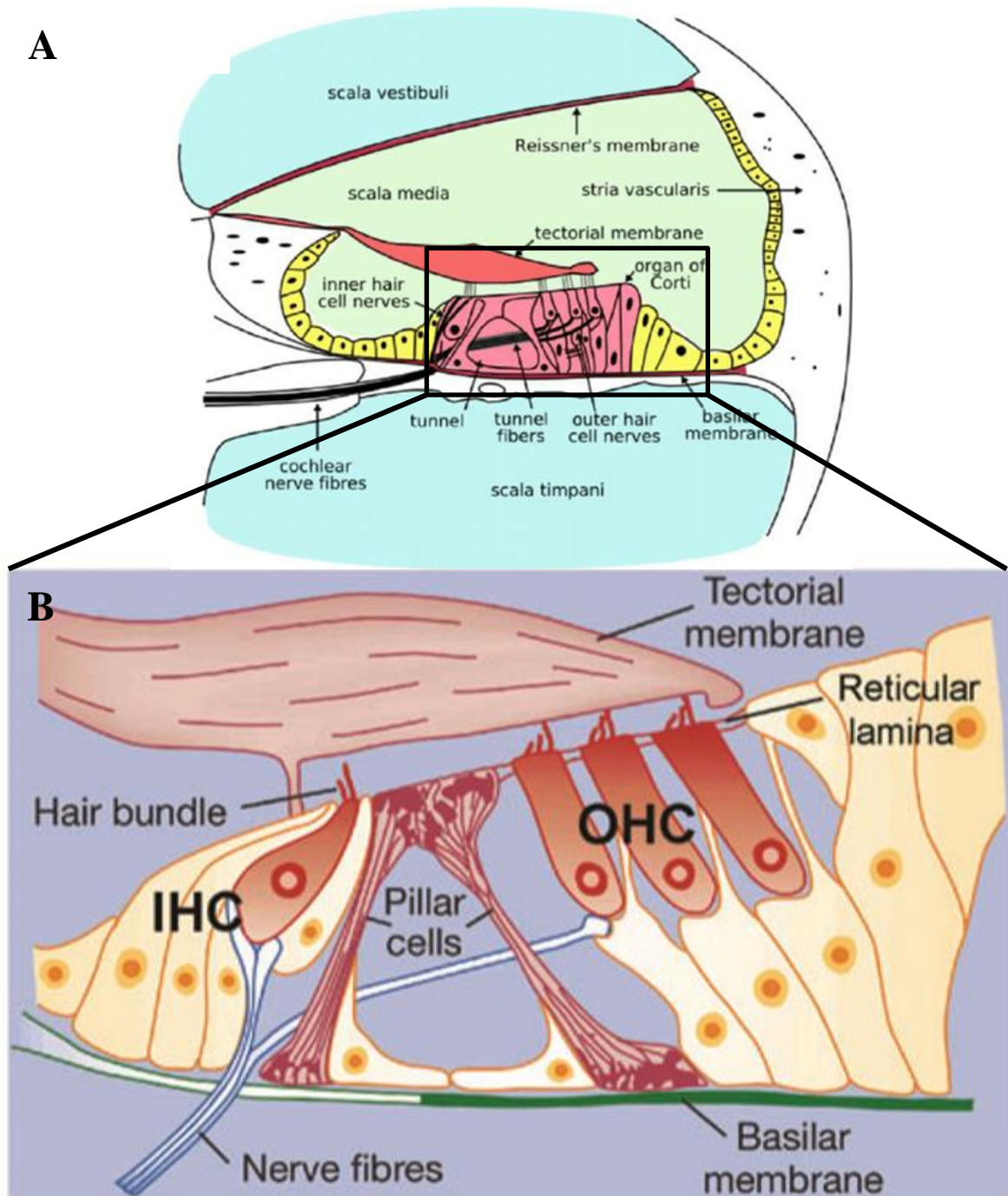


Figure 1.2 – Structure of the organ of Corti – (A) Cross section of the cochlear spiral showing the three chambers; the scala vestibuli, scala tympani, and the scala media which houses the organ of Corti. (B) Expanded view of the region highlighted with the black box in A. The three rows of outer hair cells are responsible for the amplification of sound, and in the mature system the tallest stereocilliary row is

physically linked to the tectorial membrane. Upon sound stimulation, the movement induces outer hair cells stereocilia deflection, which stimulates the cells to amplify the displacement via changes in length. This force is transmitted through the Deiter cells and amplifies basilar membrane movement. The inner hair cells then detect this fluid motion through their longer and free standing stereocilia rows. Images adapted from commons.wikimedia.org/wiki/File:Cochlea-crosssection.png and Marcotti 2012 respectively.

The entirety of the organ of Corti is tonotopically organised from the base to the apex, meaning that sound waves entering the cochlea induce the greatest vibration at a specific location along the spiral cochlea structure (von Békésy 1960). Treble frequencies induce the greatest vibration amplitude at the base, and the bass frequencies induce the largest amplitude at the apex. This is mainly possible due to the differences in membrane properties along the length of the cochlear spiral. The tectorial membrane above the organ of Corti and the basilar membrane beneath it are both wider and thinner at the apex of the cochlea compared to the base (**Figure 1.3**, Raphael and Altschuler 2003). Meaning that high frequencies can better resonate with the stiffer structure, and low frequencies continue to move along the cochlea until they come into contact with the looser structure of the apex.

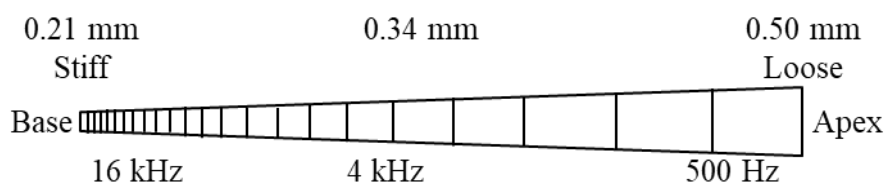


Figure 1.3 – Tonotopic organisation of the basilar membrane – Image representing the uncoiled basilar membrane that supports the organ of Corti. At the base of the cochlea, this membrane is thin and stiff, and is thus better suited to vibrating at high frequencies. At the apex, the membrane is wider and more floppy, and thus is better suited to vibrating at lower frequencies. This image was redrawn from Kim and Koo 2015.

The hair cells themselves also possess differing properties along the length of the organ of Corti. Inner and outer hair cell stereocilia become taller closer to the apex (Fettiplace and Hackney 2006), and the outer hair cells themselves become taller as you move away from the base (Oghalai *et al.* 1998). The taller stereocilia are more suited to detecting bass frequencies, unlike the short and stiff stereocilia at the base, and the shorter outer hair cells more suited to the rapid depolarisation required to detect higher frequencies on a cycle-by-cycle basis. It is this system of property gradients along the cochlear spiral, modelled as the travelling wave (von Békésy 1960), which forms the entire structural basis of frequency discrimination.

The exquisite sensitivity of the organ of Corti is achieved thanks to highly specialised structures within the cochlear partitions. As mentioned above, the function of the three rows of outer hair cells is to amplify the sound induced movement of the basilar membrane, and this is accomplished via electromotility. Upon stereocilia deflection in the excitatory direction, the outer hair cell is depolarised due to the opening of the MET channels at the tips of the shorter transducing stereocilia rows (Beurg *et al.* 2009). This depolarisation induces a voltage-dependent (Brownell *et al.* 1985) elongation and contraction of the outer hair cells on a cycle-by-cycle basis (Mammano and Ashmore 1993). This applies force to the tectorial membrane and as such amplifies the sound induced displacement of the organ of Corti by a magnitude of over 1000x (Ren *et al.* 2011). Mutations that affect this amplification system result in a hearing threshold increase of 60dB SPL in mice, across all frequencies (Dallos *et al.* 2008). Not only does this amplification enhance the sensitivity of the cochlea, but it also enhances the frequency tuning by generating the greatest amplification at the characteristic frequency (Olson 2004), which are dictated by the membrane properties covered earlier. The protein responsible for the electromotility of the outer hair cells is the modified 80kDa transmembrane anion transporter prestin (SLC26A5; Zheng *et al.* 2000a). Upon depolarisation, prestin undergoes a chloride-dependent conformational change (Oliver *et al.* 2001) that alters the width of the protein. Due to the transmembrane nature and high density of prestin in the lateral wall of the hair cell (10,000/ μm^2 , Mahendrasingham *et al.* 2010), this conformational change causes the overall length of the outer hair cell to change in response to stereocilia deflection. The mutation (Dallos *et al.* 2008) or pharmacological inhibition (Muller *et al.* 2003) of prestin completely nullifies the cochlea amplification by the outer hair cells, and results in severe frequency wide hearing loss.

The second method by which the cochlea amplifies the detection of basilar membrane movement is by the endocochlear potential (EP). As previously discussed, the cochlea is composed of three chambers, and the upper (scala vestibule) and lower (scala tympani) chambers are connected via the helicotrema at the very apex. These two chambers contain the same solution, termed perilymph, which bathes the cell bodies of the hair cells. This high sodium solution is composed of (in mM): 148 Na⁺, 4 K⁺, 1.3 Ca²⁺, 1 Mg²⁺, 119 Cl⁻ and 21 HCO₃⁻. The solution in the central chamber, which bathes the stereocilia of the hair cells, is composed of a very different solution, termed the endolymph. This low sodium and calcium, high potassium solution is composed of (in mM): 1 Na⁺, 157 K⁺, 0.02 Ca²⁺, 0.01 Mg²⁺, 132 Cl⁻ and 30 HCO₃⁻ (Wangemann 2006). The significantly different composition of these two solutions is possible due to the claudin based tight junctions present between the cells that line the scala media (Ben-Yosef *et al.* 2003), entirely sealing it from the other chambers. The endolymph also possesses an electrical potential of +80mV (Tasaki *et al.* 1954), compared to the resting membrane potential of a mature hair cell of around -60mV. It is this combined difference in ionic composition and 140mV difference in electrical potential that provides a strong driving force for cations, mainly potassium and calcium, to enter the hair cells through the MET channels upon deflection of the stereocilia. This effectively increases the depolarisation induced by the MET channels opening and amplifies the signal generated by sound. The significance of the EP can be assessed by disrupting it with either loop diuretics, which prevent potassium secretion by inhibiting the NKCC (**Figure 1.4**) co-transporter (Hannaert *et al.* 2002), or transient hypoxia, which both result in loss hearing sensitivity (Evans and Klinke 1982) and frequency tuning (Brown *et al.* 1983).

The EP is both set up and maintained by the stria vascularis, which is located on the lateral wall of the cochlear spiral (Wangemann 2006) and is composed of three cell layers. The basal cells are exposed to the perilymph, and are connected to the fibrocytes of the spiral ligament with gap junctions, forming an ionic syncytium. These cells are also connected with gap-junction channels to the second layer of the stria vascularis, the intermediate cells. The intermediate cells and the marginal cells, the third cell layer of the stria vascularis which lay adjacent to the endolymph, are separated with the intrastrial space (**Figure 1.4**). The basal and marginal cells are connected to their adjacent partners with claudin tight junctions (Kitajiri *et al.* 2004), which allows them to seal both the intrastrial space and the endolymph. Potassium enters the stria vascularis through the electrical

syncytium, and after passage through the various gap junctions, is secreted into the intrastrial space through the inward rectifying potassium channel Kir4.1 (Nin *et al.* 2008). It is this secretion of potassium through the apical surface of the intermediate cells which establishes the positive endolymphatic potential (Liu and Zhao 2008), and disruption of Kir4.1 abolishes the EP (Marcus *et al.* 2002). Potassium is then taken up by the marginal cells through a Na-2Cl-K co-transporter (Flagella *et al.* 1999), and flows out of the marginal cells down the concentration gradient into the endolymph through KCNQ1+E1 subunit containing potassium channels (Neyroud *et al.* 1997). The net result of this potassium movement is an intrastrial space with a high electrical potential but low potassium concentration (Salt *et al.* 1987), and an endolymph with both a high potassium concentration and a high electrical potential.

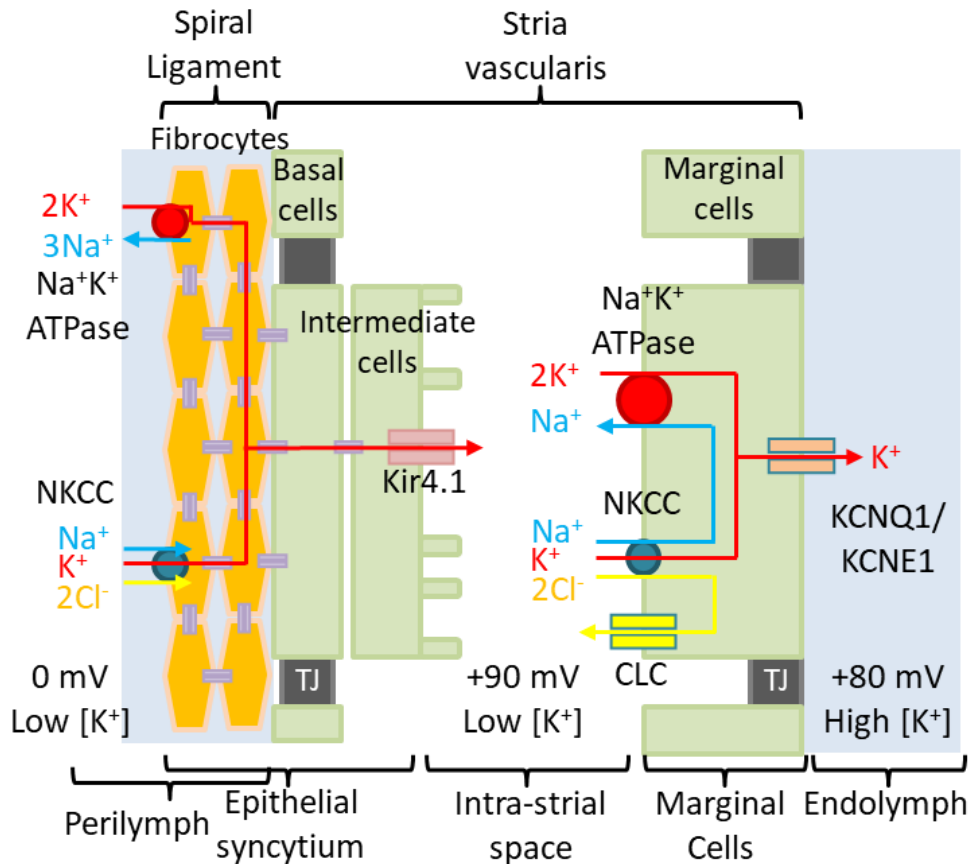


Figure 1.4 – The cell layers and channels of the stria vascularis – Potassium flows down the concentration gradient and through the ionic syncytium of the spiral ligament into the basal and intermediate cells of the stria vascularis. Potassium then flows into the intrastrial space through the inwardly rectified potassium channel Kir4.1, located on the apical surface of the intermediate cells. This potassium is taken into the marginal cells through the Na-2Cl-K co-transporter, resulting in a low potassium concentration in the intrastrial space. Chloride ions are recycled into the intrastrial space through CLC channels. The potassium then flows out of the marginal cell through KCNQ1/KCNE1, and the result is an endolymph with a high potassium concentration and a high electrical potential of +80mV. This image was redrawn from Nin *et al.* 2008.

In order to maintain this system, potassium must be recycled following mechanotransduction back to the stria vascularis. Upon mechanotransduction, potassium entering the hair cells through the MET channels is then extruded via voltage-gated basolateral potassium channels (Kros *et al.* 1998). Following uptake by the various

supporting cells within close proximity to the hair cells, the potassium follows the concentration gradient through the electrical syncytium of the lateral wall. Potassium moves through the Deiter cells and fibrocytes of the spiral ligament until it reaches the stria vascularis (Kikuchi *et al.* 2000), where it is then re-secreted in order to maintain the EP. In mice, the EP is not entirely matured at the onset of hearing at P12, and fails to reach a mature calcium concentration (Johnson *et al.* 2012) and EP of +80mV until the age of around P17 (Sadanaga and Morimitsu 1995). As such hearing thresholds continue to improve over the first post-hearing week in mice (Corns *et al.* 2018).

1.2 – Development and maintenance of the mechanotransduction machinery

1.2.1 – Structure of the stereocilia and the mechanotransduction apparatus

As mentioned in section 1.1, it is the hair bundles that reside on the apical surface of the hair cells which are responsible for the mechanotransduction of acoustic stimuli into changes in membrane potential. These hair bundles are precisely set up, such that their staircase structure of stereocilia of different height is always orientated with the surrounding cells and in line with the modiolus. The stereocilia themselves, similar to other factors of the tonotopic gradient described earlier, show a height gradient along the length of the organ of Corti, with the stereocilia at the apex being longer and thicker than those at the base (Wright 1984). The heights of the stereocilia are not only very similar within each row, but also between adjacent hair cells in the frequency range. These hair bundles, which have to be precisely maintained throughout the life-course, require a plethora of mechanisms to be created and stabilised.

Each stereocilium possesses a stiff core of tightly packed actin filaments, uniformly polarised such that the barbed ends of the actin filaments reside at the distal stereocilia tips (Flock *et al.* 1977). These bundles of actin are stabilised with cross-linkers roughly once per 10 subunits, and knocking out one of the proteins associated with these cross-linkers, such as espin, results in deafness due to short and thin stereocilia (Zheng *et al.* 2000b). At the base of each stereocilium, the tubular structure tapers briefly before insertion into the cuticular plate, a thick base of non-polarised actin, at the apical membrane of the hair cells (DeRosier and Tilney 1989). This stiff core structure and tapered insertion into the stable cuticular plate means that the stereocilia, upon sound-induced deflection, pivot around the

cuticular plate rather than bending (Flock *et al.* 1977). This pivoting results in a shearing movement between the stereocilia, which optimally stretches the coiled double stranded link between the tips of the shorter stereocilia and the shaft of their taller adjacent partner (Kachar *et al.* 2000, Pickles *et al.* 1984). It is the stretching of this link that results in opening of the MET channel at the tip of the shorter stereocilium (Beurg *et al.* 2009), and thus it is this link that the process of hearing is entirely dependent on. Deflection of the bundle towards the tallest row opens the MET channel, resulting in hair cell depolarisation, whereas movement towards the shortest row closes the MET channel, and results in hair cell hyperpolarisation (Hudspeth and Corey 1977). Lateral movement on the bundle has no effect on the MET channel opening probability, as these movements do not result in stretching of the tip links (Shotwell *et al.* 1981).

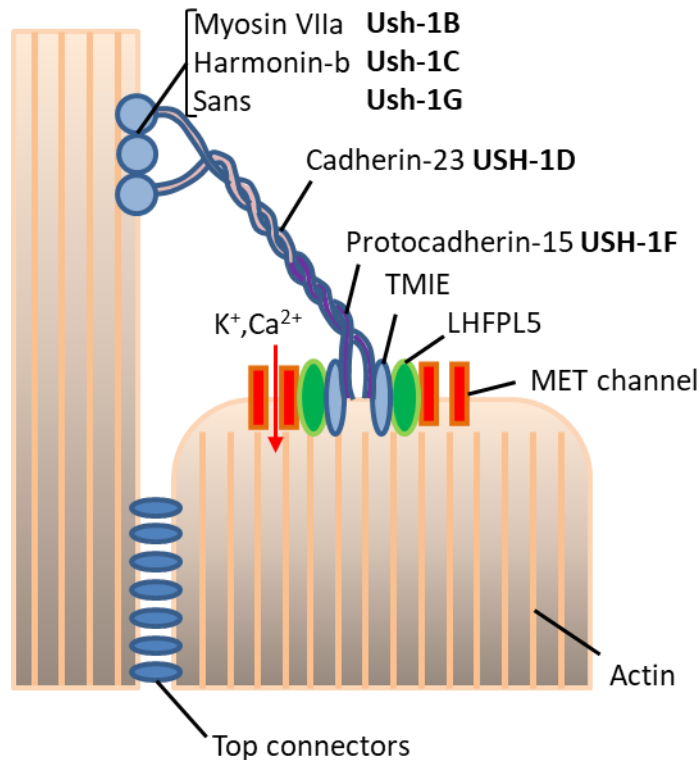


Figure 1.5 – Structure and composition of the tip-links – The protocadherin-15 and cadherin-23 connects the tip of the shorter stereocilium to the shaft of the adjacent taller partner in a calcium dependent manner. The base of the link interacts directly with the MET channel and increased tension due to stereocilium deflection results in channel opening and cell depolarisation. The link is connected to the taller stereocilium through myosin VIIa, harmonin-b and sans, which allow for the adjustment of tip-link tension by moving the anchoring point up and down the stereocilium. This figure was redrawn from Fettiplace 2017.

Tip links are present at birth in the mouse (Goodyear *et al.* 2005), and composed of protocadherin-15 near the tips of the shorter stereocilia, and cadherin-23 towards the shaft of the taller stereocilia (**Figure 1.5**, Kazmierczak *et al.* 2007). The interaction between these two components is calcium dependent, and removing calcium from the surrounding solution causes them to break (Assad *et al.* 1991). However, the link can be repaired if broken by mechanical force or low calcium (below the physiological concentration of 20-40 μM), and the new link is initially entirely composed of protocadherin-15 (Zhao *et al.* 1996; Indzhykulian *et al.* 2013). The lower side of the tip link, in a mechanism that is still mostly unknown, results in opening of the MET channel, but the upper anchor of the link

also possesses a crucial role. The upper tip link density contains, likely among many others, myosin VIIa, harmonin-b and sans (Grati and Kachar 2011), which anchor the cadherin-23 and also control the resting tension of the link by moving the anchor point up and down the stereocilium shaft, at least in lower vertebrates (Howard and Hudspeth 1987). This resting tension results in a resting opening probability of the MET channels, which can be visualised with patch-clamp experiments that utilise a fluid jet for hair bundle stimulation (Corns *et al.* 2014). While not directly involved in mechanotransduction, other types of links are also important for bundle stimulation and morphology (Petit and Richardson 2009). Ankle links, by the tapered bases of the stereocilia, and lateral links, which interconnect adjacent stereocilia along the shafts, are present only during development (Goodyear *et al.* 2005, Petit and Richardson 2009). These transient links function to hold the bundle together and prevent splaying before more mature links can be developed (Hackney and Furness 2013). At the onset of hearing most of these links have been lost, and replaced with stereocilin associated top connectors (Verpy *et al.* 2011), which remain throughout life and function to ensure the bundle moves as a single coordinated unit in response to sound. This ensures the stereocilia remain together and don't splay in response to sound stimuli, and all move in synchrony to ensure a maximal MET current during stimulation.

The MET channel is a large pore, large conductance, non-selective cation channel present at the tips of the shorter rows of stereocilia (Farris *et al.* 2004, Beurg *et al.* 2009). The identity of the MET channel has been a mystery for some time, but is now believed to be at least comprised of the transmembrane channel-like protein 1 (TMC1) in the mature system and TMC2 in the developing cochlea (Vreugde *et al.* 2002). TMC1 localises to the site of mechanotransduction (Kurima *et al.* 2015), interacts directly with protocadherin-15 (Maeda *et al.* 2014) and knocking out the protein results in the complete loss of mechanotransduction after P8, when TMC2 is entirely replaced by TMC1 (Kawashima *et al.* 2011). The TMC proteins require the presence of TMIE (Zhao *et al.* 2014) to properly localise to the site of mechanotransduction. Further evidence for the role of TMC1 as the MET channel lies with the tonotopic expression of the protein. Conductance of the MET channel at the base is up to three times greater than that at the apex (Ricci *et al.* 2003), which likely functions to increase the sensitivity of the system when dealing with much shorter opening periods of the channels. The TMC1 channel possesses a higher expression level at the base compared to the apex, and using fluorescently tagged TMC1 subunits it

was discovered that the expression is three-fold higher in the base, aligning perfectly with the conductance gradients (Beurg *et al.* 2018).

As well as possessing a high conductance, the MET channel also displays another interesting property necessary for efficient auditory transduction, which is adaptation. The MET channel displays a two-stage adaptation in response to a stepping stimulus; a fast adaptation in the sub-millisecond timescale and a slower component that acts over tens of milliseconds (Crawford *et al.* 1989; Wu *et al.* 1999; Vollrath and Eatok 2003). The slower component of this adaptation is thought to be based on the downwards movement of the upper tip-link density discussed earlier, which is dependent on myosin VIIa (Kros *et al.* 2002). Upon a sustained excitatory deflection, through a mechanism that is still poorly understood, the stretching of the tip-link results in the anchoring point slipping down the taller stereocilium, resetting the resting tension to prevent saturation of the bundle. When the stimulus is removed, the tension in the link decreases, and is re-tightened by the myosins in the upper tip link density to reset the resting position of the hair bundle (Howard and Hudspeth 1987). Exactly how the tallest row myosins can respond, when calcium enters only the shorter two rows through the MET channel (Beurg *et al.* 2009), remains unknown. The fast component of adaptation is thought to be based on calcium entering during transduction and acting as a permeant blocker of the MET channel, although this is still under some debate. When extracellular calcium is decreased from a perilymphatic 1.3 mM to an endolymphatic 20-40 μ M, the conductance of the MET channel increases by 50% (Ricci *et al.* 2003, Corns *et al.* 2014). Also, in these physiological conditions the channel is thought to be around 50% open at rest, due to the low calcium and resting tip-link tension alone (Beurg *et al.* 2010a). The fast component of adaptation can also be slowed down by lowering the extracellular calcium (Ricci and Fettiplace 1998, Ricci *et al.* 1998, Corns *et al.* 2014), and depolarising the cell to +80 mV to prevent calcium influx also abolishes fast adaptation (Assad *et al.* 1989).

1.2.2 – Development of the hair bundle, and the mechanisms responsible for the establishment and maintenance of the staircase architecture

Development of the stereocilia bundle begins at around embryonic day 14. At this stage, the apical surface of the hair cells possess a lawn of small and thin microvilli (**Figure 1.6**, Lim and Anniko 1985, Nishida *et al.* 1998), and a single microtubule-based projection called the kinocilium. Initially near the centre of the apical membrane, the kinocilium later migrates to the position of the future vertex of the hair bundle (Tilney *et al.* 1992), and in the case of outer hair cells this refers to the point of the V-shape. The kinocilium is believed to be necessary for the proper orientation and gross morphology of the bundle, and requires physical linkage to the future stereocilia with cadherin-23 and protocadherin-15 to carry out its function (Jones *et al.* 2008, May-Simera *et al.* 2015). Following the migration of the kinocilium, and just before birth, the microvilli closest to the kinocilium widen and elongate to become stereocilia, the microvilli that do not are eventually reabsorbed by the cell (Sekerková *et al.* 2011). At birth, the stereocilia staircase architecture is apparent, but not mature, as the height differences between the rows is still small. The development of stereocilia in the mouse then goes through an elongation phase, a widening phase which coincides with the acquisition of the MET current, and a final elongation phase of row 1 and a slight shortening of row 2 (Tadenev *et al.* 2019, Krey *et al.* 2020).

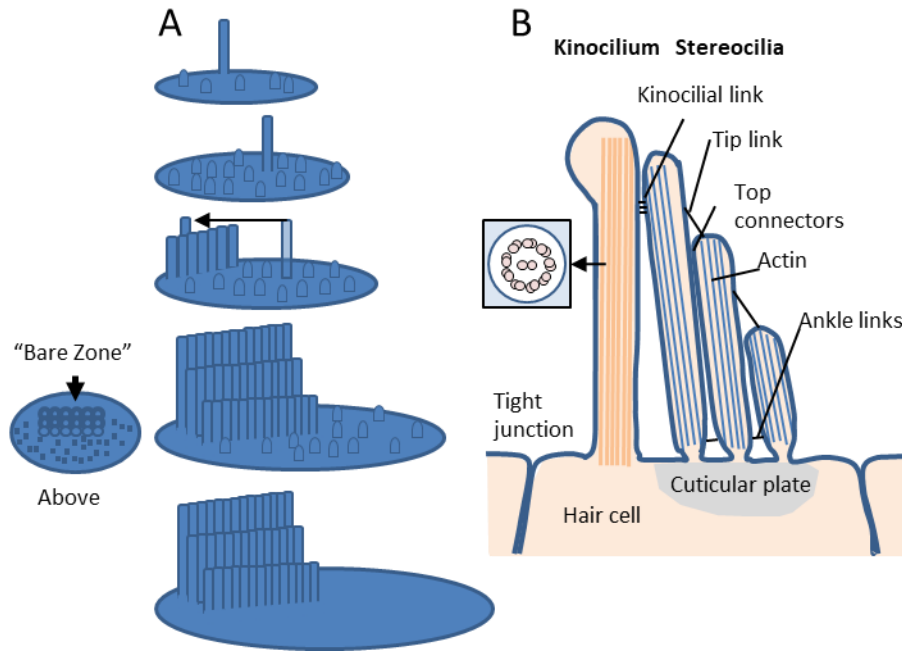


Figure 1.6 – Initial development of the hair bundle – (A) Hair bundle development starts with the kinocilium, which is a microtubule-based projection on the apical surface of the hair cell surrounded by a lawn of small actin-based microvilli (Lim and Anniko 1985, Nishida *et al.* 1998). The kinocilium then migrates to the future vertex of the bundle, and this is closely followed by the growth of the nearby actin protrusions into immature stereocilia (Tilney *et al.* 1992). The staircase structure is then gradually established and any non-stereocilia actin protrusions are gradually lost. The region behind the tallest row of stereocilia is strangely devoid of actin protrusions, and is termed the “bare zone” (Tarchini *et al.* 2013). (B) The physical linkage of the kinocilium and the stereocilia is essential for proper bundle orientation and morphology (Jones *et al.* 2008, May-Simera *et al.* 2015). The mature stereocilin associated horizontal top connectors can also be seen here, alongside the transient ankle links necessary for normal development (Verpy *et al.* 2011, Goodyear *et al.* 2005, Petit and Richardson 2009). This image was redrawn from Schwander *et al.* 2010.

Ionic flux through the MET channel is required for the stereocilia to develop as normal, and loss of the MET current results in deficits in stereocilia morphology (Krey *et al.* 2020) as well as hair cell maturation defects (Marcotti *et al.* 2006). The MET current is first

recordable in basal hair cells at around birth and P1 at the apex in both mice and rats (Kim and Fettiplace 2013, Chen *et al.* 2014, Beurg *et al.* 2016), and reaches a maximal current at around P6 (Corns *et al.* 2016). In contrast, the hair bundles are fully mature at around P16 (Peng *et al.* 2009), and are between 4-8µm tall depending on the position along the organ of Corti. The hair bundles of inner hair cells are longer and thicker than their outer hair cell counterparts (Garfinkle and Saunders 1983). The component of stereocilia height regulation which is of pivotal interest for the following work is the establishment and maintenance of the stereocilia staircase and the molecular cues which underlie the different time points of development and maturation. This is carried out through the differential localisation of actin capping and cross-linking proteins at the tips of the different rows of stereocilia, regulating their height by modulating the balance of actin polymerisation versus depolymerisation (Tilney *et al.* 1992).

Epidermal growth factor receptor kinase substrate 8 (EPS8) is a regulator of the intracellular actin cytoskeleton. EPS8 can affect actin indirectly through the regulation of Rac GTPase activity (Scita *et al.* 1999), or directly bind to f-actin barbed ends to bundle and cap the filaments, stabilising them to promote growth (Croce *et al.* 2004, Hertzog *et al.* 2010). Among other interesting roles, EPS8 has been implicated in the regulation of synaptic spine density and volume, with knock-outs resulting in a high density of immature synapses and learning deficits (Menna *et al.* 2013). Of particular interest to this project, EPS8 is involved in the growth and regulation of actin-based protrusions. In the gut, EPS8 functions alongside the I-BAR (Inverse bin-amphiphysin-Rvs) protein member BAIAP2L1 to regulate the length of the actin-based intestinal microvilli in the epithelial cells (Postema *et al.* 2018). When EPS8 is mutated, the result is decreased fat absorption due to a significant decrease in the length of these microvilli (Tocchetti *et al.* 2010). In the cochlea at E16.5, EPS8 is localised to the tips of all the stereocilia by MYO15a (Zampini *et al.* 2011, Manor *et al.* 2011). At this stage, another pair of proteins important for stereocilia growth regulation, GPSM2 (G-protein signalling modulator 2) and GNAI3 (Inhibitory G protein alpha 3), are strictly localised to the “bare-zone”, a region behind the hair bundle which is devoid of actin protrusions (Tarchini *et al.* 2013, Tadenev *et al.* 2019). At later ages, after around P4, GPSM2-GNAI3 uses the whirlin (WHRN) adapter protein to migrate specifically to the tips of the tallest row of stereocilia (Tadenev *et al.* 2019). This movement induces EPS8 and the short isoform of MYO15a (MYO15aS) to

concentrate to the tips of the tallest row as well and stabilises them there, with only a small amount of EPS8 being detectable in the second row (**Figure 1.7**, Zampini *et al.* 2011, Manor *et al.* 2011, Tadenev *et al.* 2019). GNAi3 can move with WHRN independently of GPSM2 to the stereocilia tips of row 1, but requires the presence of GPSM2 to maintain its localisation at this site (Tadenev *et al.* 2019). Thus, in the mature system, row 1 contains a complex of EPS8-MYO15aS-WHRN-GPSM2-GNAi3, which acts to identify and selectively lengthen row 1 relative to the other rows. Knocking out EPS8 shows effects similar to other proteins in this complex (Belyantseva *et al.* 2003, Mburu *et al.* 2003, Tarchini *et al.* 2016), and results in dramatically shortened stereocilia, and extra rows within the hair bundles (Zampini *et al.* 2011). MET currents can still be elicited from these bundles using a fluid jet, but the resting current of the bundle is entirely lost (Zampini *et al.* 2011). This results in inner hair cells which fail to mature, likely due to the loss of ion influx through the MET channel (Krey *et al.* 2020), and also display immature potassium currents and spiking behaviour (Zampini *et al.* 2011). Interestingly, and for an unknown reason, the basolateral properties of the outer hair cells remained unaffected. EPS8 knock-out mice show a dramatic increase in hearing threshold from the onset of hearing across the entire frequency range (Zampini *et al.* 2011). Thus, it is this EPS8 based complex at row 1 which is important for the initial elongation and definition of row 1, as well as the control of the number of rows. However, there is another complex which is concentrated predominantly in the second row, to define the row apart from row 1.

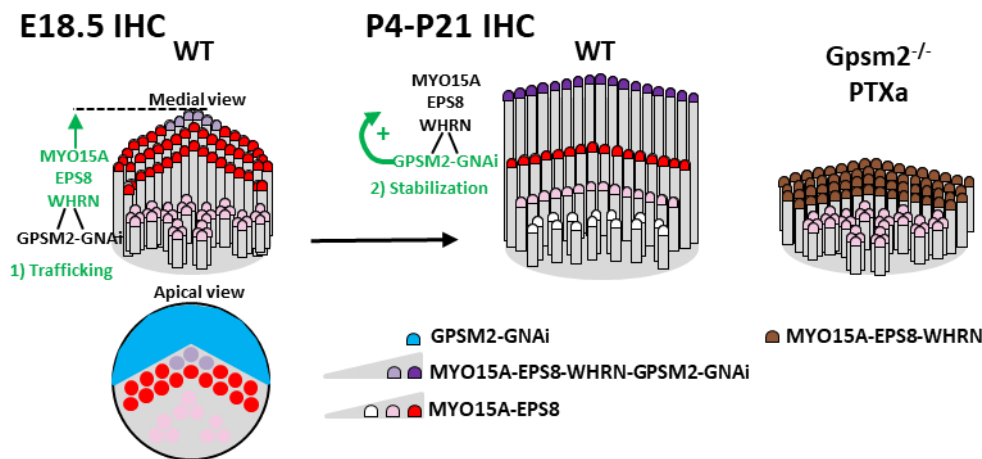


Figure 1.7 – Development and stabilisation of the row 1 complex – In the late embryonic and early post-natal stages of development, EPS8 and MYO15aS is present at the tips of all of the stereocilia, and the GPSM2-GNAi3 complex is only present in the “bare zone” (Zampini *et al.* 2011, Manor *et al.* 2011, Tarchini *et al.* 2013, Tadenev *et al.* 2019). In later stages, the GPSM2-GNAi3 complex moves into the tips of the tallest stereocilia where it stabilises the EPS8-MYO15aS, which is mainly concentrated to the tallest row and the 2nd row in smaller amounts (Tadenev *et al.* 2019, Zampini *et al.* 2011). When GPSM2 is knocked out or GNAi3 is disrupted with pertussis toxin subunit A (PTXa), the result is stereocilia rows of similar length due to the loss of the differential localisation of the row 1 complex (Tadenev *et al.* 2019). This image was redrawn from Tadenev *et al.* 2019.

With a similar two-stage timeline, EPS8 like 2 (EPS8L2) is present at the tips of all the stereocilia rows at P4.5 alongside the long isoform of MYO15a (MYO15aL, Fang *et al.* 2015, Krey *et al.* 2020). EPS8L2 possesses a similar sequence and domain organisation to EPS8 (Offenhäuser *et al.* 2004), and possesses similar barbed end actin capping and cross-linking activity (Avenarius *et al.* 2014). Similar to EPS8, through a mechanism that is not as well understood, EPS8L2 then becomes concentrated at the tips of the shorter rows only (Furness *et al.* 2013) at approximately P11.5. After this time point, the EPS8L2-MYO15aL complex recruits CAPZB (Avenarius *et al.* 2017), TWF2 (Peng *et al.* 2009) and gelsolin (Mburu *et al.* 2010) to the tips of these shorter stereocilia. This complex then inhibits actin polymerisation via their actin capping activity, shifting the equilibrium of polymerisation

to depolymerisation which results in their rows being shorter than row 1 (Peng *et al.* 2009, Mburu *et al.* 2010). Knocking out EPS8L2, a core component of this row 2 and 3 complex, results in a milder phenotype than that seen in the EPS8 knock-out (Furness *et al.* 2013, Zampini *et al.* 2011). MET currents with normal properties can be obtained from the EPS8L2 knock-outs at P8, with no apparent effect on the resting current (Furness *et al.* 2013). However, knock-out mice show progressive hearing loss, particularly at the high frequencies, detectable from around 2 months of age. Scanning electron microscopy revealed that the shortest row of stereocilia begins to show signs of degeneration at the age of 1 month, becoming progressively worse. The third row is almost entirely lost at 8 months of age, and the shorter rows of stereocilia generally become thinner relative to row 1, which appears unaffected (Furness *et al.* 2013). Thus, the complex present in row 1 is required for the establishment of the mature staircase structure, and the complex present in the subsequent rows is required for maintenance of the shorter stereocilia into adulthood.

As mentioned previously, the MET current is required for proper maturation of the hair cells and mutations such as the EPS8 knock-out, which affects the resting current, results in hair cell maturation defects (Marcotti *et al.* 2006, Zampini *et al.* 2011). However, the resting current is also required, through a currently unknown mechanism, to maintain the differential localisation of these actin capping and bundling proteins. When the resting current was entirely removed, by knocking out the MET channel components TMC1 and 2, the differential localisation of EPS8 and EPS8L2 was lost (Krey *et al.* 2020). The two actin capping proteins, and their associated MYO15a long/short isoform, remained at the tips of all the stereocilia rows. Thus, the bundle effectively remained in the early post-natal stage of stereocilia development. The later stage proteins CAPZB, TWF2, GPSM2 and GNAi3 all entirely failed to accumulate to any of the stereocilia tips. The resulting morphology was a reduced height difference between row 1 and 2, as well as a thicker row 3 and a reduced uniformity of stereocilia height even within rows (Krey *et al.* 2020). This indicates how much is still left to be done within the field; to understand what links ionic movement through the MET channel and the differential localisation of these actin effector proteins. Also, the exact mechanisms by which these proteins are so specifically targeted to each row is still poorly understood, and there are likely a plethora of proteins involved that the field is still unaware of. Without a detailed understanding as to how the system develops and works under normal physiological scenarios, we have no hope in the development of potential therapeutics.

1.3 – Ribbon synapses

1.3.1 – Structure and function of ribbon synapses in the cochlea

Ribbon synapses are a specialised form of synapses found within hair cells of the cochlear and vestibular system, photoreceptors and bipolar cells of the retina, and pinealocytes within the pineal gland. One common property of some of these primary sensory cells, particularly hair cells and retinal photoreceptors, is the ability to respond to stimuli with a graded change in membrane potential rather than the action potential, which permits a greater bandwidth (Baden *et al.* 2013, Jarsky *et al.* 2011, Oesch and Diamond 2011, Rutherford *et al.* 2016, Simmons and Van Steveninck 2005). Ribbon synapses allow for this graded information to be carried to nerve fibres, by providing release with a millisecond time frame (Nouvian *et al.* 2006) that can be sustained for an extended period of time (Singer 2007, Thoreson 2007). In the cochlea, this rapid release allows hair cell afferent fibres to “phase lock” to incoming sine waves (Palmer and Russell 1986), meaning the fire rate within the fibres corresponds to the pattern of the sine wave. This permits for sound localisation by comparison of the incoming waveforms between the two ears, for sounds with frequencies below a few kHz only (Rayleigh 1907, Palmer and Russell 1986, Goldberg 1990). At higher frequencies this phase-locking is not possible, and hair cells instead respond with sustained graded changes in membrane potential in an attempt to better reflect the sound intensity information for sound localisation (Palmer and Russell 1986). The exquisitely fast release by ribbon synapses also allows for sound localisation by detecting which cochlea responded to the stimulus first (Hudspeth 2000, Fuchs 2005, Moser *et al.* 2006) as well as through sine wave comparison and intensity differences. Other organ systems do not benefit as greatly from the quick transmission permitted by ribbon synapses. For example, within the retina a 1ms flash of light results in an 80ms hyperpolarisation in cone photoreceptors, and thus the ribbons do not assist particularly in speeding up the kinetics in this system, but rather utilise their sustainable release (Cao *et al.* 2014, Pahlberg *et al.* 2017, Schneeweis and Schnapf 1995).

Within the mature cochlea, the ribbon synapse itself is an electron dense structure (Smith and Sjöstrand 1961) with an oval pre-synaptic body decorated with 20-60 vesicles of neurotransmitter (**Figure 1.8**, Sobkowicz *et al.* 1982, Jean *et al.* 2018). At the base of the oval body, at the site of synaptic release also known as the active zone (AZ), 5-30 vesicles reside proximal to the membrane and primed for vesicular fusion (Jean *et al.* 2018, Jung *et*

al. 2015a, Kroll *et al.* 2019, Wong *et al.* 2014). Of these membrane proximal vesicles, a proportion are tethered to the AZ similar to the tethering that occurs at a conventional synapse, with between one and three filaments (Jung *et al.* 2015a, Vogl *et al.* 2015, Chakrabarti *et al.* 2018). This population of membrane proximal vesicles likely corresponds to the readily releasable pool (RRP) within the inner hair cells (von Gersdorff *et al.* 1996). The RRP is responsible for the fast component of exocytosis, which shows an exponential decrease with prolonged stimuli (Liley and North 1953) with time constants as fast as 0.5ms, which reflects the high probability of release for these vesicles (Mennerick and Matthews 1996, Grabner *et al.* 2016). The concentration of these primed vesicles of the RRP decreases further away from the ribbon, which suggests a role for the structure in efficiently priming vesicles for quick and sustainable release (Frank *et al.* 2010, Chakrabarti *et al.* 2018). Vesicles are captured from the cytosol, and move down the ribbon towards the AZ where they are eventually tethered to the membrane ready for exocytosis (Chakrabarti *et al.* 2018, Cooper *et al.* 2012, Jung *et al.* 2015a, Zampighi *et al.* 2011). The rate at which the ribbon can replenish the vesicles at the AZ dictates the sustainable release portion of exocytosis following RRP depletion (Moser and Beutner 2000, Spassova *et al.* 2004), which is mediated by the secondary releasable pool (SRP) of vesicles. Also, the replenishment of the RRP of membrane proximal vesicles and SRP of ribbon associated vesicles has been shown to be somewhat dependent on calcium. Calcium speeds up the rate of RRP replenishment (Babai *et al.* 2010) and the replenishment of the SRP is currently believed to be dependent on intracellular calcium (Schnee *et al.* 2011).

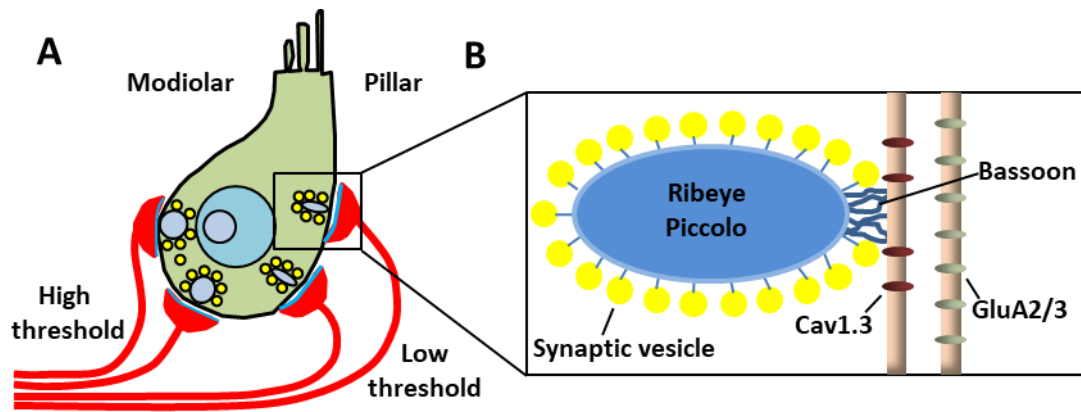


Figure 1.8 – Gross morphology of the synaptic ribbon – (A) The extensive innervation of IHCs by afferent fibres, with a morphological gradient depending on the position within the hair cell. (B) The gross morphology of the synaptic ribbon, which is an electron dense structure tethered to the membrane and decorated extensively with vesicles of neurotransmitter. The ribbon itself is within close proximity of $Ca_v1.3$ channels to permit the efficient coupling of calcium entry and neurotransmitter release (Neher 1998). This image was redrawn from Fettiplace 2017.

Inner hair cells are innervated extensively by afferent fibres, which reflect their role as the cells responsible for all conscious sound perception, with each fibre possessing its own characteristic firing threshold (Lieberman and Kiang 1978). The activity in each unbranched afferent fibre (Spoendlin 1975) is driven by a single AZ (Glowatzki and Fuchs 2002), with the nerve fibre terminal possessing a ring of concentrated AMPA receptors in order to form a highly sensitive glutamate detector (Chapochnikov *et al.* 2014, Matsubara *et al.* 1996, Choquet and Triller 2003). During prolonged stimulation, the afferent fibres show a spike rate adaptation which is currently thought to be primarily based on the depletion of the RRP (Spassova *et al.* 2004). This spike rate adaptation is thought to further support sound encoding over a wide dynamic range, by preventing spike rate saturation and allowing the fibre to transmit an increase in signal intensity (Wen *et al.* 2012).

The trigger for vesicular release at the ribbon synapse is calcium influx through the $Ca_v1.3$ voltage-dependent calcium channels, which are fast activating and show minimal inactivation (Koschak *et al.* 2001, Platzter *et al.* 2000, Schnee and Ricci 2003). These

channels, which open near the resting membrane potential of hair cells (Zampini *et al.* 2014), are clustered within close proximity to the synaptic ribbon (Wong *et al.* 2014). The close proximity between the calcium channels and the primed vesicles, with a distance of around 30nm (Neher 1998), means that entry of calcium through a single channel can initiate the fusion of a synaptic vesicle (Kim *et al.* 2013). This system is known as a calcium nano-domain, and allows for the cells to better transfer the graded sound information to the afferent fibres (Graydon *et al.* 2011). Nano-domains are naturally noisier than a more cell-wide response, as the random opening of a single channel can cause vesicular fusion in the absence of sound (Moser *et al.* 2020). However, the calcium entry with such a close proximity means that the calcium sensor of the synapse is quickly saturated regardless of stimulus intensity, which reduces stimulus based differences in release kinetics (Moser *et al.* 2020). The prevalence of calcium nano-domain control is not uniform across the tonotopic axis however, and is more utilised by the lower frequency cells which can phase lock to incoming sound (Johnson *et al.* 2017). Basal hair cells favour micro-domain control of synaptic release, in which multiple channels must open in order to release vesicles positioned slightly further away from the channel cluster (Kim *et al.* 2013). This difference in the calcium properties is reflected in the relationship between exocytosis and calcium influx in the hair cells. Low frequency hair cells show a non-linear relationship between calcium influx and exocytosis, with a power of 2-3, whereas hair cells at the base show a linear relationship between the two (Johnson *et al.* 2005, Schnee *et al.* 2005, Keen and Hudspeth 2006). These properties reflect how the cells respond to the incoming sound stimuli. The basal cells cannot phase lock, and thus need to be able to better transmit intensity information with small graded changes in membrane potential, and better carry this to the afferent fibres with a linear calcium induced exocytosis relationship (Johnson *et al.* 2008, Johnson *et al.* 2009). The cause of this tonotopic difference in calcium kinetics is currently unknown.

The number and morphology of ribbon synapses themselves also varies tonotopically, and hair cells within the middle region of the cochlear spiral possess the greatest number of ribbon synapses and afferent connections (Meyer and Moser 2010). This region is the most sensitive to sound, but how this innervation pattern is established and maintained is unknown. Ribbon synapses at the base of the cochlea are also more ellipsoid than those at the apex (Johnson *et al.* 2008), which may correspond to their differences in membrane potential response upon sound stimulation. Finally, ribbon synapses also vary in structure

based on their subcellular localisation within the hair cell. At the modiolar side the ribbon synapses possess larger AZs with larger ribbons and Ca_v1.3 channel clusters than those at the pillar side (Lieberman *et al.* 2011, Meyer *et al.* 2009). This corresponds to the characteristic differences in the threshold properties of the different afferent fibres (Merchan-Perez and Lieberman 1996). Afferent fibres at the pillar side have a higher spontaneous rate and a lower firing threshold than those at the modiolar side (Lieberman 1982). This likely plays a major part in the hair cells ability to translate a wide dynamic range, as the modiolar fibres will saturate at higher volumes, and better convey the intensity information to the brain.

1.3.2 – Ribbon synapse molecular composition

Ribbon synapses vary greatly in molecular composition compared to conventional synapses (Pang and Südhof 2010), and one protein specific to ribbon synapses is RIBEYE (Khimich *et al.* 2005, Schmitz *et al.* 2000). RIBEYE is transcribed from the same gene as the ubiquitously expressed co-repressor CtBP2, but due to its unique promoter RIBEYE is expressed only in ribbon synapses (Schmitz *et al.* 2000). Through the A domain, RIBEYE is able to interact with three other RIBEYE molecules (Magupalli *et al.* 2008), which enables the protein to form the pre-synaptic scaffold for the ribbon synapse machinery. When RIBEYE is knocked out, the result is a complete loss of pre-synaptic ribbon in the mouse, with the rest of the synaptic machinery remaining intact (Becker *et al.* 2018). The auditory phenotype in this mouse model was relatively minor, with a small decrease in fast and sustained release (Maxeiner *et al.* 2016), due to the presence of apparent compensatory mechanisms. The knock-out resulted in the appearance of multiple AZs per afferent fibre with larger associated post-synaptic densities, and also resulted in a disorganisation of the tightly controlled Ca_v1.3 clusters (Jean *et al.* 2018). This resulted in calcium currents of normal amplitude, but a decrease in exocytosis upon weak depolarising stimuli, which suggests that RIBEYE is important for the recruitment/stabilisation of calcium channels to the pre-synaptic machinery (Becker *et al.* 2018, Jean *et al.* 2018). As such, the knock-out resulted in a decrease in the peak and sustained firing rate in the afferent fibres, which caused the apparent threshold shift seen in the mutant (Becker *et al.* 2018). In zebrafish, knocking down both RIBEYE genes they possess results in a complete loss of the Ca_v1.3 clusters (Sheets *et al.* 2011), and double knock-out results in ribbon with a decreased

electron density that appear “ghost” like (Lv *et al.* 2016). These “ghost” ribbons could however still possess tethered vesicles, which highlights the difference between the mouse and zebrafish models (Lv *et al.* 2016). Finally, overexpression of RIBEYE in neuromast cells resulted in the generation of numerous large ribbon structures (Sheets *et al.* 2011). Taken together this data suggests that RIBEYE is the major scaffolding molecule of the mammalian ribbon synapse.

Bassoon and piccolo are large scaffolding proteins that are also present at the ribbon synapse (Dick *et al.* 2003, Regus-Leidig *et al.* 2013) and structurally quite similar to one another (Fenster *et al.* 2000). Bassoon and piccolo can both bind directly to RIBEYE (Ivanova *et al.* 2015), and bassoon knock-out results in ribbon detachment from the AZ, which suggests a primary function for bassoon is to anchor the pre-synaptic ribbon in place (Dick *et al.* 2003). The mutation also results in Ca_v1.3 clustering deficits and errors in pre and post synapse alignment, which causes exocytosis and sound encoding deficits in the inner hair cells (Buran *et al.* 2010, Frank *et al.* 2010). In contrast, knocking out piccolo, and as a result its short splice isoform piccolino, results in deficits in the ultrastructural development of the pre-synaptic ribbon in the retina (Regus-Leidig *et al.* 2014, Regus-Leidig *et al.* 2013). From a functional perspective, the knock-out showed a very mild phenotype with only slight delays in the b-wave of an electroretinogram (ERG) (Müller *et al.* 2019). Thus the differences in phenotype severity between the two knock-out models suggests that bassoon is of greater importance to the ribbon synapse structure and function than piccolo.

Another class of proteins, known as Rab3-interacting molecules (RIMs) are known to be present within the ribbon synapses of the cochlea, particularly RIM2 α , RIM2 β and RIM3 γ (Jung *et al.* 2015b). Deficiency of RIM2 α resulted in a reduction in the cluster of Ca_v1.3 calcium channels and an overall decrease in calcium influx, and therefore deficits in sound encoding, but no loss of nano-domain controlled exocytosis (Jung *et al.* 2015b). Loss of RIM2 β seemed to slightly worsen the phenotype, and loss of RIM3 γ had no effect on the calcium channels or the ABR responses. RIM2 α is known to interact with Ca_v1.3 directly through an interaction with the proteins C-terminus (Picher *et al.* 2017), which, when taken together with the knock-out data, suggests that the RIM proteins serve to facilitate normal calcium channel clustering to the synapse. This function appears to be shared by RIM-binding proteins (RIM-BP) present at the ribbon synapse of inner hair cells. It was shown through a similar knock-out study that loss of RIM-BP2 similarly promotes

clustering of the calcium channel to the synapse as well as regulating replenishment of the RRP (Acuna *et al.* 2015, Krinner *et al.* 2017).

Cochlear ribbon synapses lack the proteins classically associated with vesicle fusion and exocytosis at the conventional synapse, such as the neuronal SNAREs (Nouvian *et al.* 2011), synaptotagmins calcium sensors 1-3 (Südhof 2002, Beurg *et al.* 2010b, Reisinger *et al.* 2011), synaptophysins and synapsins (Safieddine and Wenthold 1999). In the absence of the majority of the synaptotagmins, the protein currently believed to be responsible for detecting intracellular calcium is otoferlin (Roux *et al.* 2006). Otoferlin, which is encoded by the OTOF deafness gene (Yasunaga *et al.* 1999), is capable of binding to calcium directly, and thus acting as the synaptic calcium sensor, through its 6 C₂ domains (Johnson and Chapman 2010, Roux *et al.* 2006, Ramakrishnan *et al.* 2009). Removal of otoferlin results in the near complete loss of exocytosis at cochlear hair cell ribbon synapses and severe deafness, which can in some cases be temperature dependent (Strenzke *et al.* 2016, Pangršič *et al.* 2012, Santarelli *et al.* 2015). Otoferlin localises to the membrane of hair cells, and is particularly focused at the AZ of the ribbon, where it has also been shown to assist in vesicular resupply (Strenzke *et al.* 2016, Pangršič *et al.* 2012, Santarelli *et al.* 2015).

As mentioned earlier, ribbon synapses do not possess synaptotagmins 1-3 calcium sensors, but synaptotagmin 4 (SYT4) is expressed in the base of the cochlear spiral and not the low frequency apex (Johnson *et al.* 2010). As stated previously, the higher frequency base of the cochlea shows a different dependency on calcium for exocytosis, showing a more linear relationship than the apex to reflect the different in stimulus response (Schnee *et al.* 2005, Keen and Hudspeth 2006). When SYT4 was knocked out, the result was a loss of this calcium linearization at the base of the cochlea (Johnson *et al.* 2010). SYT4 is unable to bind directly to calcium itself (Südhof 2002), but is known to be able to form hetero-oligomers with other synaptotagmins (Chapman *et al.* 1998). This suggests that SYT4 may be regulating synaptic responses to calcium by forming hetero-oligomers in the hair cells, possibly even with otoferlin (Marcotti 2012), to linearize the calcium response in the base relative to the apex. Interestingly, another factor known to affect this basal linearization is the hair cells innate activity. Prior to the onset of hearing, inner hair cells fire spontaneous calcium-induced action potentials, the shape of which is modulated by the SK2 potassium channel (Johnson *et al.* 2007). Knocking out this channel causes broader spikes and sustained depolarisation, the result of which is a loss of calcium linearization (Johnson *et*

al. 2007). This suggests the electrical activity of the cells is partly driving the maturation of the synapses, possibly by permitting and modulating calcium entry into the cell. Calcium is known to modulate ribbon size (Sheets *et al.* 2012), and loss of intracellular calcium results in complete ribbon disassembly (Spiwox-Becker *et al.* 2004). How this intracellular calcium modulates the synaptic ribbon and the calcium sensing machinery is unknown.

1.3.3 – Ribbon synapse development and maturation

Ribbon synapse development begins with the formation of afferent fibre contacts on the inner hair cells at around embryonic day 16 (E16), which is then followed by the appearance of floating and membrane anchored ribbons at E18 (Michanski *et al.* 2019). The ribbons that are anchored to the membrane show multiple anchors to the membrane, which later matures into a single anchor point (Michanski *et al.* 2019). Floating ribbons are still prevalent in the first post-natal week, rarely in post-hearing animals, and likely correspond to ribbon precursors (Sobkowicz *et al.* 1986). These precursors show a close proximity to microtubules, and appear to interact with the plus-end motor protein KIF1a, which may be involved in shuttling these ribbons to the prospective AZ (Michanski *et al.* 2019). At this stage, the number of vesicles associated with the immature ribbon steadily begins to increase, from ~4-5 at E18 up to the mature number of 30-40 at P48 (Michanski *et al.* 2019). This reflects the size change in the ribbons themselves, which grow steadily until P12 (Michanski *et al.* 2019). At E18, dense core vesicles also appear (Michanski *et al.* 2019), which have been proposed to modulate synapses by carrying neurotrophins (Fariñas *et al.* 2001, Wu *et al.* 2004, Kersigo and Fritzsche 2015) and transporting synaptic proteins such as bassoon and piccolo to the future AZ (Shapira *et al.* 2003, Zhai *et al.* 2001). Interestingly, at birth the differential distribution of ribbons with different morphology, in which the modiolar side of the cell contains larger ribbons with a higher chance of multi-ribbon synapses than the pillar side (Merchan-Perez and Liberman 1996, Liberman *et al.* 2011), is already present (Liberman and Liberman 2016). This pattern later inverts around the onset of hearing, and then reverts to the mature morphology after P21, with no effect on the post-synaptic morphology (Liberman and Liberman 2016). This suggests the process is entirely pre-synaptic in nature, but the exact mechanisms underlying this peculiar shift, and even the purpose of the pattern inversion, is unknown.

During the first post-natal week the ribbon count per AZ is steadily decreased to ~1, with the exception being the multi-ribbons of the modiolar side, in order to achieve the mature ribbon number (**Figure 1.9**, Wong *et al.* 2014, Huang *et al.* 2012, Merchan-Perez and Liberman 1996, Sobkowicz *et al.* 1982). The mechanism by which the number of ribbons is decreased is currently under debate, but one interesting theory is that the multiple ribbons of an immature AZ fuse to create a single ribbon of a mature morphology (Michanski *et al.* 2019). Consistent with this idea, the volume of the ribbon in the mature animal roughly corresponded to the volume of the precursors seen in embryonic stages, but much work is still to be done to validate this hypothesis (Michanski *et al.* 2019). The post-synapse also matures during this time, and in the period of P6-P20 several immature post-synaptic densities fuse to form the mature machinery seen in the adult AZ (Wong *et al.* 2014, Michanski *et al.* 2019).

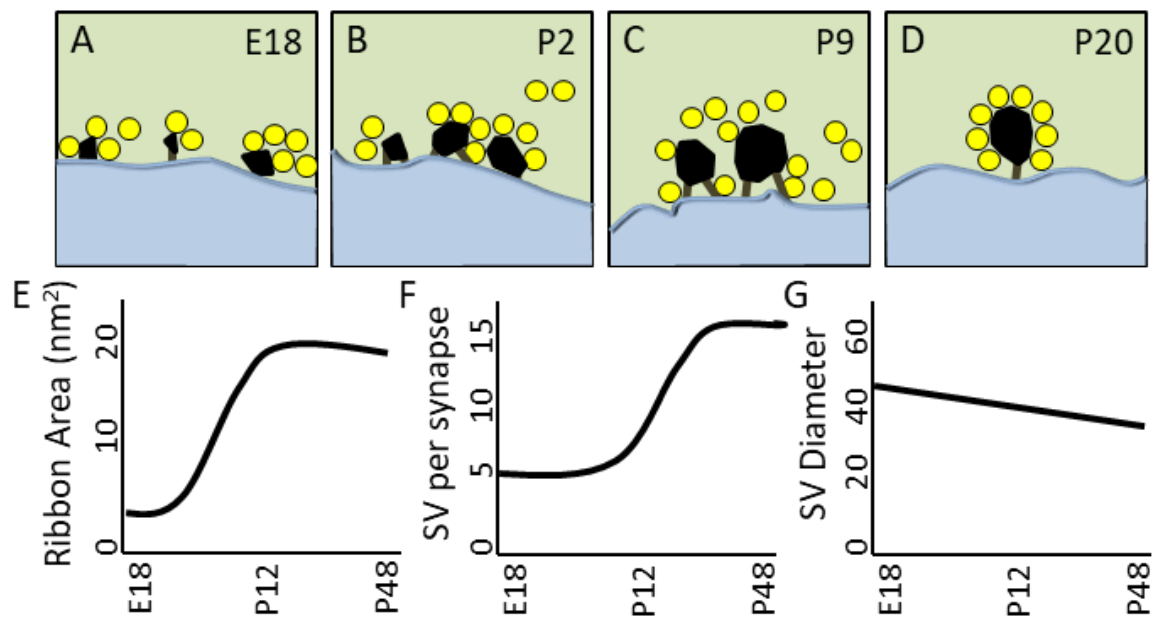


Figure 1.9 – The morphological development of synaptic ribbons throughout maturation – (A-D) Between the late embryonic stages and the end of the third post-natal week the number of ribbons per active zone steadily decreases, likely due to the fusion of multiple immature ribbons (Michanski *et al.* 2019). Also, the size of the ribbons gradually increases (E) alongside the associated number of synaptic vesicles (F). The number of tethering filaments of each ribbon also steadily decreases (C) until a single filament (D) anchors each ribbon by P20. The size of the ribbon associated vesicles also decreases during maturation (G) and the occurrence of floating ribbon precursors also decreases, to the point where they are rarely seen in the mature animal. This figure was redrawn from Michanski *et al.* 2019.

Currently, the little that is known about the mechanism behind the development and maintenance of the afferent connection with the inner hair cell is based on observational knock-out studies. For example, knocking out neuronal cell adhesion molecule (NrCAM), a member of the immunoglobulin family of adhesion molecules, results in an increased number of immature synapses in P10 mice (Harley *et al.* 2018). However, mice at later stages show no visible defects in ABR experiments, indicating some form of recovery (Harley *et al.* 2018). Due to the homophillic interactions between NrCAM molecules, the current hypothesis is that the interaction between NrCAM molecules across the synaptic cleft modulates synapse number, pruning or maturation through a currently unknown

mechanism (Mauro *et al.* 1992, Harley *et al.* 2018). Another molecule of the immunoglobulin class of adhesion molecules has been shown to be somewhat involved in ribbon synapse formation. Neuroplastin-65 was shown to be expressed within the basolateral membrane of hair cells and within the cuticular plate (Carrott *et al.* 2016). Loss of neuroplastin-65 resulted in misalignment of the pre and post synapse, with no effect on the final number of synapses, which suggests a possible role in the refinement or maintenance of the afferent contact (Carrott *et al.* 2016). The resulting phenotype was elevated hearing threshold in ABR experiments, caused by an apparent disruption of the SRP.

Currently, our understanding of the process of ribbon synapse formation and maintenance is entirely dependent on targeted knock-out studies analysing ribbon phenotypes. This type of mutation driven work needs to be continued until a more detailed model of development and maintenance can be constructed. When we have this level of understanding, we can then begin to focus efforts on the development of therapeutic strategies which may be able to protect ribbon synapses or restore those that have failed to properly develop.

1.4 – The electrophysiological maturation of hair cells and their innervation

1.4.1 – Innervation of cochlear hair cells following birth

As previously mentioned, inner hair cells are extensively innervated with afferent fibres. In fact, 95% of the spiral ganglion neurons afferents (SGNs) that enter the cochlea are responsible for innervating an inner hair cell with a single unbranched and myelinated projection, these fibres are known as type I fibres (Keithley and Fieldman 1982, Burda and Branis 1988, Pujol *et al.* 1998). Conversely, the remaining 5% are unmyelinated type II fibres, which make contact with between 3-10 outer hair cells each in mice (Berglund and Ryugo 1987). The difference in innervation reflects the functionality of the cell types. Inner hair cells are responsible for all conscious sound perception, and as such are extensively innervated with fast-transmitting myelinated fibres. Whereas outer hair cells do not transmit conscious sound, and while the role of the type II fibres is still under debate, they are currently believed to be responsible for cochlear nociception (Liu *et al.* 2015) or involved in fine tuning the output of the cochlear amplifier (Jagger and Housley 2003, Ashmore *et al.* 2010). This fine segregation of type I fibres to the inner hair cells and

type II to the outer hair cells is not a single stage process, and undergoes a number of developmental stages before reaching maturity.

At birth, inner and outer hair cells are innervated by both types of afferent fibre, and show the specificity of the adult system at the end of the first post-natal week (Perkins and Morest 1975, Echteler 1992, Simmons 1994, Huang *et al.* 2007). At this stage, type I fibres are bifurcated, and both types synapse with an inner hair cell as well as extending into the outer hair cell rows and forming synapses there (Huang *et al.* 2007). Type II fibres, upon reaching the rows of outer hair cells, turn and begin to grow basally to further increase the number of outer hair cell contacts (Echteler 1992). At this point the type II fibres are in competition with the type I fibres for contact with the outer hair cells, and type II fibres that fail to form lasting connections at this stage undergo apoptosis (Reuda *et al.* 1987, Echteler and Nofsinger 2000, Barclay *et al.* 2011). The innervation by both types of fibres at this stage results in 40-50 ribbon synapse puncta on each outer hair cell and 50-60 on each inner hair cell (Huang *et al.* 2012). Interestingly, type I fibres show very little apoptosis at this early stage, which perhaps reflects the difference in the number of contacts the fibre must make before being “worth” keeping, which is dependent on the type of fibre (Barclay *et al.* 2011). Type II fibres then lose their synaptic contacts with the inner hair cells, and continue to project basally (Echteler 1992). This loss of contact, paired with the fusion of ribbons mentioned earlier (Michanski *et al.* 2019), results in a gradual decrease in ribbon synapse puncta on each hair cell, reaching approximately 20 synapses per cell depending on the tonotopic position (Liberman *et al.* 1990). The neurites of the type I fibres extending into the outer hair cell rows then retract, and maintain a single connection with a single inner hair cell in the mature configuration (**Figure 1.10**, Huang *et al.* 2007, Huang *et al.* 2012). This results in a drop in the number of ribbon synapse puncta on the outer hair cells from 40-50 to less than 10 in the adult cochlea (Huang *et al.* 2012). At this stage the fibres and their contacts show the classical specific innervation seen in the mature system.

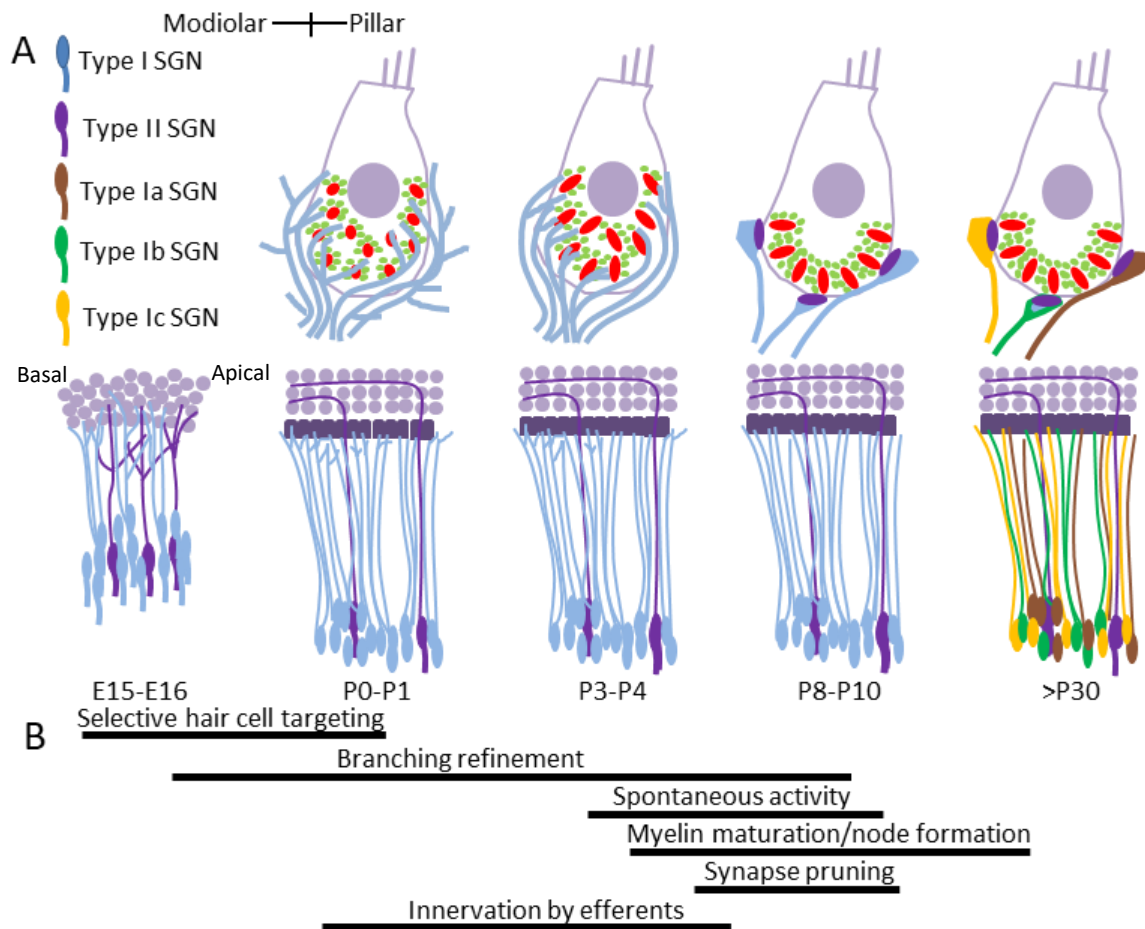


Figure 1.10 – The development of hair cell innervation throughout the first two post-natal weeks – (A) Early in the first post-natal week the type I fibres make branched connections with the inner hair cells and the type II fibres have extended into the outer hair cells, where they turn basally and extend to contact more cells. By P10 the synapses of the type I fibres refine to create a single pre-synaptic bouton with the inner hair cells, creating the distinct pillar and modiolar populations with distinct synapses and firing thresholds (Liberman 1982). (B) Timeline for the maturation of hair cell afferent and efferent innervation. This figure was redrawn from Coate *et al.* 2019.

The mature cochlea also possesses inhibitory efferent inputs. Fibres of the lateral olivocochlear innervate the boutons of the type I fibres, and fibres of the medial olivocochlear project onto the cell bodies of the outer hair cell directly (Warr and Guinan 1979). As with the afferent system, the exclusivity of the fibres is not established at earlier stages. Fibres of the medial olivocochlear contact inner hair cell bodies for a short time,

before projecting beyond the cells and making contact with the outer hair cells specifically by around P8 (Simmons *et al.* 1996, Glowatzki and Fuchs 2000, Roux *et al.* 2011). At this point, inner hair cells are contacted by approximately 16 efferent fibres from the lateral olivocochlear, and these fibres contact the cell body directly (Glowatzki and Fuchs 2000). This connection is later refined such that the fibre contacts the afferent fibre bouton only (Darrow *et al.* 2006). The exact function of the efferent input to the cochlea is still under debate, but the current theory is that the cholinergic inhibitory inputs hyperpolarise the outer hair cells to dampen the cochlear amplifier and ameliorate noise induced cochlea damage. Acetylcholine release results in calcium entry through the $\alpha 9\alpha 10$ -acetylcholine receptors, which in turn open the calcium activated SK2 channels on the hair cells and results in hyperpolarisation via an outward potassium current (Elgoyhen *et al.* 1994, Elgoyhen *et al.* 2001, Nenov *et al.* 1996). The function of the efferent contact on the afferent fibres is also unclear, but it is thought to assist in sound localisation or perhaps protection of the fibres from excitotoxic damage (Darrow *et al.* 2006).

1.4.2 – Electrophysiological maturation of inner and outer hair cells in mice

Alongside the development of the mature innervation, the hair cells themselves also undergo drastic biophysical maturation over the course of the first few post-natal weeks. Outer hair cells are the first to reach maturity, defined as the point when they show electro-motility, at around P8 (Marcotti *et al.* 1999, Abe *et al.* 2007), followed by inner hair cells which are mature at P12 (Kros *et al.* 1998), which corresponds to the onset of hearing in mice. Notably, while the outer hair cells possess electro-motility at P8, the expression of prestin continues to rise until around P10 (Belyantseva *et al.* 2000). Prior to the onset of maturation, inner and outer hair cells have a resting membrane potential of around -60 mV and fire spontaneous calcium based action potentials, which is thought to be crucial in the development of the cochlea and downstream auditory pathway (Kros *et al.* 1998, Ceriani *et al.* 2019). Conversely, mature cells possess a resting membrane potential of -80mV *in vitro*, show no spiking activity and instead respond to ionic influx with graded changes in membrane potential (Marcotti and Kros 1999, Kros *et al.* 1998). This drastic change obviously involves a large shift in the channel repertoire of the cells, which will be discussed separately based on the ion carrying the current.

Immature hair cells possess three different potassium currents. One is the delayed rectifier known as $I_{K,DR}$, which activates upon cell depolarisation at about -60 mV, and the second is the inward rectifier known as I_{K1} which activates upon hyperpolarisation below -80 mV (Marcotti *et al.* 1999, Marcotti *et al.* 2003a). The identity of the channels responsible for these two currents is still under debate, but their naming is based on the shapes created in classical voltage clamp traces. The third potassium current present in immature inner hair cells is carried by the SK2 channel mentioned earlier, which is activated indirectly following acetylcholine release from the inhibitory efferent fibres that directly contact the cell (**Figure 1.11**, Marcotti *et al.* 2004a). Hair cells retain $I_{K,DR}$ into adulthood, and outer hair cells alone express I_{SK2} at adult stages, but lose the I_{K1} current (Marcotti *et al.* 1999, Marcotti *et al.* 2003a). This is replaced with another current termed $I_{K,n}$, which is activated positive to around -120 mV and almost entirely open at -60 mV, thus this current is of particular importance for establishing the resting membrane potential (Housley and Ashmore 1992, Kubisch *et al.* 1999, Marcotti and Kros 1999, Marcotti *et al.* 2003a). The appearance of $I_{K,n}$, which is carried by KCNQ4 channels (Kubisch *et al.* 1999), also prevents any future spiking activity by lowering the resting membrane potential towards the mature value of -80 mV (Marcotti and Kros 1999, Marcotti *et al.* 2003a). Mature inner

hair cells, but not outer hair cells, also express a fast-activating calcium and voltage activated current known as $I_{K,f}$, which is carried by the BK potassium channel (Kros *et al.* 1998, Marcotti *et al.* 2004b). This fast BK current allows for the swift repolarisation of the cell following mechanotransduction, which is necessary for the cell to properly reflect the sinusoidal stimulation in the membrane potential of the bundle.

Hair cells possess a calcium current (I_{Ca}) both before and after maturation, which is carried by the $Ca_v1.3$ channel discussed earlier. This current is activated close to the resting membrane potential at around -70 mV, and is crucial for the generation of the spontaneous spiking activity, which is characteristic of the immature hair cells and for exocytosis at the synaptic ribbon (Marcotti *et al.* 2003b, Brandt *et al.* 2003, Zampini *et al.* 2010, Platzner *et al.* 2000). The expression of these channels does not change, but rather it is their close association and co-localisation with the synaptic ribbon that is developed and refined throughout hair cell maturation (Frank *et al.* 2010, Wong *et al.* 2014), with the gradual decline of extra-synaptically localised channels.

The final current present in the immature hair cells is the sodium current, possibly carried by the $Na_v1.1/1.6$ voltage gated channels, which open close to the resting membrane potential of the cell, similar to the calcium current, at around -60 mV (Marcotti *et al.* 2003b, Eckrich *et al.* 2012). These channels appear to possess the singular function of modulating the spiking activity seen in the immature cells, and as such the expression of the current is lost in the mature system (**Figure 1.11**, Marcotti *et al.* 2003b).

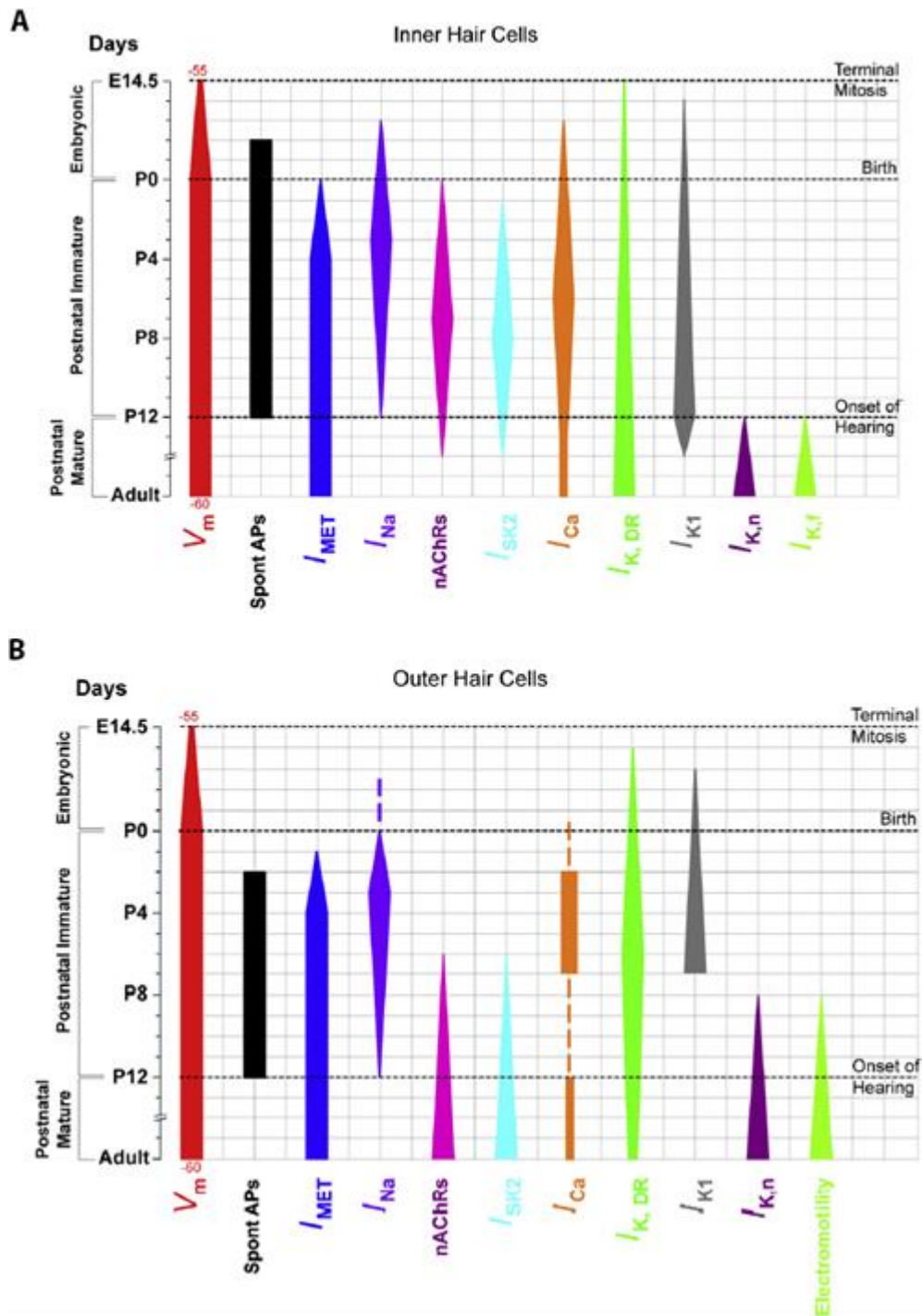


Figure 1.11 – The development of the different currents within both inner and outer hair cells – Following terminal mitosis of the inner and outer hair cells, both populations go through drastic changes in their current repertoire, the size of which is indicated by the width of the vertical bars shown above (A and B). Both cells transiently express sodium currents that facilitate the action potentials seen before the onset of hearing, and both gain and lose the expression of the negatively activating

$I_{K,1}$. Some currents, such as $I_{K,DR}$ and I_{Ca} appear early and persist until the onset of hearing. This image was taken from Corns *et al.* 2014.

1.4.3 – The use of mice in mammalian hearing research

The vast majority of our understanding of the auditory system has been obtained with the use of the mouse as a model organism, and mice are still the organism of choice in the field of hearing research. One of the most significant aspects of the mouse model is the fact that the pups are born deaf, and the cochlea continues to develop after birth until around three weeks of age, though mice are able to hear at around P12 (Marcotti 2012, Johnson *et al.* 2012). As such, this permits experiments such as electrophysiology on pre-hearing immature hair cells and supporting cells without the need for working with embryonic animals. Another crucial aspect of a model is the similarity to humans, and indeed 99% of genes in mice have a matching human orthologue (Bowl and Dawson 2015). To date, of the >340 genes identified in mice as being important in hearing, approximately a third of these have already been associated with hearing phenotypes in humans, and this proportion is likely to rise as slower work on humans “catches up” (Steel 2014, Ohlemiller 2019). Finally, with a lifespan of around two to three years, the mouse model permits research on the aging mammalian cochlea that can be carried out within a reasonable timeframe.

Despite the remarkable similarity to the human cochlea, there are differences worth considering. For example, mice possess a different range of perceivable frequencies, and can hear between 1 - 100 kHz (Heffner and Heffner 2007) compared to the human range of 20 Hz – 20kHz (Neely 1998). This shift to higher frequencies makes the mechanisms of low frequency sound localisation (<3 kHz), such as afferent fibre phase locking (Section 1.2.1), less utilised in mice. Another significant difference between mice and humans is the non-coding expression regulatory sequences of the genome that show a remarkable divergence in mice relative to humans (Vierstra *et al.* 2014). This can result in differences in protein expression and thus discrepancies between the phenotypes seen in mice versus those seen in humans due to differences in functional redundancy (Hosoya *et al.* 2016).

1.5 – Dystroglycan and the dystrophin glycoprotein complex

1.5.1 – The dystrophin glycoprotein complex and the role it plays at the sarcolemma

Dystroglycan (DG) is a ubiquitously expressed heterodimer, composed of a heavily glycosylated alpha subunit (120-180kDa) and a transmembrane beta subunit (43kDa), linked together by non-covalent interactions (Sciandra *et al.* 2001). The two subunits are encoded by a single gene with two exons and a single intron, and separated with an early proteolytic cleavage in the ER which is thought to be induced through autoproteolysis at the sea urchin, eneterokinase, agrin (SEA) domain (Holt *et al.* 2000, Esapa *et al.* 2003, Akhavan *et al.* 2008). Dystroglycan forms the core component of the dystrophin glycoprotein complex (DGC), which was originally purified from muscle tissue (Ervasti *et al.* 1990). Interestingly, the protein was identified before this in neuronal tissue under the aliases of cranin and LBP120, which were later revealed to be dystroglycan (Smalheiser and Schwartz 1987, Douville *et al.* 1988). The DGC is composed of dystroglycan, sarcospan, sarcoglycans (α , β , γ and δ), syntrophins (α , β 1, β 2, γ 1 and γ 2), dystrobrevin (1-3), and dystrophin (**Figure 1.12**, Ervasti *et al.* 1990, Blake *et al.* 1996). The alpha subunit of dystroglycan (α DG) is heavily modified with both N and O-linked sugar residues, with O-linked modifications being particularly prevalent within the central mucin domain which is flanked by two globular domains in the immature protein (Brancaccio *et al.* 1995). The N-terminal globular domain of the subunit is later cleaved off by furin during the maturation process (Singh *et al.* 2004). The glycosylation of α DG is essential for the binding of the protein to its extracellular matrix binding partners that contain laminin-G domains, which include laminin, agrin, pikachurin, perlecan, neurexins and slits (Sciandra *et al.* 2013, Sato *et al.* 2008, Barresi *et al.* 2006, Ervasti and Campbell 1993, Ibraghimov-Beskrovnaya *et al.* 1992). The affinities of these interactions can be dependent on the presence of calcium, in the case of laminin α 1 (Ervasti and Campbell 1993), or influenced by the extent of the glycosylation of α DG; particularly the length of the matriglycan chains synthesized by LARGE1 (Beltrán *et al.* 2019, Briggs *et al.* 2016, Sciandra *et al.* 2013).

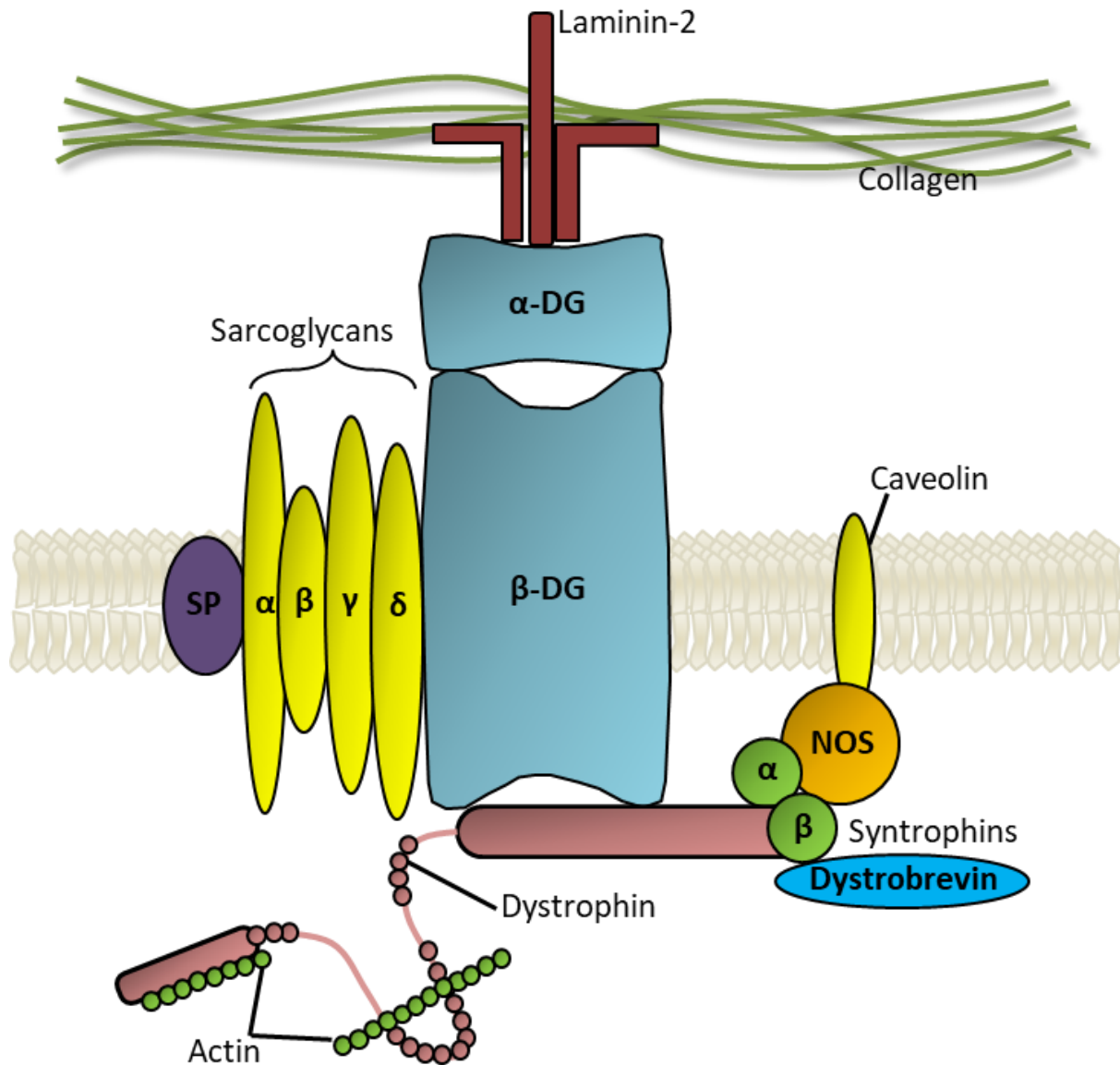


Figure 1.12 – Structure of the dystrophin glycoprotein complex – The extracellular α DG subunit, the transmembrane β DG subunit and dystrophin forms a physical link between the extracellular matrix and the intracellular cytoskeleton. This link allows the sarcolemma to impart tension to the surrounding matrix, and prevents contraction induced muscle damage (Batchelor and Winder 2006). Dystroglycan forms the core subunit of the DGC, and associates with several transmembrane and intracellular accessory proteins. This image was taken from Cossu *et al.* 2004.

The beta subunit of dystroglycan (β DG) can interact with utrophin or dystrophin, the latter of which is a large 427kDa intracellular protein, by binding with the WW domain on dystrophin via the PPxY motif on the intracellular tail of dystroglycan (James *et al.* 2000, Jung *et al.* 1995, Rentschler *et al.* 1999). This WW domain is a motif of around 30 amino acids which contains a conserved pair of tryptophan residues, which is where the designation is derived from, that allows for the binding of proline rich sequences similar to those found in both the PPxY motif and SH3 domains (Sudol 1996). While the WW domain on dystrophin or utrophin is necessary for dystroglycan binding, it is not sufficient, and requires the presence of the EF-hand region on dystrophin to first stabilise the C-terminal tail of dystroglycan and permit the stable binding (Chung *et al.* 1999, Rentschler *et al.* 1999, Xin *et al.* 2000, James *et al.* 2000). The binding between dystroglycan and dystrophin or utrophin can also be modulated by phosphorylation of the tyrosine within the PPxY motif, but this will be discussed in greater detail later (James *et al.* 2000, Ilsely *et al.* 2001). Dystrophin is able to bind directly to the actin cytoskeleton of the cell (Way *et al.* 1992), and thus dystroglycan creates a physical link between the extracellular matrix and actin cytoskeleton. Thus, when members of the DGC are lost the result is commonly a form of muscular dystrophy due to contraction induced muscle damage. For example, when dystrophin is lost from the DGC in the case of Duchenne muscular dystrophy (Duchenne 1868) or mutated such that it is no longer able to bind actin (Beggs *et al.* 1991), the DGC is destabilised and eventually lost (Ervasti *et al.* 1990, Matsumura *et al.* 1993, Blasi *et al.* 1996). This leads to the sarcolemma of the muscle cells being unable to withstand contraction induced tension from the surrounding matrix or contractile apparatus, which results in continuous damage, muscular dystrophy, and ultimately death due to cardio-respiratory failure (Duchenne 1868, Batchelor and Winder 2006). Dystroglycan also appears to function within the satellite cells of the muscle and modulate muscle regeneration (Cohn *et al.* 2002), which explains why muscle specific knock-outs of dystroglycan show a milder phenotype than more widespread knock-outs (Côté *et al.* 1999).

Obtaining a complete overview as to all the functions dystroglycan possesses in both the mature animal and during development is difficult in mice, as deletion results in embryonic lethality at embryonic day 5.5 due to a failure in the formation of Reichert's membrane (Williamson *et al.* 1997). As stated earlier, the glycosylation of α DG is necessary for it to be able to bind extracellular binding partners (Yoshida-Moriguchi *et al.*

2010, Sheikh *et al.* 2017), and as such mutations that lead to the hypoglycosylation of dystroglycan can give an indication as to various the roles dystroglycan can play. These conditions are known as secondary dystroglycanopathies, and up to 18 genes have been identified as causative mutations. The conditions can range from severe conditions such as Walker-Warburg, which is characterised as severe muscle wasting, poor muscle tone, cobblestone lissencephaly, hydrocephalus, intellectual disability and other brain development deficits which usually results in death before the age of three years. This condition can be caused by mutations in POMT1, POMT2, B3GNT1 and LARGE, which are all involved in the proper glycosylation of α DG (**Figure 1.13**, De Bernabé *et al.* 2002, Van Reeuwijk *et al.* 2005, Buysse *et al.* 2013, Longman *et al.* 2003). The conditions can also take a milder form of congenital muscular dystrophy without any brain involvement in the case of FKRP mutation or adult onset muscular dystrophy in the case of ISPD mutation (Brockington *et al.* 2001, Cirak *et al.* 2013).

Glycosyltransferases

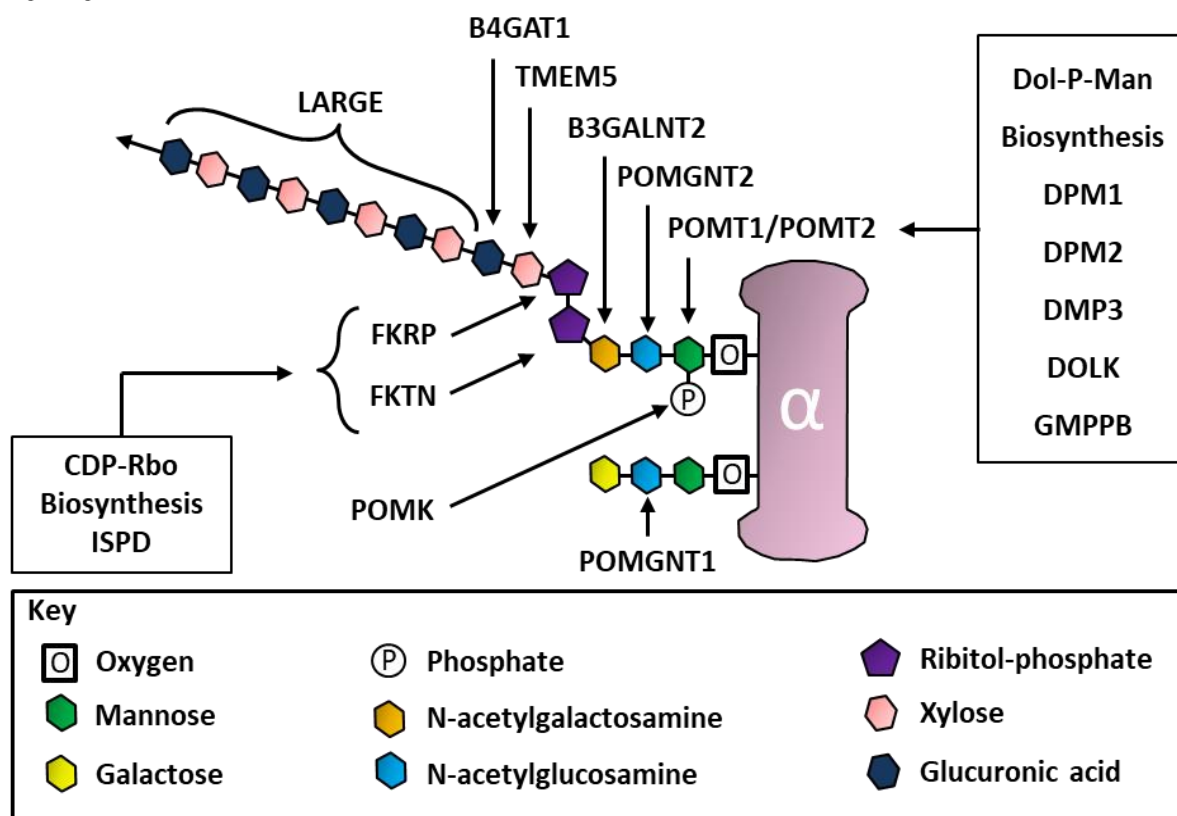


Figure 1.13 – The extensive glycosylation of alpha-dystroglycan – This diagram is a simplified representation of the extensive glycosylation of αDG alongside the various enzymes responsible, to give an indication of the complexity of the system. Some of the enzymes shown here do not directly modify αDG, and are instead responsible for the synthesis of cytidine diphosphate ribitol (CDP-Rbo) or dolichol phosphate mannose (Dol-P-Man), used by other enzymes in the modification process. This image was re-drawn from Nickolls and Bönnemann 2018.

Conversely, direct mutations in the dystroglycan gene are rarer, and only a select few cases have been reported in humans. These primary dystroglycanopathies also show a spectrum of possible conditions, the more severe of which can show neonatal death or severe neuronal involvement in the cases of muscle-eye-brain disease caused by a mutation at C669F (Riemersma *et al.* 2015, Pihko *et al.* 2015). In accordance with the name, patients with this condition show muscle hypotonia and atrophy, visual impairment including glaucoma and myopia, and cognitive impairment with epilepsy and seizures (Pihko *et al.* 1995). This particular mutation results in dystroglycan accumulation and degradation in

the ER (Signorino *et al.* 2018). The conditions associated with primary dystroglycanopathies can also be relatively mild, for example in the G220A mutation, and result in asymptomatic hyperCKemia and mild muscular dystrophy (Dong *et al.* 2015). The variety of symptoms that can arise from dystroglycan dysfunction give an indication as to the vast array of functions the DGC carries out.

1.5.2 – The role of dystroglycan in non-muscular tissues

The first piece of evidence linking the DGC to a neuronal role was the original reports by Duchenne (1868), who reported a lower intelligence in Duchenne muscular dystrophy (DMD) patients. In fact, both cognitive impairment and epilepsy are common features of dystroglycanopathies (Messina *et al.* 2009, Di Rosa *et al.* 2011). It was shown via an *in vitro* siRNA knockdown that the loss of dystroglycan results in a reduction in dendritic complexity and reach in hippocampal neurons, which is linked to cognitive impairment and retardation in humans (Kulkarni *et al.* 2012, Bijata *et al.* 2015). Furthermore, dystroglycan is highly expressed in the glial cells of the central nervous system that contact the basement membranes that cover the brain and blood vessels (Zaccaria *et al.* 2001). Knock-out results in degradation of these basement membranes, and displacement of central nervous system neurons outside of their usually boundaries (Yamamoto *et al.* 1997, Yamamoto *et al.* 2008).

Within the central and peripheral nervous system dystroglycan also seems to possess a role in neuronal myelination. Morphological alterations can be seen in the white matter tracts of patients with dystroglycanopathies (Bönnemann *et al.* 2014), and dystroglycan is upregulated during the myelination of regenerating peripheral nerve fibres (Masaki *et al.* 2000). It was shown that disruption of the binding between α DG and laminin resulted in a reduction in central nervous system fibre myelination by oligodendrocytes (Colognato *et al.* 2007, Eyermann *et al.* 2012). Knock-out studies demonstrated that the cooperation between α DG and integrin- α 6 β 4 is important for both the proper folding of the myelin sheath and development of the nodes of Ranvier (Nodari *et al.* 2008, Saito *et al.* 2008).

The possible role of dystroglycan as an extracellular signal transducer is becoming more and more detailed (Moore and Winder 2010). Dystroglycan is known to be able to act as an adapter for the ERK/MAPK signalling cascade, but the details of how dystroglycan is

able to transduce extracellular signals is still largely unknown (Spence *et al.* 2004). It was shown that the knock-out of dystroglycan in the retina resulted in the excessive branching of blood vessels in the retina as a result of notch pathway activation (Biswas *et al.* 2018). How the pathway is being activated in this scenario is unknown, but it is thought to be triggered by the binding of laminin $\gamma 3$ to α DG (Biswas *et al.* 2018). In a similar study, it was shown that the binding of the extracellular matrix protein agrin to dystroglycan could trigger the proliferation of cardiomyocytes in the heart of the neonatal mouse (Bassat *et al.* 2017). The mechanism by which this binding transduces the signal is similarly unknown, but it is thought to act by activating the hippo pathway (Bassat *et al.* 2017).

As well as regulating dendritic complexity, regulating the basement membranes of the central nervous system, and regulating myelination, dystroglycan also possesses a role in axonal guidance. As mentioned previously, slit is a ligand of α DG, and in the spinal cord dystroglycan regulates normal axonal guidance by localising slits to the floorplate and maintaining a permissive growth substrate for developing axons (Wright *et al.* 2012). The disruption of α DG function by mutating glycosylated enzymes B3GNT1 and ISPD resulted in an increase in stalled projections and projections that failed to properly turn after crossing the midline (Wright *et al.* 2012). Elsewhere in the central nervous system, dystroglycan is involved in a second example of axonal guidance. Under normal conditions, at the optic chiasm, 95% of retinal ganglion cell axons cross to the contralateral fibre tract (Petros *et al.* 2008). At embryonic day 13, dystroglycan is enriched in the ventral forebrain at the site of retinal axon crossing (Clements and Wright 2018). Similar to the spinal cord, disrupting the glycosylation of α DG by mutating ISPD results in an increased prevalence of axonal stalling and failure to properly cross the midline into the contralateral fibre tract (Clements and Wright 2018). By the time of birth in this model, only ~50% of the axons successfully crossed the optic chiasm, further highlighting the significant role dystroglycan plays in localising the slits at these sites. Once again, further work is required to properly understand the molecular mechanisms underlying this localisation, but expands on the ever growing list of functions dystroglycan possesses.

As well as modulating dendritic complexity and regulating myelination, dystroglycan is also involved in the layering of retinal and cortical tissues. In line with this, disruption of the DGC is often associated with retinal defects, including microphthalmia, retinal detachment and delayering, and cataracts (Dubowitz 2000, Toda *et al.* 2000, Hino *et al.* 2001, Kano *et al.* 2002). In the retina, the layers of cells including photoreceptors and

bipolar neurons are encapsulated by two membranes; the inner limiting membrane which resides adjacent to the vitreous humor, and Bruch's membrane which is positioned beneath the photoreceptors. In dystroglycan knock-down and conditional knock-out models, in *Xenopus* and mice respectively, results in a loss of the integrity of these membranes and aberrant cell migration resulting in cells breaching the inner limiting membrane, past their usual layer boundaries (Lunardi *et al.* 2006, Clements *et al.* 2017). Thus, the DGC is not necessary for the formation of the membranes, but rather acts to maintain them as well as their proper connection to the surrounding cells to ensure normal cellular migration within the retina (Lunardi *et al.* 2006, Clements *et al.* 2017). In the absence of normal migration, it was observed that the knock-down model possessed ten times the amount of cell death compared to the control animal, as revealed with a TUNEL assay, with no impact on cell proliferation (Lunardi *et al.* 2006).

Similar delayering phenotypes in disrupted DGC models can be observed in the cortex. In the cerebellum it has been reported that the conditional deletion of fukutin from E10.5, resulting in α DG glycosylation defects (**Figure 1.13**), results in radial glia disorganisation and thus cell migration defects (Sudo *et al.* 2018). External granule cells, which usually migrate inwards via the Bergmann radial glia scaffold, stalled at the surface of the cortex (Sudo *et al.* 2018). Earlier knock-outs of fukutin as E9.5 results in a more severe phenotype, which presents as disruption of the pial membrane as well as fusion of the two cerebral hemispheres (Sudo *et al.* 2018). In the rostral cortex, knocking out fukutin related protein and thus disrupting α DG glycosylation (**Figure 1.13**), results in migration deficits in the Cajal-Retizius cells where the cells fail to form their normal layer (Booler *et al.* 2017). At E11.5, brain lesions caused by cell migrating beyond their normal boundaries were apparent. The amount of reelin signalling, which is essential for normal neuronal migration and brain development (Boyle *et al.* 2011), appears to be unaffected within the knock-outs, and instead it is the localisation of the signal that is defective (Booler *et al.* 2017).

Thus in both the retina and the cortex, the DGC plays a role in normal tissue layering via the maintenance of key membrane structures and ensuring normal cell migration. However, much work is still to be done to elucidate the mechanism by which the DGC is acting in these contexts.

1.5.3 – The role of dystroglycan in synapse formation and maintenance

To date, dystroglycan has been implicated in the development of synaptic components in two different contexts: the regulation of the receptor clustering at the post-synaptic cleft of the neuromuscular junction (NMJ), and the control of terminus invagination and ultrastructure in retinal ribbon synapses.

At the NMJ, multiple components of the DGC have been implicated in the proper clustering of acetylcholine receptors (AChRs). While dystrophin is localised throughout the sarcolemma of the muscle tissue, the protein is particularly enriched at the NMJ (Miike *et al.* 1989, Bewick *et al.* 1992, Porter *et al.* 1992). Dystrophin co-localises to the post-synapse with acetylcholine receptors and rapsyn, which is responsible for the formation of receptor clusters (Ramarao and Cohen 1998, Dmytrenko *et al.* 1993). When full length dystrophin is knocked out, in the case of MDX mice (Hoffman *et al.* 1987), the result is a fragmentation of the receptor clusters in regenerating muscle fibres, but not established fibres (Kong and Anderson 1999, Zaccaria *et al.* 2000). The synaptic phenotype in this model was subtle, and shows that dystrophin appears to perform a non-critical function at the NMJ. It was reported that fewer large receptor clusters were visible in the MDX mouse, suggesting that dystrophin may only be responsible for the formation of larger receptor patches with slight effect on receptor cluster degradation rate (Xu and Salpeter 1997, Lyons and Slater 1991). The physiological consequences of the clustering defects in MDX mice is progressively reduced end-plate potential amplitudes, and an increase in the quantal content of synaptic vesicles, likely as a compensatory mechanism (Nagel *et al.* 1990). As discussed previously, the DGC can also bind utrophin to the intracellular domain of β DG as well as dystrophin (Chung *et al.* 1999), and utrophin is also concentrated at the NMJ (Tinsley *et al.* 1992, Khurana *et al.* 1990, Grady *et al.* 1997a). Similarly, the effects of utrophin knock-out at the NMJ were relatively subtle, with the only impact being a decrease in receptor cluster density with minimal functional consequences (Grady *et al.* 1997b, Deconinck *et al.* 1997a). The mild nature of the phenotypes in mice can be explained by the fact that the removal of dystrophin results in utrophin upregulation in a compensatory mechanism (Deconinck *et al.* 1997b). As such, both dystrophin and utrophin have to be knocked out in mice to recapitulate the phenotype seen in patients that entirely lack dystrophin (Van Putten 2012).

Similar to the actin binding components of the complex, other components of the DGC are also concentrated to the NMJ. Dystroglycan, both alpha and beta, are localised to the NMJ through the binding of ankyrin (Ayalon *et al.* 2008). At the synapse, α DG binds to both agrins and laminins to facilitate the formation of normal NMJs and post-synaptic receptor cluster (Campanell *et al.* 1994, Sugiyama *et al.* 1994, Sugiyama *et al.* 1997, Gee *et al.* 1994). Knocking out or disrupting dystroglycan results in disorganised and unstable cluster of acetylcholine receptors (Jacobson *et al.* 2001). Alongside this, larger clusters of receptors can be induced via the addition of laminin (Sugiyama *et al.* 1997), which suggests that perhaps dystroglycan stabilises and modulates these synapses through laminin rather than agrin. To lesser extents, alpha sarcoglycan (Zhang *et al.* 2008, Zhao *et al.* 2018), alpha syntrophin (Adams *et al.* 2000), and alpha dystrobrevin (Grady *et al.* 2000) have also been linked to receptor turnover rates and clustering at the NMJ. Overall, the DGC appears to play significant role in receptor clustering, but is not crucial for the establishment or functionality of these synapses.

As mentioned earlier, dystroglycan also possesses a role in the ribbon synapses of the retina. Pikachurin is a secreted ECM like protein, and a ligand of α DG (Sato *et al.* 2008). At the retinal ribbon synapse, the DGC is present at the pre-synaptic membrane and pikachurin is expressed selectively in the synaptic cleft (Sato *et al.* 2008). When pikachurin is knocked out, the ON bipolar cell terminus fails to properly invaginate into the photoreceptor terminals of the rods and cones (Sato *et al.* 2008). This results in a delayed b-wave in an electroretinogram trace, which reflects inefficient synaptic transmission between the photoreceptors and the bipolar neurons. The localisation of pikachurin and the DGC to the synapse is dependent on dystrophin first arriving at the synapse, which occurs earlier and independent of the two (Omori *et al.* 2012). Both dystrophin and dystroglycan knock-outs result in a similar delayed b-wave phenotype to the pikachurin mutant (Pillers *et al.* 1999, Omori *et al.* 2012). Interestingly, while this b-wave impairment has been compared to ERG traces observed in patients with stationary night blindness, this does not appear to significantly impact the vision of DMD patients (Fitzgerald *et al.* 1994). At the post-synaptic side, pikachurin binds to the orphan G-protein coupled receptor GPR179, which itself binds to the GTP-ase accelerating protein (GAP) complex proteins RGS7 and RGS11 (**Figure 1.14**, Orlandi *et al.* 2018). The amount of these GAP complex proteins dictates both the kinetics and sensitivity of the synapse by accelerating the inactivation of the $G\alpha$ subunit (Hollinger and Hepler 2002). Mutating

GPR179, and thus disrupting the GAP complex proteins, does not impact synaptic invagination like the pikachurin and dystroglycan mutants, but does result in an entirely absent b-wave (Peachey *et al.* 2012, Orlandi *et al.* 2018). Consistent with this, and unlike dystrophin, mutations in GPR179 have been associated with recessive stationary night blindness in humans. Thus, while GPR179 binds to pikachurin, it is not responsible for localisation of the protein to the synaptic cleft like dystroglycan (Orlandi *et al.* 2018). Therefore, at the retinal ribbon synapse, dystrophin, dystroglycan, pikachurin and GPR179 form a trans-synaptic complex that both modulates the invagination of the bipolar terminus and the kinetics of the G-protein coupled receptor signalling (Hollinger and Hepler 2002, Sato *et al.* 2008, Omori *et al.* 2012, Orlandi *et al.* 2018). The role dystroglycan plays in the retina opens the possibility that the complex may be functioning similarly in other ribbon synapses, such as those within the cochlea. This could be similarly dependent on pikachurin or possibly acting through an entirely different mechanism.

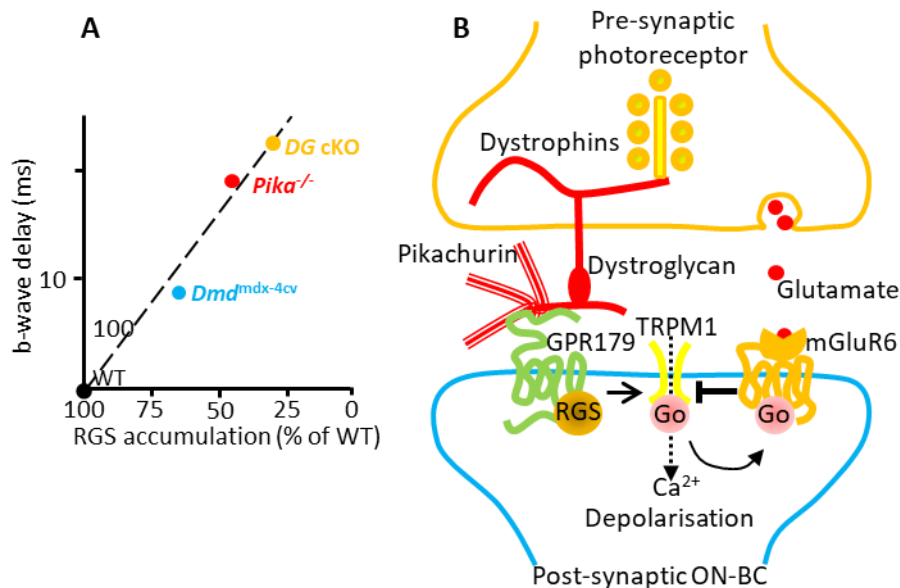


Figure 1.14 – The role of the DGC in the formation of proper ribbon synapses between photoreceptors and ON bipolar cells – (A) The spectrum of phenotypes associates with mutations in the dystrophin-dystroglycan-pikachurin-GPR179 trans-synaptic complex. Dystrophin mutation, resulting in a premature stop codon, leads to the mildest phenotype with the smallest increase in b-wave implicit time. In order of severity from mildest to worst, this is followed by pikachurin knock-out and then dystroglycan knock-out. The severity of this knock-out can be attributed to the differential effect on the accumulation of the post-synaptic RGS7/11 protein accumulation. The fact that dystroglycan possesses the most severe phenotype suggests that it may be functioning to facilitate proper ribbon synapse development

in another manner independently of pikachurin.(B) Schematic of the trans-synaptic complex, and how it functions to regulate synaptic kinetics through the regulation of the G-protein receptors through the RGS proteins. This figure was redrawn from Orlandi *et al.* 2018.

1.5.4 – The possible functions of phosphorylated dystroglycan within the organ of Corti

The first piece of evidence linking the DGC to hearing was the finding that a mutation in the Xp21.2 locus, which corresponds to dystrophin, resulted in non-syndromic X-linked hearing loss (Lalwani *et al.* 1994). Female carriers also showed a mild increase in hearing threshold, though it was significantly less severe than the male patients. Furthermore, it was reported that secondary dystroglycanopathies caused by mutations in B3GALNT3 can result in sensorineural hearing loss alongside a plethora of other neurological symptoms (Al Dhaibani *et al.* 2018). No work has been done to further investigate the exact mechanism of this hearing loss in patients in either case, and much work is to be done to determine how the mutation exerts the phenotype. Interestingly, while dystrophin and α DG have been reported as present within the organ of Corti, β DG has previously been reported entirely absent (Dodson *et al.* 1995, Heaney and Schulte 2003). This is curious, as the two subunits are translated together as a single propeptide and separated via early proteolytic cleavage (Ibraghimov-Beskrovnaya *et al.* 1992), which suggests that an apparent complete absence must be due to rapid degradation or a masked antibody epitope. Previous work in our lab identified that phosphorylated β DG (p β DG), but not unphosphorylated β DG, is present within the organ of Corti using a phospho-specific antibody (Prof Matthew Holley, unpublished observations). The phosphorylation of the PPxY tyrosine is known to block the binding epitope of antibodies commonly used for the localisation of β DG such as Mandag2 (James *et al.* 2000, Pereboev *et al.* 2001), explaining the absence reported previously.

The apparent phosphorylation of the entire β DG content of the organ of Corti is peculiar, as this phosphorylation is known to result in internalisation into recycling endosomes alongside c-src (Sotgia *et al.* 2003) or for degradation (Lipscomb *et al.* 2016). The phosphorylation is also known to trigger localisation to the nucleus via the importin α 2 β 1 system, where dystroglycan is known to regulate nuclear structure (Martínez-Vieyra *et al.* 2013, Gracida-Jiménez *et al.* 2017, Lara-Chacón *et al.* 2010, Oppizzi *et al.* 2008). Finally,

the phosphorylation of β DG is also known to reduce the binding affinity with dystrophin and utrophin, by physically preventing the C-terminus of dystroglycan from fitting within the hydrophobic pocket created by the WW domain (James *et al.* 2000, Winder 2001). Thus, while dystrophin appears to perform some unknown function in hearing (Lalwani *et al.* 1994), this appears to perhaps not involve the binding of dystroglycan (James *et al.* 2000).

The final piece of evidence that could link dystroglycan to a role in hearing and hearing loss is the potential interaction with the actin-binding proteins EPS8 and EPS8L2, responsible for the establishment and maintenance of the hair bundle staircase respectively (Section 1.2.2). In an SH3 phage display interactome screen it was found that the SH3 domain of EPS8L2 is a potential interactor of the cytoplasmic domain of β DG (Thompson *et al.* 2008). The exact binding location on dystroglycan, whether this binding occurs *in vivo*, and the role of this interaction in the cochlea remains unknown.

Thus the hypothesis I set out to test was: Dystroglycan possesses a role in the maintenance of cochlear ribbon synapses and/or stereocilia by interacting with pikachurin or EPS8L2 respectively.

Therefore, in order to address this hypothesis, the aims for the project were:

- Investigate whether EPS8L2 interacts with dystroglycan using biochemical approaches
- Further analyse the distribution of phosphorylated beta-dystroglycan within the organ of Corti, and specifically visualise whether it co-localises with EPS8L2 at the tips of the shorter rows of stereocilia
- Analyse the effects of knocking out dystroglycan specifically from cochlear hair cells on hearing thresholds, ribbon synapses and hair cell maturation

2 – Materials and methods

2.1 – Animal techniques

2.1.1 – Ethical statement and animal strains

All procedures were performed at the University of Sheffield, licenced by the Animals (Scientific Procedures) Act (1986) and approved by an ethical review committee. For all *in vitro* experiments, mice were killed via cervical dislocation and then quickly decapitated. For the auditory brainstem response (ABR) and distortion product oto-acoustic emission (DPOAE) experiments, mice were anaesthetised via the intraperitoneal injection of ketamine (100mg/kg, Fort Dodge, USA) and xylazine (10mg/kg Rompun 2%, Bayer Healthcare LLC, USA). Depending on the experimental plans for the animal, mice were either culled via schedule 1 at the end of the experiment or recovered via a second intraperitoneal injection of atipamezole (1mg/kg). Recovering mice were placed into a separate cage on a heat mat (37°C) and monitored at all times until they were moving and responding as normal (2-4 hours in normal conditions). Fully recovered mice were then returned to their rack. The wild-type animal strains used in this work were: C57BL/6J (6J) and C57BL/6NTac (6N), which both have a fixed hypomorphic allele in *Cadherin 23* (*Cdh23^{ahl}*: Johnson *et al.* 1997; Noben-Trauth *et al.* 2003). Some experiments were also performed using C57BL/6NTac mice in which the *Cdh23^{ahl}* allele was ‘corrected’ using CRISPR/Cas9 homology-directed repair (C57BL/6NTac^{*Cdh23*⁺}: Mianné *et al.* 2016). In addition, the transgenic mice 129S1-DAG1<tm2Kcam>/J (The Jackson Laboratory, Cohn *et al.* 2002), EPS8 knockout (Offenhäuser *et al.* 2006), MYO15-Cre (Caberlotto *et al.* 2011) and *BAIAP2L2^{tm1b}* (MRC Harwell) were also used, which are all on the C57BL/6NTac background.

For the DAG1 floxed line, the nomenclature DAG1^{-/-} represents a mouse homozygous for the floxed allele that will continue to produce functional DG in the absence of Cre, and DAG1^{+/+} represents a homozygous wild-type. For the Myo15Cre line, Myo15Cre^{+/-} represents a mouse heterozygous for the Cre carrying allele that will produce Cre in hair cells only after P2, and Myo15Cre^{+/+} represents a mouse not carrying a Cre containing allele.

2.1.2 – Tissue preparation

All electrophysiology experiments performed for this thesis were done on hair cells within the 9-12 kHz region of the apical coil, as described previously (Muller *et al.* 2005). Apical coils of the cochlea were dissected out shortly after death in extracellular solution. This solution was composed of (in mM): 135 NaCl, 5.8 KCl, 1.3 CaCl₂, 0.9 MgCl₂, 0.7 NaH₂PO₄, 5.6 D-glucose, 10 HEPES-NaOH, 2 sodium pyruvate, amino acids and vitamins were added from concentrates (Thermo Fisher Scientific, UK). The pH of the solution was then adjusted to 7.48 using 1M NaOH, and the osmolality checked with an osmometer (308 ± 3 mOsm/kg H₂O, Advanced Instruments model 3300). Once the dissection was complete, the apical turn was transferred into a custom glass-bottom microscope chamber and immobilised with a nylon mesh attached to a stainless steel ring (**Figure 2.1**). The specimen was then viewed on an upright microscope (Nikon FN-1, Japan) with Nomarski differential interference contrast (DIC) optics (63x water immersion objective) and a 15x eyepiece. In order to maintain cell health, new extracellular solution was constantly perfused through the chamber at room temperature (20-25°C) using a peristaltic pump at around 3 ml/minute.

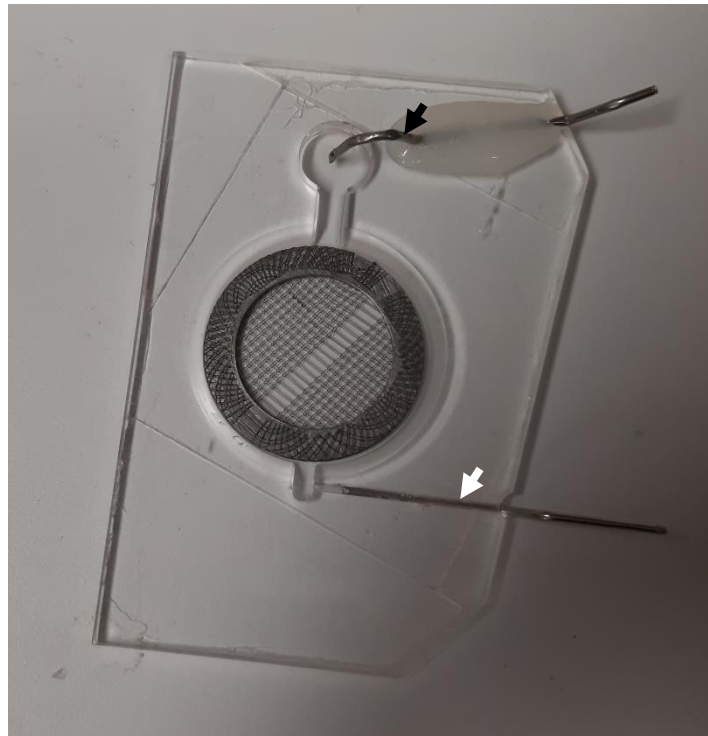


Figure 2.1 – Grid and chamber used for the immobilisation of cochlear sensory epithelia – Once dissected, cochlear sensory epithelia were immobilised underneath the centre of the nylon grid. Fresh extracellular solution was then be pumped into the chamber through the inlet tube (White arrow) and removed via the outlet tube (Black arrow), positioned such that the height of the outlet tube hole dictated the fluid level in the chamber.

2.1.3 – Whole-cell patch clamping and mechanotransduction

In order to record whole-cell potassium currents, patch electrodes were first pulled from soda glass capillaries using a 2-stage upright pipette puller (Narishige PC-10) to a resistance of ~2-3 MOhm for inner hair cells and 3-4 MOhm for outer hair cells. In order to try and reduce the capacitance charge generated by the pipette, it was then coated with surf wax (Zogg's sex wax), ensuring the wax was as close to the tip as possible. The intracellular solution used for inside the pipette comprised (in mM): 131 KCl, 3 MgCl₂, 1 ethylene glycol-bis(β-aminoethyl ether)-N,N,N',N'-tetraacetic acid (EGTA)-KOH, 5 Na₂ATP, 5 HEPES-KOH and 10 Na-phosphocreatine. The pH of the solution was then

adjusted to 7.28 with 1M KOH, and the osmolality was then checked ($\sim 293 \pm 3$ mOsm/kg H₂O). Positive pressure was maintained within the patch pipette at all times while it was in solution and not contacting a cell, in order to ensure the patch pipette contained only intracellular solution. Unwanted cells were removed from the preparation to expose the basolateral membrane of hair cells with a borosilicate cleaning pipette pulled to a diameter of around 3 μ m, which was attached to a syringe via a tube for fine control of negative and positive pressure. Following cell contact with the patch pipette and the formation of a giga-ohm seal, breakthrough into the whole cell configuration was achieved via sharp negative pressure applied through a mouthpiece. All the data presented here was collected using an Optopatch patch clamp amplifier (Cairn Research LTD, UK). Data acquisition was controlled by pClamp software using a DigiData 1440A low noise board (Molecular Devices, USA). All traces were filtered at 2.5 kHz with an 8-pole Bessel filter, sampled at 5 kHz and then stored on a computer for offline analysis using Origin (OriginPro, Version 2020. OriginLab Corporation, Northampton, MA, USA). All data was then corrected for the liquid junction potential between the intracellular and extracellular solution, which was previously measured to be -4 mV. Recordings were normally corrected for series resistance after compensation (usually $\sim 80\%$ depending on the experiment). In some cases it was necessary to transiently change the composition of the extracellular solution, such as when testing sensitivity to low calcium (40 μ M Ca²⁺), and this was achieved with a gravity fed multi-channel pipette positioned close to the area of recording.

In order to record mechanotransducer currents, inner and outer hair cells were patched with a different intracellular solution, one based on caesium and not potassium. This solution blocks the majority of the potassium current and allows us to visualise the mechanotransducer currents more easily. This solution comprised (in mM): 131 CsCl, 10 Na-phosphocreatine, 3 MgCl₂, 5 Na₂ATP, 5 HEPES and 1 EGTA-CsOH. The pH was then adjusted to 7.29 and the osmolality checked ($\sim 290 \pm 3$ mOsm/kg H₂O). Hair bundles were then stimulated using a borosilicate fluid jet (8-10 μ m diameter) driven by a piezo-electric disc. The placement of this fluid jet was fine-tuned prior to the recordings in order to achieve a saturated signal from the hair cell, which was visible as a flat peak in the trace with little noise during the excitatory stimulus. Hair bundles were either stimulated with a 50Hz sinusoid or voltage steps, with all stimuli being filtered at 2.5 kHz on an 8-pole Bessel filter.

2.1.4 – Auditory Brainstem Response (ABR) and Distortion Product Oto-Acoustic Emissions (DPOAE) recordings

Following the onset of anaesthesia as described in section 2.1.1, and after the loss of the foot retraction reflex after a toe pinch, mice were placed into a soundproof chamber (MAC-3 acoustic chamber, IAC Acoustic, UK) on a heat mat (37°C) to maintain body temperature. Three subdermal electrodes were then placed below the skin; one behind the pinna of each ear (one reference, one ground) and a third electrode beneath the skin of the scalp (active). The quality of the electrode placement was checked as the signal to noise achieved from a continuous heart rate trace, which also allowed continuous checks of the health of the animal throughout the experiment. The ear canals of the animals were also checked prior to the start of the experimental protocol, to ensure they had not been occluded while placing the electrodes. Sound stimulation was delivered with calibrated loudspeakers (MF-1 multi-field speaker, Tucker-Davis Technologies, USA) which were always 10 cm away from the pinna of both ears. These loudspeakers were pre-calibrated using a white noise protocol and a low noise microphone (ER10B+, Etymotic, USA), which was also placed 10 cm from the speaker. Recording were collected using customised software (Ingham *et al.* 2011) which was driving an RZ6 auditory processor (Tucker-Davis Technologies, USA). Sound stimulation ranged from 3-42 kHz, including “click” (broadband white noise), and the amplitude was varied from 5-95 dB SPL in 5dB steps. The stimulation waveform for 3 and 6 kHz was inverted halfway through each set of repetitions, in order to better eliminate electrical artefacts and other noise. Each stimulation comprised a 5 ms pulse with a 1 ms on/off ramp time, and these pulses were presented at 42.6/second, and each trace produced by the software was a product of 256 averaged repetitions. Hearing thresholds were estimated as the lowest volume capable of producing any distinguishable feature of the ABR waveform. This was done by looking at the higher volumes, and comparing those traces down the list of amplitudes until no convincing feature remained in the trace (**Figure 2.2**). Where possible, traces were judged by scientists blinded to the genotype of the animal, to mitigate any implicit bias that can easily appear in experiments that require manual judgement.

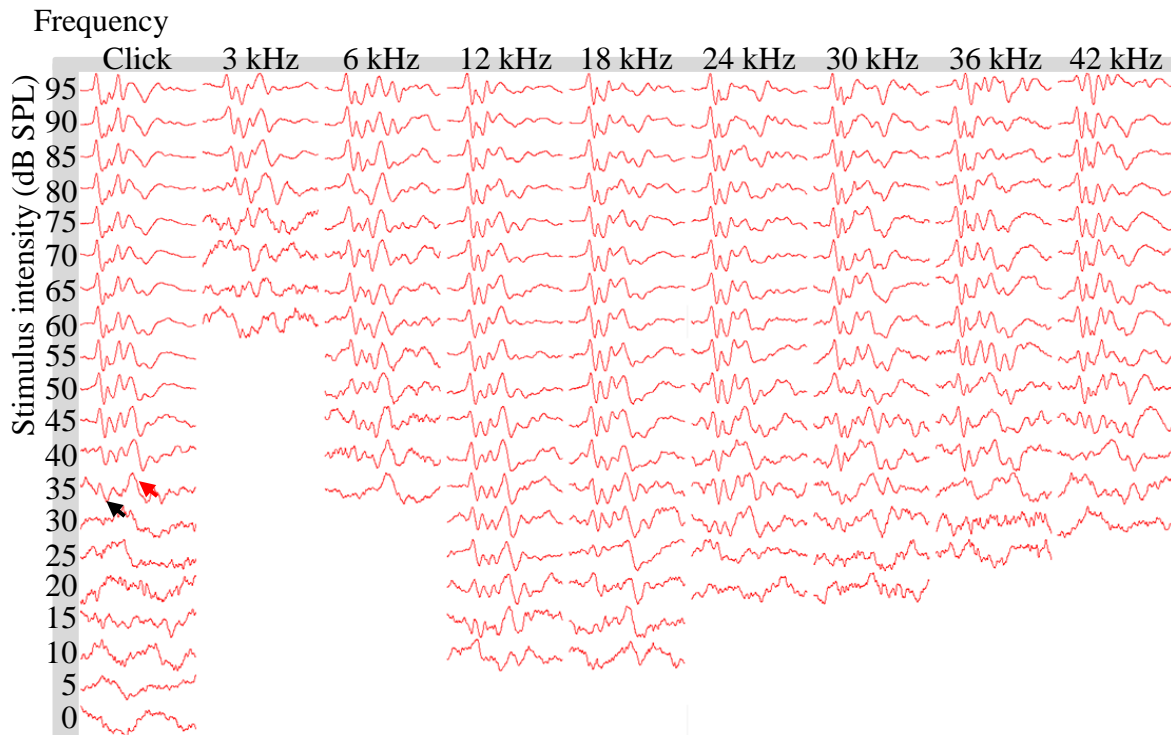


Figure 2.2 – Manual analysis of ABR hearing thresholds – Hearing thresholds were manually estimated from the traces shown, which have been normalised by the amplitude of each trace to fill the space and best represent the shape. The threshold is defined as the minimum amplitude (dB SPL, Y-axis) needed to elicit any features of the ABR waveform. For example, for the click broadband white noise column shown above, the hearing threshold would be 35, as traces at lower amplitudes than this lose the recognisable trough (Black arrow) and peak (Red arrow) of the waveform.

While the mouse was still anaesthetised, we utilised the remaining time to perform DPOAE experiments to test and measure outer hair cell amplification. In order to perform this experiment, the subdermal electrodes were first removed and a metal coupler was placed into one of the ear canals to create a closed system. This coupler was connected to two pre-calibrated loudspeakers (MF1-S, multi-field speaker, Tucker-Davis Technologies, USA) and one low noise microphone (ER10B+, Etymotic Research INC, USA). During the experiment, two primary tones, denoted as f_1 and f_2 (where $f_1/f_2 = 1.2$), were played into the ear while the DPOAE artefacts were recorded from the frequency $2f_1-f_2$. The amplitude of f_1 and f_2 was always equal, and varied from 20-80 dB SPL in 10 dB steps throughout the experiment. The f_2 frequency was also changed throughout the experiment,

stepwise from 3 to 36 kHz (3, 6, 12, 18, 30 and 36 kHz). For each set of frequency and amplitude 500 repetitions were collected and averaged. Data was collected using BioSig RZ software driving an RZ6 auditory processor (Tucker-Davis Technologies, USA). The threshold for a DPOAE response was pre-defined as one standard deviation above the noise, and all collected data was plotted as threshold vs frequency.

2.1.5 – Cochlea whole-mount immunofluorescence

Following cervical dislocation, the cochlea (younger than P12) was swiftly dissected from the skull and either dropped directly in 4% paraformaldehyde (PFA) in phosphate-buffered saline (PBS) or for adult cochleae the fixative was first perfused through the round and oval window after a hole was cut in the apex. After the brief perfusion, adult cochlea were then placed into fresh PFA and left to incubate for 20 minutes on a rocker, the same time used for the younger mice. The apical turn was then dissected out and subjected to three 10 minute washes in PBS. The specimen was then placed into blocking buffer (5% foetal calf serum (FCS), 0.1% triton x-100 in PBS) and left to incubate at room temperature for an hour. Following this, the blocking buffer was replaced with a suitably diluted primary antibody (**Appendix 2.1**) in incubation buffer (1% FCS, 0.1% triton x-100 in PBS) and left to incubate overnight at 37°C in a sealed chamber. Samples were then washed in PBS as before, and placed into a suitably diluted Alexa secondary antibody (**Appendix 2.1**) in incubation buffer for an hour at 37°C. The samples were washed a final time in PBS, and then mounted with hydromount (National Diagnostics, with added 1% w/v 1,4-diazabicyclo(2.2.2)octane (DABCO) and 1 µg/ml 4',6-diamidino-2-phenylindole (DAPI)). After this was left to fully set, usually overnight in a dark container, the samples could then be imaged on either a Nikon A1 confocal or a Zeiss LSM 880 confocal with Airyscan, depending on the resolution required. All data collected were then suitably processed using Fiji (Schindelin *et al.* 2012).

2.1.6 – Cryostat sample prep, sectioning and staining

In order to prepare samples for cryostat sectioning, cochleae were first fixed with 4% PFA using the same method utilised for whole-mount immunostaining as detailed above. The cochlea samples were then decalcified overnight in 5% ethylenediaminetetraacetic acid

(EDTA) in water (pH adjusted to 8 with NaOH pellets as the EDTA dissolved) at 4°C on a roller. The cochleae were then placed sequentially into tubes of increasing sucrose concentration until they sank, including 10, 20 and 30%, in order to allow the sucrose to penetrate the cochlea and support the hollow structure during the sectioning. The samples were then placed into disposable foil moulds with optimal cutting temperature (OCT) compound (Fisher Healthcare, UK) and orientated such that the blade cut through the centre of the modiolus and gave the best image of the organ of Corti spiral possible. This mould was then flash frozen in isopentane which had been pre-equilibrated with dry ice to create a freezing pool, and once entirely frozen the sample was stored in -80°C until the time of sectioning.

Prior to cutting, the samples embedded in OCT were first transferred into the cryostat chamber (-20°C starting temperature) for 30 minutes to equilibrate. The OCT block was then removed from the mould and attached to a small slice of cork with more frozen OCT. This was then attached to the chuck with the same method. This setup allowed cutting to be stopped and the block placed back into storage more easily. Thick sections of the cochlea were then taken and disposed of until the centre of the modiolus was reached, at which point 10µm sections were cut and collected on SuperFrost Plus glass slides (Thermo Fisher Scientific, UK). Up to 6 samples were collected on each slide to prevent unnecessary wastage, and stored at -80°C until the staining procedure.

To stain the sections, the slides were first removed from -80°C and kept at room temperature for 30 minutes to stop the slide from possibly cracking due to the temperature difference between the freezer and the solutions. During this time, a hydrophobic barrier pen was used to separate the sections to make the future steps easier. The slides were then placed in PBS for 10 minutes on a rocker to re-hydrate the sample and remove the OCT, and 100 µl of blocking buffer (5% foetal calf serum (FCS) and 3% bovine serum albumin (BSA) in PBS) was applied to each section. The hydrophobic barrier meant that each sample could be incubated with a different solution, and the blocking buffer formed a separate droplet over each sample. The samples were incubated with the blocking buffer for an hour at room temperature in a humidified chamber. This buffer was then removed, replaced with a suitable primary antibody diluted in blocking buffer and left to incubate at room temperature for two hours at room temperature or overnight at 4°C (**Appendix 2.1**). The slides were then washed three times for 10 minutes in PBS on a rocker, before incubation with Alexa secondary antibodies (1:1000) for one hour at room temperature

(**Appendix 2.1**). The washing steps with PBS was then repeated before hydromount (National Diagnostic, with added 1% DABCO w/v and 1 µg/ml DAPI) was added to the slide and the sample covered with cover glass. This was then left to set overnight in a dark container and imaged on either a Leica DMIRE2 epifluorescent microscope or a Zeiss LSM880 confocal microscope with Airyscan.

2.1.7 – Utricle twist-off

For collection of lysates enriched with stereocilia, a modified protocol of the original bullfrog twist-off (Gillespie and Hudspeth 1991) was employed. First, chambers were prepared by coating the centre of Eppendorf caps with a mixture of 10 µl Cell-Tak (Corning), 5 µl of 0.1M sodium bicarbonate and 5 µl of a 1 M sodium hydroxide stock solutions. This mixture was left to coat the chamber for a minimum of one hour at 4°C, and then removed. The resulting chambers could then be stored at 4°C for no more than a week. To carry out the twist-off, whole cochleae were quickly dissected out from wild-type mouse pups between postnatal day 6 (P6) and P8 in PBS, and the utricle was dissected out. The otoconia and otolithic membrane was removed, and up to four utricles were placed into a pre-prepared twist-off chamber containing 100 µl of PBS with freshly added protease inhibitor cocktail (cOmplete EDTA-free protease inhibitor cocktail, Roche). The utricles were then finely manipulated in order to attach them to the base of the chamber, at which point the PBS was replaced with 37°C 4.5% low melting point agarose in PBS with protease inhibitors. The chamber was then placed in a 37°C incubator for a minute, and then into 4°C for ten minutes to fully set. The agarose cap was then separated from the edge of the Eppendorf cap with a large gauge needle, and inverted. The utricles were then pulled off the gel cap laterally, leaving the stereocilia embedded in the agarose. To check the efficacy, gel discs were fixed with 4% PFA in PBS for 10 minutes, permeabilised with 0.1% triton x-100 for one minute and then labelled with Texas Red phalloidin (1:1000, Molecular Probes, Life Technologies). To collect samples for further experimentation, the stereocilia patches were excised from the gel and placed into 1 ml of PBS with protease inhibitors. This was then heated to 80°C until the gel was entirely melted, at which point the solution was centrifuged at 15000 x g for 15 minutes to separate the PBS and agarose from the protein pellet, which could then be resuspended later.

2.1.8 – Genotyping

DNA was extracted from either ear clips or tail sections with the Phire Animal Tissue Direct PCR Kit (Thermo Fisher Scientific, UK) as per the manufacturer's protocol. Firstly, 22.5 µl of F123L buffer was added to each tissue segment. Then, 0.6 µl of the DNA release mix was added, followed by gentle flicking to mix and incubation at room temperature for 4 minutes. The reaction was then stopped by heating to 98°C for two minutes, at which point the DNA could then be stored at 4°C until the time of the PCR. In order to setup the PCR reaction, 1µl of DNA was mixed with 10 µl 2x tissue master mix, 0.4 µM forward and reverse primers (**Appendix 2.2**) and water up to a final volume of 20µl. Following the reaction, the products were then run on a SyBr safe stain DNA gel as described below and imaged with a UV protocol on a Bio-Rad ChemiDoc XRS+.

2.2 – Bacterial techniques

2.2.1 – Creation of chemically competent bacteria

In order to create chemically competent *E. coli* (DH5 α), for plasmid amplification, or *E. coli* (BL21 DE3), for protein expression, the *E. coli* was first grown in 10-15 ml of 2xYT (16 g tryptone, 10 g yeast extract and 5 g NaCl in 1 L of dH₂O, autoclaved) overnight at 37°C in a shaking incubator. The following day, 1.5 ml of this starter culture was used to inoculate 100 ml of 2xYT, and left to grow in a shaking incubator until the media reached an OD₆₀₀ between 0.4 and 0.6. This culture was then split into two 50 ml falcon tubes and centrifuged for 10 minutes at 6000 x g on a table top centrifuge pre-cooled to 4°C. The medium from these tubes was then decanted completely, and the tubes were left inverted for a minute to ensure all media was removed. The cells were then resuspended in 10 ml of ice cold 100mM CaCl₂ per tube, and left on ice for an hour. The centrifugation step was then repeated, and the cell pellets were resuspended in 2 ml of 15% glycerol in 70 mM CaCl₂. The resulting suspension was then divided into 50 µl aliquots and snap-frozen in liquid nitrogen. The cells were now chemically competent, and could be stored in -80°C for up to 6 months.

2.2.2 – Plasmid purification

All purifications were performed with Qiagen mini, midi or maxi kits, depending on the amount of DNA require. The purification of plasmids from DH5 α E.coli was achieved by first growing a suitable volume of bacteria (5ml for mini, 500 ml for midi and 1 L for maxi) overnight at 37°C. The manufacturer's protocol was followed exactly, and the concentration of DNA obtained from the purifications was quantified on a NanoDrop Lite (Thermo Fisher Scientific, UK). For electroporations, all plasmid DNA required a 260/280 ratio greater than 1.8 to ensure there was no contamination significant enough to trigger arcing of the current and poor efficiency.

2.2.3 – Bacterial transformation

In order to transform DH5 α or BL21 E.coli bacteria, the plasmid DNA and bacteria were first thawed on ice. Once thawed, 1 μ l of DNA (usually from a mini-prep and 100-200 ng/ μ l) was added to 20 μ l of the competent bacteria and left to incubate on ice for 30 minutes. The bacteria were then immediately heat shocked at 42°C for 40 seconds and then placed back on ice for 2 minutes. Following this, 400 μ l of 2xYT (without antibiotics) was added to the tube and the bacteria were incubated at 37°C on a shaking incubator for one hour to allow the cells to recover. Next, 100 μ l of the bacteria was placed onto a 2xYT agar plate containing either ampicillin (100 μ g/ml) or kanamycin (50 μ g/ml), depending on the plasmid resistance, and spread until dry with a flame sterilised glass rod. The plate was then inverted, and left to grow in an incubator at 37°C overnight or at room temperature over the weekend, at which point individual colonies were visible and easily collected.

2.2.4 – Glutathione S-transferase (GST) protein purification

In order to purify GST tagged proteins from BL21 E.coli, a 5ml starter culture of 2xYT containing the antibiotic dictated by the plasmid (Ampicillin 100 μ g/ml or kanamycin 50 μ g/ml) left to grow overnight in a shaking incubator at 37°C. The following day, all of this culture was transferred into 1L of 2xYT with antibiotic and grown in a shaking incubator until the OD₆₀₀ was within 0.6-0.8. The culture was then stimulated to begin producing the target protein by the addition of IPTG to a final concentration of 1mM. This culture was

then placed back in the shaking incubator for a further three hours before centrifugation at 6000 x g for 15 minutes to pellet the cells. After the supernatant was decanted, the pellet was placed into a falcon tube and either processed immediately or frozen such that the protocol can be carried out at a later date.

The BL21 pellet was then resuspended in 10 ml of sterile PBS with 1x protease inhibitor cocktail (cOmplete, EDTA-free protease inhibitor cocktail, Roche) and 1mM EDTA. The cells were then lysed by four 30 second periods of sonication with 30 second rests in between. The solution was then centrifuged at 21000 x g for 45 minutes in a table top centrifuge pre-cooled to 4°C. During this centrifugation step, 120 µl of glutathione sepharose 4B (Thermo Fisher Scientific, UK) bead slurry was briefly washed three times with 10 ml of PBS, centrifuged between each wash at 3800 x g for a minute to pellet the beads. Extra care was taken during the removal of the supernatant to ensure that as many beads were kept within the tube as possible. After the centrifugation of the sample was completed, the supernatant from this step was mixed with the now pre-equilibrated beads and left to mix on a roller at 4°C for an hour. The sample was then centrifuged at 3800 x g for one minute, the supernatant was removed, and the resulting beads were washed three times with 10 ml of PBS as before. After the final wash and removal of the PBS, 500 µl of elution buffer (10 mM reduced glutathione in 50mM tris pH 8) as added and the solution was transferred to an Eppendorf tube. The solution was then left to incubate at 4°C for 30-60 minutes on a roller. The resulting mix was then centrifuged at 500 x g for 5 minutes and the supernatant, containing the purified protein, divided into aliquots as necessary. This final elution step could be repeated if required with half the volume of elution buffer to remove any extra proteins still bound to the beads.

2.3 – Cell culture techniques

2.3.1 – KM155, VOT-E36 and VOT-N33 cell culture methods

For all cell lines used, cells were thawed from liquid nitrogen by quickly placing into a pre-heated water bath (37°C) until no ice crystals were visible. The vial was wiped with ethanol, and the cells were then rapidly transferred into a T75 with 12 ml pre-warmed media (composition and temperature dictated by the individual line, **Appendix 2.3**) and left to settle. Once cells were attached, the media was replaced in order to remove the

DMSO used in the freezing media. The cells could now be split as normal, but not used for experiments until 3-4 days after their removal from liquid nitrogen.

KM155 human muscle myoblasts (Mamchaoui *et al.* 2011) were maintained in skeletal muscle growth medium (Promocell) with the supplement added and 10% FCS. The cells were kept at 37°C with 5% CO₂ and split approximately once every 2-3 days. The VOT-E36 and VOT-N33 cells (Lawoko-Kerali *et al.* 2004) are the developmental precursors to the sensory epithelia and spiral ganglion neurons respectively (kindly provided by Professor Matthew Holley). The maintenance of these lines required minimal essential media (MEM, Thermo Fisher Scientific, UK) with 10% FCS, 50 units/ml gamma interferon (γ INF), and a 33°C incubator with 5% CO₂. The basis of the immortality of these lines is a temperature sensitive variation of the SV40 tumour antigen, which is unstable at 37-39°C, meant that the line can be differentiated by removing the γ INF and growing at a higher temperature. This was not required for any of the experiments documented here, but the lines association with the cochlea made them an ideal candidate for these early *in vitro* experiments.

All lines used for the experiments documented in this thesis were passaged in the same way. The media was first aspirated away, and then cells were first briefly rinsed with pre-warmed PBS. This was aspirated off, and pre-warmed trypsin-EDTA (0.05% trypsin with 0.5 mM EDTA pH 7.4 – Thermo Fisher Scientific, UK) was added to cover the cells. The flask was then placed back into their incubator and occasionally checked to see if the cells had detached. As soon as all cells had detached from the surface, with gentle tapping if required, a volume of media equal to that of the trypsin was added. The cells were then briefly mixed with the media using a stripette which facilitated cell separation to prevent the accidental selection of colonies and deactivated the trypsin due to the serum in the media. Cells were then centrifuged in a 15 ml falcon tube for 3 minutes at 300 x g on a table top centrifuge. The media and trypsin was removed by aspiration and the cells were then resuspended in suitable growth media, which could then be distributed between different flasks as required.

In order to freeze cells in liquid nitrogen, while maintaining acceptable viability, a suitable amount of cells were first passaged as normal, but instead of normal media the cell pellet was resuspended in 1 ml of freezing media (90% FCS and 10% dimethyl sulfoxide (DMSO) v/v). Cells were then transferred immediately into a cell freezing container

(CoolCell, Merck, UK) and placed into a -80°C freezer and left to gradually freeze overnight. The vials could then be transferred directly into liquid nitrogen for long term storage, and thawed as above then necessary.

2.3.2 – Electroporation

All the electroporations used in this work were performed using the Neon Transfection System (Thermo Fisher Scientific, UK). Firstly, the protocol started as the normal passage procedure outlined above, but upon resuspension in the media the cell density was measured using a haemocytometer. The cells were then centrifuged at 1000 rpm for 3 minutes, the media was aspirated and the cells were washed with 4 ml of PBS. The centrifugation step was then repeated and the cells were resuspended in PBS to a density of 5×10^6 cells/ml. The cells were then ready for the electroporation step, and the electroporation was carried out in either a 10 μl or 100 μl capacity tip, depending on the experiment. For the smaller volume tip 11 μl of cell suspension was mixed with 1 μg of DNA, pulled into the electroporation tip and then electroporated with 2 pulses of 1,150 V for 20 ms in a chamber filled with buffer E (included in the kit). For the larger tip volume, 110 μl of cell suspension (5×10^7 cells/ml) was mixed with 10 μg of DNA, pulled into the tip and electroporated using a different protocol (1350 V in two 20 ms pulses) in buffer E2. In both cases, the electroporated cells were then placed immediately into pre-warmed media (33°C) containing no antibiotic and left to incubate overnight before fixation or lysis collection.

2.3.3 – Cell immunofluorescence

In order to obtain cell coverslips for imaging, cells were seeded into 6 well plates containing a suitable number of sterile coverslips at a density of 1×10^5 /well. The cells were then left to settle overnight before being subjected to three rinses with cold PBS to remove the media followed by immediate fixation with 4% PFA in PBS for 10 minutes at room temperature. The cells were then permeabilised with 0.1% triton x-100 for one minute, and then rinsed three times with cold PBS. Coverslips were then removed from the 6-well plate and blocked with blocking buffer (5% FCS and 3% BSA in PBS) for one hour. This stage and the following antibody incubation stages were performed by inverting the coverslips

onto a 10 μ l droplet on a parafilm base in a humidified chamber, to reduce antibody and buffer usage. The coverslips were then placed onto droplets of suitably diluted primary antibodies (**Appendix 2.1**) in blocking buffer and incubated for two hours at room temperature. Coverslips were then rinsed six times in PBS, before being immediately placed onto a droplet containing suitably diluted Alexa secondary antibodies (Usually 1:1000, **Appendix 2.1**) in blocking buffer and left to incubate for an hour at room temperature. The coverslips were then rinsed six times in PBS and mounted using hydromount (National Diagnostics, with added 1% w/v DABCO and 1 μ g/ml DAPI).

2.3.4 – Cell lysate collection

In order to collect cell lysates, the growth media was aspirated and the cells were rinsed twice with ice cold PBS. All the PBS was then aspirated before the addition of a suitable volume of RIPA-lysis buffer (50 mM tris-HCl pH 7.5, 150 mM NaCl, 1 mM EGTA, 1 mM EDTA, 1% triton x-100 v/v, 0.5% sodium deoxycholate, 0.1% SDS, 1 mM sodium azide and 1x protease inhibitor cocktail (cOmplete, EDTA-free protease inhibitor cocktail, Roche) which was added fresh). The cells were then scraped into a single corner and transferred into an Eppendorf tube on ice, where they were sonicated twice for 10 seconds in order to break up any remaining cells and shear the DNA. The lysate was then centrifuged in a pre-cooled rotor at 15000g for 15 minutes. The supernatant was then pipetted off and aliquoted as necessary before long term storage at -20°C.

2.4 – Biochemistry and molecular biology techniques

2.4.1 – SDS-PAGE

In order to create the two-stage gels employed for protein electrophoresis, we first created the resolving gel working solution. For each gel this solution was composed of 4.15 ml of 30% acrylamide bis-acrylamide stock (Severn Biotech), 3.75 ml resolving gel stock (1.5 M tris, 0.4% SDS, pH 8.8) and 2 ml of water. In order to start the polymerisation the gel, 5 μ l of tetramethylethylenediamine (TEMED) and 100 μ l of 10% ammonium persulfate (APS) in water were added. Following mixing by inversion the solution was then transferred into the 1mm gel cast (Biorad), covered with a layer of isopropanol to remove bubbles, and left

to set for an hour. Following this, 5 ml of stacking gel solution was mixed, comprising 0.8 ml 30% acrylamide bis-acrylamide stock (Severn Biotech), 0.625 ml gel stock (1 M tris, 0.75% SDS, pH 6.8) and 3.525 ml of water. Again, to set the gel, 15 µl of TEMED and 50 µl of 10% APS was added. The tube was then inverted as before and, following removal of the isopropanol and washing with water, added to the top of the resolving gel layer. The 15-well comb was then placed into the cast and the gel was left to fully set for another 30 minutes.

In order to prepare the samples for electrophoresis, they were first boiled at 95°C for five minutes with added Laemmli sample buffer from a 2x stock (20% glycerol, 100 mM Tris pH 6.8, 4% SDS, 0.2% bromophenol blue, 2% β-mercapto-ethanol). The samples were then briefly cooled to room temperature and then run on the gel at 150 V until the dye-front formed by the bromophenol blue reached the bottom.

2.4.2 – Coomassie staining

Gels designated for Coomassie staining were, following removal from the tank and glass plates, placed directly into methanol based Coomassie stain (0.5 g Coomassie R250 and 100 ml of acetic acid in 1 litre of water) and left to stain for an hour on a rocker. The staining solution was then replaced with de-stain (10% acetic acid and 40% methanol in water) and incubated on a rocker for an hour. At this point, if the bands on the gel were clearly visible and the contrast was good, the gel could be immediately imaged. If required, de-stain could be refreshed, and the gel could be further incubated on the rocker until the image quality improves.

2.4.3 – Western blot

In order to transfer the proteins from the SDS gels to a suitable membrane for antibody probing the necessary components of the transfer tank were first soaked in 1x Towbin (14.40 g of glycine, 3.03 g of tris and 20% methanol in water). This included two pieces of filter paper, three sponges and a piece of PVDF membrane (Immobilon-P, Merck) which is first activated by rinsing with pure methanol. The transfer tank was then assembled in the following order: 2x sponge, filter paper, PVDF membrane, gel, filter paper, sponge. This

assembly was then clamped together and placed in the correct orientation in the BioRad transfer tanks, which was then filled with 1x Towbin and an icepack to prevent heat build-up. The tank was then connected to a powerpack and subjected to 100 V for 75 minutes. The tank was then disassembled and the membrane placed into a falcon tube, where it was then rinsed with TBST before being placed directly into blocking buffer (5% w/v skimmed milk powder in TBST) and left to incubate on a roller for one hour. Following this incubation, the buffer was then swapped with a primary antibody (**Appendix 2.1**) containing solution, in which the antibody was diluted in blocking buffer. After incubation of one hour at room temperature, or overnight at 4°C, the membrane was rinsed three times with TBST and then washed three times for 10 minutes in TBST. The secondary antibody (**Appendix 2.1**) containing buffer was then swapped into the tube, also diluted in blocking buffer, and left to incubate for one hour at room temperature. The membrane was then rinsed and washed with TBST as before, and then developed by the application of ECL western blotting detection reagent (Amersham, GE Life Sciences). The membrane was then imaged on a Bio-Rad ChemiDoc XRS+ system using a cumulative western blot protocol. The exposure times were adjusted after the first image was collected, and exposures ranged from a minute to half an hour, depending on the antibody. The resulting images were then processed with Image Lab Software as necessary.

2.4.4 – Western blot membrane stripping

In order to reuse and re-probe western blot membrane, we utilised the Abcam mild stripping protocol (Abcam 2013). Used blots were placed directly into stripping buffer (7.5g glycine, 0.5g SDS and 5 ml tween-20 in 500 ml of water, pH 2.2) on a roller for 15 minutes. This was then repeated with fresh buffer, and the membranes were then washed twice for 10 minutes in PBS. Following this, the membranes were washed twice for 5 minutes in TBST, and were then ready to be blocked and re-probed as before.

2.4.5 – Silver staining

Following SDS-PAGE, gels to be used in silver staining were first washed for 30 minutes in a solution of 20% methanol and 10% acetic acid in water. The gel was then washed three times for 15 minutes in 50% methanol in water and incubated with the silver staining

solution for 20 minutes. This solution was composed of 0.076% sodium hydroxide, 70mM ammonium hydroxide, 1% silver nitrate in water. The gel was then washed twice for 10 minutes in water and then developed with 0.02%PFA and 0.5% citric acid in water until the signal was at a suitable level. This reaction was then halted with a wash of 50% methanol and 10% acetic acid in water. The resulting gel was the imaged on a Bio-Rad ChemiDoc XRS+ system using a standard visible light protocol.

2.4.6 – SPOT arrays

Custom Celluspot arrays (Intavis) representing the intracellular tail of β DG (**Appendix 2.4**, Thompson *et al.* 2010, James *et al.* 2000) were probed in a manner similar to that used for a western blot membrane. The arrays were blocked for an hour in 5% skimmed milk powder in TBST and then incubated with the GST-tagged SH3 domain of interest at a concentration of 20 μ g/ml in blocking buffer for 2 hours. The array was then subjected to three rinses and three 5-minute washes with TBST and incubated with the primary antibody for one hour. The array washed as before, incubated with horse radish peroxidase (HRP) secondaries (**Appendix 2.1**) in blocking buffer for an hour, washed a final time with TBST, and then developed with western blot ECL solution (Amersham). Images were collected on the Bio-Rad ChemiDoc XRS+ system with a cumulative exposure protocol, and then processed with Image Lab Software.

2.4.7 – SPOT array stripping

In order to strip for reuse, the SPOT arrays were first washed three times for 10 minutes with water, and then incubated with stripping buffer A (8% Urea, 1%SDS and 0.5% beta-mercaptoethanol in water) for 30 minutes at 50°C. The arrays were then washed three times for 10 minutes each with buffer B (50% ethanol and 10% acetic acid in water), followed by three washes of 10 minutes with 100% ethanol. From this point, the arrays were air dried and then placed in a 50 ml falcon for further use after a brief wash with TBST, or immediately rinsed with TBST for faster reuse.

2.4.8 – DNA electrophoresis

For all DNA electrophoresis to check plasmid size or insert size, the DNA was first digested with a suitable enzyme and buffer combination (NEB) for one hour at 37°C. The samples were then mixed with 6x loading dye (50% glycerol and 0.15% orange G in tris-acetate EDTA (TAE) buffer – from 50x stock [242 g tris, 57.1 ml glacial acetic acid and 100 ml 500 mM EDTA pH8, brought up to 1L with dH₂O]) and were then ready to run. The gel was composed of either 0.8% or 1.5% agarose in TAE, depending on the size of the DNA fragment, and heated in a microwave until entirely dissolved. The gel was then allowed to cool until it could be comfortably handled. At this point 30 ml of gel was mixed with 1 µl of 10mg/ml ethidium bromide in a falcon tube, and transferred into the gel mould. Once the gel was entirely set the samples could be run at 100 V until the orange G band had migrated approximately halfway through the gel. The resulting gel was then imaged on a Bio-Rad Chemi-Doc XRS+ with a UV protocol.

2.4.9 – Plasmid cloning

In order to generate pcDNA3.1MycHisB(-) mammalian expression vectors of the EPS8L2 and EPS8L3 SH3 pGEX-4T1 vectors, kindly provided by Kalle Saksela (Kärkkäinen *et al.* 2006), the SH3 domain of the codon optimised sequence was copied from the original plasmids via PCR. To do so, 1µl of miniprep (Qiagen) purified plasmid was mixed with 1.25 µl of 10 pmol forward and reverse primers containing BamHI and HindIII restriction sites respectively (**Appendix 2.2**). This was then mixed with 2x Phusion High-Fidelity PCR Master Mix (Thermo Fisher Scientific, UK) and water to a final volume of 25 µl. The mix was then placed in a thermocycler and the DNA fragment was amplified with 35 cycles of PCR (**Appendix 2.2**) and run on a 1.5% agarose gel to check the fragment size and remove the PCR components. These DNA bands were then excised from the gel under a UV light and purified from the agarose using a gel extraction kit (Qiagen). Both the amplified L2 and L3 SH3 fragments as well as the pcDNA3.1MycHisB(-) target vector were digested with BamHI and HindIII restriction enzymes (1 unit per µg of DNA for 1 hour at 37°C in CutSmart buffer, New England Biolabs). The linearized target vector was then run on a 0.8% agarose gel and purified from the gel as before to remove the small excised fragment. The SH3 fragments were then ligated into the target vector in a 20 µl reaction incubated at 25°C for 2 hours and 30 minutes with the following components: 2 µl

10x T4 ligase buffer (New England Biolabs), 10 µl SH3 PCR fragment (L2 or L3), 1 µl linearised pcDNA3.1MycHisB(-) target plasmid, 1 µl T4 ligation enzyme (New England Biolabs) and 6 µl ddH₂O. Following the ligation, 10 µl of ligated plasmid was used to transform chemically competent *E. coli* (DH5α, section 2.2.3), from which the final vectors were amplified (Section 2.2.2) and checked via sequencing.

2.4.10 – GST pull-down

In order to first pre-clean lysates for pull-down, one T75 flask worth of E36 cell lysate was collected as above for each pull-down in RIPA buffer with protease inhibitors. To pre-clean the lysate, 30 µl of glutathione sepharose 4B (Thermo Fisher Scientific, UK) beads were washed three times in 1 ml of cold PBS, and each time separated via centrifugation at 500 x *g* for 1 minute at 4°C. After the removal of the final wash of PBS, the cell lysate was transferred into the Eppendorf containing the beads and incubated at 4°C on a roller for two hours. The lysate was then removed from the beads after centrifugation as before, and mixed with 300 µg of the GST linked “bait” protein and 50 µl of pre-equilibrated glutathione beads. This mixture was incubated at 4°C for two hours on a turner before separation via centrifugation, after which the supernatant was extracted and stored at -20°C. At this point, a 10 µl sample of the beads was taken and stored at -20°C, and the remaining beads were washed three times with ice cold PBS with a 10 µl sample taken after each centrifugation. To visualise the pull-down, 5 µl of the supernatant and each bead sample was run on a western blot (as described above) and probed for βDG before stripping and reprobing for the “bait” GST protein tag.

2.4.11 – Co-immunoprecipitation

In order to carry out the electroporations for the co-immunoprecipitation experiments, two T175 flasks worth of E36 cells at ~80% confluency were electroporated with 10 µg of myc tagged EPS8, EPS8L2 or EPS8L3 in a 100 µl tip as described above. Some of the cells (approximately 10%) were then placed into a six well plate containing glass coverslips, to check efficiency via immunolabelling, and the rest was placed into a T75 flask with pre-warmed media. The cells were left to grow overnight, and any glass coverslips were fixed and immuno-labelled using the protocol described above. In order to collect the cell lysates

for the co-immunoprecipitation a different protocol for lysate collection had to be employed, as sonication can disrupt the binding we needed to preserve. To collect the lysates, the media was first aspirated and the cells were briefly washed with 10 ml ice cold PBS. This PBS was then aspirated, and replaced with 500 μ l of Co-IP buffer (20 mM tris-Cl pH 8, 137 mM NaCl, 1% triton X-100 and 2 mM EDTA) with fresh protease inhibitors (cOmplete, EDTA-free protease inhibitor cocktail, Roche). Using a cell scraper, the cells were scraped into a corner and transferred into an Eppendorf tube, which was then briefly vortexed and incubated at 4°C for 30 minutes on a roller. Following this, the solution was then centrifuged at 15000 x g for 15 minutes in a pre-cooled rotor, and the supernatant was stored in -20°C until needed.

On the day of the experiment, the lysates were thawed on ice while 50 μ l of protein A beads (Amintra, Expedeon) were equilibrated with three cycles of 1 ml washes in PBS followed by centrifugation at 800 x g for 1 minute. The PBS was then removed from the beads, and the whole lysate from one T75 of electroporated cells was added. This mixture was incubated at 4°C on a roller for one hour, and separated via centrifugation at 800g for 5 minutes. The resulting supernatant, and now a pre-cleaned lysate, was then mixed with anti-myc 1:100 (9E10, Invitrogen) and incubated at 4°C on a roller for 3 hours. After this incubation, 100 μ l of pre-equilibrated protein A beads were added to the solution, and left to incubate at 4°C for another hour. This mixture was then centrifuged at 800 x g for 5 minutes at 4°C, and 10 μ l samples of the supernatant and beads were taken. The beads were then washed three times with 1 ml of PBS and separated with centrifugation at 800 x g for 5 minutes, with another sample of the beads being taken between each step. The resulting samples of the supernatant and beads were then run on a 12.5% SDS-PAGE gel as described above, and probed on a western blot for β DG and the myc tag of the mammalian expression constructs.

2.4.12 – Buffer exchange

Whenever buffer exchange was required, such as clearing up purified antibodies or removing glutathione from GST purified proteins, the G25 (GE Healthcare) buffer exchange column was used as per the manufacturer's protocol. The column was first pre-equilibrated with 2 column volumes of the target buffer. Exactly 500 μ l of the protein sample (diluted if necessary to this volume) was added to the column and left to entirely

penetrate. The target protein was then eluted with the addition of another millilitre of the buffer of choice, and collected as it left the column as seven individual equal fractions. Each fraction was then quickly tested for protein content by adding 2 μ l of the fraction to a 50 μ l droplet of Bradford reagent, which allows for easy visualisation of the protein peak. The peak fractions were then pooled and the proteins frozen for later use.

2.4.13 – Protein A IgG purification

To purify rabbit IgGs, the pH of the crude sera was first adjusted with the addition of 1/10 volume 1 M tris-Cl pH 8. One millilitre of the sera was then passed through 1 ml of compacted protein A beads (Amintra, Expedeon) twice, in order to ensure the binding of the IgGs was complete. The flow through from this stage was kept, and the column bed was washed with 10 column volumes of 100 mM tris-Cl pH 8. The column was then washed a final time with 10 column bed volumes of 10 mM tris-Cl pH 8, and the bound IgGs eluted with 4 ml of 50 mM glycine pH 3 added in 0.5 ml steps. Each step was collected in a tube containing 1/10 column bed 1M tris-Cl pH 8 and stored separately, the peak fractions were then identified via spectrometry at 280 nm and then pooled.

2.4.14 – Antibody affinity purification

In order to create a column capable of specifically binding p β DG IgGs, 1.72 ml of compacted streptavidin beads (Amintra, Expedeon) was first equilibrated by washing three times with 10 ml of 0.5 M sodium phosphate pH 7.5, similar to the glutathione beads protocols. Then, 1.2 mg of the original immunisation peptide (biotin-KNMTPYRSPPpYVPP), which was enough to fully saturate the beads, was bound to the resin by incubation at 4°C for two hours on a roller in 0.5M sodium phosphate pH 7.5. The resin was then separated via centrifugation as before. The absorbance of the peptide containing solution was checked on a spectrometer at 280 nm before and after the incubation in order to ensure the peptide was entirely bound. The resin required for a single purification (100 μ l) was then washed twice with 10 ml of 0.5 M sodium phosphate pH 7.5 and once with 10 ml 1 M NaCl 0.05 M sodium phosphate pH 7.5, and the rest of the resin stored in the sodium phosphate buffer with 0.02% sodium azide. Next, to ensure that anything bound to the column at this stage could not be eluted with the steps to follow,

the column was subjected to all the solutions used for the affinity purification. First, the column was sealed and incubated with 1 ml of ethanolamine pH 7.5 for four hours at room temperature on a roller. The resin was then washed twice with 1 ml of PBS, followed by 1 ml of 10 mM tris-Cl pH 7.5, 1 ml of 100 mM glycine pH 2.5, 1 ml of 10 mM tris-Cl pH 8.8, 1 ml of fresh 100mM triethylamine pH 11.5 and enough 10 mM tris-Cl pH 7.5 for the pH to reach ~7.

The column was now ready for the affinity purification, and the peak fractions of the IgG purification protocol were applied. The column was then sealed with parafilm and incubated on a roller at 4°C for two hours to bind target antibodies. The column was then washed with 2 ml of 10 mM tris-Cl pH 7.5 and 2 ml of 500 mM NaCl 10 mM tris-Cl pH 7.5. The acid sensitive IgGs were eluted by adding 1 ml of 100mM glycine pH 2.5, sealing the column and then incubating at 4°C for an hour. This elution was then collected, and the column was washed with 10 mM tris-Cl pH 8.8 until the pH reached ~8. The base sensitive IgGs were then eluted by adding 1 ml 100 mM triethylamine pH 11.5 and incubating at 4°C on a roller for an hour. After this elution was collected the column was washed with 2 ml of 10 mM tris-Cl pH 7.5, sodium azide was added to 0.02%, and the resin was stored at 4°C. Both the acidic and basic elutions were combined, and buffer exchanged into PBS with 0.02% sodium azide. The peak fractions from the buffer exchange were checked via spectrometry at 280 nm, and pooled for further checks and validation.

2.4.15 – mRNA extraction and DNase I treatment

mRNA was extracted from DAG1^{-/-}xMYO15Cre^{+/+} control and DAG1^{-/-}xMYO15Cre^{+/-} knock-out animals using the Ambion RNAqueous 4PCR total RNA isolation kit, as per the manufacturer's instructions. In brief, whole cochleae were quickly dissected from 3 month old animals in PBS following cervical dislocation and decapitation as with the protocols discussed in earlier sections (2.1.1). These cochleae, minus the vestibular system, were placed into 200 µl lysis buffer (Included in the kit) in Eppendorf tubes and homogenised using a pestle, pre-cleaned with RNaseZap solution, three times for ten seconds. Another 200 µl of lysis buffer was added to each cochlea and the samples were then centrifuged at 15000 x g at 4°C for 3 minutes. Following this, 350 µl of each sample was removed and mixed with 350 µl of 64% ethanol, placed in a filter cartridge, and centrifuged at 15000 x g

for 1 minute. The filter cartridges were then washed with 700 µl wash solution 1 followed by another minute at 15000 x g, and washed 2 times with 500 µl of wash solution 2, with a similar centrifugation after each wash. The cartridges were then centrifuged again for 1 minute at 15000 x g to remove any residual wash solution. Following placement into a fresh collection tube, 60 µl of pre-heated elution solution (80°C) was added to each tube, left to incubate for 1 minute at room temperature, and then centrifuged at 15000 x g for 30 seconds. To ensure all mRNA was eluted, this same 60 µl of solution was run through the column a second time, followed by another 30 seconds at 15000 x g.

In order to carry out the DNase treatment (Included in the same Ambion kit) to remove any DNA contamination, 6 µl of DNase I buffer and 1 µl of DNase I was added to each sample and incubated at 37°C for 30 minutes. The DNase I was then deactivated with the addition of 6.7 µl of inactivation solution and incubation at room temperature for 4 minutes. The samples were then centrifuged a final time at 15000 x g for 90 seconds, placed into a fresh tube and measured for mRNA concentration with a NanoDrop.

2.4.16 – cDNA synthesis

cDNA was synthesised from purified mRNA using the high capacity RNA to cDNA kit (Applied Biosystems) as per the manufacturer's instructions. In brief, the 20 µl reaction was composed of 10 µl RT buffer, 1 µl enzyme mix and up to 9 µl of mRNA sample. The amount of mRNA added to each reaction was the same between samples (Up to 500 ng/reaction), and nuclease free water was added to bring the reaction volume to 20 µl as necessary. For each mRNA sample, a 10 µl reverse transcription (RT) negative reaction was set up with identical proportion, with the only difference being that instead of enzyme mix, water was added. The reactions were then vortexed, briefly centrifuged to collect the solution at the bottom, and incubated at 37°C for 60 minutes in a thermocycler, followed by 95°C for 5 minutes to inactivate. The cDNA was now synthesized and ready for use in the subsequent RT-PCR or RT-qPCR experiments.

2.4.17 – qPCR

In order to carry out the DAG1 knock-out validation qPCR on a 384 well plate, a standard curve created from one of the control cDNA samples was created for the DAG1 and HPRT qPCR primers, containing two repeats of non-diluted, 1:5, 1:25, 1:125, 1:625 and a dH₂O negative. Each reaction was 10 µl, and comprised; 5 µl Fast SYBR Green Master Mix (ThermoFisher Scientific), 1 µl cDNA (At a suitable dilution), forward and reverse primers (500 nM for HPRT and 200 nM for DAG1), and dH₂O up to 10 µl final volume. This qPCR acts to validate the primers, ensuring that a single product is created from the cDNA with a high efficiency, and the standard curve created is linear on a logarithmic scale, allowing for the quantities of unknown samples to be accurately extrapolated. Following the validation, the standard curves were recreated on a plate alongside three control and three dystroglycan knock-out animals, each possessing three technical repeats and a reverse transcription enzyme negative control. Results were then analysed via the $2^{-\Delta\Delta Ct}$ method described elsewhere (Livak and Schmittgen 2001). In brief, cycles to threshold (Ct) values for the housekeeping gene HPRT were subtracted from their respective DAG1 Ct values, to yield the ΔCt . One of the DAG1 Ct values was randomly chosen as the reference value, and this value was subtracted from all three biological repeats, yielding the $\Delta\Delta Ct$. This value was then substituted into $2^{-\Delta\Delta Ct}$ for each sample to give the final comparative value for the experiment, which allows for the comparison of DAG1 expression relative to the chosen reference sample.

2.4.18 – Statistical Analysis

The statistical significance of data was determined with either a Student's two-tailed unpaired t-test or, for ABR and DPOAE data that is non-parametric due to the amplitude limit of our system, a two-way ANOVA with Šidák's post-test. For all experiments, a P value of $P < 0.05$ was defined as the threshold for statistical significance. In all graphs presented here, the error bars represent the standard deviation of the data, and is plotted alongside the mean. In cases where ratiometric percentage data was statistically compared via a parametric test, the log to the base 10 of the percentages was used in the tests to compensate for the non-parametric nature of the data. Graphpad Prism 8 was used to carry out all statistical analysis.

Chapter 3 - Investigating the *in vitro* interaction of beta-dystroglycan and EPS8L2

3.1 – Introduction

It was previously identified in a human interactome screen that the SH3 domain of EPS8L2 is a potential interactor of β DG, binding specifically to the intracellular cytoplasmic domain (Thompson *et al.* 2008). While our knowledge of the complex present at the shorter rows of stereocilia is improving, exactly how EPS8L2 is localised to this location remains largely unknown. If β DG can in fact bind to EPS8L2 *in vitro* and is expressed in the organ of Corti, it opens up a possible role for localising or stabilising EPS8L2 to the shorter stereocilia tips alongside MYO15L (Fang *et al.* 2015), CAPZB (Avenarius *et al.* 2017), TWF (Peng *et al.* 2009) and gelsolin (Mburu *et al.* 2010).

In order to further investigate the possible interaction between β DG and EPS8L2, and attempt to determine whether an interaction occurs *in vivo*, we employed the use of peptide SPOT arrays representing the intracellular domain of β DG (Thompson *et al.* 2010). These arrays could then be probed with the GST-tagged SH3 domains of EPS8, EPS8L1, EPS8L2 and EPS8L3 kindly provided by Professor Kalle Saksela (Kärkkäinen *et al.* 2006). This allowed us to visualise whether there is a distinct binding domain for EPS8L2 on β DG, and whether this binding is specific to EPS8L2 only. However, the method does not allow for a quantifiable comparison of binding affinity, or an indication of whether the interaction still occurs in more complicated *in vivo* situations. As such, the next step was to attempt to pull dystroglycan from a cell lysate using the same GST-linked constructs.

The binding of SH3 domains to β DG has been well characterised before. Both Grb2 and vinexin bind through their SH3 domains to the PxxP SH3 interaction motif on the intracellular tail of β DG (Cavaldesi *et al.* 1999, Russo *et al.* 2000, Thompson *et al.* 2010). This binding motif on β DG overlaps with the PPPY motif which interacts with the WW domain of dystrophin, and as such the two interactions are inherently competitive (Yang *et al.* 1995, Moore and Winder 2010). Also, due to the overlapping nature of the motifs, both SH3 domains and the WW domains of dystrophin and utrophin are similarly disrupted by phosphorylation at Y890 (James *et al.* 2000, Ilsley *et al.* 2001). Therefore, although only phosphorylated dystroglycan was detectable in the organ of Corti, the literature suggests that this phosphorylation should block any possible interaction with the SH3 domain of EPS8L2. Thus we hypothesised that EPS8L2 possesses a distinct binding site on β DG at the PxxP motif which is blocked by Y890 phosphorylation.

3.2 – Results

3.2.1 – Investigating the binding site of EPS8L2 on the cytoplasmic region of β DG

Following GST purification of the tagged and codon optimised SH3 constructs, and consistent with the results obtained from the SH3 interactome screen (Thompson *et al.* 2008), SPOT arrays of the intracellular domain of β DG appear to indicate binding of EPS8L2 (**Figure 3.1**). The arrays cannot be used to quantify the binding relative to the other EPS8 family members, but the binding does appear to show a distinct proline rich consensus sequence, whereas other family members show a complete lack of any binding in the case of EPS8. While EPS8L1 did appear to show a distinct single binding sequence, difficulties in expressing EPS8L1 resulted in poor yields and the need to use a much more of the elution for each experiment, which may explain the poor signal seen in the array. EPS8L3 also showed consistent signal across the array, though the appearance of multiple sites makes the consensus binding sequences somewhat less convincing. It is worth noting that the exposure times for these experiments were not consistent, due to the innate variability in the signal intensity produced. Some arrays, such as EPS8L2, were over-saturated within a minute, whereas others such as EPS8L3 showed a much weaker signal and were exposed for the full 30 minutes. Also, some of the scans shown here show consistent binding of the biotinylated spot, which is an artefact caused by a newer batch of the α GST primary antibody, and not the expressed proteins. Secondary antibody only experiments also indicated no binding to the array (data not shown), suggesting that the signal seen in all but the biotinylated spot is facilitated by the GST-fusion products only. The GST only control experiment indicated no consistent binding across the three repeats of the array, and thus the binding seen in the other experiments is not an artefact of the GST tag.

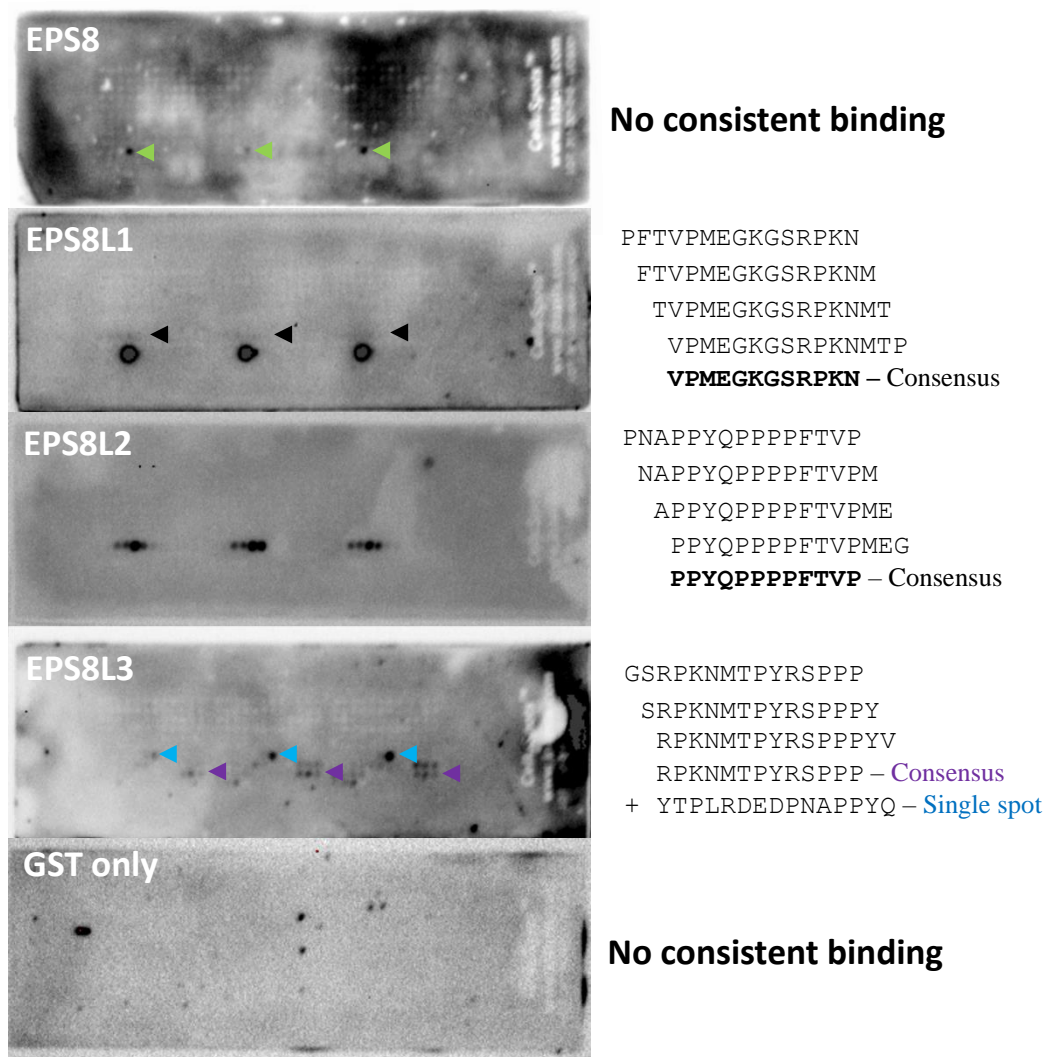


Figure 3.1 – The distinct binding site of EPS8L2 on the cytoplasmic tail of β DG – Peptide SPOT arrays representing the cytoplasmic tail of β DG (Thompson *et al.* 2010, James *et al.* 2000) probed with the GST fused SH3 domains of EPS8 (n=3), EPS8L1 (n=3), EPS8L2 (n=3), EPS8L3 (n=2) or GST only control (n=2) at 20 μ g/ml. Bound fusion products were revealed with α -GST 1:1000 primary and α -mouse HRP 1:10000 secondary antibodies. Each array possesses three repeats, and consensus sequences were obtained by determining which sequence is absolutely necessary for signal within a particular spot. Some of the scans show illumination of the biotinylated control spot across all three of the array repeats (Green arrow).

3.2.2 – Validating the VOT-N33 and E36 lines as sources of β DG and p β DG

Following the promising results of the SPOT array experiments, which appear to indicate a distinct binding site for the SH3 domain of EPS8L2 on the intracellular domain of β DG, we decided to further investigate this interaction by attempting a pull-down of β DG. This was performed with the same GST linked SH3 domains using a β DG and p β DG containing cell lysate. This not only determined whether the two proteins interact in a cellular context, but also provided a way to directly compare the binding affinities of the SH3 domains and confirm whether the phosphorylation of Y890 blocks the interaction as it does with Grb2 (Cavaldesi *et al.* 1999, Russo *et al.* 2000). Thus, in order to carry out these experiments it was necessary to identify whether the otic cell lines we had our disposal possessed a suitable content of both phosphorylated and non-phosphorylated β DG. Using cell immunofluorescence, both the N33 (**Figure 3.2**) and E36 (**Figure 3.3**) cell lines show comparable signal strength using antibodies for both Y890 phosphorylated (pY890 β DG antibody 1709 – pY890 Ab) and non-phosphorylated β DG (β DG monoclonal antibody Mandag2 – β DG Ab). In line with the literature, a particularly strong pY890 Ab signal could be regularly seen proximal to the nucleus (**Figure 3.2** and **3.3**, white arrow), consistent with the idea that phosphorylation canonically leads to internalisation (Sotgia *et al.* 2003). Western blots of the two cell lines indicated that both lines show strong signal at the expected size for β DG (43kDa) with both the β DG and pY890 antibodies (**Figure 3.4A** and **B** respectively). Using the housekeeping protein glyceraldehyde-3-phosphate dehydrogenase (GAPDH) as a loading control, quantification revealed that there was no significant difference in β DG or pY890 β DG expression between the two cell lines (**Figure 3.4C**). As such, both cell lines were deemed suitable for further experimentation as they could both act as a good source of phosphorylated and non-phosphorylated β DG. However, due to the fact that the E36 lines is derived from precursors of the organ of Corti, and thus possesses the ability to theoretically differentiate into hair cell cells, the E36 line was preferred over the neuronal N33 line. It is worth noting that neither cell line was able to replicate the expression seen in the organ of Corti, where β DG signal is entirely absent and only pY890 β DG signal is apparent (Heaney and Schulte 2003, Holley unpublished observations).

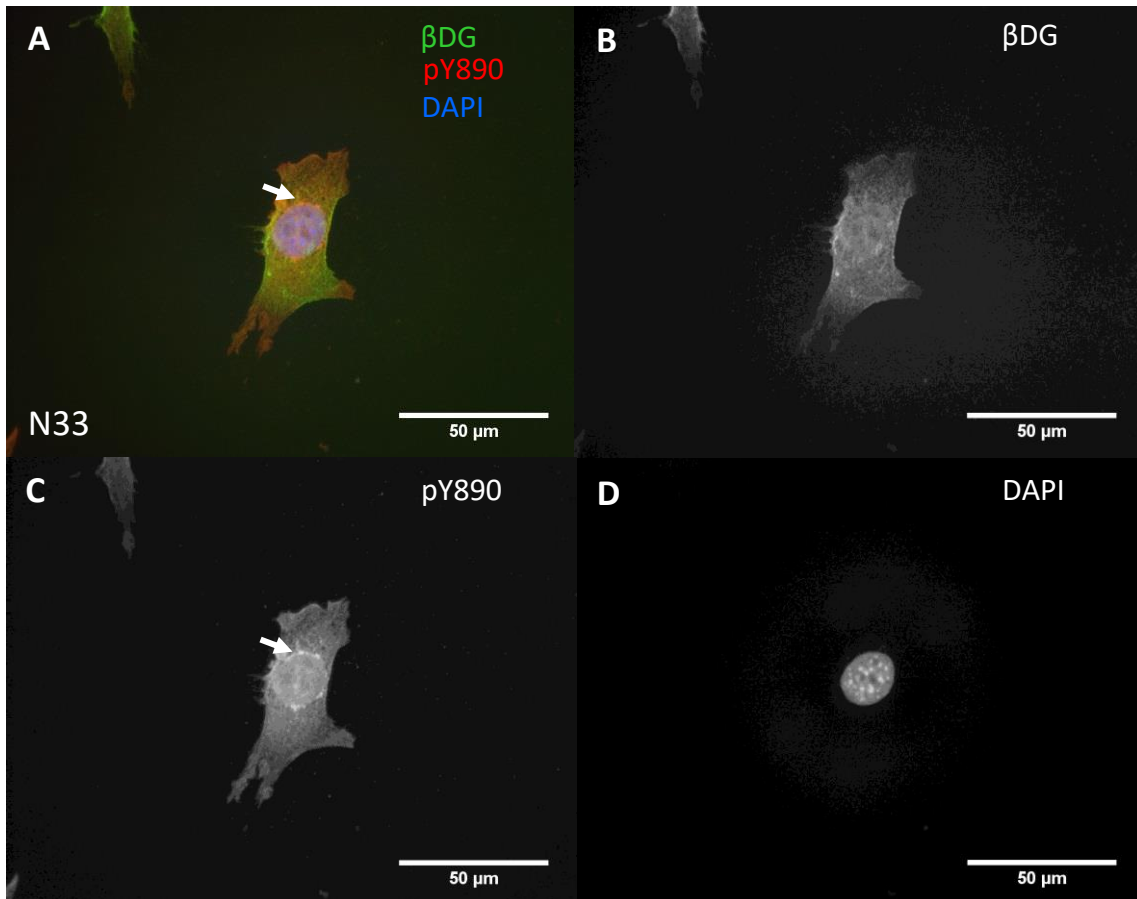


Figure 3.2 – Visualisation of phosphorylated and non-phosphorylated dystroglycan expression in the VOT-N33 cell line – Composite immunofluorescence of the N33 cell line (A) showing strong signal with both antibodies, indicating red pY890 Ab signal (C, 1:100) particularly proximal to the nucleus (white arrow) and more uniform green βDG Ab signal (B, 1:20). (D) DAPI 1μg/ml (blue) was used as a nuclear marker. This image is representative of three separate experiments.

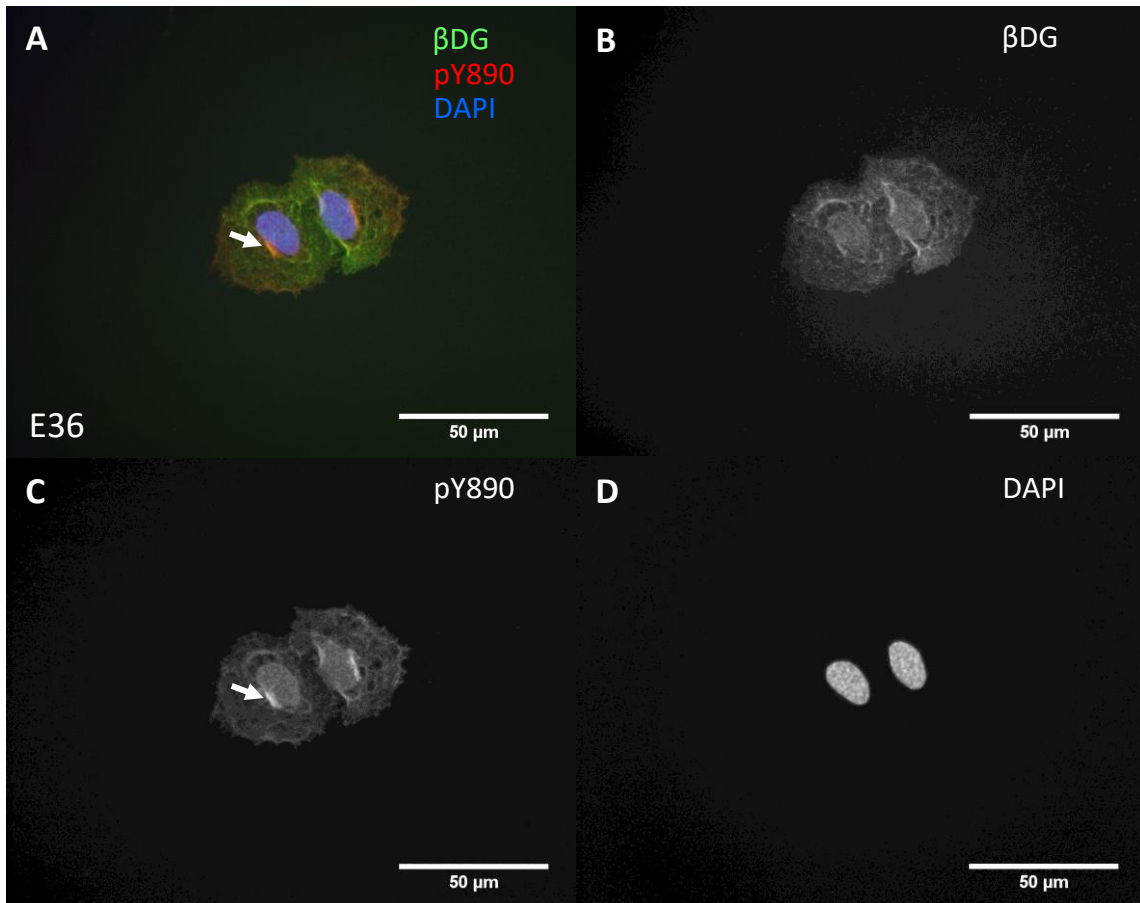


Figure 3.3 – Visualisation of phosphorylated and non-phosphorylated dystroglycan expression in the VOT-E36 cell line – Composite immunofluorescence of the N33 cell line (A), again showing strong signal with both antibodies, indicating red pY890 Ab (C, 1:100) signal particularly proximal to the nucleus (white arrow) and more uniform green βDG Ab (B, 1:20). (D) DAPI 1μg/ml (blue) was used as a nuclear marker. This image is representative of three separate experiments.

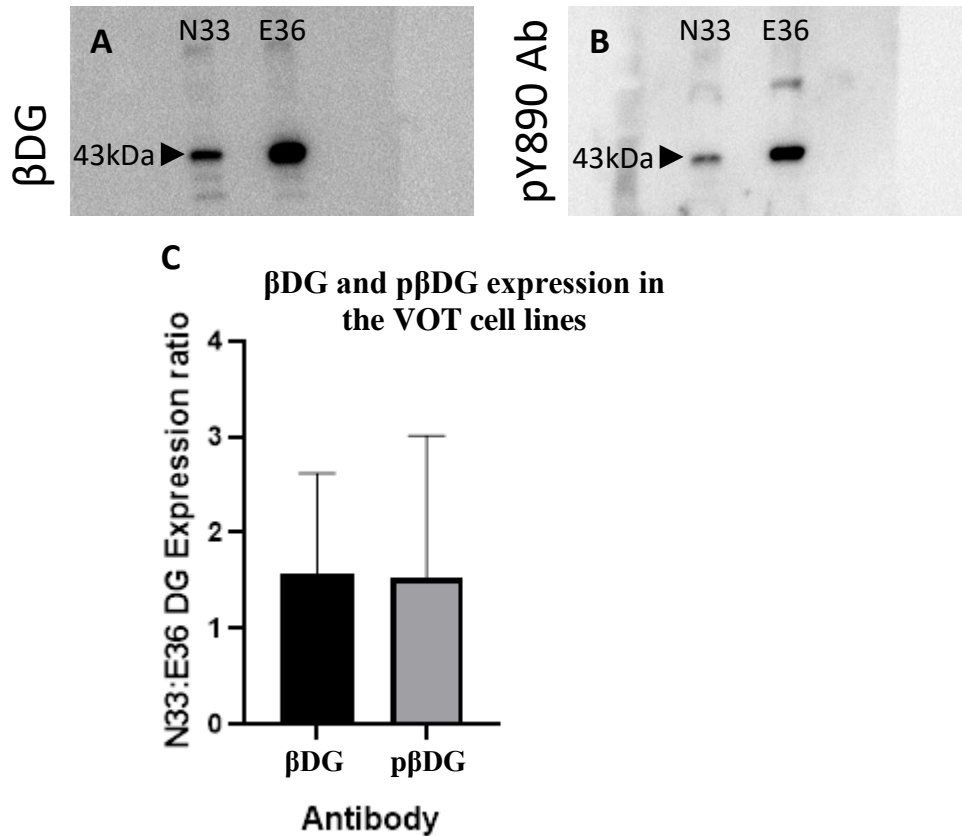


Figure 3.4 – Western blot quantification of the ratio of β DG to p β DG in the VOT-N33 and E36 cell lines – (A and B) Western blot of the two lines using β DG Ab (A, 1:200) and pY890 Ab (B, 1:500) in the VOT-N33 and E36 cell lines. (C) Expression ratio between the two lines, with GAPDH as the loading control. (n=3, P = 0.808, unpaired two-tailed Students t-test). Error bars represent the standard deviation. For the statistics the log to the base 10 of the data was used to permit the parametric assuming test.

3.2.3 – Pull-down of β DG using the GST-fused SH3 domains of the EPS8 family

With the cell line established as a source of both β DG and pY890 β DG, we could then use the E36 cell lysate to further investigate the potential binding between β DG and EPS8L2 and try to facilitate a pull-down of dystroglycan. This could be done using the same buffer exchanged bacterial GST constructs used for the SPOT array experiments, and the complex could be spun down using glutathione beads. Due to issues in the expression of the EPS8L1 SH3 domain, that construct could not be used in the pull-down experiments. Despite attempts at optimisation, the quantity of protein purified was always insufficient.

Western blot experiments with samples taken throughout the purification appeared to indicate a sequestering of the expressed protein into the pellet after the sonication step (data not shown).

As seen in **Figure 3.5**, the entire signal from both antibodies was lost from the beads following a single wash with ice-cold PBS. Though this appears to indicate that the binding seen between the SH3 domain of EPS8L2 and β DG in the SPOT arrays may not be strong enough to facilitate a pull-down, too many variables are present to make a definitive conclusion. The interaction could be behaving differently with the whole of β DG present, or β DG could be subject to competition for the SH3 domain and the binding affinity for β DG is weaker than the other potential binders. It is also possible that an error with the methodology meant that all proteins bound to the SH3 domain were eluted in the washing stage, and only the SH3-GST construct remained bound to the beads. Therefore, it was decided that we would simplify the system, and use only purified proteins to better reflect the conditions of the SPOT array.

Thus, a similar experimental protocol was performed again, but using 55.2 μ g of the purified cytoplasmic domain of β DG instead of a cell lysate. This particular amount was determined through western blot, as a concentration that would not over-saturate the western blot when running the 5 μ l bead sample used for the previous GST based pull-down. Notably, as this cytoplasmic dystroglycan was produced in bacteria the sample contains only non-phosphorylated β DG, and as such the pull-down was only probed with the β DG antibody. As seen in **Figure 3.6**, when using purified β DG for the pull-down, signal can be seen in the EPS8L2 SH3 lane that persists throughout all three washes with PBS. The GST probe, though of poor quality, indicates that there appears to be a comparable level of bait protein throughout the samples. The other SH3 domains do not show the same binding capacity, reflecting the results seen in the SPOT arrays.

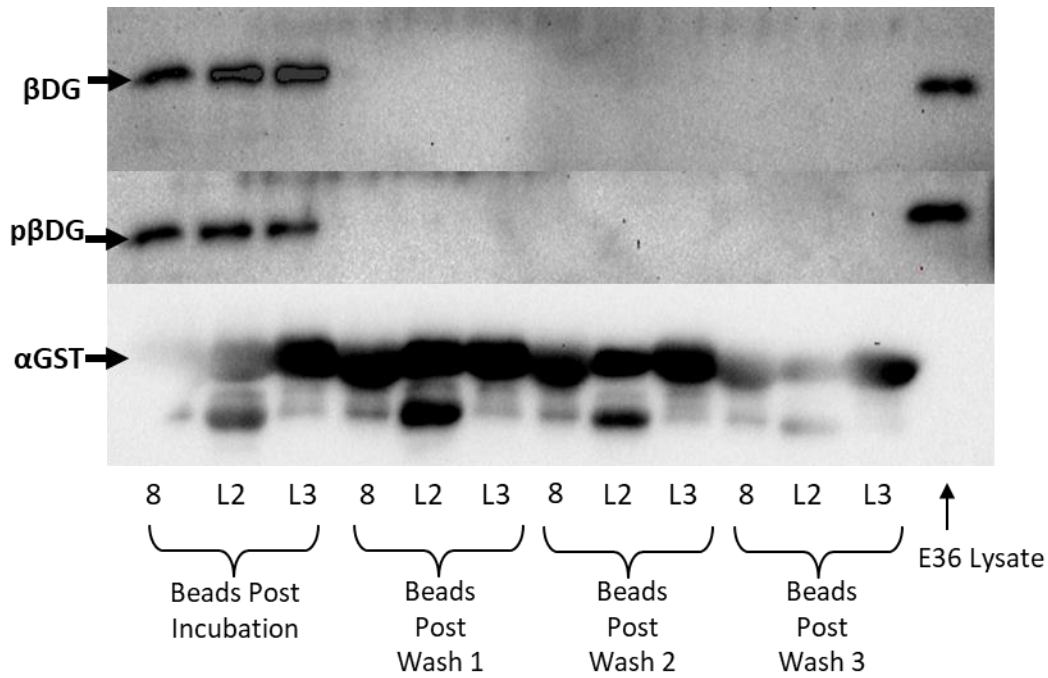


Figure 3.5 – Pull-down of β DG from the VOT-E36 cell line using the GST-fused SH3 domains of the EPS8 family – 5 μ l samples of glutathione Sepharose 4B bead slurry following the binding incubation period and throughout the subsequent washes. The amount of β DG and p β DG bound to the beads throughout the three washes of PBS was monitored using β DG Ab (1:200) and pY890 Ab (1:500) respectively. The final lane contains a sample of VOT-E36 lysate to act as a positive control for the dystroglycan antibodies. The same blot was stripped and re-probed with α GST (1:1000) in order to monitor the amount of GST-SH3 bound to the beads relative to the dystroglycan signal. This result is representative of three separate experiments.

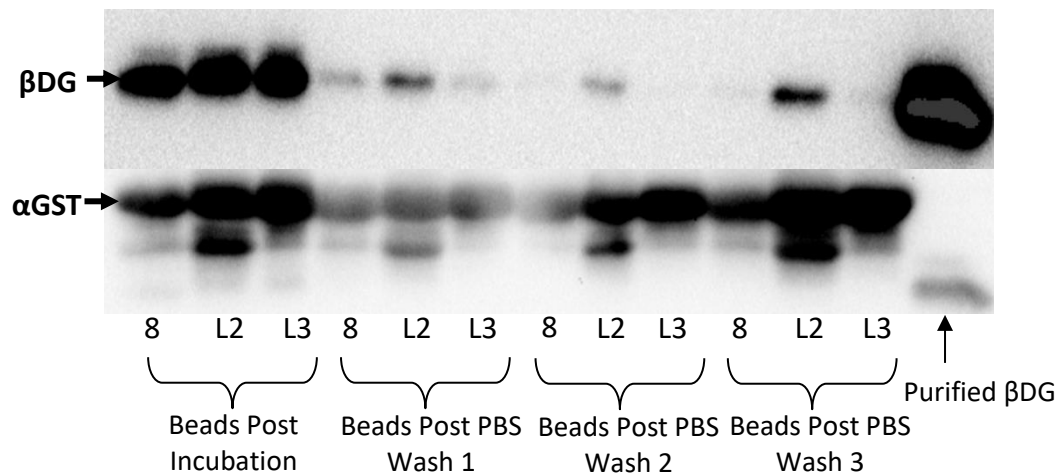


Figure 3.6 – Pull-down of the purified cytoplasmic tail of β DG using the GST fused SH3 constructs - 5 μ l samples of glutathione beads following incubation with 55.2 μ g of cytoplasmic β DG and 300 μ g of GST-SH3 domain throughout the PBS washes. The membrane was probed with β DG Ab (1:200), stripped, and then reprobed for GST (1:1000). The final lane contains a sample of the purified dystroglycan as a positive control for the antibody. As before, the amount of bait protein needed for this experiment was more than could be harvested from the EPS8L1-SH3 purifications. This result is representative of three separate experiments.

3.2.4 – Creating mammalian expression vectors of the EPS8 family SH3 domains and using them for the co-immunoprecipitation of β DG

In order to re-attempt the pull-down of β DG under more physiological conditions, we first generated mammalian expression construct versions of the bacterial EPS8L2 and L3 SH3 domains. This allows for the expression of the constructs in the cells without the need to use SH3 domains created in bacteria as bait, and provides a more physiological context to determine whether β DG and EPS8L2 bind *in vivo*, with EPS8L3 acting as the negative control. Full length versions of myc-EPS8 and HA-EPS8L1 were kindly provided by Kalle Saksela (Kärkkäinen *et al.* 2006). Firstly, the SH3 domain was amplified from the pGEX-4T1 using the PCR protocol detailed above (Section 2.4.9), using primers that would integrate a HindIII and BamHI cut-site (**Appendix 2.2, Figure 3.7A**). This fragment, and the target pcDNA3.1MycHisB(-) vector, were then both digested with HindIII and BamHI before ligation. The presence of the ligated fragment was then checked with a second double digest (**Figure 3.7B**), and the vectors that showed successful ligation were checked via sequencing from the T7 promoter. Following the sequencing, one of each validated construct was used in a test electroporation to ensure expression of the Myc tag (**C, D and E**). The efficiency of the electroporations seemed highly variable, but the constructs all demonstrated that they could induce expression of the Myc tag in the VOT-E36 line.

Due to the fact that the EPS8 and EPS8L1 constructs were full length, it was decided that the SH3 only L2 and L3 constructs would be used for the preliminary co-immunoprecipitations (Co-IPs). After electroporation of the Myc tagged mammalian expression constructs into the VOT-E36 cell line, the pre-cleared lysates were incubated with α Myc (1:100) and subjected to the PBS washing steps with samples of the beads taken at every step. As seen in **Figure 3.8**, the β DG signal in the EPS8L2 lanes appear to indicate no difference in binding compared to the EPS8L3 lane. However, no β DG signal was evident in the lysate lanes which was surprising given the amount of cells used, and when probing for the Myc tagged construct no signal could be identified at the expected size of 8kDa (data not shown).

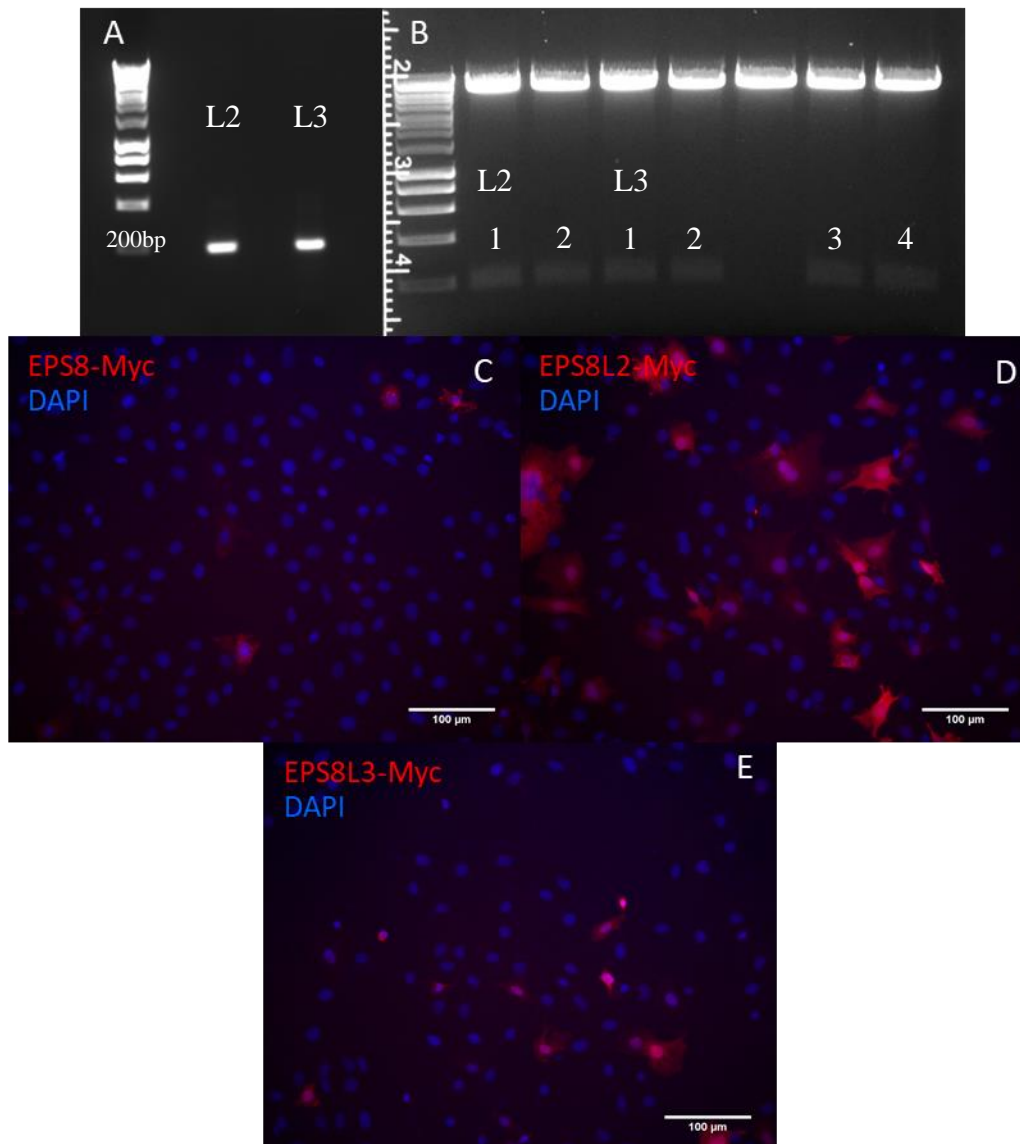


Figure 3.7 – The creation and validation of the mammalian EPS8 SH3 expression constructs – (A) The 200bp SH3 domain of the bacterial EPS8L2 and EPS8L3 GST fusion constructs was amplified via PCR as described earlier and run on a 1.5% agarose gel. Following digestion of the fragments and the linearization of the pcDNA3.1MycHisB(-) target vector, the final construct was ligated. (B) Test double digestion of the transformed constructs indicated most of the bacterial colonies had taken up the successfully ligated plasmid, termed 1-2 for L2 and 1-4 for L3. Test electroporation of the EPS8 (C), EPS8L2 (D) and EPS8L3 (E) constructs into the E36 cell line immunostained for Myc tag expression (α Myc 1:100, red) alongside a DAPI nucleus marker (1 μ g/ml, blue).



Figure 3.8 – Co-immunoprecipitation of β DG from the electroporated E36 lysates - 5 μ l samples of protein A beads following co-immunoprecipitation of β DG from E36 lysate using an α Myc antibody (1:100) and the SH3 domains of EPS8L2 and L3. Identification of any β DG (β DG Ab 1:200) band is difficult, as both this antibody and the α Myc used for the co-IP are from mice.

3.3 – Discussion

The two lines at our disposal for these *in vitro* experiments were the VOT-E36 and VOT-N33 immortal lines (Lawoko-Kerali *et al.* 2004). The VOT-E36 line corresponds to sensory and non-sensory progenitors of the cochlear sensory epithelia, derived from the Immortomouse, and as such theoretically possesses the capacity to differentiate into hair cells (Jat *et al.* 1991, Rivolta and Holley 2002). The second line, VOT-N33, represents progenitor cells that would have gone on to become neurons of the spiral ganglion, which are responsible for hair cell afferent innervation (Lawoko-Kerali *et al.* 2004). The immortality of both cells is maintained by the expression of a temperature sensitive version of the SV40 virus large T-antigen and gamma interferon (Lawoko-Kerali *et al.* 2004). Therefore, if required, gamma interferon can be removed from the media and the temperature can be raised from the maintenance level of 33°C to 37°C to induce differentiation. However, for the experiments planned, we simply required a supply of the same phosphorylated dystroglycan that was detected within the organ of Corti. This allows for pull-down experiments using normal cell lysates as a source of DG and allows us to further investigate the possible binding between β DG and EPS8L2.

The results in this chapter appear to indicate that EPS8L2 may bind to the intracellular domain of β DG in simple purified situations. In the SPOT arrays, GST pull-downs of purified cytoplasmic β DG, and the original SH3 interactome screen, the two do appear to bind. However, in more complicated scenarios such as pull-downs or co-immunoprecipitations from cell lysates, this binding is not apparent. Whether the two no longer bind due to competition, or a possible modification on dystroglycan occurring in the lysates is unknown. No modifications have been reported on the cytoplasmic tail of dystroglycan in the region of 860-870 in humans or mice (Bateman 2019), highlighted as the consensus sequence for the binding of EPS8L2 by the SPOT arrays. It is possible a modification proximal to the site could influence the binding when considering the secondary structure. However, more work is needed in order to determine whether modification or competition is preventing the binding of the two.

Notably, the consensus sequence for the binding of EPS8L2 and β DG is entirely separate from the phosphorylation site, and EPS8L2 does not appear to show any binding to the phosphorylated peptide fragment in the SPOT arrays. Also, the successful GST pull-downs were of cytoplasmic β DG produced in bacteria, and therefore did not contain any

phosphorylated β DG. Thus, we cannot conclude whether the Y890 phosphorylation of β DG affects the interaction with EPS8L2, and further experiments would be needed to make a definitive conclusion. For example, the purified intracellular domain β DG pull-down using the GST linked SH3 domains could be performed alongside a Y890 phosphomimetic version of β DG. We should then theoretically be able to see whether the presence of phosphorylation affects the binding of EPS8L2 as it does with Grb2 (Cavaldesi *et al.* 1999, Russo *et al.* 2000). Because of the difficulties in obtaining clear evidence for the *in vitro* interaction, the possibility of the interaction was further interrogated with signal localisation experiments detailed later.

Due to our inability to detect any of the myc-tagged SH3 domains in western blots, either due to issues with electroporation efficiency or a general lack of cells, the negative results of the co-immunoprecipitation should be considered unreliable. Due to the presence of the myc signal in the immunofluorescence, and the sequencing data indicating that the construct is indeed intact (data not shown), the construct does appear to express correctly. If this particular experiment was to be repeated, more time would be spent in optimising the electroporation in order to ensure a decreased variability in transfection efficiency. However, due to results that will be discussed in later chapters, the outcome for this experiment became a less crucial piece of the puzzle, and as such spending further time on this particular area of the project was deemed inefficient.

Had the binding between β DG and EPS8L2 been apparent, this could have opened up a role for dystroglycan at the tips of the shorter rows of stereocilia, alongside TWF2, CAPZB and Gelsolin (Furness *et al.* 2013, Peng *et al.* 2009, Avenarius *et al.* 2017, Mburu *et al.* 2010). At this location, dystroglycan could have perhaps functioned to link the underlying actin effector proteins, and thus the force of actin polymerisation, to the overlying membrane (**Figure 3.9**). By binding to EPS8L2, which is initially localised to this site via the specialised motor proteins MYO15L, β DG could have perhaps also acted to maintain EPS8L2 at this specific site by preventing protein diffusion (Fang *et al.* 2015). Thus, if dystroglycan was lost, we would not expect EPS8L2 to be entirely absent from this site, but present at a lower intensity and possibly resulting in a milder version of the progressive hearing loss seen in the EPS8L2 knock-out model (Furness *et al.* 2013).

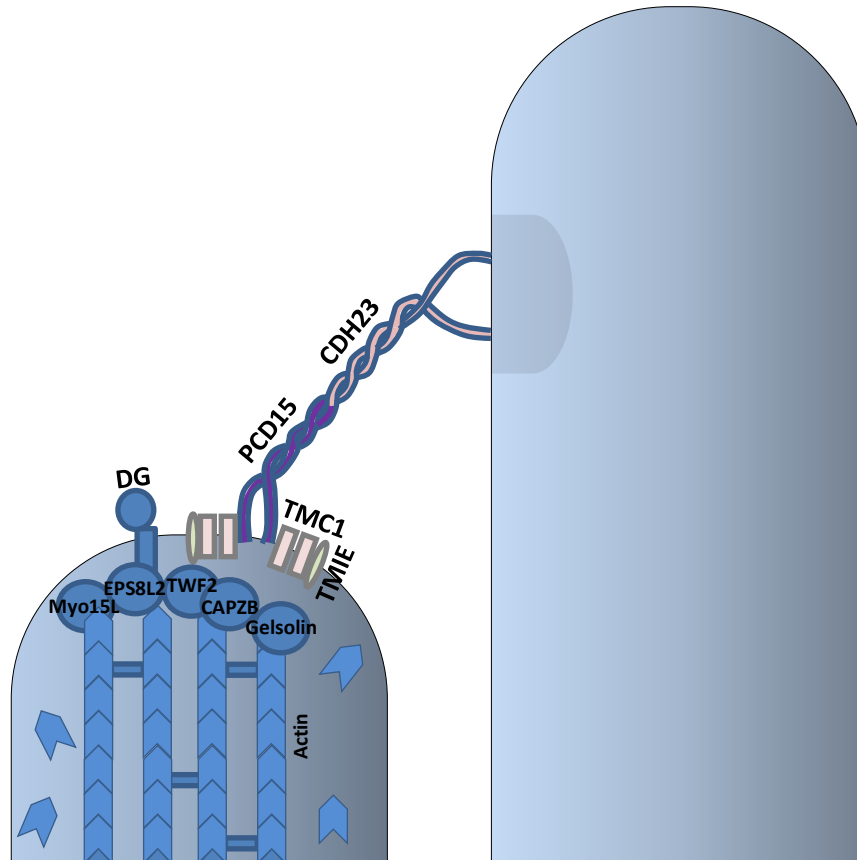


Figure 3.9 – Theoretical role of β DG at the shorter rows of stereocilia – If β DG bound to EPS8L2 *in vitro*, this could have perhaps indicate a role for β DG in maintaining EPS8L2 at the shorter rows of stereocilia alongside the other members of the row 2 complex. As MYO15L is responsible for the initial localisation of EPS8L2, we would expect the relative amount of the actin capper to decrease in a DG knock-out, with some correctly localised proteins remaining. In this model, exactly how β DG would localise specifically remains unknown.

Chapter 4 - Investigating the expression and distribution of phosphorylated beta-dystroglycan in the cochlea using the Y890 phospho-specific antibody

4.1 – Introduction

Previous reports have concluded that α DG, but not β DG, is present within the organ of Corti (Heaney and Schulte 2003). This is peculiar, as both subunits are translated together as a single precursor polypeptide which is separated via an early autoproteolytic cleavage (Ibraghimov-Beskrovnaya *et al.* 1992, Akhavan *et al.* 2008). Thus, if only the alpha subunit was detected as present, this would either suggest that the beta subunit is immediately degraded or the antibody initially used for β DG localisation was not able to properly detect the protein. Phosphorylation of β DG at the Y890 residue is known to prevent the binding of commonly used antibodies such as Mandag2 (Pereboev *et al.* 2001). When an antibody specific for Y890 phosphorylated β DG (pY890 Ab 1709, Ilsley *et al.* 2001) was used to stain cochlea sections, the resulting signal was both within the spiral ganglion projections and the organ of Corti itself (**Figure 4.1**, Matthew Holley unpublished). This raises the possibility that β DG is in fact present within the organ of Corti, but exists only in a phosphorylated state. These preliminary experiments were performed on cryostat sections and utilised simple light microscopy, and thus the first stage in a further investigation was to use confocal immunofluorescence microscopy to define the localisation of the pY890 Ab signal. By using Zeiss LSM 880 confocal Airyscan super-resolution alongside immunolabelling, it is possible to identify from which stereocilia row an immunofluorescent signal is originating. One particular area of interest was the tips of the shortest rows of stereocilia, where EPS8L2 resides (Furness *et al.* 2013). If pY890 Ab signal was present at this location, it would further support the hypothesis that the two may be interacting to somehow facilitate normal stereocilia development or maintenance. Alongside this work, a second aspect of the original hypothesis is a proposed role for dystroglycan in the formation and maintenance of ribbon synapses. In the retina, α DG, β DG and dystrophin accumulate at the synaptic cleft to facilitate normal synapse kinetics and terminus invagination (Omori *et al.* 2012). Thus, staining whole mount sections of the cochlear sensory epithelia should reveal whether the components also accumulate at the cochlear ribbon synapse. Any function this accumulation plays at the cochlear synapse was then investigated using a conditional DAG1 knock-out mouse. By analysing the auditory brainstem response (ABR) waveforms

and using immunostaining to investigate ribbon number and alignment with the post-synapse, any potential role for dystroglycan in ribbon synapses can be fully investigated.

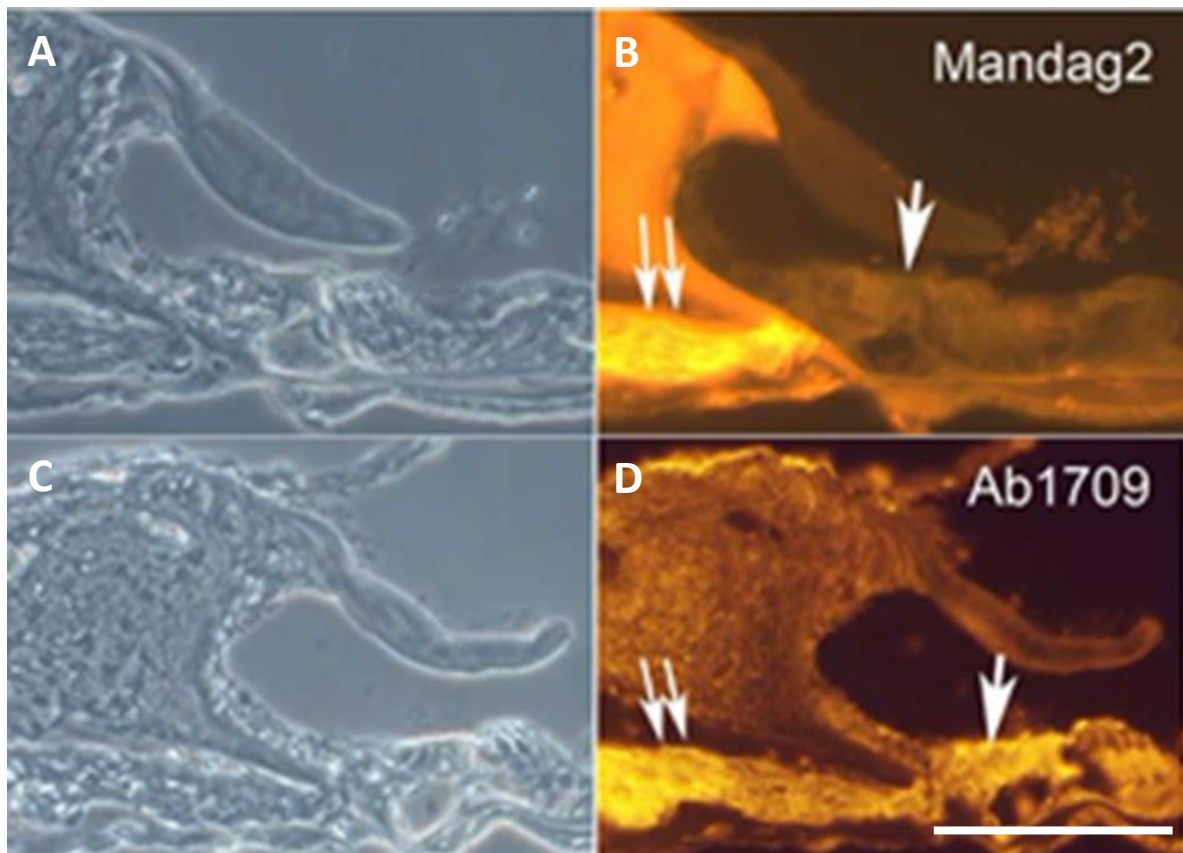


Figure 4.1 – Preliminary staining of the cochlea with β DG (Mandag2 monoclonal) and pY890 Ab (1709 polyclonal sera) – Cryostat sections of the organ of Corti, stained with either Mandag2 (1:20, B) or the pY890 Ab sera (1:100, D). (A and C) The accompanying bright field images are shown as a location reference. This preliminary data was collected by Professor Matthew Holley (unpublished) and reproduced with permission. Scale bar is approximately 50 μ m.

In order to validate any signal seen with the pY890 Ab, the ideal negative control for the antibody would be a DG knock-out mouse which should show no organ of Corti signal if the antibody was specific; however this was unfortunately not available. As such, focus was shifted onto affinity purifying the antibody to remove any IgGs which were not specific to p β DG. This would provide us with two fractions; a specific fraction and a negative control fraction that is depleted of p β DG specific IgGs. This experiment alone would not give sufficient proof that the signal in the organ of Corti corresponds to p β DG,

as the specific fraction could still be binding to a protein other than β DG. This would however provide a more trustworthy fluorescent signal than the crude sera and provide a low noise antibody fraction which could be used in further experimentation.

Thus, the aim of this section of the project was to investigate the signal seen in the pY890 Ab preliminary staining and determine whether this is indeed specific to p β DG. Further investigating the subcellular localisation of this signal may suggest either a stereocilia or synaptic role for dystroglycan in the cochlea, and therefore provide a basis for later and more specific experimentation.

4.2 – Results

4.2.1 – The subcellular localisation of the pY890 Ab signal within the cochlear hair cells

In order to investigate the signal distribution of the pY890 crude sera, whole mount sections of the apical cochlea of P6-P8 mice were stained with pY890 Ab and phalloidin. Phalloidin was used to mark cell borders and the organised F-actin of the stereocilia. At this age, the maturation of the hair cells and their stereocilia is still incomplete, as discussed in section 1.2.2, but the preservation of sample quality is much easier due to incomplete cochlea calcification. As such, whole-mount sections of this age make an ideal starting point for this type of investigation. As seen in **Figure 4.2A**, pY890 Ab signal appears to stain the stereocilia of the three rows of outer hair cells, but not the single row of inner hair cells. Using standard confocal microscopy, the resolution is too low to visualise where along the stereocilia this signal is located. When focusing deeper into the specimen to the basal part of the hair cells (**Figure 4.2B**), it is apparent that the pY890 Ab signal does not demonstrate any ribbon synapse-like puncta which would reside proximal to the nucleus. In order to visualise both the location of the pY890 Ab signal along the stereocilia, and any specificity between the rows, we utilised Zeiss LSM880 Airyscan super-resolution fluorescent microscopy. As in **Figure 4.2C**, the pY890 Ab signal can be seen at the tips of all three stereocilia rows, encompassing the sites of both EPS8 and EPS8L2 expression (Zampini *et al.* 2011, Furness *et al.* 2013).

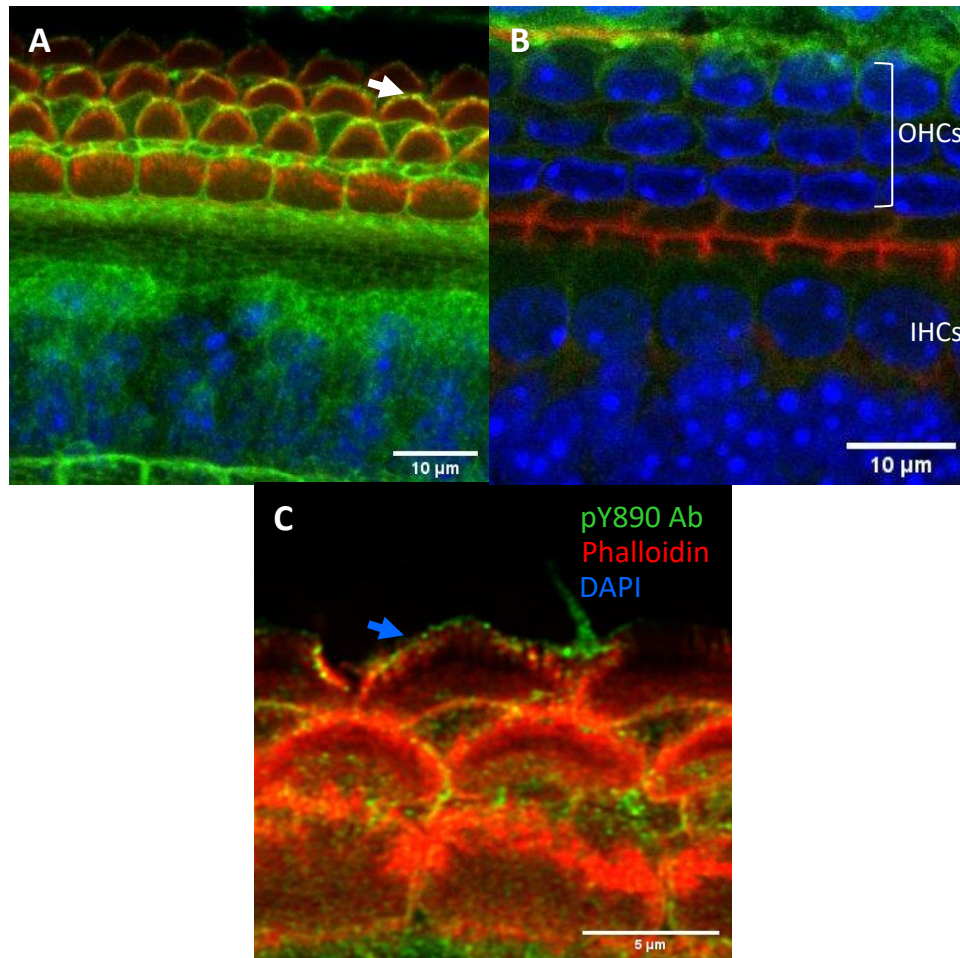


Figure 4.2 – The specific localisation of pY890 Ab signal within the organ of Corti – (A-C) Representative images of apical whole mount section of a P6 organ of Corti stained with the pY890 Ab sera (1:100, green), phalloidin (1:1000, red) and DAPI (1 μg/ml, blue). (A) Standard confocal microscopy image of the apical surface of the hair cells, at the level of the stereocilia of the three rows of outer hair cells (white arrow). (B) Confocal image of the nuclei of the hair cells from the same sections, taken at the approximate level of the ribbon synapses. (C) Airyscan super-resolution image of the outer hair cell stereocilia, the blue arrow indicates green signal at the tips of the red stereocilia. (A-C) Images shown are representative of three individual experiments.

4.2.2 – Affinity purification of pY890 Ab and validation of the resulting fractions

In order to investigate whether the signal at the stereocilia was specific, the pY890 Ab crude sera was first purified for IgGs with a protein A column and then for pY890 DG specific antibodies with an antigen column. This affinity column was composed of the immunizing peptide used to create pY890 Ab linked to biotin and bound to a resin of streptavidin beads. The antibodies that flowed through the column without binding should contain no pY890 β DG binding antibodies, known as the depleted pY890 Ab fraction, and the antibodies that bound should be p β DG specific, termed affinity purified pY890 Ab (AP pY890 Ab)

Following the purification, and before use on any cochlear sections, it was imperative to check whether the purification had been successful in providing a specific positive and non-specific negative fraction. When used for western blots of cochlear sensory epithelia and E36 lysates, the affinity purified fraction appears to yield fewer non-specific bands when compared to the original sera (**Figure 4.3A**). Furthermore, when used in the peptide SPOT arrays used in previous experiments, AP pY890 Ab binds primarily to the phospho-mimetic peptide on the β DG array, with some weaker signal in the neighbouring non-phosphorylated peptides (**Figure 4.3B**). Conversely, the depleted pY890 Ab fraction shows no binding to this phosphorylated SPOT even with extended exposures, only showing noise across the array with no consistent signal across the three repeats. In order to gauge whether the AP pY890 Ab fraction was visibly cleaner than the crude sera, and whether it is in fact specific for p β DG, we utilised sgRNA control and DG knock-out KM155 myoblasts. As seen in **Figure 4.4**, AP pY890 Ab appears to show a cleaner intracellular signal in the sgRNA control cells (**B**) compared to the crude sera (**A**). In line with this, the depleted pY890 Ab fraction shows a more uniform signal across the cell with reduced punctate signal (**C**). In DG knock-out cells, the AP pY890 Ab fraction shows a significantly weaker signal at identical exposure settings, indicating that the signal seen in the sgRNA cells is indeed specific (**D**).

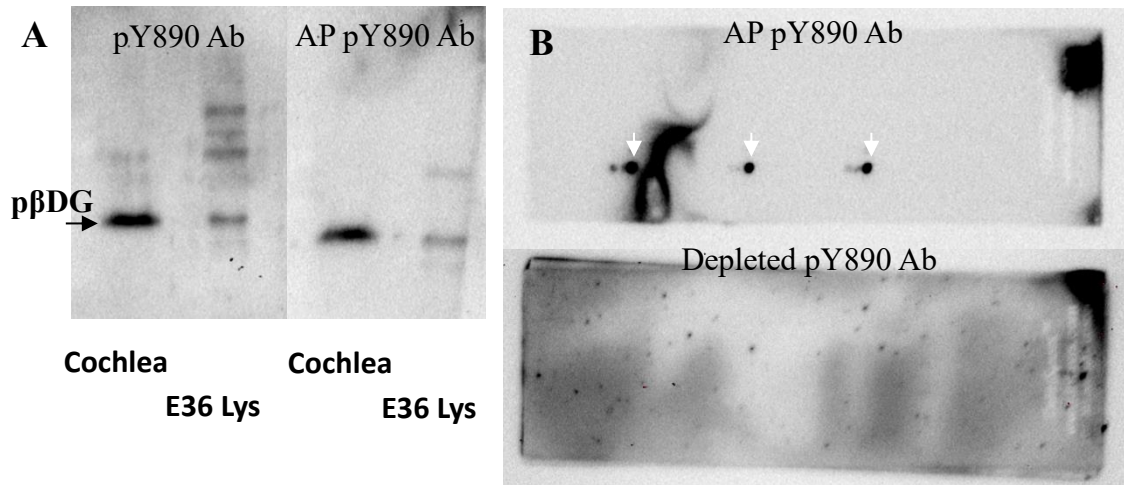


Figure 4.3 – Western blot and SPOT array validation of the AP pY890 Ab and depleted pY890 Ab fractions – (A) Single western blots of cochlear sensory epithelia lysate and VOT-E36 cell lysate probed with pY890 Ab (1:500) or the affinity purified antibody fraction AP pY890 Ab (1:20). (B) Peptide SPOT arrays representing the cytoplasmic domain of β DG probed with AP pY890 Ab (1:20) and depleted pY890 Ab (1:100). The white arrow indicates signal at the phosphorylated peptide spot of the array across all three repeats.

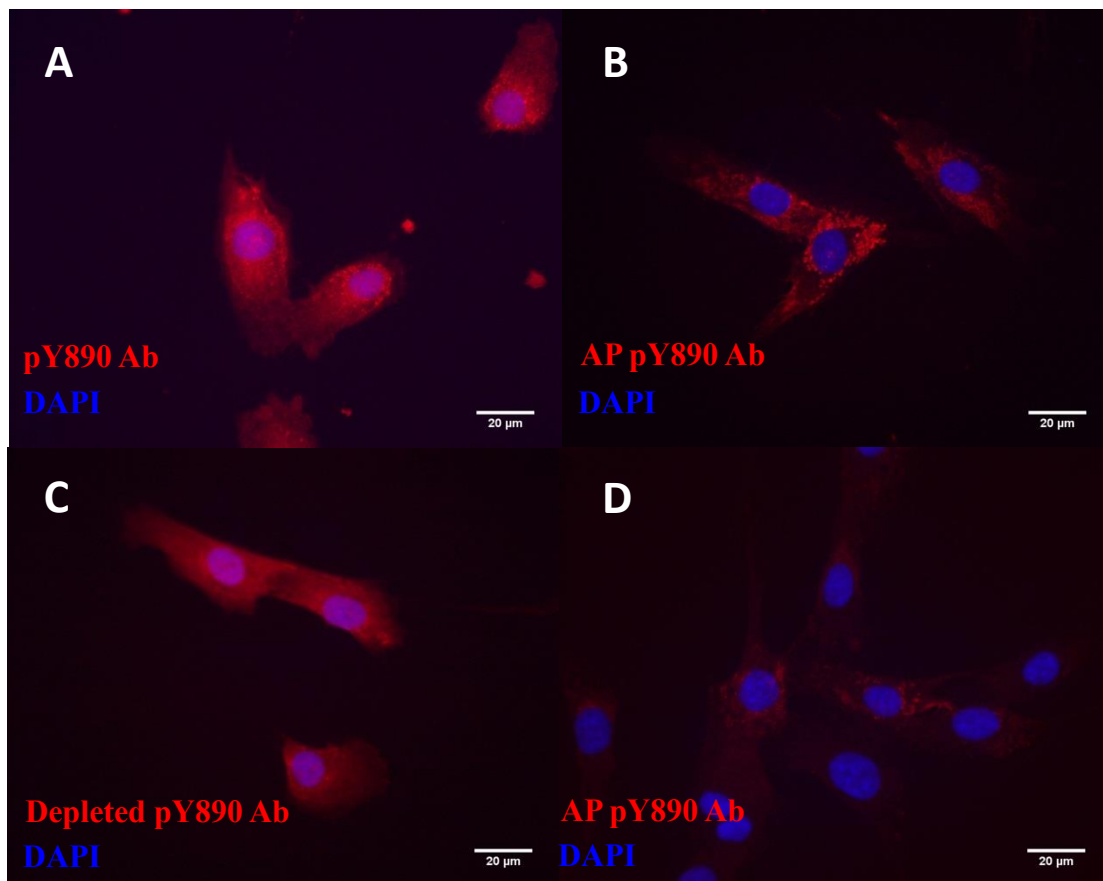


Figure 4.4 – Further validating the purified AP pY890 Ab fraction using sgRNA control and DG knock-out KM155 myoblasts – (A-C) Representative images of sgRNA KM155 cells stained with the pY890 crude sera (1:100)(n=3)(A), AP y890 Ab fraction (1:10)(n=3)(B) and depleted pY890 negative control fraction (1:100)(n=3)(C). (D) Representative image of DG knock-out KM155 myoblasts stained with AP pY890 Ab (1:10), showing a mixed population with some cells still showing weak p β DG signal (n=3). All cell immunofluorescence experiments were also marked for nuclei with DAPI (1 μ g/ml, blue).

4.2.3 – AP pY890 Ab signal within the organ of Corti

At this stage, we had a purified fraction of pY890 Ab that specifically binds p β DG in both KM155 myoblasts and SPOT arrays, and a depleted pY890 Ab which can no longer bind p β DG and can act as an ideal negative control. When P6 cochlea sections were stained with these fractions, using the same methods as the previous experiments, the AP pY890 Ab fraction showed no signal at the tips of the outer hair cell stereocilia (**Figure 4.5A**). Interestingly, the depleted pY890 Ab appeared to show signal at the tips of the shorter

rows of stereocilia specifically in the outer hair cells (**Figure 4.5B**). This suggests that the signal seen at the tips of the stereocilia originally was probably an artefact, and did not represent the distribution of p β DG in hair cells. Exactly why the affinity purification removed the antibodies binding to the tallest row of stereocilia tips from the depleted pY890 Ab fraction is unknown. However, the interesting signal distribution in the depleted pY890 Ab stained sections raises the interesting question of exactly what the antibody is binding to. The lack of any apparent signal at the stereocilia when using the AP pY890 Ab raises the concern that the antibody may not be working correctly in this context. When focusing below the inner hair cells, and using a neuronal fibre marker (Type III β -tubulin), it is apparent that the purified fraction is capable of staining the p β DG in the myelin surrounding the afferent fibres (**Figure 4.5C and D**). Thus, the antibody does appear to be capable of detecting dystroglycan in expected structures such as the myelin sheath (Saito *et al.* 1999) and capable of detecting p β DG in the stained sections, it simply appears that p β DG is not present within the stereocilia.

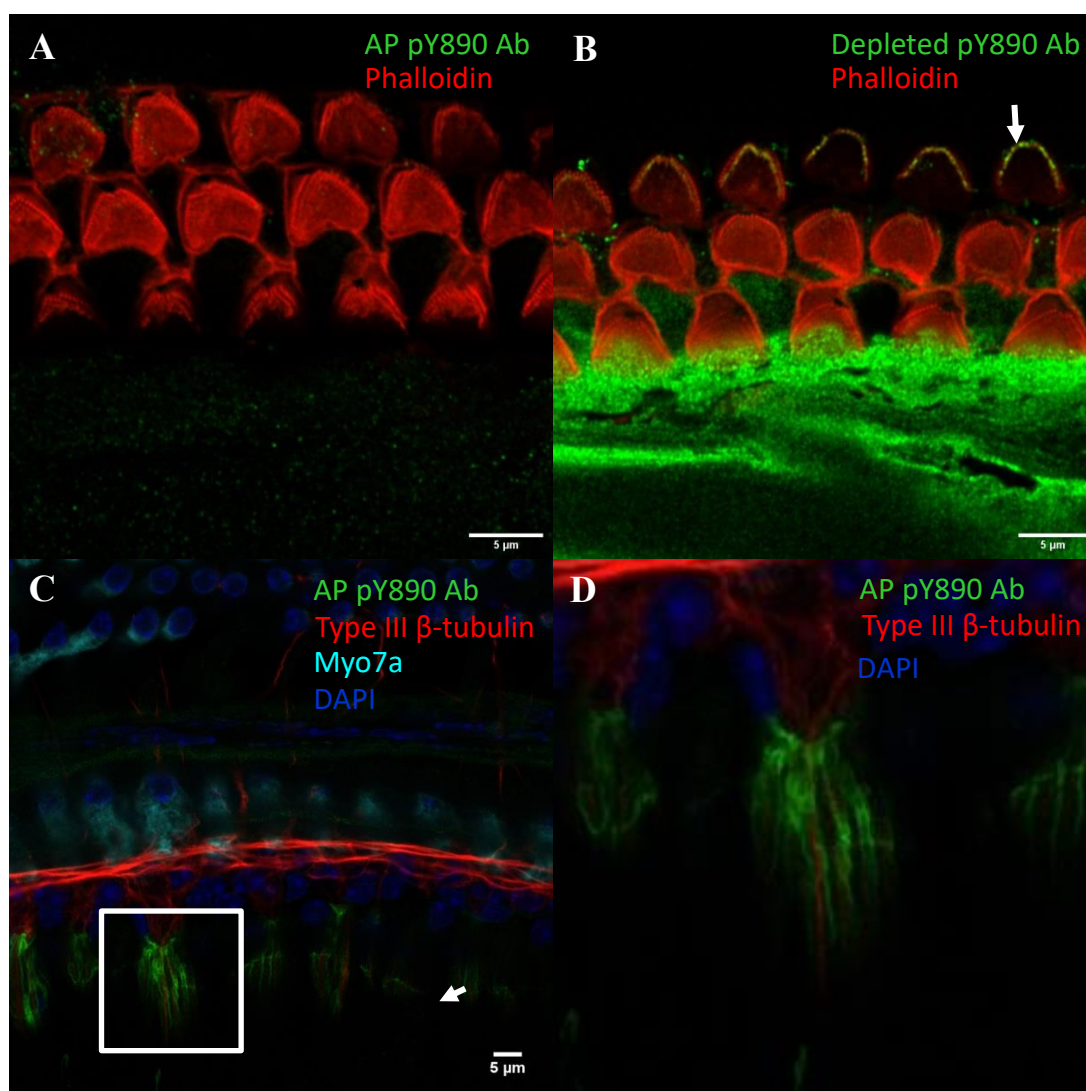


Figure 4.5 – Staining P6-8 cochlea sections with affinity purified 1709 and the depleted IgG negative control – Representative image of whole-mount apical sections taken at the level of the outer hair cell stereocilia labelled with the purified (A) fraction of pY890 Ab (1:4, green)(n=3) or the depleted pY890 Ab negative (B) fraction (1:100, green)(n=3). The white arrow indicates green signal at the tips of the shorter rows of stereocilia, which are stained for F-actin with phalloidin (1:1000, red). (C) Representative image of cochlea sections stained for pβDG (AP pY890 Ab 1:4), nerve fibres (Type III β-tubulin 1:50), hair cells (Myo7a 1:500) and DAPI (1μg/ml)(n=3). Below the inner hair cells, the AP pY890 Ab signal can be seen surrounding the nerve fibres. (D) Blown up image of the region highlighted by the white square in C, highlighting the structure labelled by the AP pY890 Ab.

4.2.4 – Investigating the possibility of pikachurin expression within the hair cell ribbon synapses

Following the discovery that purification results in the complete loss of pY890 Ab signal within the organ of Corti, we next investigated the possibility of pikachurin in the ribbon synapses of hair cells. As discussed previously, dystroglycan functions at the ribbon synapses of the retina to facilitate normal synaptic kinetics and bipolar terminus invagination (Sato *et al.* 2008). Thus, although we have yet been unable to visualise β DG with any of the antibodies at our disposal, finding pikachurin in a ribbon synapse-like distribution would support the hypothesis that alpha dystroglycan may function to facilitate normal synapse formation in the cochlea. When labelling cryostat sections of the cochlea with a commercially available affinity purified pikachurin antibody, the organ of Corti does appear to show particularly enriched pikachurin signal (**Figure 4.6**). When swapping to whole-mount confocal images, closer inspection reveals that pikachurin signal is particularly prevalent at the neck of inner hair cells and the basal cell bodies of the outer hair cells (**Figure 4.6**). However, this signal does not appear to show a ribbon synapse like punctate pattern in either cell type.

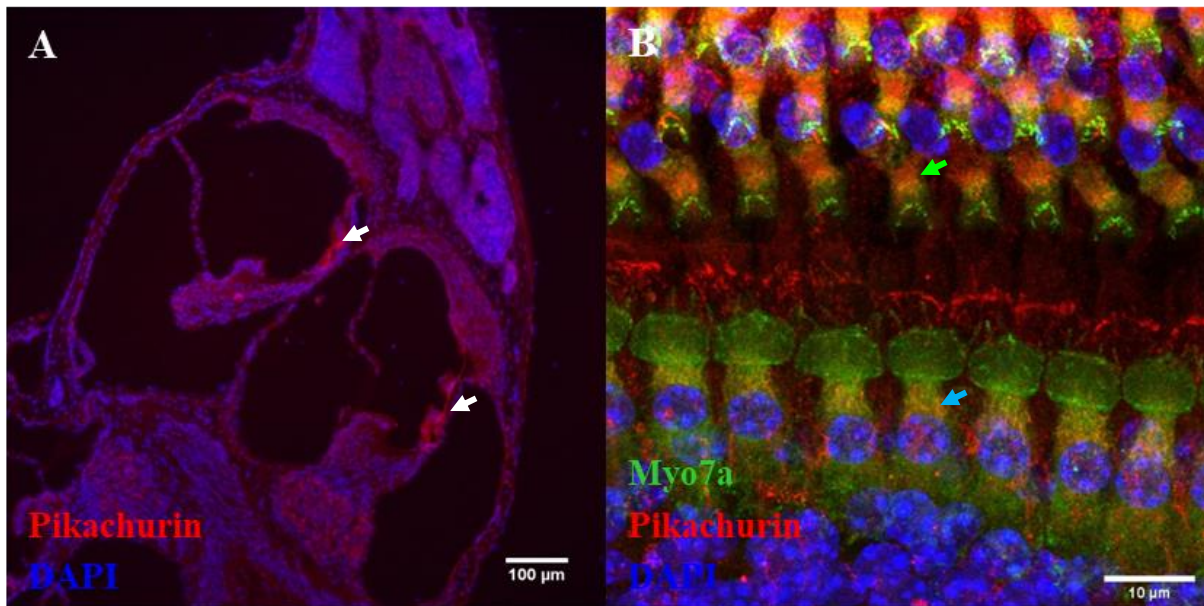


Figure 4.6 – The expression of pikachurin within the mammalian cochlea – (A) Representative cryostat section of the cochlea stained for pikachurin (1:100, red) and nuclei with DAPI (1 μ g/ml, blue) at a low magnification. The white arrow indicates the organ of Corti, showing apparent red signal (n=7). (B) Representative whole-mount max intensity cochlea sections labelled for pikachurin (1:100, red) alongside a hair cell myo7a marker (1:500, green) and nuclei with DAPI (1 μ g/ml, blue), imaged on a Zeiss LSM880 equipped with Airyscan for super-resolution confocal microscope (n=6). Red signal appears to be particularly enriched at the necks of the inner hair cells (blue arrow) and the basal cell bodies of the outer hair cells (green arrow).

With the discovery of apparent pikachurin expression in the organ of Corti, we next investigated whether pikachurin interacted with α DG in this context similar to within the retina (Sato *et al.* 2008). Using cryostat sections imaged on an epifluorescent microscope, one of the α DG antibodies at our disposal, IIH6 (sc-53987, Santa Cruz Biotechnology), appears to co-localise with pikachurin at the basolateral membrane of inner hair cells (**Figure 4.7A-C**). However, in whole mount cochlea sections, the signal does not appear to show any co-localisation (**Figure 4.7D**). Thus, whilst the pikachurin antibody does appear to show high expression within the organ of Corti, the lack of ribbon synapse like puncta and co-localisation with α DG suggest that the association taking place within the retina is likely not present in the cochlea.

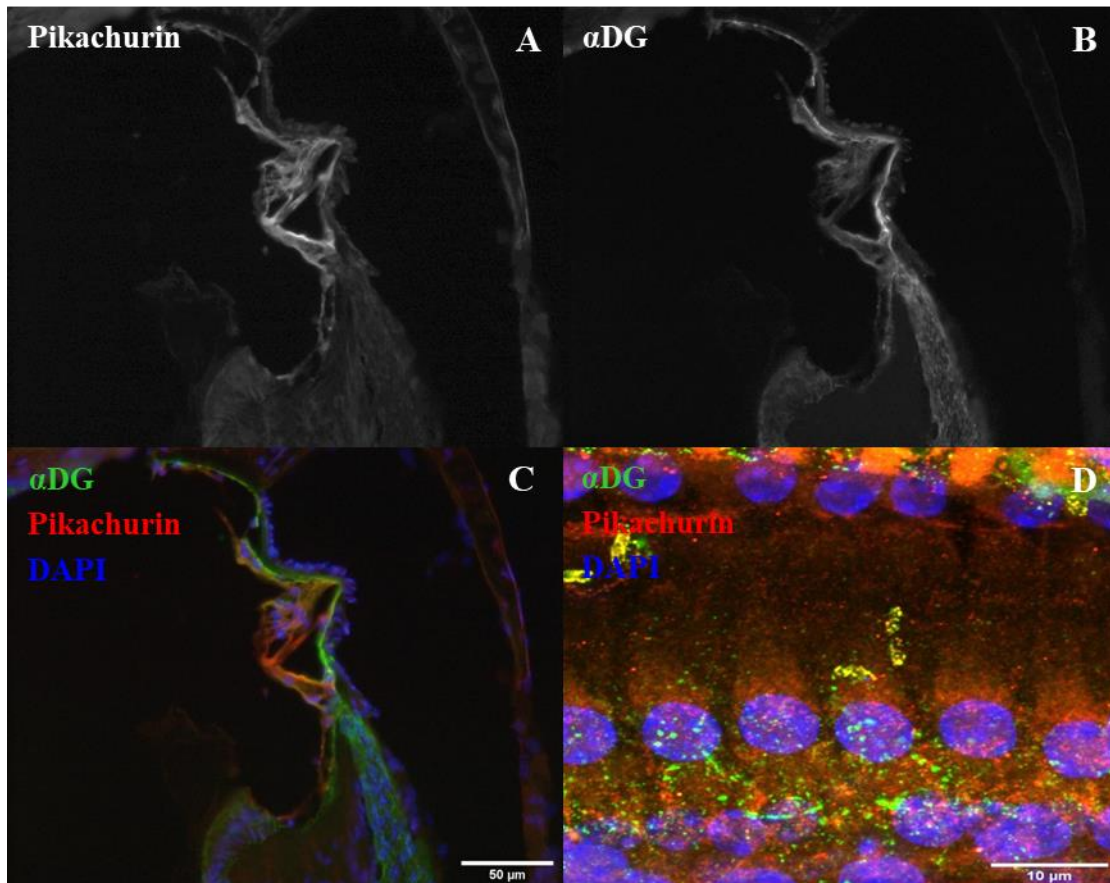


Figure 4.7 – Investigating whether pikachurin interacts with DG in the organ of Corti – Representative cryostat section of the organ of Corti with labelled pikachurin (1:100, red)(A) and α DG (IIH6 1:100, green)(B). (C) Composite image of both antibody channels, alongside a DAPI nuclei stain (1 μ g/ml)(n=3). (D) Representative whole-mount super-resolution max intensity projection of inner hair cells immunolabelled using the same antibodies.

4.2.5 – Attempted identification of the protein responsible for the depleted pY890 Ab stereocilia signal

The signal of the depleted Y890 Ab in cochlear stereocilia, showing signal in only the shorter rows of stereocilia in outer hair cells only, is unique (Section 1.2.2) and the protein responsible for this signal is unknown. Thus, identifying this protein could elucidate a new actin effector or actin effector localising protein that function to maintain the shorter rows of stereocilia alongside the EPS8L2 containing row 2/3 complex. In order to try and identify this protein, we employed a modified version of the hair bundle “twist-off”

method originally used to isolate hair bundles from bullfrog utricles (Gillespie and Hudspeth 1991). In brief, this method involves dissecting out several vestibular utricles in PBS with protease inhibitors and trapping the long stereocilia in low melting point agar. Thus, by then cutting out the patches of stereocilia, and extracting the stereocilliary proteins by melting the agar disc, we had hoped to create a concentrated enough sample to perform an immunoprecipitation using the depleted IgGs. This would allow us to mass spec the protein A resin and identify the proteins that bound to the antibody fraction. Preliminary data indicated that the depleted pY890 Ab showed stereocilia tip staining in the vestibular utricle (data not shown), and phalloidin staining of the gel cap indicated that the method appears to be capable of selectively isolating vestibular hair bundles (**Figure 4.8A**). However, eight utricles worth of stereocilia lysate were required to provide even a faint band when probed for actin, the major protein component of stereocilia, in a western blot (**Figure 4.8B**). Therefore, an immunoprecipitation would require a huge amount of animals and would be extremely time consuming. As such, due to limited time remaining on the PhD period, the side project was stopped.

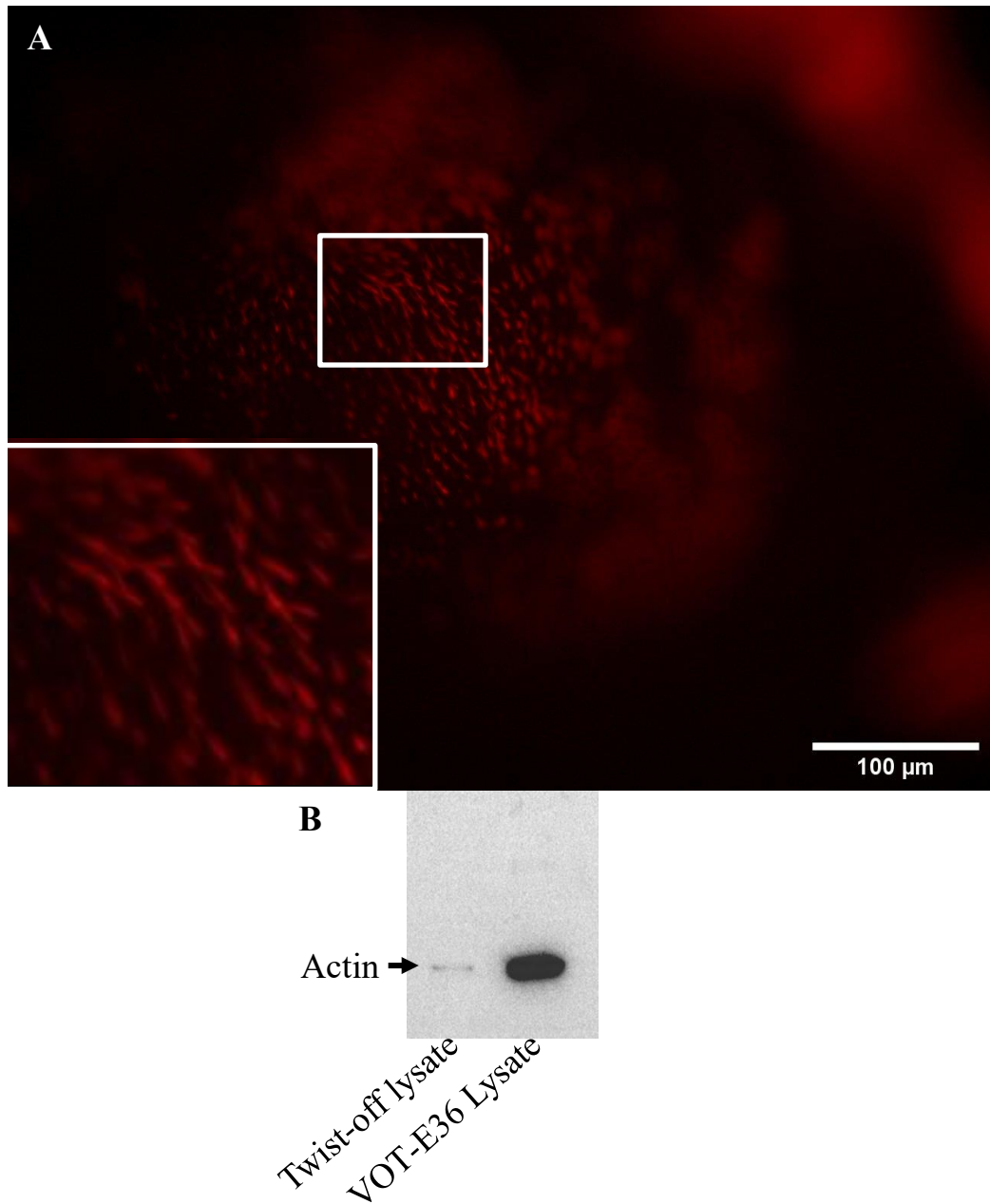


Figure 4.8 – Collection of a stereocilia enriched lysate using the “twist-off” technique – (A) Representative epifluorescent image of an agarose gel disc following the “twist-off” procedure stained with phalloidin (1:1000, red) to mark F-actin with a zoomed in image of the central region (n=2). (B) Representative western blot of 8 utricles worth of stereocilia harvested via the “twist-off” method compared to 5 μ l of VOT-E36 lysate (Chapter 3) used as a positive control for the actin probe (α actin 1:1000)(n=2).

4.3 – Discussion

Initially, the crude sera of pY890 Ab appeared to indicate that p β DG is present at the tips of all three rows of the outer hair cell stereocilia. The presence of this signal in the outer hair cells is peculiar, but the inner and outer hair cell stereocilia are very different. Inner hair cells stereocilia are much longer and wider, compared to the shorter and stiffer outer hair cell stereocilia (Fettiplace 2017). Thus it is expected that there is a difference in actin effector protein expression between the two cell types, in order to both establish and maintain this morphology difference. However, when the pY890 Ab serum was purified via protein A and affinity columns, this stereocilia signal was entirely lost. The affinity purified fraction was shown to be functional and specific for p β DG using both SPOT arrays and KM155 immunofluorescence experiments. Alongside this, the purification process also yielded a non-specific fraction depleted of all p β DG binding antibodies, providing an ideal negative control for the subsequent staining experiments. Interestingly, it is this non-specific fraction which displayed signal at the tips of the shorter rows of stereocilia in the outer hair cells. Why exactly this signal remained throughout the purification while the signal at the tallest row was lost is currently unknown. The precise signal distribution this fraction displays is unique. The protein the depleted serum is binding to at the stereocilia tips is an interesting question, the answer to which may reveal an important protein involved in row specification or maintenance.

Based upon the previous reports of dystroglycan and pikachurin functioning to facilitate normal ribbon synapse development in the ribbon (Sato *et al.* 2008), the cochlea was labelled to try and identify whether pikachurin signal is present within the organ of Corti. Interestingly, while pikachurin signal did appear to be present at the hair cells, this signal did not show a ribbon synapse like punctate pattern or any detectable co-localisation with α DG. Also, the lack of any apparent ribbon synapse puncta was not due to the inability to detect the signal, as experiments in the following chapters utilising the same methodology were able to detect ribbon puncta (**Figure 5.8**). Interestingly, α DG has been reported present within the organ of Corti, but only one of the antibodies at our disposal possessed any detectable signal at this location. Thus, while these staining experiments are indicative of DG not being involved in ribbon synapse formation in the cochlea, the experiments are not conclusive.

Therefore, due to the apparent staining artefacts present with anti-DG antibodies, in order to make a definitive conclusion on the role of dystroglycan in ribbon synapses the use of a conditional dystroglycan knock-out model was required. By monitoring hearing thresholds with age and carrying out further immunofluorescence and patch clamping experiments, the phenotype and the mechanism of the DG knock-out can be deduced.

Chapter 5 – Investigating the phenotype associated with the hair cell specific knock-out of dystroglycan

5.1 – Introduction

Following the results from the biochemical interaction and immunofluorescence experiments, the only way to proceed to definitively determine whether dystroglycan possesses a role in cochlear stereocilia or ribbon synapses was by using a knock-out model. This model had to be driven by a tissue specific promoter with an onset late in development for the following three reasons. Firstly, as discussed previously, embryo-wide deletion of dystroglycan in mice results in early embryonic lethality due to a failure in the formation of Reichert's membrane (Williamson *et al.* 1997). Secondly, even if the embryos could survive to adulthood, dystroglycan has been shown to be involved in a vast array of functions, including neuronal guidance (Wright *et al.* 2012, Clements and Wright 2018). Therefore an animal-wide deletion could affect hearing thresholds by impairing the downstream auditory pathway or spiral ganglion neuron guidance. This would be completely independent of any ribbon synapse or stereocilia phenotype, overcomplicating the analysis of the mutant. Finally, the stages of stereocilia and ribbon synapse development of our interest occur postnatally, such as the refinement of EPS8L2 row specificity and the maturation of ribbon synapse connections. Thus, dystroglycan expression being present in the hair cells through-out embryonic development, based on our hypothesis, should not impact the result of the hair cell specific knock-out. Therefore, it was decided that the floxed 129S1-DAG1^{tm2Kcam}/J line (The Jackson Laboratory, Cohn *et al.* 2002) would be crossed with a hair cell specific MYO15-Cre recombinase line (Caberlotto *et al.* 2011). This promoter begins to express Cre-recombinase in basal cochlear hair cells at P0, and this expression gradually moves through to the apex until P3, at which point all hair cells express the recombinase. This model will therefore remove dystroglycan from all the cochlear hair cells from approximately P6 onwards, depending on protein stability kinetics (Caberlotto *et al.* 2011, Corns *et al.* 2018).

The initial priority for this model was the ABR/DPOAE experiments, as the age of onset and frequencies affected could provide clues as to how the deletion was causing the phenotype. If the phenotype was particularly marked at the higher frequencies, and progressive with age, this would reflect the EPS8L2 knock-out and suggest a deficit in stereocilia maintenance (Furness *et al.* 2013). Conversely, if the thresholds were poor across all frequencies, and resulted in a reduction in wave I amplitude, this would suggest

a deficit in ribbon synapse formation or maintenance (Buchwald and Huang 1975). Furthermore, the DPOAE experiments directly assess the function of the outer hair cell cochlear amplifier (Kemp 2002). Thus, if the phenotype results in frequency wide hearing loss with a severe effect on the DPOAE thresholds, this would indicate a role for dystroglycan in the function of the outer hair cells.

5.2 – Results

5.2.1 – Analysing the hearing thresholds and outer hair cell function of 1 month old DG knock-out mice

Following the necessary crosses, we generated both a DG knock-out mouse ($DAG1^{-/-}MYO15Cre^{+/+}$) and a litter-matched control ($DAG1^{-/-}MYO15Cre^{+/+}$). The first preliminary ABR/DPOAE experiments were carried out at the age of 1-month, well after the onset of hearing at a point where the hearing thresholds should be at their lowest. At this age, the ABR hearing thresholds were comparable, and appeared to indicate no major increase in the mutant across any of the tested frequencies (**Figure 5.1**). As this was a preliminary experiment, the thresholds were not judged by a blinded participant, and as such may have been subject to implicit bias. In preliminary DPOAE experiments, the thresholds of the knock-out and control animals at this age appears to be very similar, suggesting that the outer hair cell function is not significantly perturbed (**Figure 5.2 and 5.3**).

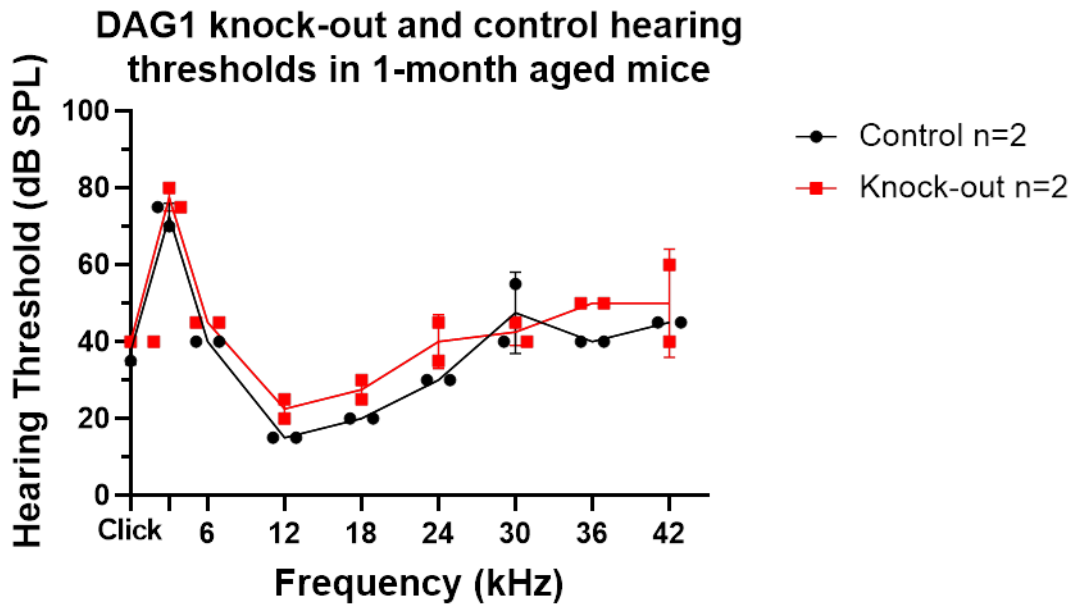


Figure 5.1 – DAG1 knock-out and control hearing thresholds in 1-month aged mice
 – Preliminary ABR hearing thresholds of the DAG1 knock-out and control animals in response to a white noise click and pure tone frequencies (3-42 kHz). Individual hearing thresholds for each animal are plotted alongside the mean which shown as a connecting line, and statistics is not viable due to the limited number of animals per genotype (n=2 animals per genotype). Error bars represent the standard deviation.

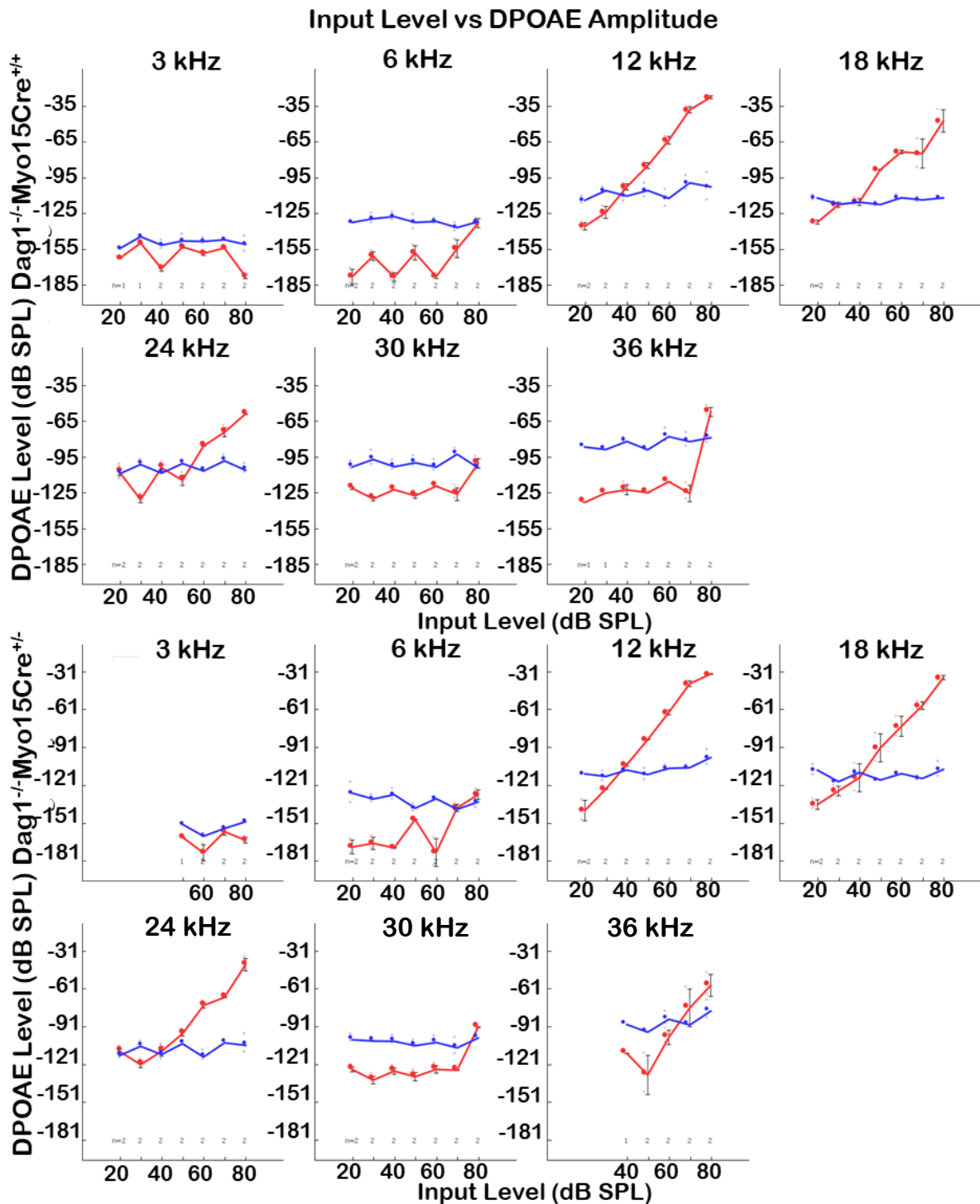


Figure 5.2 – The effect of dystroglycan knock-out on distortion product amplitude against stimulus volume for each frequency in 1 month old mice – The amplitude of the distortion product (blue) plotted alongside the noise floor (red), to allow the threshold for each frequency (3-36kHz) to be determined for the knock-out (n=2) and the control (n=2) genotype. These thresholds can then be plotted separately to allow for easy comparison. The error bars here represent the standard deviation of the data. DPOAEs could not be obtained at 42 kHz and were therefore omitted.

DPOAE thresholds of 1-month old DAG1 knock-out and control mice

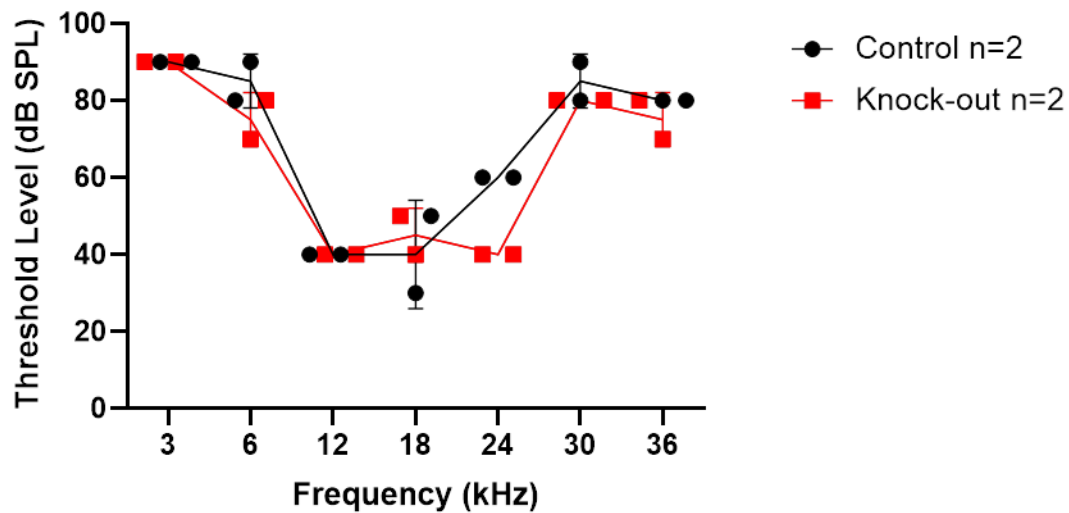


Figure 5.3 – DPOAE thresholds of 1 month old DAG1 knock-out and control mice – DPOAE threshold graph of DAG1 knock-out and control mice generated from the data in **Figure 5.2**, with the threshold for each frequency (3-36 kHz) defined as the volume at which the distortion product rises above the noise floor. Statistical analysis of this data is not possible due to the low animal number (n=2 animal per genotype). 80dB was the highest stimulus amplitude used for the experiment, and as such DPOAEs that failed to cross the threshold were reported as 90dB. Individual thresholds for each animal are plotted alongside the mean which shown as a connecting line. Error bars represent the standard deviation.

5.2.2 – Analysing the hearing thresholds and outer hair cell function of 2 month old DG knock-out mice

Performing the same ABR and DPOAE experiments in 2 month old mice yields a similar result, with knock-out mice showing similar hearing thresholds to the control mice (**Figure 5.4**). The large variability at the high frequencies in this set of experiments appears to have been caused by some issue with the mouse strain’s background unrelated to the DAG1 or MYO15Cre loci. This resulted in complication when comparing the two groups, but the mice unaffected by this issue from both genotypes showed a similar hearing threshold. All of the ABR thresholds obtained from this experiment and the following experiments were judged by a blinded individual to ameliorate implicit bias. Similar to the ABR thresholds,

the DPOAE thresholds are very similar between both the knock-outs and the controls (Figure 5.5 and 5.6). Thus, the conditional deletion of dystroglycan does not appear to negatively affect either hearing thresholds or outer hair cell amplification in 1 month or 2 month old animals.

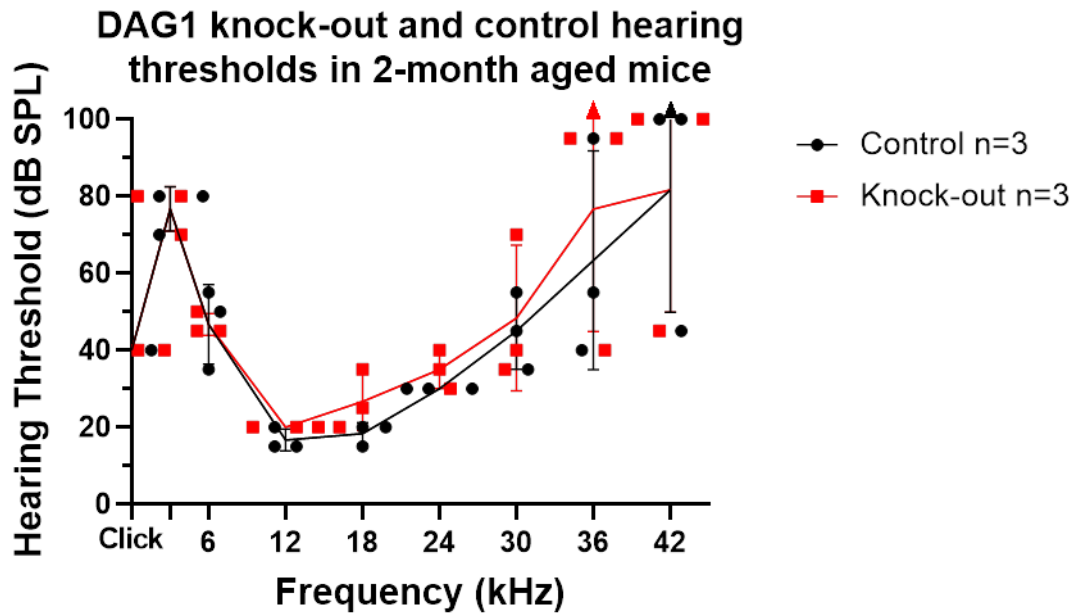


Figure 5.4 – DAG1 knock-out and control hearing thresholds in 2-month aged mice – ABR hearing thresholds of both DAG1 knock-out and control animals in response to a white noise click and pure tone stimuli (3-42 kHz). When an ABR waveform could not be elicited at the highest stimulus amplitude of 95dB, the value was recorded as 100dB. This results in non-parametric data, and as such statistical analysis on all ABR thresholds was performed using a two-way ANOVA with Šidák’s post-test. Individual hearing thresholds for each animal are plotted alongside the mean which shown as a connecting line. Error bars represent the standard deviation and arrowheads indicate where error bars have exceeded the graph boundary.

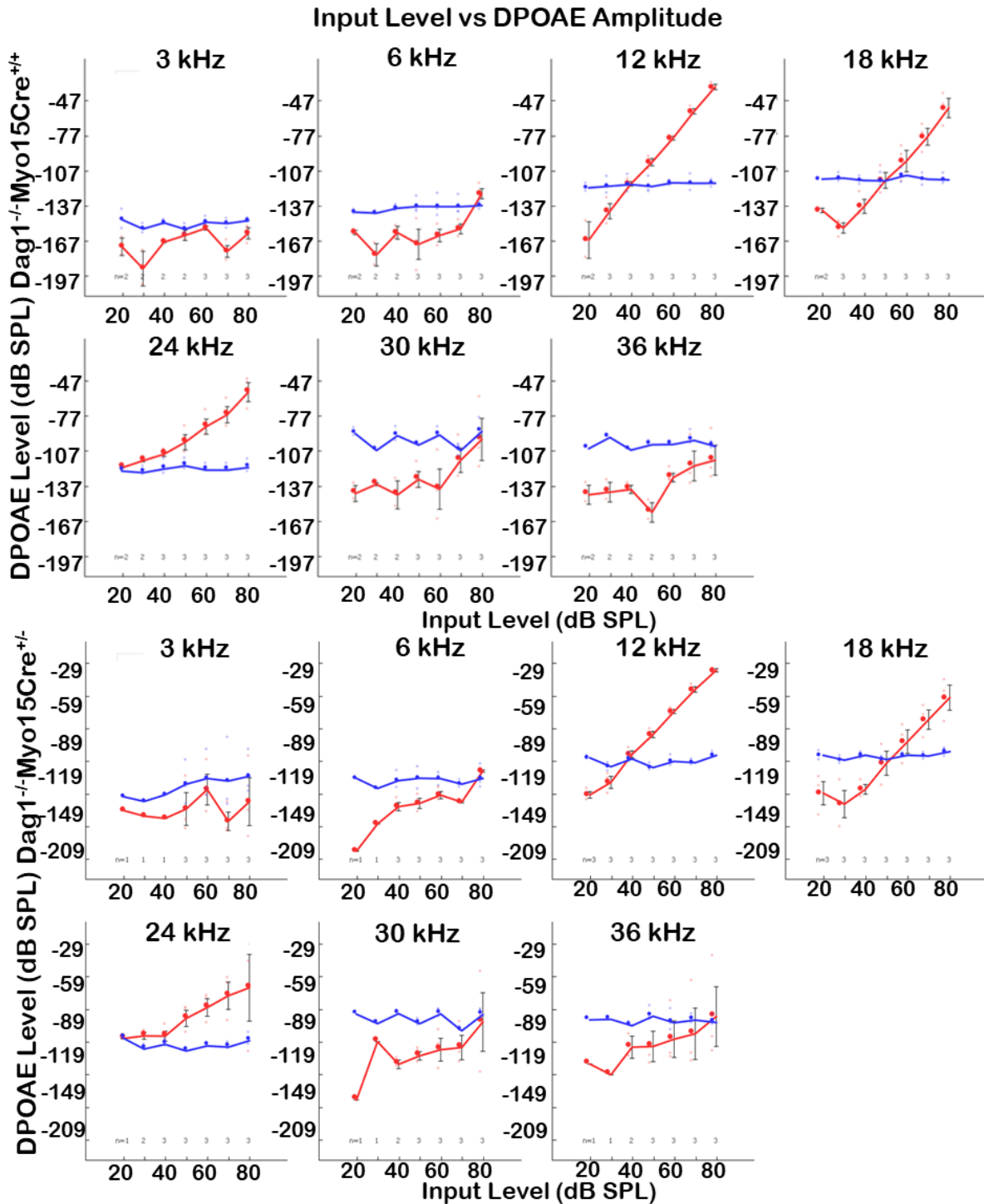


Figure 5.5 – The effect of dystroglycan knock-out on distortion product amplitude against stimulus volume for each frequency in 2 month old mice – Sound level of the distortion product (red) against the noise floor (blue) for each frequency (3-36 kHz) for both the DAG1 knock-out (n=3) and control (n=3) genotypes. The hearing threshold for each frequency is determined as the stimulus volume at which the distortion product rises above the noise floor. Error bars represent standard deviation. DPOAEs could not be obtained at 42 kHz and were therefore omitted.

DPOAE thresholds of 2-month old DAG1 knock-out and control mice

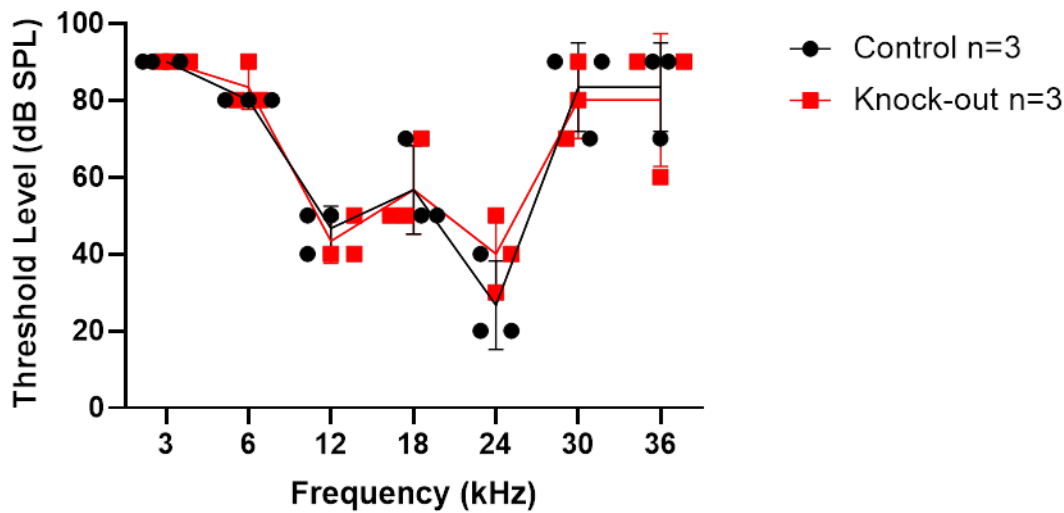


Figure 5.6 – DPOAE thresholds of 2 month old DAG1 knock-out and control mice – Distortion product thresholds for each frequency (3-36 kHz) plotted from the data in **Figure 5.5** for both the knock-out (n=3) and control (n=3) genotypes ($P = 0.748$, two-way ANOVA with Šidák's post-test). DPOAE responses that never reached the threshold were graphed as 90dB. Thresholds of individual animals are plotted alongside the mean which is represented as a connecting line. Error bars represent the standard deviation.

5.2.3 – Analysing the hearing thresholds of 6 month old DG knock-out mice

Following the results that the hearing thresholds in 1 month and 2 month old knock-outs were comparable to the controls, we next looked at aged mice. While we would expect the phenotype of an EPS8L2 related phenotype to begin showing hearing loss by a month of age, it is possible that the dystroglycan deletion could result in hearing loss in more aged mice by destabilising ribbon synapses. Therefore, we performed ABR experiments on 6-month old knock-out and control animals. As seen in **Figure 5.7**, both sets of genotypes show very similar hearing thresholds across all the frequencies analysed. In summary, it appears as though the deletion of dystroglycan does not appear to significantly impair hearing thresholds in young or old animals.

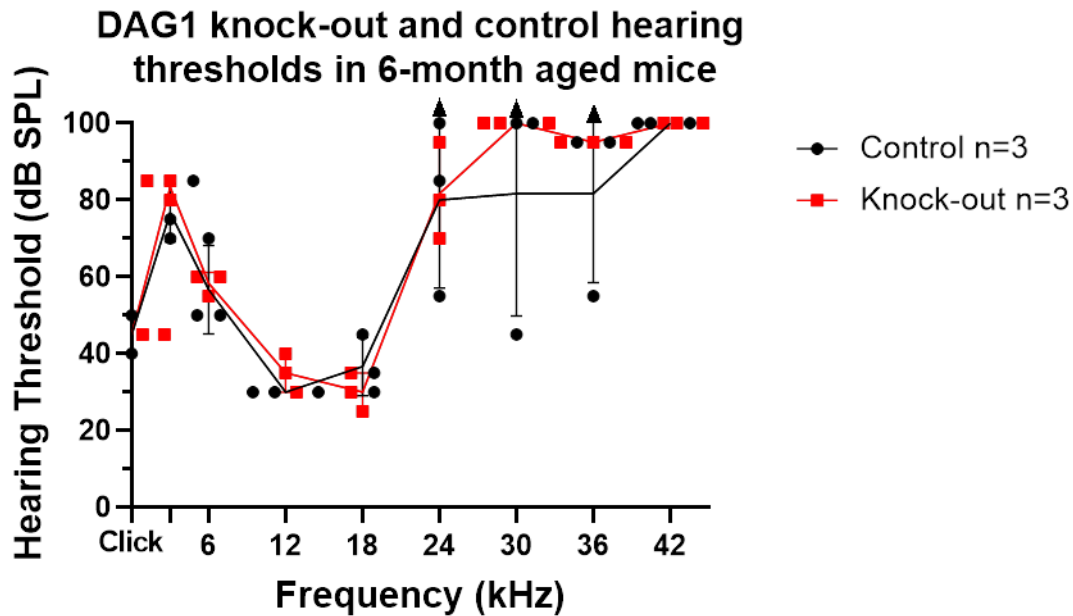


Figure 5.7 – DAG1 knock-out and control hearing thresholds in 6-month aged mice = ABR hearing thresholds in control (n=3) and knock-out (n=3) animals in response to a white noise click and pure tone (3-42 kHz) stimuli (P = 0.180, two-way ANOVA with Šidák's post-test). The large degree of variability in the higher frequency thresholds is due to the issue with the line discussed earlier. Consistent with the previous ABR graph, when an ABR waveform could not be elicited at the highest stimulus amplitude of 95dB, the value was recorded as 100dB. Error bars represent the standard deviation, and arrowheads indicate where error bars have exceeded the boundaries of the graph.

5.2.4 – Investigating the quantity and alignment of ribbon synapses in the conditional DG knock-out

Due to the results of the ABR and DPOAE experiments, which appeared to indicate that the DG deletion had no effect on hearing thresholds or on outer hair cell amplification, we next investigated the ribbon synapses. It is possible that the mutation could have reduced the number of functional ribbon synapses within the hair cells while maintaining normal hearing threshold, commonly known as hidden hearing loss. Therefore, we used immunostaining of P19 control and knock-out animals to analyse whether the number of ribbon synapses or their association with a post-synaptic density was affected by the mutation. As shown in **Figure 5.8**, the number of CtBP2 positive pre-synaptic ribbons was

comparable between the control and knockout animal, showing no significant difference between the two (**Figure 5.8A-C**). Furthermore, the number of misaligned synapses, defined as the number of CtBP2 pre-synaptic puncta without an adjacent PSD95 positive post-synaptic density, was also unaffected (**Figure 5.8D**). While these experiments do not rule out fine ultrastructure defects, such as those seen in the retinal knock-out of DG (Sato *et al.* 2008), it does suggest that DG is not crucial for the formation of cochlear ribbon synapses.

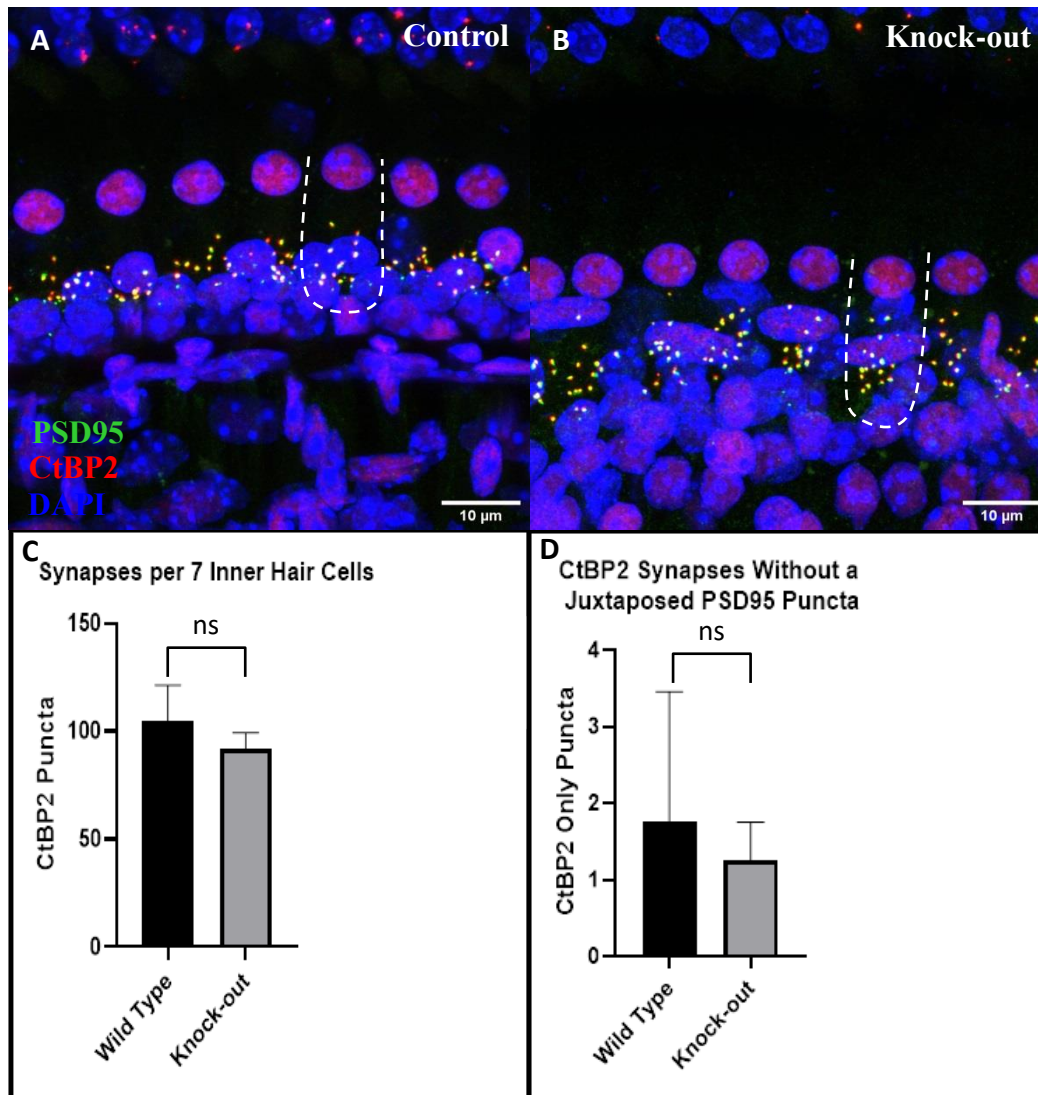


Figure 5.8 – The impact of DG deletion on the number and alignment of ribbon synapses in the cochlea – (A and B) Maximal intensity projections of whole-mount cochlea sections of P19 control and DG knock-out animals stained for both the pre-synaptic ribbon with CtBP2 (1:500, red) and the post-synaptic density marker PSD95 (1:1000)(n = 4 cochleae from 4 separate animals per genotype). Each image stack was taken with identical settings and the dimensions were identical between samples

(66 x 66 μm). The dashed white line denotes an example perimeter of an inner hair cell. (C) Quantification of the number of CtBP2 puncta per 7 inner hair cells for each maximal intensity projection (n=4 cochleae per genotype). (D) The number of CtBP2 puncta lacking a PSD95 post-synapse in 7 inner hair cells for each of the maximal intensity projections (n=4 cochleae per genotype). Statistical analysis was performed using an unpaired two-tailed Student's t-test (ns = $P > 0.05$). Error bars represent the standard deviation.

5.2.5 – Investigating the maturation of inner hair cells in the DG knock-out mice

In order to investigate possible additional and subtle phenotypes the DG deletion may be presenting in the inner hair cells, we next investigated the maturation of these cells. Inner hair cell maturation defects are apparent in the EPS8, but not EPS8L2, knock-out mutant due to the early onset mechanotransduction defects (Zampini *et al.* 2011, Furness *et al.* 2013). EPS8 knock-out results in absence of the mature fast activating $I_{K,f}$ potassium current and the retention of immature spiking activity in response to depolarising currents, instead of the mature graded and sustained responses. Thus, although the DG deletion appears to have no effect on the hearing thresholds, if the protein is modulating the EPS8/EPS8L2 axis this could theoretically result in maturation defects due to early deficits in mechanotransduction. As discussed previously (Section 1.4.2), the maturation of inner hair cells coincides with the loss of direct efferent innervation and the loss of the SK2 channel clusters located proximal to these efferent contacts (Marcotti *et al.* 2004a, Marcotti *et al.* 2004b). Maturation also results in the appearance of the large conductance potassium current $I_{K,f}$ carried by the BK channel (Kros *et al.* 1998). Therefore, we performed immunofluorescent microscopy experiments to investigate whether mature IHCs expressed BK channels. As seen in **Figure 5.9A** and **B**, inner hair cells from both genotypes express BK channel clusters while lacking the immature SK2 channels. Quantification revealed that the intensity of the BK signal, taken as an average of the entire maximal intensity image stack, was not significantly different between the control and knock-out animals (**Figure 5.9C**). Furthermore, the area of the BK channel patches was not significantly different between the two genotypes (**Figure 5.9D**). However, it is worth noting that this area measurement is inherently inaccurate, as separate patches can be stacked on top of each other by the maximal intensity projection. Taken together, this

staining experiment appears to indicate that the inner hair cells of the knock-out animals are expected to mature as normal and express the expected repertoire of potassium channels.

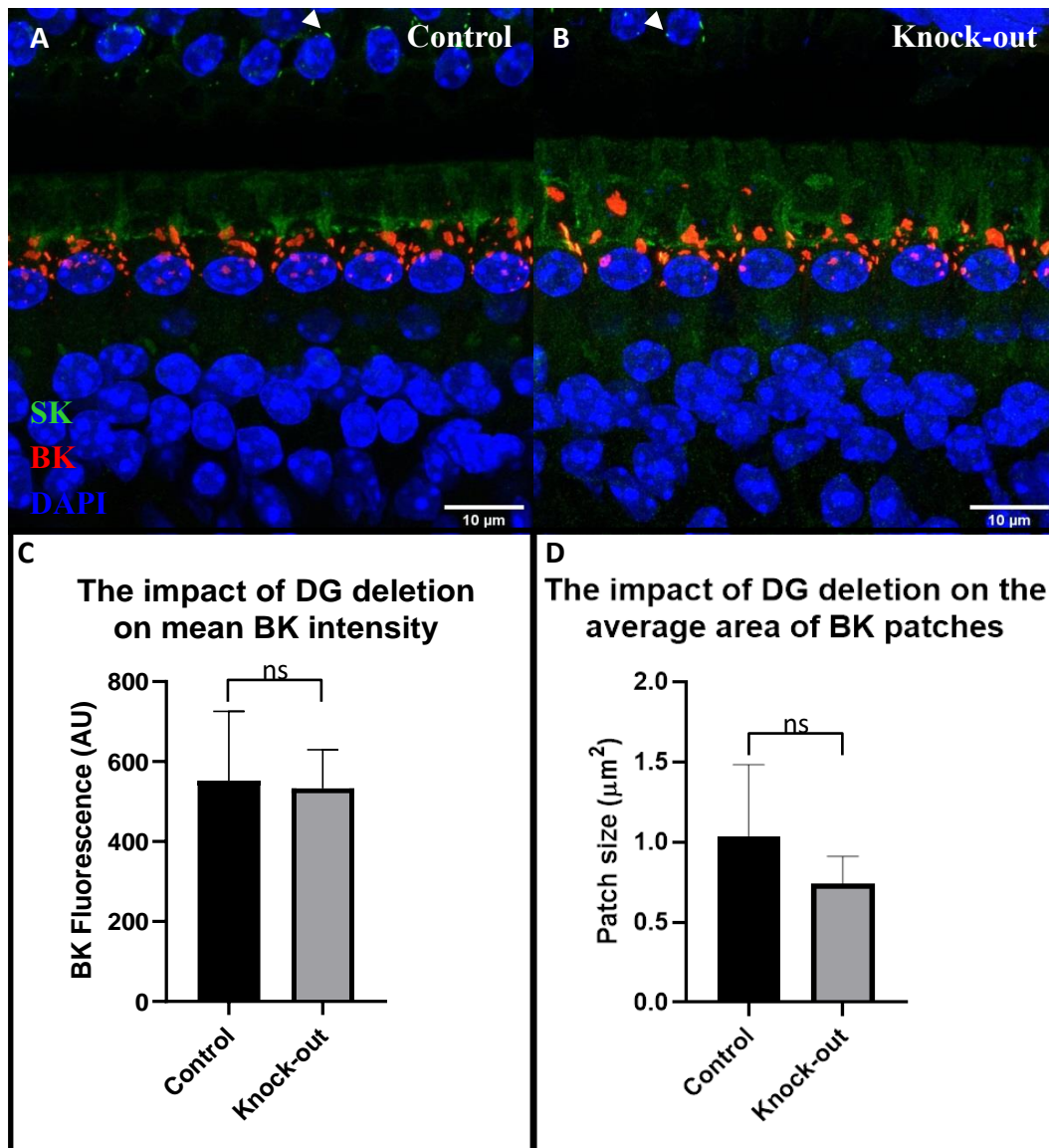


Figure 5.9 – Analysing the expression of the BK and SK2 potassium channels in the control and knock-out mice – Representative whole-mount immunofluorescence maximal intensity projections of both control (A) and DG knock-out P19 cochlea (B) labelled for BK (1:200, red), SK2 (1:200, red) and nuclei (DAPI, 1μg/ml, blue)(n = 4). (C) Quantification of the the average intensity of the red BK signal in each maximal intensity image for both genotypes (P = 0.853, n = 4). (D) Quantification of the area of the red BK potassium channel patches in A and B for each genotype (P = 0.265, n = 4). (C and D) Statistical analysis was performed using a two-tailed unpaired Student’s t-test (ns = P > 0.05).

Though the immunostaining experiments provided a generally indicator of the maturation of the inner hair cells, comparing fluorescence intensities and area is not very accurate. Thus, to more closely analyse the maturation of inner hair cell, we used whole-cell patch clamping to analyse the current and voltage responses of these cells. The voltage responses obtained under current clamp were very similar between IHCs from juvenile control (**Figure 5.10A**) and knockout (**Figure 5.10B**) mice. Neither genotype possessed inducible spiking activity upon the application of a depolarising current, characteristic of immature hair cells, but instead show mature graded and sustained responses (Kros *et al.* 1998, Marcotti *et al.* 2003a). IHCs had a resting membrane potential that was not significantly different between the two genotypes (**Figure 5.10C**). Whole cell voltage clamp traces also appear similar between the two genotypes (**Figure 5.11**). Further analysis, which has been corrected for the residual series resistance after compensation, yields similar current/voltage (I/V) curves between control and knock-out animals (**Figure 5.12A and B**). In order to statistically compare the type genotypes, current values were obtained from the sustained I/V curve at 0 mV and the fast ($I_{K,f}$) I/V curve at -25 mV (**Figure 5.12C and D**). Extracting values from the sustained I/V curve at 0 mV allows for the comparison of the sustained outward current, and thus the combined fast activating $I_{K,f}$ and slow activating $I_{K,s}$ components (Section 1.4.2). Whereas extracting values from the fast (2 ms) I/V curve at -25 mV allows for the comparison of the $I_{K,f}$ currents only, as the $I_{K,s}$ component is too slow to be contributing significantly at this time point, at a membrane potential that should result in half-maximal activation of the BK channels (Marcotti *et al.* 2003a, Latorre and Brauchi 2006). Comparison of both of these values indicates statistically similar fast ($I_{K,f}$) and sustained ($I_{K,f} + I_{K,s}$) currents between the two genotypes (**Figure 5.12**). Taken together, this electrophysiological comparison indicates that inner hair cell basolateral currents are not significantly affected in any way by the hair cell specific deletion of DG.

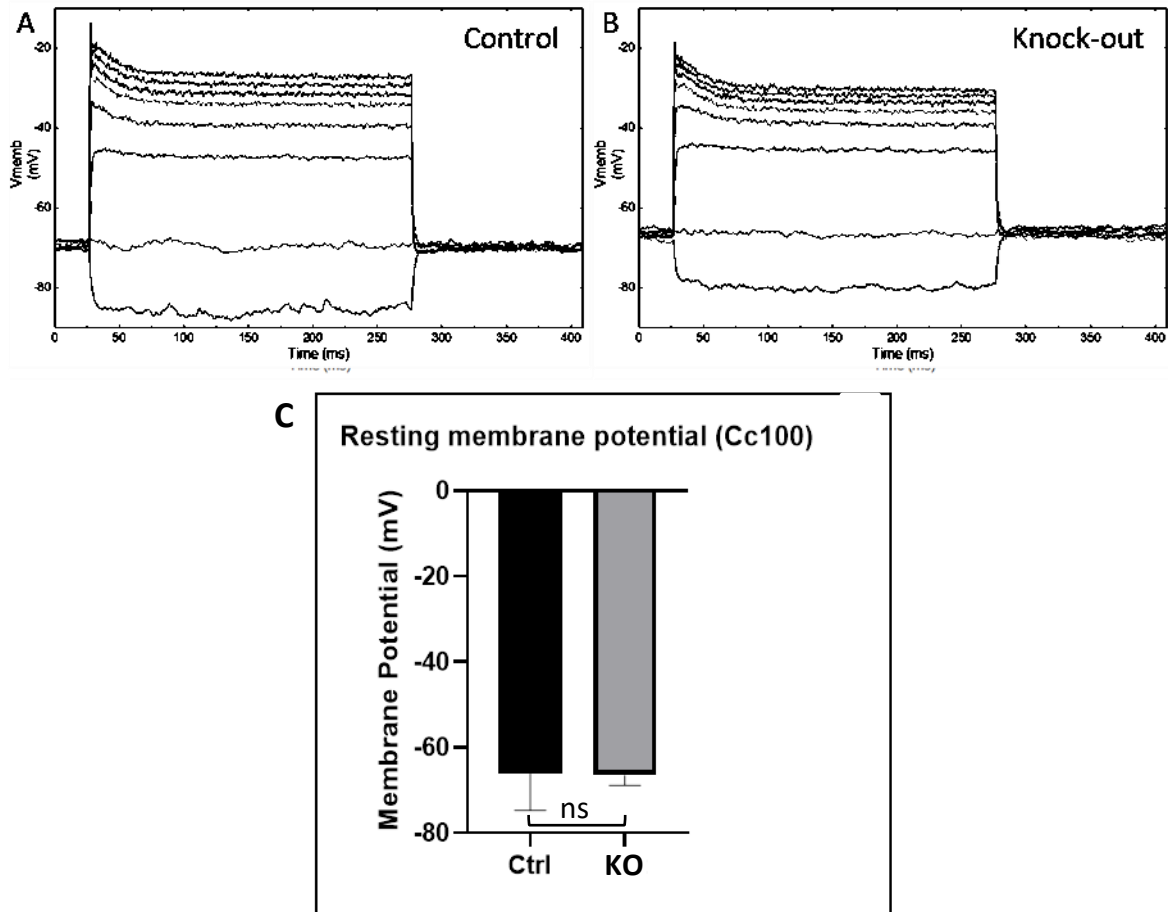


Figure 5.10 – Investigating the current clamp responses of control and DG knock-out P17-24 inner hair cells – Example voltage responses recorded from control (A, n=7) and DAG1 knock-out (B, n=6) inner hair cells obtained by applying a series of current injections from -100 to 900 pA in 100 pA steps. (C) Quantification of the resting membrane potential for control and knock-out inner hair cells measured from the raw traces obtained by averaging the membrane voltage prior to the onset of the stimulation ($P = 0.766$). Statistical analysis was performed using a two-tailed unpaired Student’s t-test (ns = $P > 0.05$).

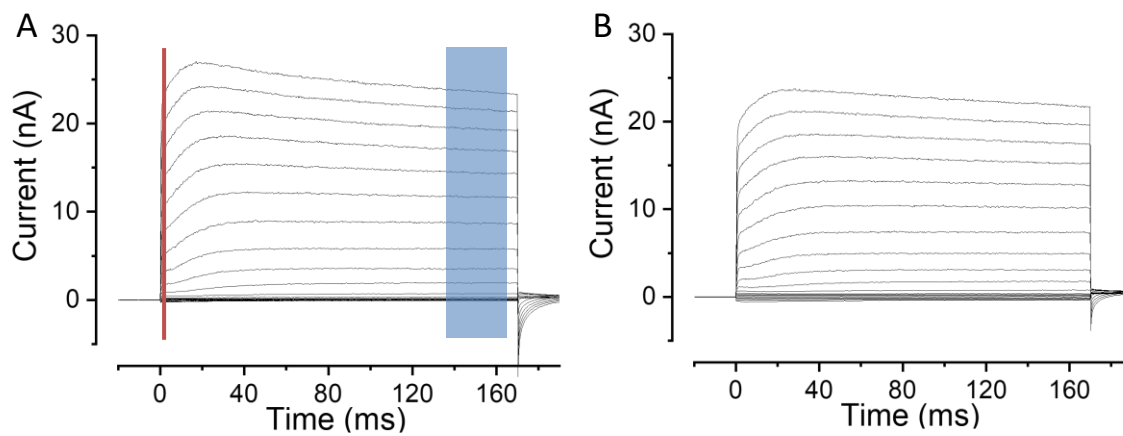
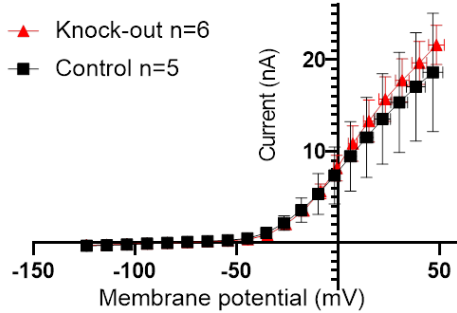


Figure 5.11 – Current recordings from control and knock-out animals – Current recordings under voltage clamp obtained by applying 10 mV steps from -124 to 66 mV (nominal increment), starting from a holding potential of -84 mV, in both control (A, n = 5) and DG knock-out (B, n = 6) animals. (A) The red line corresponds to the area of the trace used to measure the fast $I_{K,f}$ (2 ms after the onset of the voltage step) used to generate the I/V curve (see Bardhan *et al.* 2019). The blue bar corresponds to the area averaged to obtain values for the the steady-state current (see Bardhan *et al.* 2019).

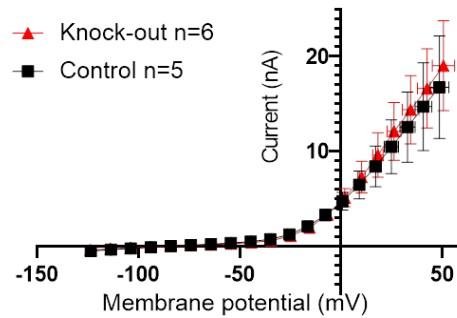
The impact of DG deletion on the sustained portion of the voltage clamp trace

A

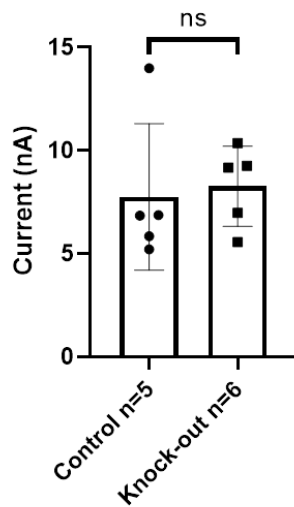


The impact of DG deletion on the fast ($I_{K,f}$) portion of the voltage clamp trace

B



C Sustained current at 0mV



D I_{Kf} (2 ms) current at -25mV

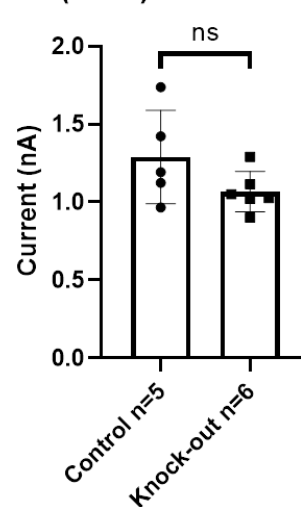


Figure 5.12 – Analysis of the control and knock-out current recordings – (A) I/V curve created using the steady-state component visualised in **figure 5.11A** after residual series resistance compensation, allowing for the comparison of voltage dependence between the control (n = 5) and knock-out (n = 6) inner hair cells. (B) Size of $I_{K,f}$ as a function of voltage in both control (n = 5) and knock-out (n = 6). The isolated $I_{K,f}$ was defined as the current at 2 ms after the voltage step. (C) Currents values extrapolated from each sustained I/V curve at 0 mV (P = 0.787). (D) Current values extrapolated from the fast ($I_{K,f}$) I/V curve at -25 mV (P = 0.183). Statistical analysis was performed using a two-tailed unpaired Student's t-test (ns = P > 0.05).

Due to our inability to localise dystroglycan to the organ of Corti with any of the antibodies at our disposal, qPCR was utilised in order to measure the difference in cochlear DAG1 mRNA expression between control ($DAG1^{-/-} \times MYO15Cre^{+/+}$) and knock-out ($DAG1^{-/-} \times MYO15Cre^{+/-}$) animals. As the knock-out is specific only for the hair cells in the whole cochlea, normal RT-PCR was not sensitive enough to detect a difference in mRNA expression (data not shown). As shown in **Figure 5.13** which uses hypoxanthine-guanine phosphoribosyltransferase (HPRT) as the selected housekeeping gene, the qPCR results did appear to show a general decrease in the amount of DAG1 mRNA present in the knock-out animals, however this difference is not significant. The mRNA for the housekeeping gene GAPDH was also trialed alongside HPRT prior to the experiment, but the standard curve created by GAPDH on a logarithmic scale of mRNA dilution indicated a poorer efficiency than HPRT (data not shown).

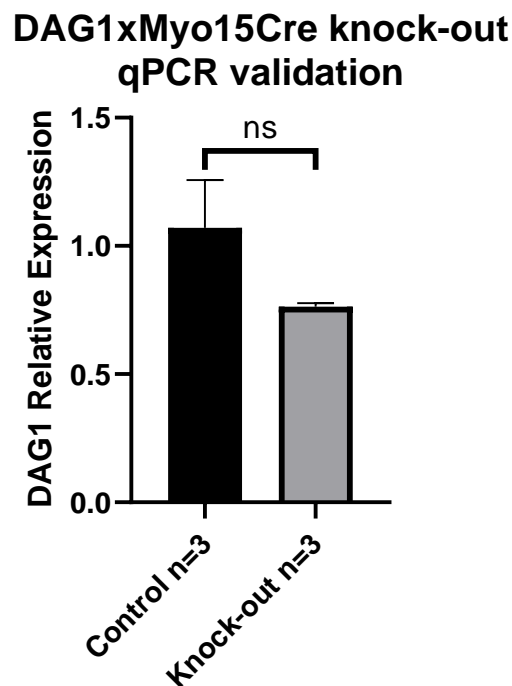


Figure 5.13 – qPCR validation of the conditional post-natal deletion of dystroglycan

– The $2^{-\Delta\Delta Ct}$ values for the amount of DAG1 mRNA present in control ($DAG1^{-/-} \times MYO15Cre^{+/+}$, 3 months of age, n=3) and knock-out ($DAG1^{-/-} \times MYO15Cre^{+/-}$, 3 months of age, n=3) cochleae with the vestibular system removed relative to the HPRT housekeeping gene ($P = 0.103$, two-tailed unpaired Student's t-test, ns = $P > 0.05$). Error bars represent the standard deviation.

5.3 – Discussion

The ABR data strongly indicate that the conditional post-natal deletion of DG from cochlear hair cells does not affect hearing thresholds in young or aged mice. The data also indicate that, unrelated to the DAG1 or MYO15Cre locus, the line appears to show a sporadic high frequency hearing loss. This hearing loss is also unrelated to the sex of the animals, as both males and females were similarly affected. While this hearing loss makes comparison of the genotypes less reliable, unaffected control and knock-out mice showed comparable hearing thresholds. In line with the ABR threshold data which indicates no apparent deficits in sound sensitivity, the statistically similar DPOAE data indicates that the outer hair cell amplification is also unaffected by the post-natal deletion at all ages tested. DPOAEs directly record the cycle-by-cycle amplification of the outer hair cells and thus if dystroglycan possessed a role in normal outer hair cell development or function we would certainly expect the DPOAE thresholds to be significantly impacted. Assuming the original hypothesis was correct, and DG is indeed functioning to facilitate normal hair cell development through the proper localisation of EPS8L2, we could expect the two phenotypes to be extremely similar. However, the DG deletion does not show any sign of the progressive hearing loss seen in the EPS8L2 knock-out animal, which is apparent in animals as young as one month old (Furness *et al.* 2013). Thus, it appears as though DG does not play a role in the maintenance of stereocilia through EPS8L2 regulation or localisation.

Given the lack of an effect on the cochlear stereocilia, we then investigated the ribbon synapses in the knock-out to investigate whether DG could indeed be functioning to facilitate normal ribbons in the cochlea as it does in the retina via a pikachurin based mechanism (Sato *et al.* 2008). Immunolabelling experiments indicated that the number and alignment of ribbon synapses was statistically similar between both genotypes which suggest that the ribbon synapses are similarly unaffected in the knock-outs. Furthermore, if a severe impairment of ribbon synapses was apparent this would have been apparent in the ABR experiments, which further supports the notion that the synaptic ribbons are fully functional in the knock-out. Had we seen some impact of the knock-out on ribbon alignment or number, the ribbon synapse function could have been further investigated with wave I amplitude analysis of the ABR traces. Wave I analysis would have provided a read-out for any deficits in the transmission to the afferent neurons, and this transmission defect could be further studied with capacitance measurement experiments. By measuring

the capacitance of the cell with whole cell patch clamping, stimulating vesicular fusion via sustained depolarisation, and then measuring the capacitance again, the release kinetics and amplitude can be quantified. However, due to the lack of any evidence supporting a defect in the synapses, these experiments were deemed unnecessary.

Thus, with no apparent impact on the stereocilia or ribbon synapses of the hair cells, the final aspect investigated in the mutant was the maturation of the inner hair cells, which should be accompanied by the onset of BK expression and the loss of SK2 puncta in normal conditions (Marcotti *et al.* 2003a, Marcotti *et al.* 2004a). Immunolabelling experiments revealed that the maturation of the inner hair cells appears comparable to the control animal, showing a statistically comparable expression of the BK potassium channel between the two genotypes. Furthermore, both the control and knock-out sections also show a lack of the SK2 potassium channel puncta seen in immature inner hair cells and mature outer hair cells (Marcotti *et al.* 2004a). More detailed investigation of the maturation with whole cell current clamping revealed that knock-out inner hair cells, similar to the control cells, do not show the spiking activity in response to depolarising currents characteristic of immature cells. The knock-out inner hair cells also showed statistically similar resting membrane potentials to the control animals (Kros *et al.* 1998, Marcotti and Kros 1999). In agreement with the BK immunofluorescence, the fast transient component ($I_{K,f}$) of voltage clamp I/V curves at -25 mV was statistically similar between the two genotypes (Kros *et al.* 1998, Marcotti *et al.* 2004b). Also, the sustained current I/V curve intersects at 0 mV was statistically comparable between the two genotypes, indicating no apparent effect on $I_{K,f}$ or $I_{K,s}$. Taken together this data suggests that the maturation of the hair cells, their ribbon synapses and their stereocilia are unaffected by the conditional deletion of DG.

Due to our inability to localise dystroglycan in the control animal, we have no simple way to validate whether our knock-out model is indeed selectively removing dystroglycan from the hair cells. While qPCR did appear to pick up a non-significant decrease in the amount of DAG1 mRNA present in the knock-out animal, this is not enough to definitively state that the dystroglycan knock-out is functioning as intended. Given more time, this experiment would be repeated using the dissected organ of Corti for the mRNA extraction, rather than the whole-cochlea minus the vestibular system. This would provide a smaller amount of starting mRNA with the intention being that this allows for the difference in DAG1 mRNA to be more easily detected in the knock-out animal, as a greater proportion

of the total DAG1 mRNA would be removed by the knock-out. If this modified protocol was also unsuccessful, fluorescent mRNA probes designed to bind in a complementary fashion to DAG1 mRNA could also be used, to allow the easy comparison of DAG1 mRNA in hair cells and the surrounding tissue.

Chapter 6 – Investigating the phenotype associated with the knock-out of BAIAP2L2, a protein that may be involved in the differential localisation of EPS8 and EPS8L2

6.1 – Introduction

With the investigation on the role of dystroglycan within the cochlea completed, we next investigated another protein hypothesised to possess a role in establishing and maintaining the differential localisation of EPS8 and EPS8L2 in the organ of Corti. The I-BAR (Inverse bin-amphiphysin-Rvs) protein family consists of BAIAP2 (IRSp53), BAIAP2L1 (IRTKS), BAIAP2L2 (Pinkbar), MIM (MTSS1) and ABBA (MTSS1L). I-BAR proteins are able to detect and induce negative membrane curvature (Zhao *et al.* 2011) by dimerising and binding to acidic phospholipids (Ahmed *et al.* 2010) via their N-terminal BAR domain. Alongside this domain, all members of the family also possess a C-terminal WH2 (Wiskott-Aldrich homology 2) domain (Zhoa *et al.* 2011) which is able to directly bind to globular actin (Lee *et al.* 2007, Saarikangas *et al.* 2008) and three members (BAIAP2, BAIAP2L1 and BAIAP2L2) possess a central SH3 domain (**Figure 6.1**, Ahmed *et al.* 2010). This SH3 domain is capable of recruiting actin effector proteins including EPS8 (Postema *et al.* 2018), mDia1 (Goh *et al.* 2012), dynamin 1 (Chou *et al.* 2014) and WAVE2 (Suetsugu *et al.* 2006). By first binding to the membrane to induce curvature, and then recruiting these actin effector proteins to the site, I-BAR proteins are able to induce and modulate the growth of actin based protrusions (Sudhaharan *et al.* 2016). One example for the role of I-BAR proteins in this context is in the brush border of the gut epithelia. It was shown that BAIAP2L1 localises to the growing tips of the microvilli alongside EPS8 (Postema *et al.* 2018), and is solely responsible in linking EPS8 to this site. The presence of BAIAP2L1 to the tip was shown to be dependent on the BAR domain, but refined further via the SH3 domain, suggesting that the curvature sensing ability of the protein is responsible for its own localisation (Postema *et al.* 2018). It was also suggested that BAIAP2L1 is capable of elongating microvilli independently of EPS8 via its WH2 domain (Postema *et al.* 2018). This interaction with EPS8 in the gut raises interesting possibilities for a role of the I-BAR proteins in the cochlea in stereocilia length regulation.

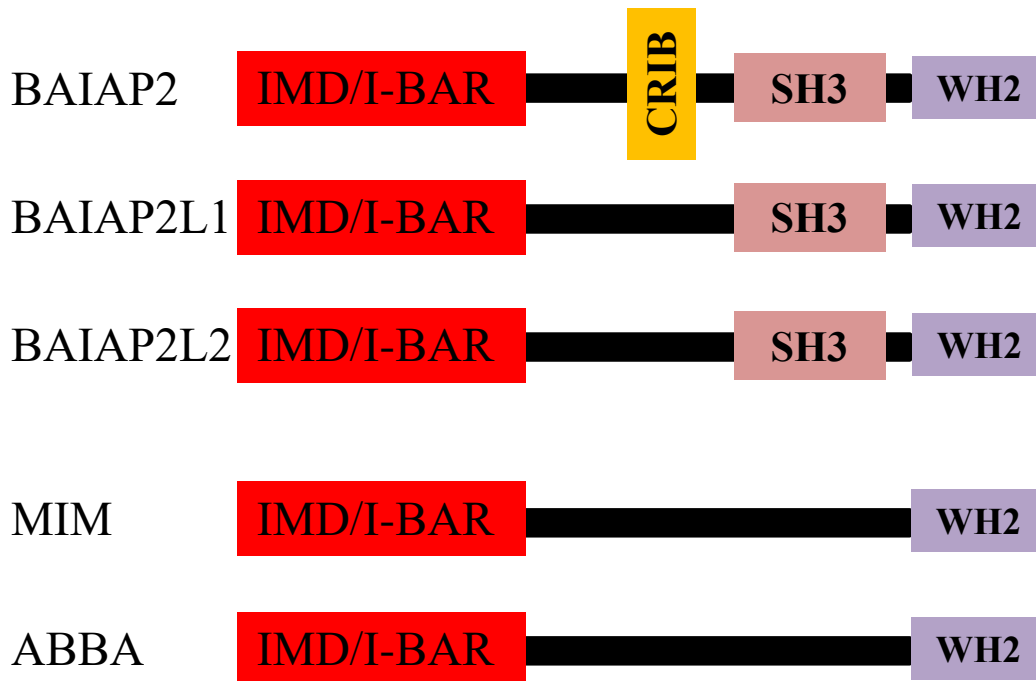


Figure 6.1 – Domain organisation of the I-BAR protein family members – All members of the Inverse Bin-Amphiphysin-Rvs (I-BAR) possess an N-terminal I-BAR domain that allows for their dimerization and binding to acidic phospholipids (Ahmed *et al.* 2010). All members also possess a C-terminal WH2 domain that binds directly to globular actin (Lee *et al.* 2007, Saarikangas *et al.* 2008). BAIAP2, BAIAP2L1 and BAIAP2L2 contain an SH3 domain which permits the recruitment of actin effectors to the tip of membrane protrusions (Ahmed *et al.* 2010). Only BAIAP2 contains a Cdc42/Rac Interactive Binding (CRIB) domain that permits binding to Rho GTPases (Ahmed *et al.* 2010). This figure was redrawn from Safari and Suetsugu 2012.

As introduced previously (Section 1.2.2), the differential localisation of EPS8 and EPS8L2, alongside other proteins that form a complex with them, is essential for the proper formation and maintenance of the stereocilia staircase (Zampini *et al.* 2011, Furness *et al.* 2013). The exact mechanism by which these proteins are precisely segregated between the rows is still not fully understood, and the ability of the I-BAR proteins to localise EPS8 in the gut suggests that they may possess a role in stereocilia morphogenesis and maintenance via EPS8 targeting. Preliminary work has indicated that BAIAP2L2, which was previously thought to only be present in the intestinal brush border and the

kidney (Pykäläinen *et al.* 2014), is present in the cochlea where it appears to interact with EPS8. Furthermore, it was identified in the IMPC screen that knocking out BAIAP2L2 results in a significant increase in hearing threshold (Dickinson *et al.* 2016). Thus the aim of the experiments within this chapter was to investigate the role of BAIAP2L2 in the cochlea, and specifically whether it plays a role in hair cell stereocilia. Our hypothesis was that BAIAP2L2 is essential for normal stereocilia morphogenesis and maintenance by facilitating the proper localisation of the row 1 protein EPS8.

6.2 – Results

6.2.1 – Investigating the severity and progression of hearing loss in BAIAP2L2 knock-out mice

The knock-out model used in the following experiments was the *BAIAP2L2*^{tm1b} homozygote, in which the fourth exon of the gene, which encodes a segment of the I-BAR domain, is deleted and replaced with a lacZ cassette. The I-BAR domain of the protein is crucial for its function, and therefore this large insertion is likely to result in a severe disruption. The lacZ cassette also possesses a splice acceptor site, and therefore also causes abnormal splicing of the BAIAP2L2 mRNA. Littermate *BAIAP2L2*^{tm1b} heterozygous mice were used as the controls for all of the experiments performed. The *BAIAP2L2*^{tm1b} mice were obtained from the International Mouse Phenotyping Consortium (IMPC).

Similar to the DAG1 work, the first priority was to use auditory brainstem response (ABR) experiments to determine the time course, frequency selectivity and severity of hearing loss in the *BAIAP2L2*^{tm1b} homozygous mice. Alongside the results of the distortion product oto-acoustic emissions (DPOAE) experiments, which are performed immediately following the ABR protocol, these experiments provide a good direction for the focused electrophysiological work. At P14, only 2 days after the onset of hearing, *BAIAP2L2*^{tm1b} homozygous mice already show a significantly elevated hearing threshold at all frequencies except 6 kHz (**Figure 6.2A**). DPOAE experiments could not be performed at this age due to the small size of the mice, as placing the metal coupler into the ear canal is extremely challenging. At this early stage, the observed hearing phenotype of the *BAIAP2L2*^{tm1b} homozygote mice was not compatible with the initial hypothesis, since it closely resembled that present in the EPS8L2 knock-out, rather than the EPS8 knock-out

mice. While EPS8 knock-out mice are profoundly deaf, EPS8L2 knock-out animals shows a progressive hearing loss (Zampini *et al.* 2011, Furness *et al.* 2013).

Performing ABR experiments on slightly older mice, at P19-22, indicates an interestingly rapid progression of the hearing loss. The homozygotes at this age show a statistically significant elevation in hearing threshold across all frequencies tested, and the hearing thresholds at the higher frequencies are higher than the P14 knock-outs (**Figure 6.2B**). The ABR hearing threshold in heterozygous mice improved between P14 and P19-22, which is expected as the endocochlear potential matures enhancing the hair cell sensitivity (Song *et al.* 2006).

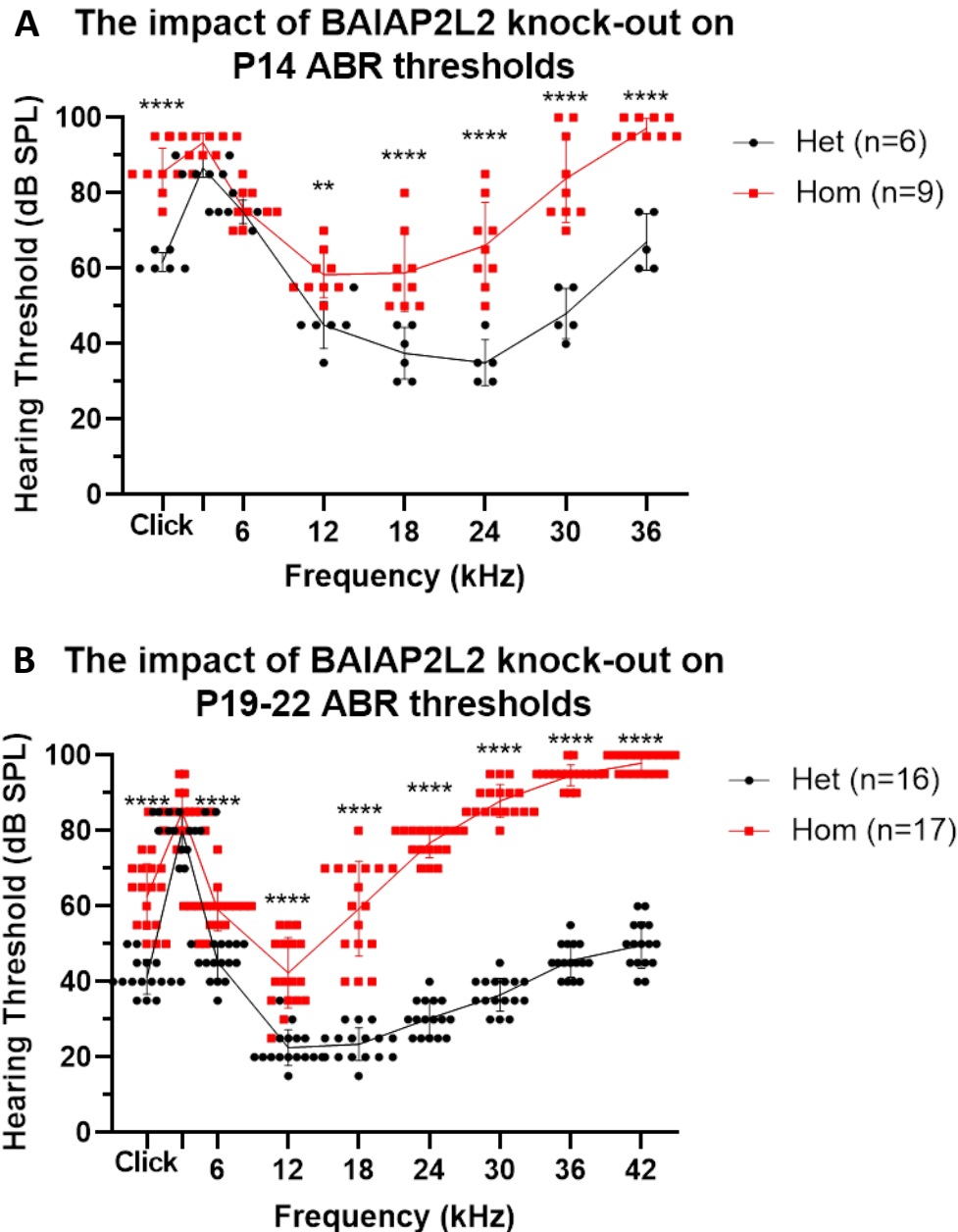


Figure 6.2 – Hearing thresholds in P14 and P19-21 *BAIAP2L2*^{tm1b} homozygous knock-out and heterozygous control mice – (A) ABR hearing thresholds in P14 heterozygote (n=6) and homozygote mice (n=9) in response to white-noise and pure tone frequencies (3-36 kHz)($P < 0.0001$). The 42 kHz point was excluded from this experiment as neither genotype possessed detectable hearing thresholds at this frequency at the highest stimulus amplitude tested of 95dB. For this and all following ABR experiments if a threshold was not detectable at 95dB the value was noted as 100dB, which naturally results in non-parametric distributions. (B) ABR hearing thresholds of P19-21 homozygous *BAIAP2L2*^{tm1b} (n=17) and heterozygous (n=16) in response to pure tone frequencies (3-42 kHz) and the broadband white noise click (P

< 0.0001). (A and B) Data is plotted as the hearing thresholds of individual animals for each frequency alongside the mean, which is plotted as the connecting line. Error bars represent the standard deviation (** = $P < 0.01$, **** = $P < 0.0001$, two-way ANOVA with Šidák's post-test).

ABR thresholds of P48-61 mice indicate that hearing loss in the homozygous mice continues to progress into adulthood, and the hearing threshold are significantly increased in the knock-out animals at all frequencies except 42 kHz (**Figure 6.3A**). At P105-115 (**Figure 6.3B**), the BAIAP2L2 knock-out homozygous mice show no detectable ABR waveform above 30 kHz, and possess thresholds which are significantly higher than the control animals at all frequencies excluding 30 and 42 kHz. By P166-245, the homozygous knock-out mice possess no detectable waveforms at the highest stimulus amplitude (95 dB SPL) across all frequencies tested, including broadband white noise (**Figure 6.4A**). Plotting just the hearing thresholds in response to white-noise stimuli for both genotypes as a function of age demonstrates how the hearing loss progresses in the knock-outs compared to the controls. Control animals show a decrease in hearing threshold between P14 and P19-22 as the endocochlear potential matures and their hearing becomes more sensitive (Song et al. 2006), and after this age the thresholds remain stable until P245 (**Figure 6.4B**). In contrast, while the knock-outs do appear to show a similar pattern of improvement between P14 and P19-22, the white-noise thresholds gradually increase after P19-222 until no waveform for a white-noise stimulus is evident at P245. Taken together, this data indicates that the BAIAP2L2 knock-out appears to show a phenotype which is more similar to the EPS8L2 than EPS8 knock-out (Zampini *et al* 2011, Furness *et al.* 2013), with a progressive age related hearing loss starting at or immediately after the onset of hearing. The phenotype seen in the BAIAP2L2 knock-out appears more severe than that seen in the EPS8L2 mutant, and by P166-245 the mice are profoundly deaf (Furness *et al.* 2013).

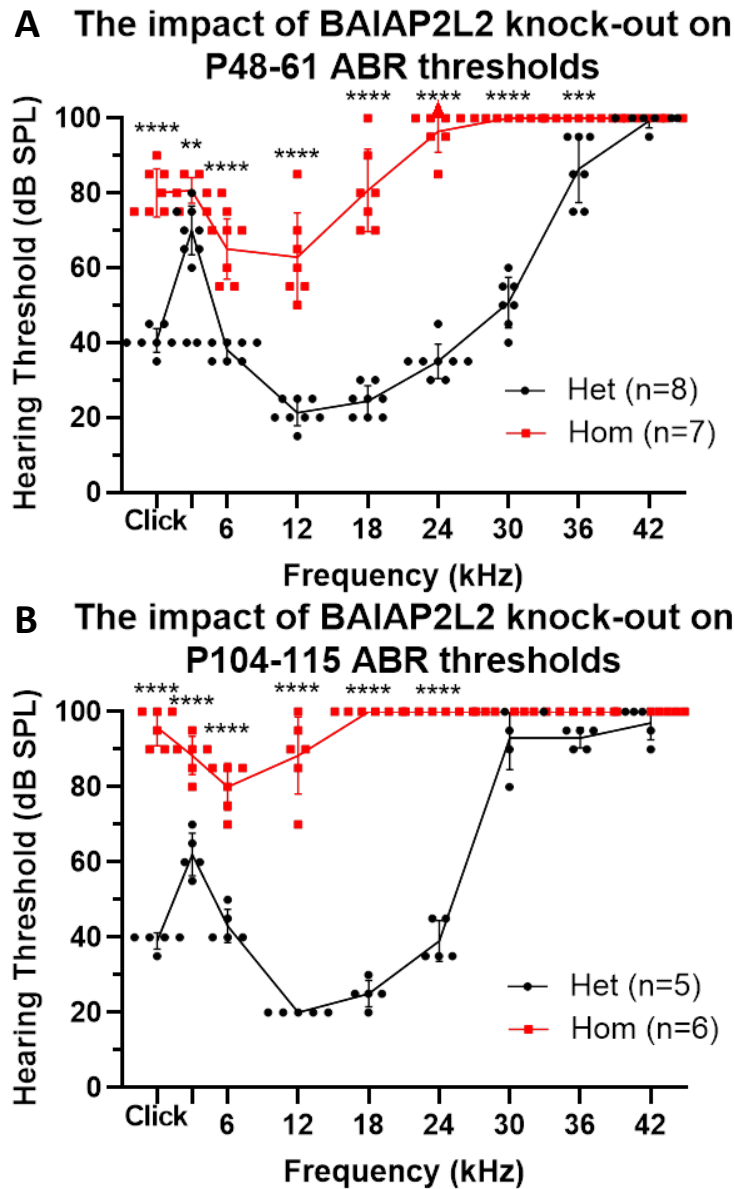


Figure 6.3 - Hearing thresholds in P48-61 and P104-115 *BAIAP2L2*^{tm1b} homozygote knock-out and heterozygous control mice – (A) ABR thresholds of P48-61 homozygous knock-out (n=7) and heterozygous control mice (n=8) in response to a click stimulus and pure-tone frequencies (3-42 kHz) ($P < 0.0001$). (B) ABR responses of P104-115 homozygous knock-out (n=6) and heterozygous control (n=5) *BAIAP2L2*^{tm1b} mice in response to the same set of stimuli ($P < 0.0001$). (A and B) Data is plotted as the hearing thresholds of individual animals for each frequency alongside the mean, which is plotted as the connecting line. Error bars represent the standard deviation and arrowheads indicate where error bars have exceeded the graph boundary (** = $P < 0.01$, *** = $P < 0.001$, **** = $P < 0.0001$, two-way ANOVA with Šidák's post-test).

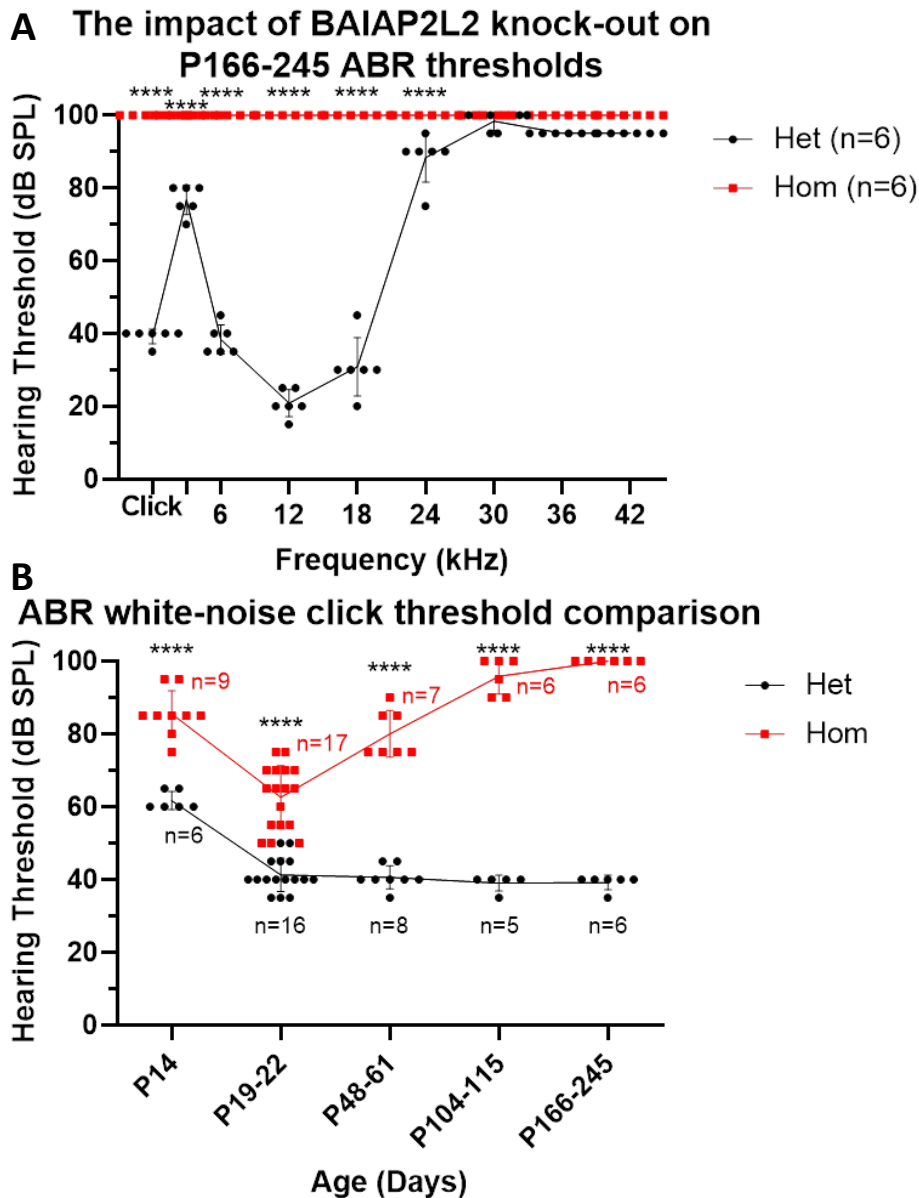


Figure 6.4 – Hearing thresholds in P166-245 *BAIAP2L2*^{tm1b} homozygote knock-out and heterozygous control mice – (A) ABR thresholds for BAIAP2L2 knock-out and control animals in response to a white-noise click and pure tone frequencies (3-42 kHz)($P < 0.0001$). (B) ABR thresholds in response to a white-noise click of knock-out and control animals for all ages tested, from P14 up to P166-245. The number of animals used for each age and genotype are shown on the graph by their relevant cluster. (A and B) Data is plotted as the hearing thresholds of individual animals for each frequency alongside the mean, which is plotted as the connecting line. Error bars represent the standard deviation (**** = $P < 0.0001$, two-way ANOVA with Šidák's post-test).

Furthermore, a more detailed analysis of the ABR waveforms at 12 kHz, which roughly corresponds to the area of the organ of Corti used in the following electrophysiological experiments, indicates that the latency was not significantly affected by the absence of BAIAP2L2 in knock-out mice (**Figure 6.5A-C**). This suggests that synaptic transmission is unlikely to be impaired by in BAIAP2L2 knock-out mice. However, the homozygous knock-out does result in a significantly increased wave I amplitude between 15 and 50 dB above hearing threshold, possibly due to differences in the shape of the amplification response (**Figure 6.5D**). The similar maximal amplitude achieved in both genotypes indicates that the inner hair cells appear to still be able to effectively transmit to the spiral ganglion afferents, which like the comparable latency suggests that synaptic transmission is unaffected. Taken together, the impact of the mutation on the ABRs and the increased amplitude of wave I suggest that the progressive degeneration in cochlear sensitivity is likely not being caused by deficits in synaptic transmission.

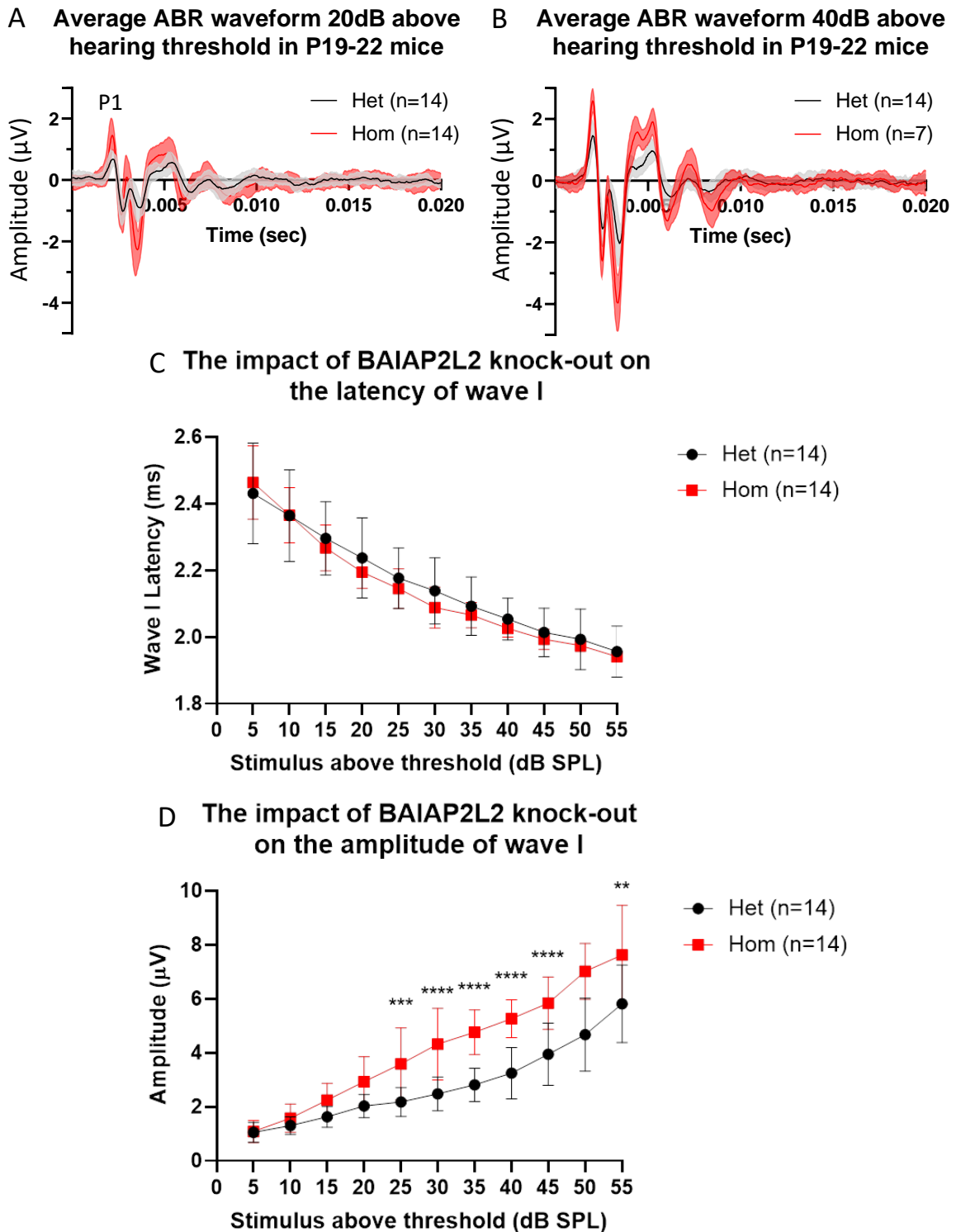


Figure 6.5 – The effect of BAIAP2L2 knock-out on the latency and amplitude of ABR wave I – (A) Average ABR waveform from P19-22 homozygous knock-out (n=14) and heterozygous control mice (n=14). Traces were averaged from the waveforms 20 dB above hearing threshold at the 12 kHz pure tone frequency. The shaded area corresponds to the standard deviation. Amplitude measurements were calculated as the difference between the first peak (P1) and trough (N1) of the ABR

waveform. (B) Similarly created average ABR waveform of knock-out (n=7) and control (n=14) mice at 12 kHz, 40 dB above the hearing threshold, with the shaded area again corresponding to the standard deviation. (C and D) The latency ($P = 0.076$) and amplitude ($P < 0.0001$) of the peak of wave I respectively, normalized with the stimulus amplitude above hearing threshold. Error bars represent the standard deviation (** = $P < 0.01$, *** = $P < 0.001$, **** = $P < 0.0001$, two-way ANOVA with Šidák's post-test).

Analysis of the DPOAE thresholds, which provide a direct indication of the functionality of the outer hair cell amplification system, reveals significantly raised thresholds in P19-22 mice relative to the control animals between 12 and 24 kHz (**Figure 6.6A**). Thus, paired with the ABR data, the DPOAE thresholds suggest that the loss of cochlear sensitivity seen in even the young mice is somewhat due to deficits in outer hair cell amplification. At P48-61 the DPOAE thresholds of the homozygous animals have degenerated further relative to the control mice, and possess significantly elevated thresholds between 6 and 24 kHz (**Figure 6.6B**). By P104-115, the DPOAE stimulation thresholds have risen further, and only achieve above-threshold values below 24 kHz, and are significantly higher than the control animals at 12 and 18 kHz (**Figure 6.7A**). At P166-245, the oldest age analysed for DPOAE thresholds, homozygous animals showed significantly higher thresholds at 12 kHz relative to the control animals (**Figure 6.7B**). The control animals also show a deterioration of the DPOAEs at this advanced age, which is expected given the use of the background strain (C57BL/6N) as a model of age related hearing loss (Kane *et al.* 2012). Thus the loss of sensitivity seen in the ABR experiment is caused in part by the progressive malfunction of the outer hair cell amplification system, which is apparent in animals as young as P19-22, the youngest that these experiments can be performed on.

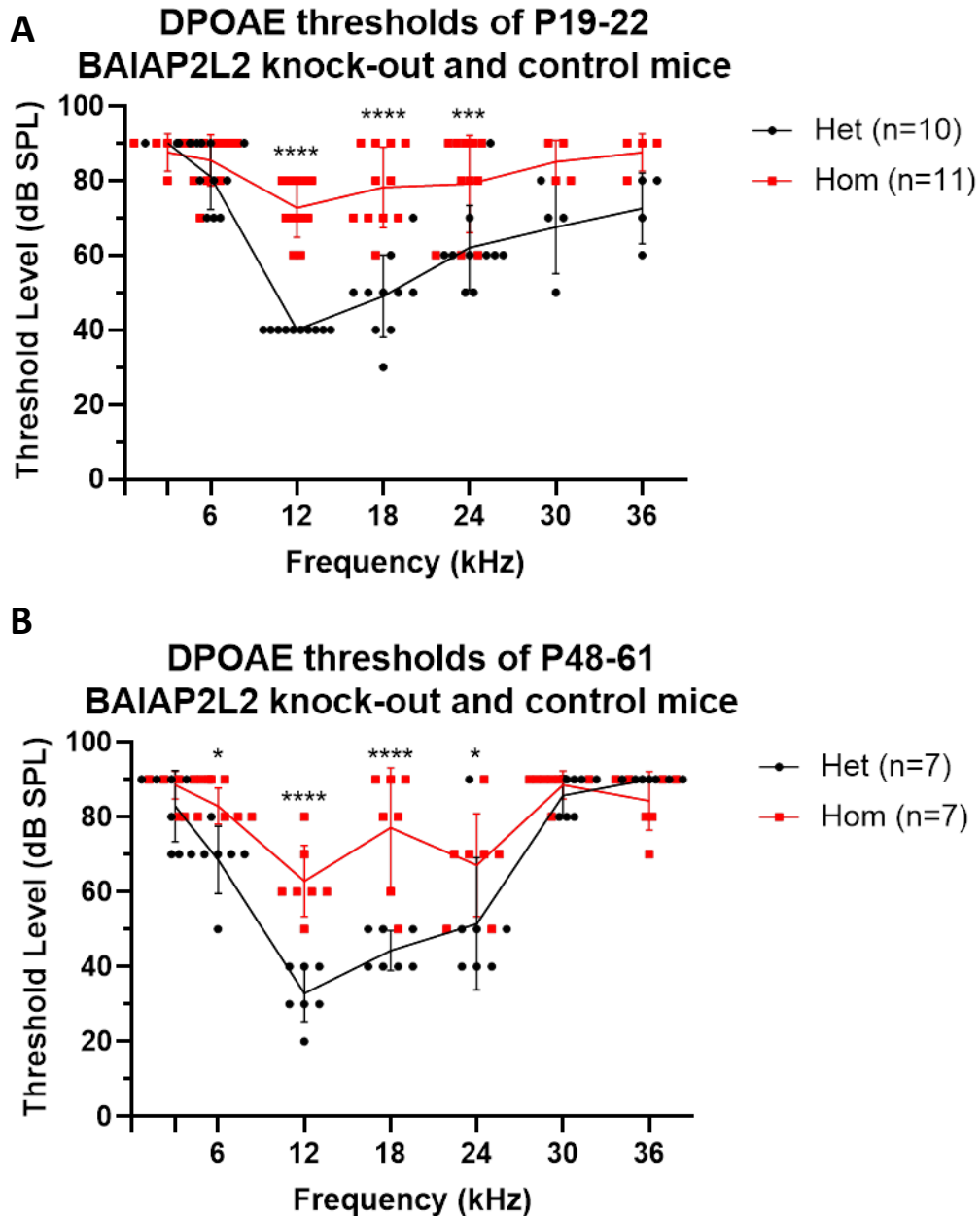


Figure 6.6 – DPOAE thresholds in P19-22 and P48-61 *BAIAP2L2*^{tm1b} homozygote knock-out and heterozygous control mice – (A) DPOAE thresholds of P19-22 homozygous knock-out (n=10) and heterozygous control mice (n=11) in response to stimulus frequencies between 3 and 36 kHz ($P < 0.0001$). (B) DPOAE thresholds of P48-61 homozygous knock-out (n=7) and heterozygous control mice (n=10) in response to the same set of stimuli ($P < 0.0001$). (A and B) Each frequency was tested from 10 to 80 dB in 10 dB steps. If DPOAEs did not exceed the threshold at the highest stimulus amplitude testable of 80 dB the value was noted as 90 dB, naturally resulting in non-parametric data distributions. Data is plotted as the DPOAE thresholds of individual animals for each frequency alongside the mean,

which is plotted as the connecting line. Error bars represent the standard deviation (* = $P < 0.05$, *** = $P < 0.001$, **** = $P < 0.0001$, two-way ANOVA with Šidák's post-test).

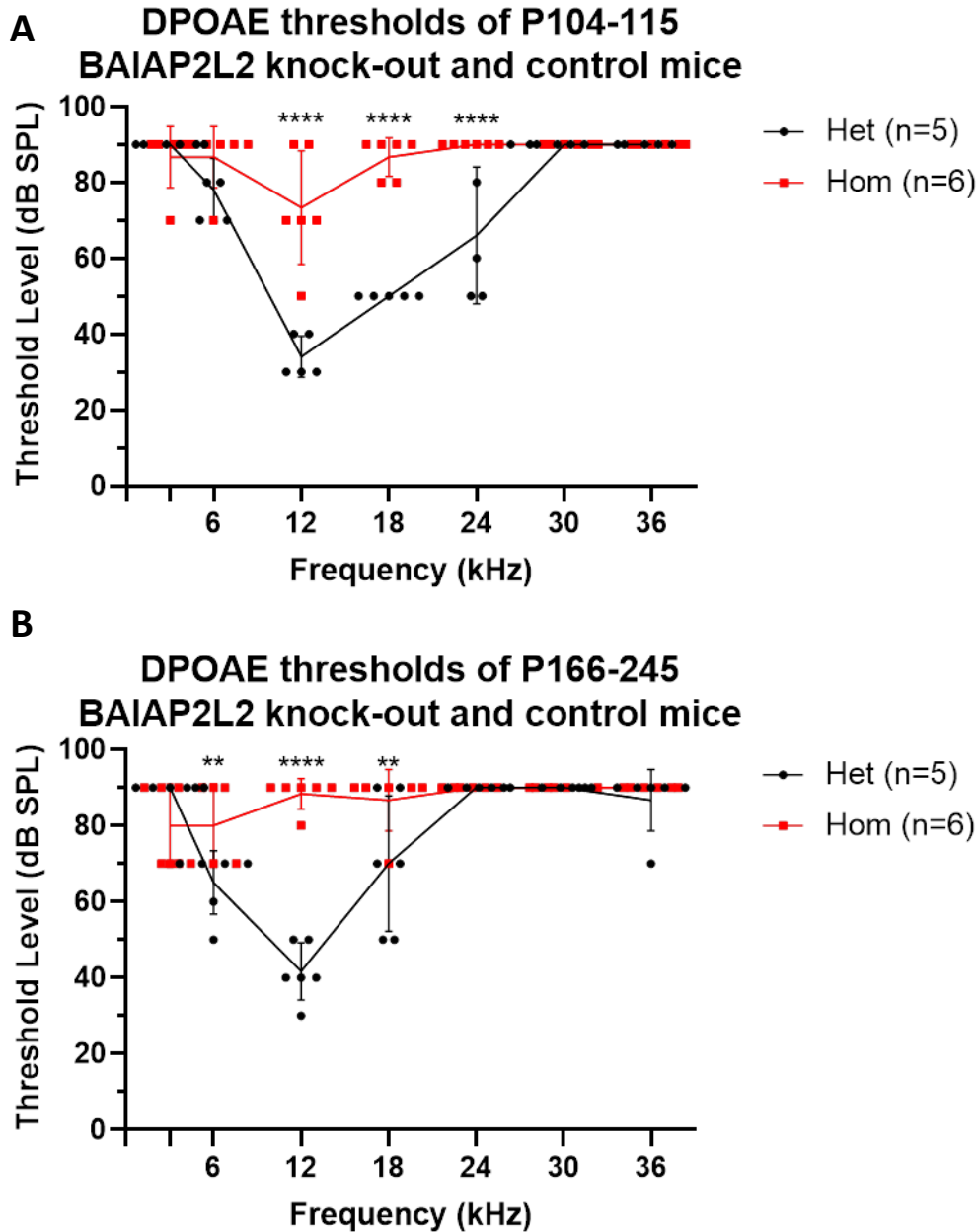
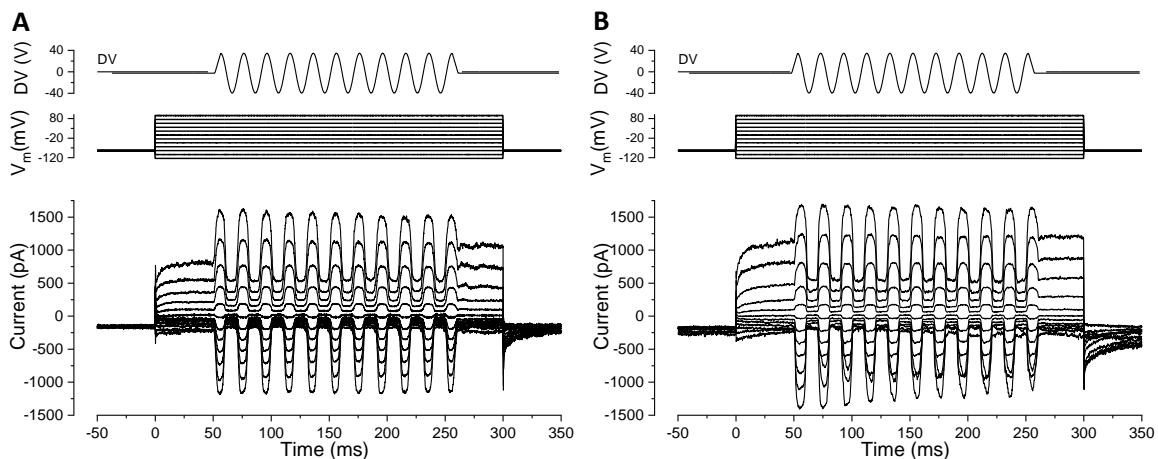


Figure 6.7 – DPOAE thresholds in P48-61 and P105-115 *BAIAP2L2*^{tm1b} homozygote knock-out and heterozygous control mice – (A) DPOAE thresholds of P48-61 homozygous knock-out (n=6) and heterozygous control (n=5) *BAIAP2L2*^{tm1b} mice in response to stimulus frequencies between 3 and 36 kHz. (B) DPOAE thresholds of homozygous knock-out (n=6) and heterozygous control (n=5) animals at P166-245, the oldest age at which the DPOAE experiment was performed, in response to

frequencies between 3 and 36 kHz. (A and B) Each frequency was tested from 10 to 80 dB in 10 dB steps. Data is plotted as the DPOAE thresholds of individual animals for each frequency alongside the mean, which is plotted as the connecting line. Error bars represent the standard deviation (** = $P < 0.01$, **** = $P < 0.0001$, two-way ANOVA with Šidák's post-test).

6.2.2 – Investigating mechanotransduction of BAIAP2L2 knock-out hair cells

Based on the hypothesis that BAIAP2L2 is functioning to localise EPS8, and thus regulate the formation of the hair bundle, we next investigated the mechano-electrical transduction (MET) in BAIAP2L2 knock-out outer hair cells. At P8-P9 both heterozygous and homozygous outer hair cells show a similar MET current response to saturating 50Hz sinusoids delivered via fluid jet between membrane potentials of -124 mV and +96 mV in 10mV nominal increment steps (**Figure 6.8A and B**). Movement of the bundle towards the taller stereocilia in the excitatory direction results in large inward currents at negative membrane potentials, which reverses for potentials positive to 0 mV due to the non-selective nature of the MET channel (Section 1.2.1). Note that both example traces show comparable amplitude at both hyperpolarised and depolarised holding potentials. From these MET traces, we can obtain values for the maximal MET current, defined as the difference between the peak and trough of the sine-induced response for each holding potential, which allows for the generation of a current/voltage curve to easily compare the two genotypes. As seen in **Figure 6.8C**, P8-9 mice of both genotypes show statistically similar MET currents across all of the holding potentials tested.



C
BAIAP2L2 knock-out and control
MET currents at P8-9

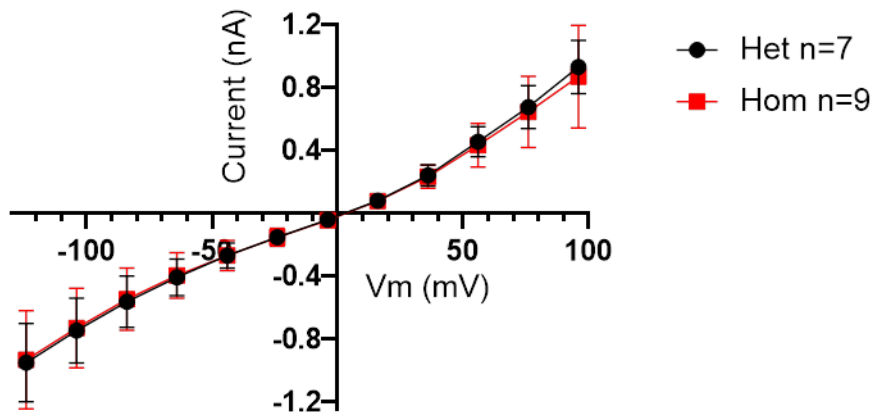


Figure 6.8 – MET recordings from P8-9 *BAIAP2L2*^{tm1b} heterozygous and homozygous outer hair cells – Current responses of outer hair cells of *BAIAP2L2* heterozygous (A, n=7 cells from 3 mice) and homozygous (B, n=9 cells from 4 mice) mice to 40V 50Hz sinusoids between -124 and 96 mV in 20 mV voltage steps from a holding potential of -84 mV. The piezo driver voltage sine wave and holding potential series are displayed above the MET traces. Fluid jet position was finely adjusted to elicit a saturated response from the hair bundle, visible as a flat peak in the current trace upon bundle deflection. (C) An I/V curve of the maximal MET current size in outer hair cells generated from the raw traces of the heterozygous (n=7 cells from 3 mice) and homozygous (n=9 cells from 4 mice) (P = 0.819, two-way ANOVA with Šidák's post-test). Note that the curve passes through the origin due to the non-selective nature of the MET channel. Error bars represent the standard deviation of the current response at each voltage step.

The resting current of the MET channels can be analysed from the sine response traces, determined from the difference between the holding current and the size of the MET current during inhibitory bundle deflection (i.e. closure of the MET channels). This resting current, when measured as a percentage of the maximal MET current, allows for the calculation of the resting open probability of the MET channels. As seen in **Figure 6.9**, the resting open probability of the MET channels is statistically comparable at the most negative potential of -124 mV and the most positive potential at +96 mV. Note how the open probability of the MET channel is higher at the depolarised holding potential which is close to the reversal potential for calcium. The reduced calcium entry into the MET channel removes adaptation and thus increases the open probability of the channel (Ricci *et al.* 2003, Corns *et al.* 2014). Thus, at least in the context of fluid jet induced currents, the hair bundle appears to be functioning normally in the BAIAP2L2 mutants at this age.

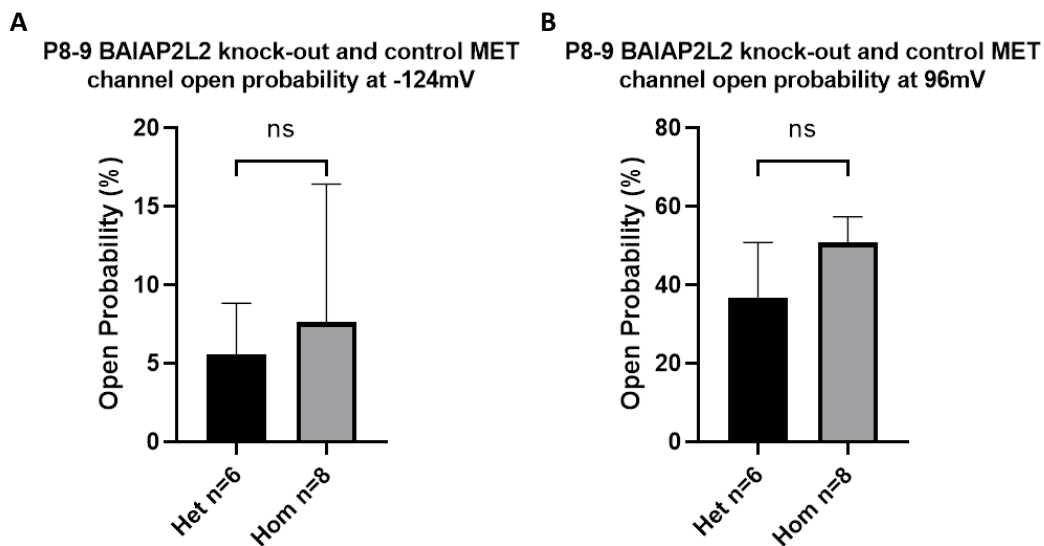
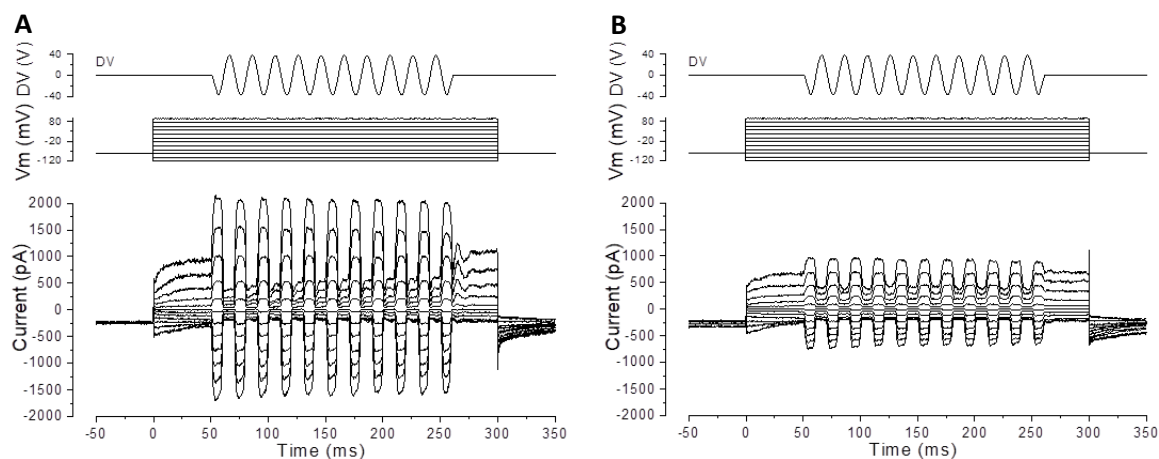


Figure 6.9 – The impact of BAIAP2L2 mutation on the resting open probability of the MET channels in P8-9 mice – Comparison of the resting open probability of heterozygous (n=6 cells from 3 mice) and homozygous (n=8 cells from 4 mice) BAIAP2L2 outer hair cells at the most hyperpolarised (-124 mV, A, P = 0.245) and depolarised (+96 mV, B, P = 0.0597) holding potentials (two-tailed unpaired Student’s t-test, ns = P > 0.05, * = P < 0.05). Error bars represent the standard deviation.

Performing similar experiments in slightly older P11 mice revealed that BAIAP2L2 appeared to possess smaller MET current at both hyperpolarised and depolarised voltage steps (**Figure 6.10A and B**). Using these traces to generate an I/V curve, as before, indicates that the *BAIAP2L2*^{tm1b} homozygous mice possess a significantly reduced MET amplitude (**Figure 6.10C**). Further analysis of the MET traces indicates that the mutation does not appear to affect the open probability of the MET channels (**Figure 6.11**). Thus BAIAP2L2 knock-out results in the rapid degeneration of the outer hair cell MET current between P8-9 and P11. Unfortunately, the progression of changes in the MET current becomes much more difficult to analyse at older ages. This is due to the gradual attachment of the tips of the outer hair cell stereocilia to the tectorial membrane (Verpy *et al.* 2011), making it difficult to remove the membrane without damaging the delicate stereocilia. Thus P11 is the oldest age at which we could reliably perform these MET experiments without mutations to weaken the stereocilia-tectorial membrane attachment (Jeng *et al.* 2020).



C
BAIAP2L2 knock-out and control
MET currents at P11

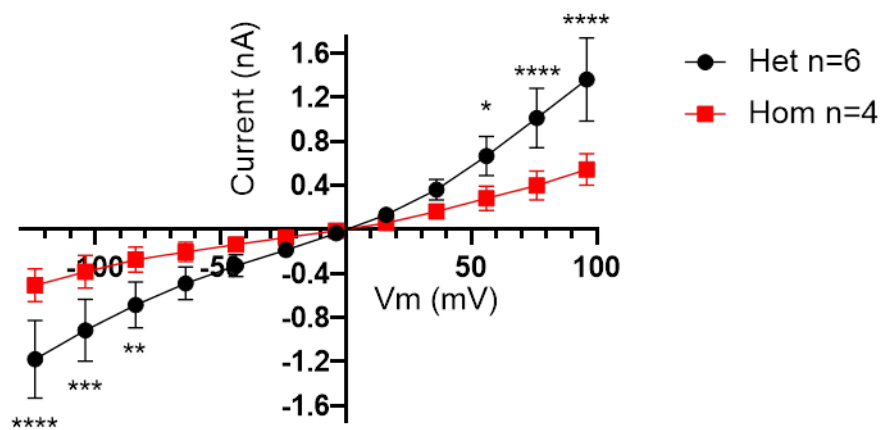


Figure 6.10 – MET recordings from P11 *BAIAP2L2*^{tm1b} heterozygous and homozygous mice – Representative outer hair cell current responses of heterozygous (A, n=6 cells from 2 mice) and homozygous (B, n=4 cells from 1 mouse) mice elicited with 40V 50Hz sinusoids between -124mV and 96mV in 20mV steps from a holding potential of -84 mV. (C) I/V curve of the maximal MET current across the range of holding potentials generated from the raw traces of heterozygous (n=6 cells from 2 mice) and homozygous (n=4 cells from 1 mouse) outer hair cells (P < 0.0001, two-way ANOVA with Šidák's post-test, * = P < 0.05, ** = P < 0.01, *** = P < 0.001, **** = P < 0.0001). Error bars represent the standard deviation.

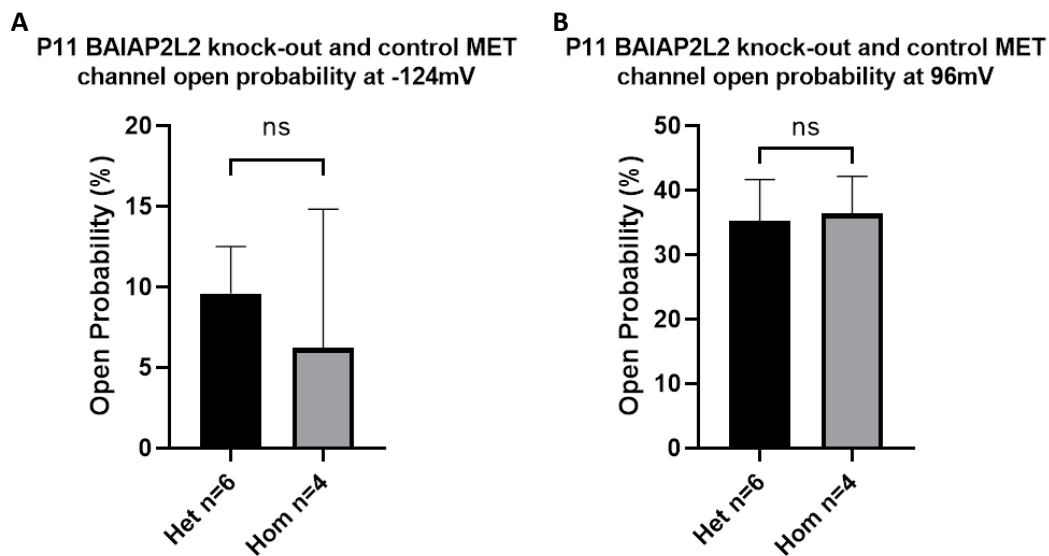


Figure 6.11 - The impact of BAIAP2L2 mutation on the resting open probability of the MET channels in P11 mice – The resting open probability of the MET channels of heterozygous (n=6 cells from 2 mice) and homozygous (n=4 cells from 1 mouse) mice at both hyperpolarised (-124mV, A, P = 0.500) and depolarised (96mV, B, P = 0.780) potentials (two-tailed unpaired Student’s t-test. ns = P > 0.05). Error bars represent the standard deviation.

To further analyse the mechanotransduction in the *BAIAP2L2*^{tm1b} mutants, the outer hair cells of P8-11 mice were also stimulated with a fluid jet step stimulation to analyse the MET channel adaptation (Crawford *et al.* 1989, Wu *et al.* 1999, Vollrath and Eatok 2003). Upon sustained bundle deflection at negative membrane potentials, MET current adapted in both genotypes, a feature which was absent when stepping to a depolarised potential (**Figure 6.12A-D**). Quantification of the amount of the MET current that is reduced over time during sustained stimulation revealed no significant difference between the two genotypes (**Figure 6.12E**). Thus it appears as though BAIAP2L2 mutation does not affect the open probability or adaptation kinetics of the MET channel in P8-11 mice.

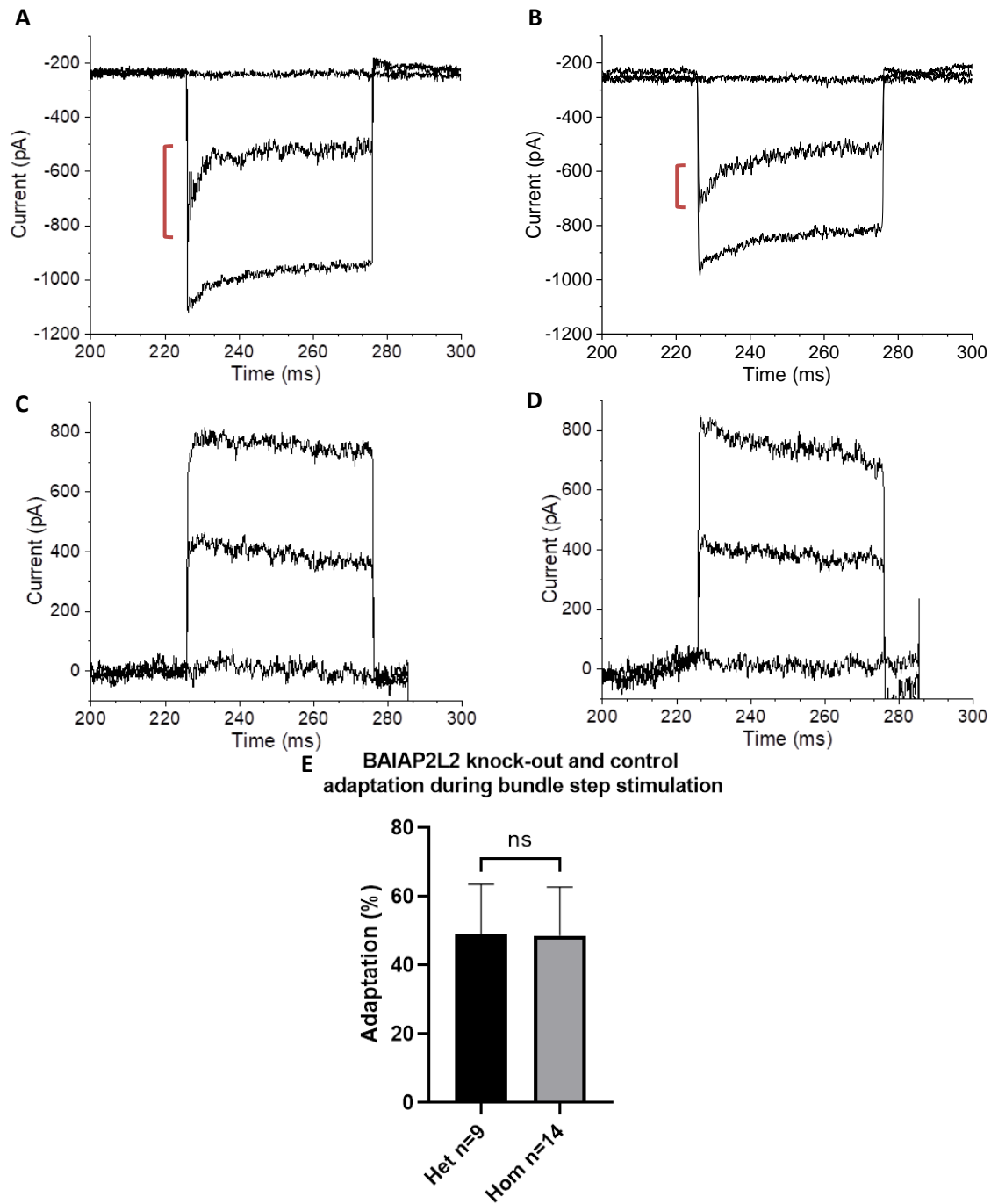


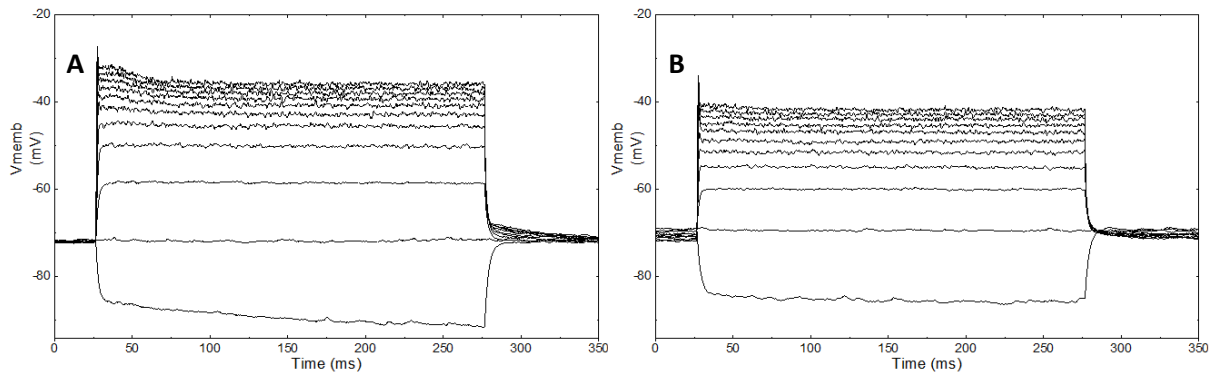
Figure 6.12 – Adaptation in the *BAIAP2L2^{tm1b}* homozygous and control mice – Representative traces of heterozygous (A, n=10 cells from 4 mice) and homozygous (B, n=14 cells from 5 mice) outer hair cells in response to fluid jet step stimulation at a hyperpolarised (-84 mV) holding potential. These traces display classic fast adaptation, particularly with non-saturating stimulation (red bars). Holding at depolarised potentials of +96 mV, and thus preventing calcium influx, prevents the fast adaptation response in heterozygous (C, n=9 cells from 4 mice) and homozygous animals (D, n=12 cells from 5 mice). (E) The percentage of the MET current

response that is adapted by the end of the fluid jet step stimulation in both genotypes ($P = 0.996$, two-paired unpaired Student's t-test, ns = $P > 0.05$, log to the base 10 of values used for statistical test to compensate for non-parametric nature of percentage data). Error bars represent the standard deviation.

6.2.3 – Investigating the maturation of BAIAP2L2 knock-out inner and outer hair cells

In order to further investigate the mechanism of the BAIAP2L2 phenotype, we next analysed the maturation of the electrophysiological properties of both inner and outer hair cells. As discussed previously, knocking out EPS8 results in inner hair cells which fail to reach maturity, showing immature spiking activity in response to depolarising currents and an absence of the fast activating $I_{K,f}$ outward current (Section 5.2.5, Zampini *et al.* 2011). Conversely, knocking out EPS8L2 has no effect on the basolateral properties of either inner or outer hair cells (Furness *et al.* 2013). Thus, by assessing the basolateral properties of the hair cells, we can further classify the phenotype in relation to the EPS8/EPS8L2 axis that the protein is hypothesized to modulate.

As seen in **Figure 6.13A** and **B**, IHCs from both the heterozygous and homozygous mice show mature graded and sustained voltage responses following hyperpolarising and depolarising current step stimulation at P28-38. The resting membrane potential of these mature inner hair cells obtained from these recordings does not indicate any significant difference between the two strains (**Figure 6.13C**).



C BAIAP2L2 knock-out and control inner hair cell resting membrane potential

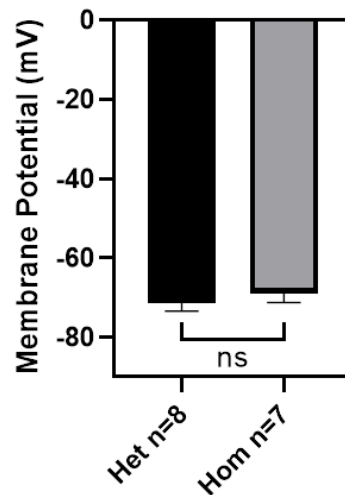


Figure 6.13 – Investigating the current clamp responses of heterozygous and homozygous BAIAP2L2 P28-38 mice – Voltage responses of inner hair from heterozygous (A, 8 cells from 3 mice) and homozygous (B, 7 cells from 3 mice) cells following current injection from -100 to 900 pA in 100 pA steps. (C) The resting membrane potential of BAIAP2L2 homozygous and heterozygous inner hair cells, obtained by averaging the first section of the raw traces prior to current stimulation onset ($P = 0.064$, ns = $P > 0.05$, two-tailed unpaired Students t-test). Error bars represent the standard deviation.

Analysis of the voltage clamp responses indicates that both the genotypes show a mature current profile possessing $I_{K,f}$, $I_{K,s}$ and $I_{K,n}$ (Section 1.4.2, **Figure 6.14**).

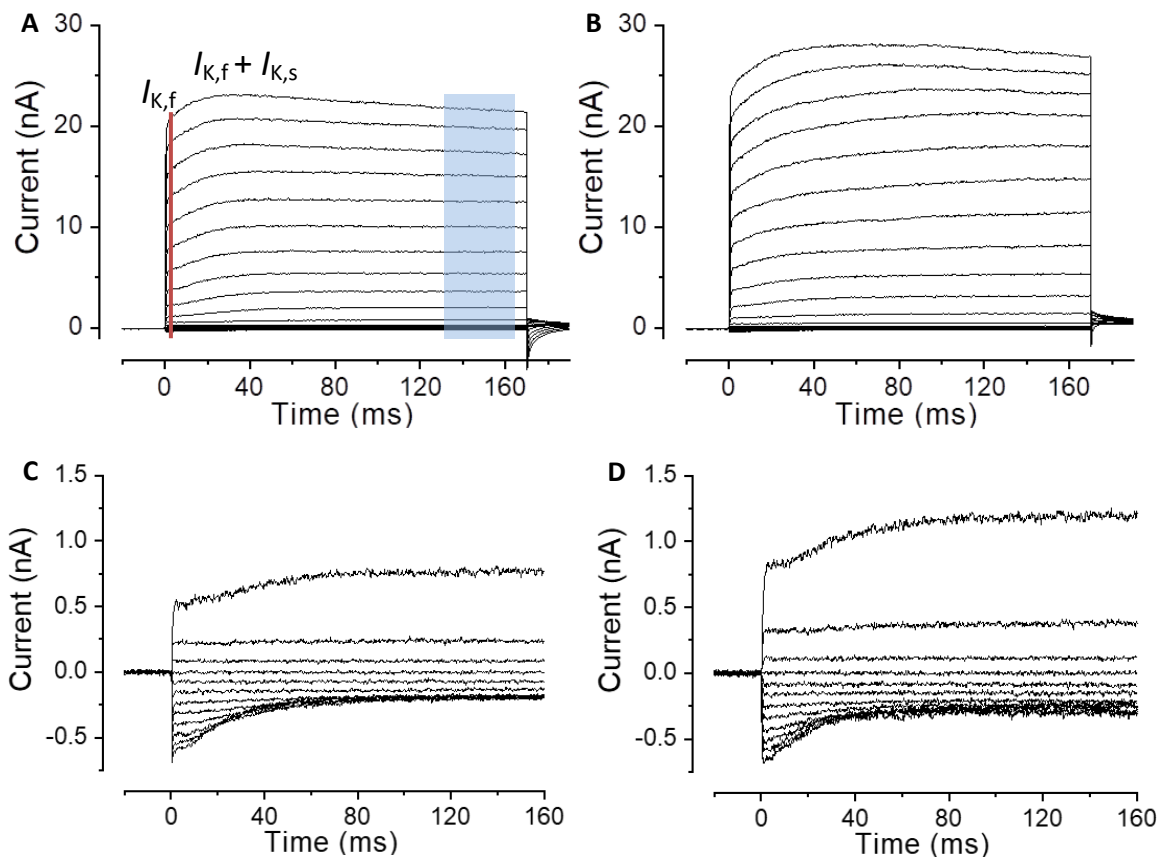


Figure 6.14 – Investigating the voltage clamp current responses from heterozygous and homozygous BAIAP2L2 P28-38 inner hair cells – Representative traces from *BAIAP2L2^{tm1b}* heterozygous (A, n=9 cells from 3 mice) and homozygous (B, n=8 cells from 3 mice) inner hair cells under voltage clamp conditions in response to voltage steps from -124 to 64 mV from a holding potential of -84 mV. Note the mature profile of both $I_{K,f}$ and $I_{K,s}$ (Section 1.4.2). The current at 2ms (red line), capturing primarily the fast activating $I_{K,f}$ current, and 134-154 ms (blue bar), capturing both the combined $I_{K,f}$ and $I_{K,s}$ sustained currents, was used to create the $I_{K,f}$ (**Figure 6.16B**) and sustained (**Figure 6.16C**) I/V curves respectively. Voltage clamp traces of heterozygous (C) and homozygous (D) BAIAP2L2 inner hair cells at a holding potential of -64 in response to 10 mV voltage steps between -144 and -34 mV to highlight the $I_{K,n}$ negatively activating inward current.

Furthermore, the measure of the steady-state (134-154 ms post voltage step) and early (2 ms post voltage step) I/V curves, which allows for statistical comparison, indicates that IHCs from both genotypes exhibited currents with similar voltage dependence (**Figure 6.15A and B**). Comparison of the current values at 0 mV from the steady-state current yields no significant difference between the two strains (**Figure 6.15C**), as do current values obtained from the early curve at -25 mV (**Figure 6.15D**). The size of $I_{K,n}$, measured as the difference between the peak and steady-state value of the deactivating tail current at -124 mV, is also unaffected by the deletion of BAIAP2L2 (**Figure 6.15E**). Thus, the absence of BAIAP2L2 does not appear to elicit any defects in the inner hair cell basolateral potassium currents, showing both a statistically comparable resting membrane potentials and voltage clamp traces.

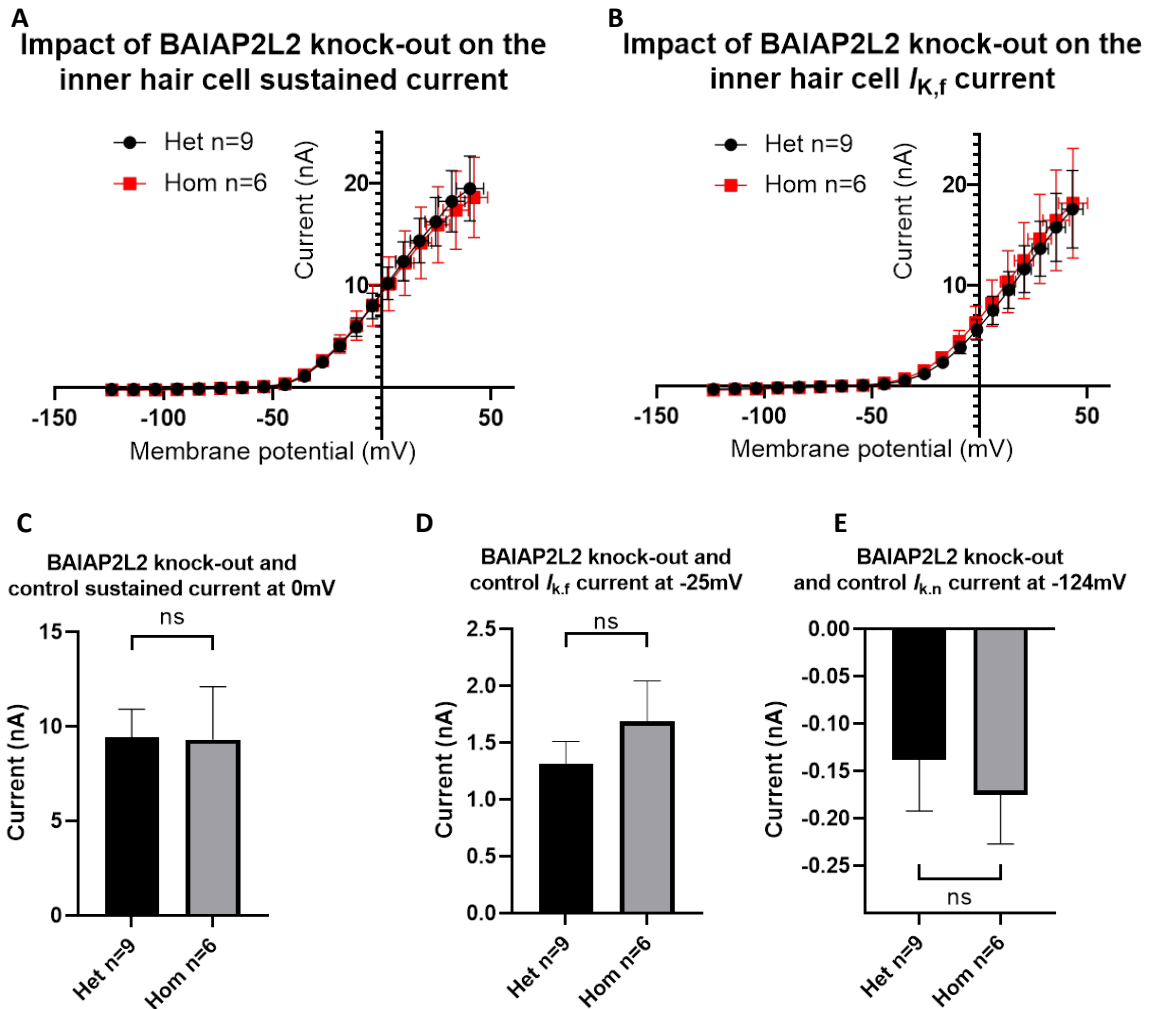


Figure 6.15 – Analysis of the voltage clamp responses from heterozygous and homozygous BAIAP2L2 P28-38 inner hair cells – I/V curves of the sustained (A) and fast (B) current responses from both BAIAP2L2 genotypes following correction of the residual series resistance after compensation (heterozygous; n=9 cells from 3 mice, homozygous; n=6 cells from 3 mice). (C) Current values extrapolated from the sustained response I/V curve at 0 mV for heterozygous and homozygous BAIAP2L2^{tm1b} inner hair cells (P = 0.633). (D) Current values extrapolated from the fast (2 ms) $I_{K,f}$ I/V curve at -25 mV for both genotypes (P = 0.055). (E) The size of the $I_{K,n}$ inward current in the inner hair cells of both genotypes, obtained from the difference between peak and steady state current at -124 mV (P = 0.217, two-tailed unpaired Student's t-test, ns = P > 0.05). Error bars represent the standard deviation.

Following the result that the inner hair cells do not appear to be severely affected by the knock-out of BAIAP2L2, we next looked towards the outer hair cells, since the DPOAE data suggests these are severely impaired by the mutation. Preliminary current clamp analysis of the outer hair cells at P12 indicates that both the genotypes are mature at this stage, both lacking any spiking activity in response to depolarising currents and responding with sustained graded membrane potential changes (**Figure 6.16A and B**). Both genotypes appear to possess similar resting membrane potentials, though the preliminary nature of the low repeat data prevents meaningful statistical analysis (**Figure 6.16C**).

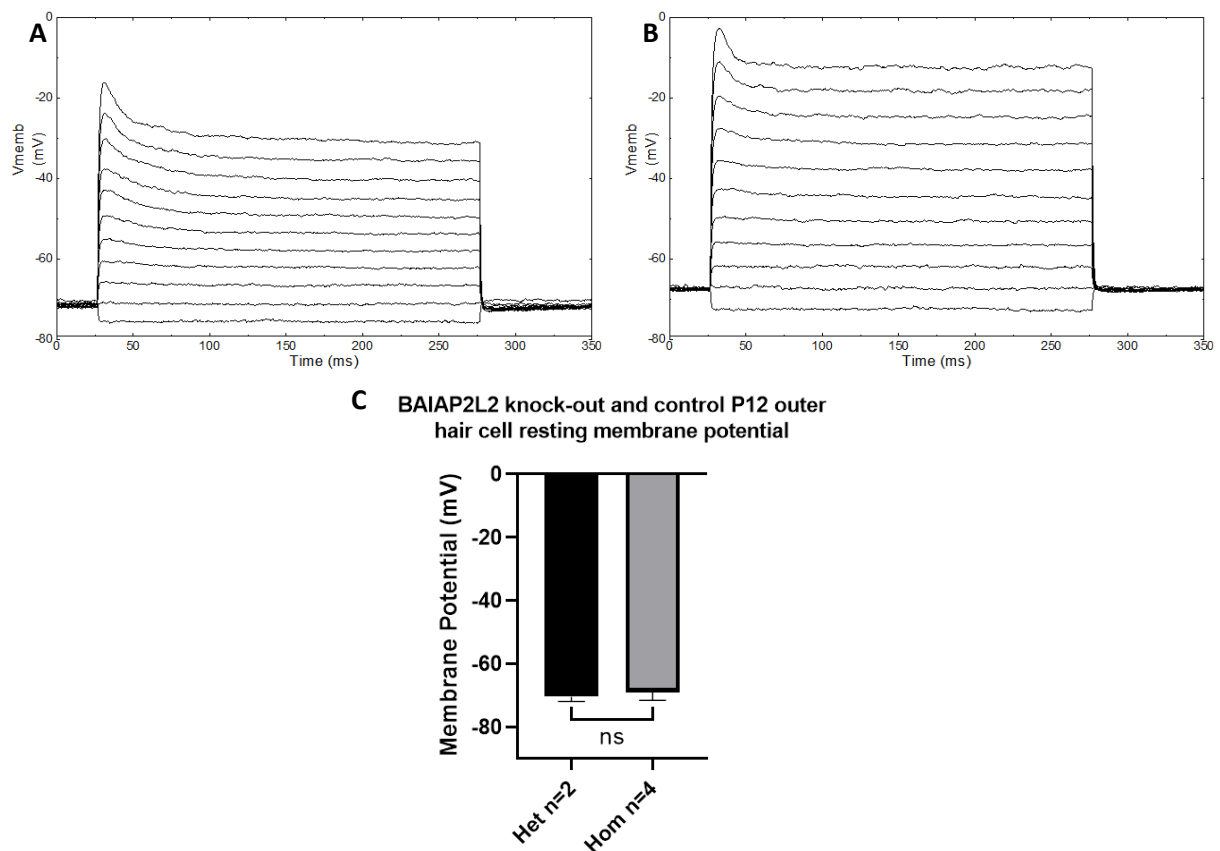


Figure 6.16 - Investigating the current clamp voltage responses from heterozygous and homozygous BAIAP2L2 P12 outer hair cells – Voltage responses from heterozygous (A, 2 cells from one mouse) and homozygous (B, 4 cells from one mouse) outer hair cells following current injection from -100 to 900 pA in 100 pA steps. (C) The mean resting membrane potential of the two genotypes, obtained by averaging the first section of the traces prior to current onset. The low sample number of this preliminary experiment prevents statistical analysis. Error bars represent the standard deviation.

Representative traces of voltage clamp experiments on the same cells reveal that both genotypes possess the mature negatively activating inward potassium current $I_{K,n}$ (Housley and Ashmore 1992, Marcotti *et al.* 1999, Marcotti *et al.* 2003a, **Figure 6.17A and B**). Interestingly, the maximal outward current in the OHCs from homozygous BAIAP2L2 mice does appear smaller compared to the heterozygous control mice. Creating an I/V curve from these traces at the point of maximal current, to allow for easy comparison between the two genotypes, indicates that the two show a very similar voltage dependence across most of the holding potentials (**Figure 6.18A**). However, at the higher holding potentials, the two appear to deviate slightly. Statistical analysis of the I/V curve, by extrapolating values for the $I_{K,n}$ current at -124 mV (**Figure 6.18B**) and the outward potassium current at 0 mV (**Figure 6.18C**), reveals no significant difference between the heterozygous and homozygous mice.

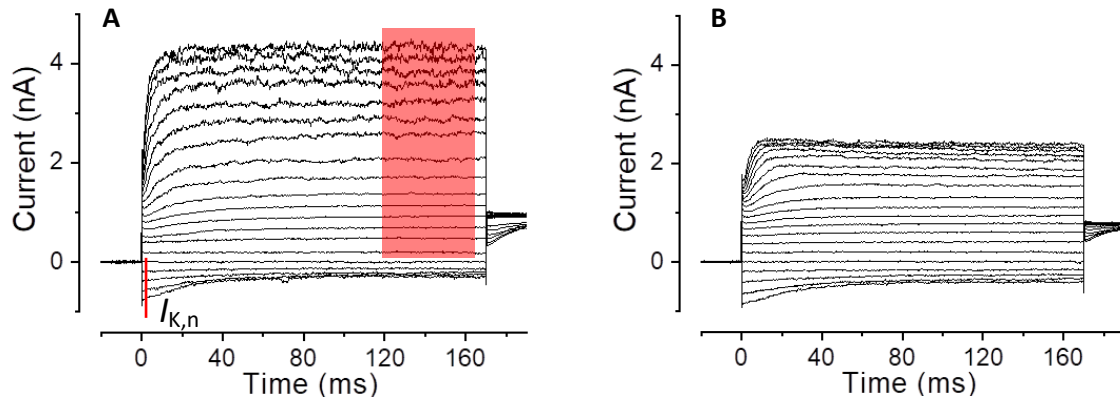
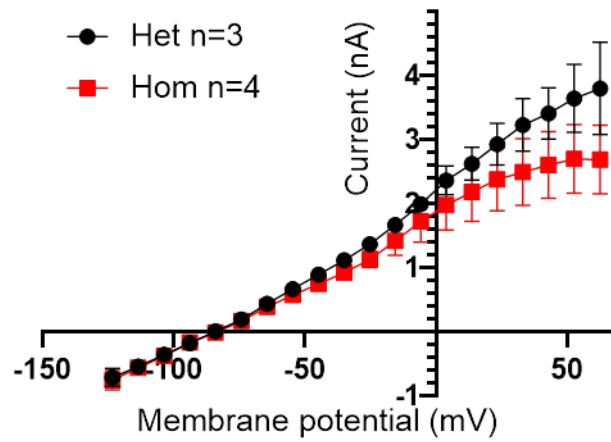
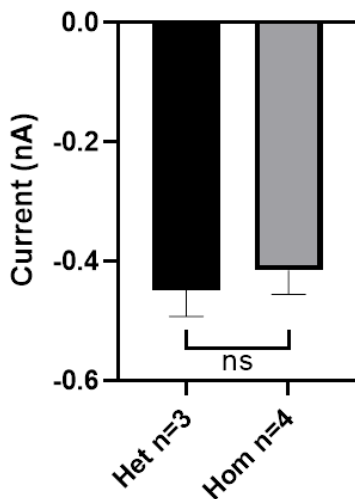


Figure 6.17 – Preliminary investigation of the voltage clamp current responses from heterozygous and homozygous BAIAP2L2 P12 outer hair cells – Representative voltage clamp traces from heterozygous (A, n=3 cells from one mouse) and homozygous (B, n=4 cells from one mouse) BAIAP2L2 mice in response to 10 mV voltage steps between -124 and 66 mV from the holding potential of -84 mV. The red line/bar in (A) indicates the averaged area of the trace used for the maximal current I/V current, capturing both the $I_{K,n}$ current from the onset of the stimulus and the averaged sustained outward current at the highest point.

A Impact of BAIAP2L2 knock-out on the outer hair cell maximum current



B BAIAP2L2 knock-out and control $I_{K,n}$ current at -124mV



C BAIAP2L2 knock-out and control current at 0mV

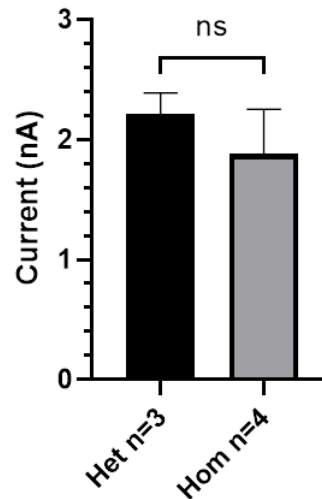


Figure 6.18 - Analysis of the voltage clamp responses from P12 heterozygous and homozygous BAIAP2L2 outer hair cells – (A) Maximal I/V curve generated from the voltage clamp traces of P12 heterozygous (n=3 cells from 1 mouse) and homozygous (n=4 cells from 1 mouse) BAIAP2L2 outer hair cells after residual series resistance compensation. Current values were recorded from the point in the trace with the largest current value, positive or negative. (B) Comparison of the size of the peak of the negatively activating inward current $I_{K,n}$ at -124 mV relative to the steady state current (P = 0.368). (C) Comparison of the size of the outward current at 0 mV (P = 0.186, ns = not significant). Error bars represent the standard deviation.

Though no synaptic phenotype was expected, based on both the literature and the analysis of the ABR data, the number and alignment of ribbon synapses in inner and outer hair cells was briefly assessed with immunofluorescence experiments, similar to the DAG1 analysis (Section 5.2.4). As expected, there was no obvious difference in the number or alignment of ribbon synapses between the heterozygous and homozygous BAIAP2L2 animals (**Figure 6.19A-D**). Immunolabelling experiments investigating the efferent innervation of outer hair cells and their proximally associated SK2 puncta similarly indicates no apparent difference between the two genotypes (**Figure 6.19E and F**). Using immunolabelling to analyse the basolateral maturation of inner and outer hair cells in the knock-out animal indicates a similar pattern. The expression of the BK potassium channel, responsible for the mature fast activating $I_{K,f}$ outward current (Kros *et al.* 1998, Marcotti *et al.* 2004b), was similar between the two genotypes (**Figure 6.20A and B**). Furthermore, the expression of prestin, the chloride based transmembrane protein responsible for outer hair cell electromotility (Zheng *et al.* 2000a), also appears similar between the homozygous knock-out animal and heterozygous control (**Figure 6.20C and D**). The prestin localisation shows the classical ring like pattern down the lateral membrane of the outer hair cells in both animals. The expression of KCNQ4, the potassium channel responsible for the mature $I_{K,n}$ negatively activating inward current in inner and outer hair cells (Kubisch *et al.* 1999), also appears normal in the knock-out outer hair cells, showing a classical localisation to the cell base (**Figure 6.20C and D**).

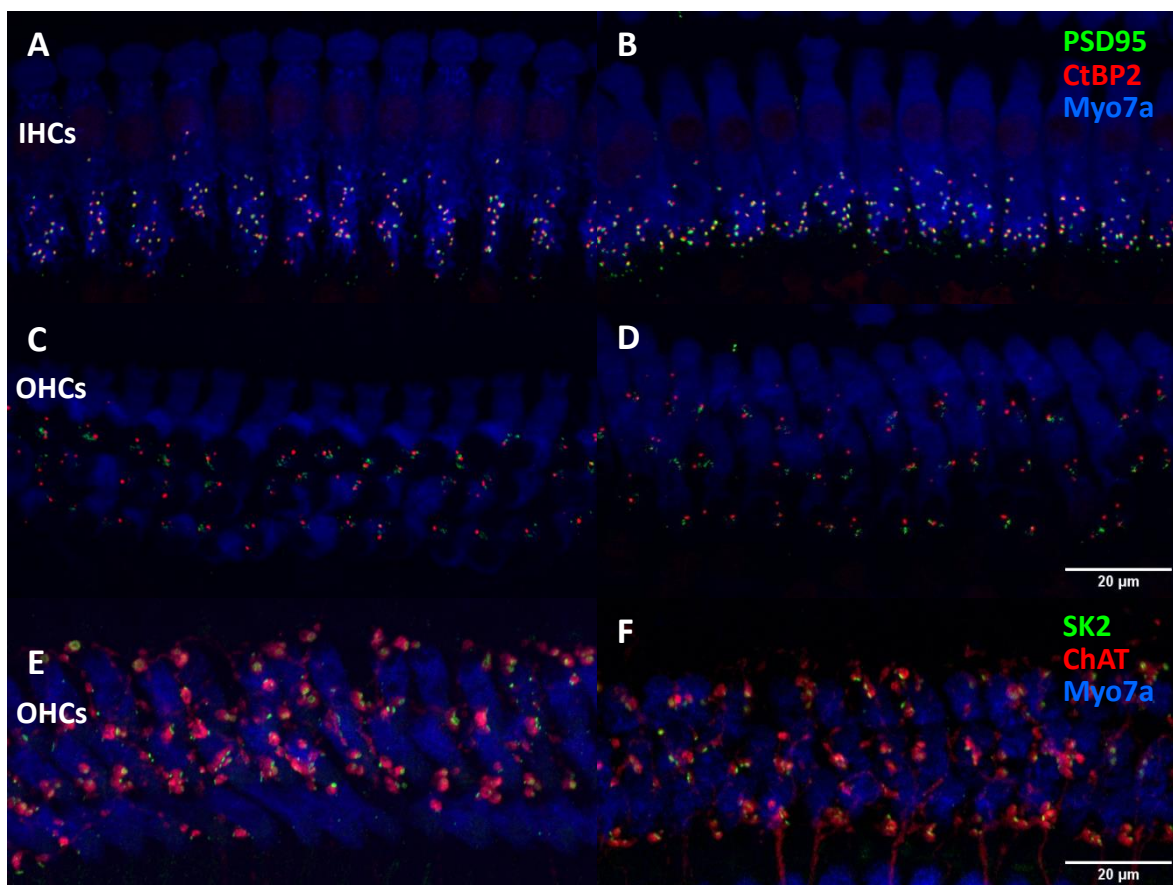


Figure 6.19 – Investigating the ribbon synapses and efferent innervation of BAIAP2L2 knock-out hair cells – Preliminary analysis of the alignment of ribbon synapses (CtBP2 1:500, red) with the post synaptic density (PSD95 1:1000, green) within BAIAP2L2 homozygous knock-out inner hair cells (B) relative to the heterozygous controls (A) (n=3 P32 animals per genotype, single representative maximal intensity projection shown). (C and D) Images obtained from the same whole-mount immunolabelled specimens as A and B, focusing on the outer hair cells (n=3 animals per genotype, single representative image shown). (E and F) Whole mount sections of the organ of Corti of control (E) and knock-out (F) animals focusing on the outer hair cells, with the efferent fibres marked with choline acetyltransferase (ChAT 1:500, red) alongside their associated SK2 (1:200, green) puncta (n=3 animals per genotype, single representative maximal intensity projection shown).

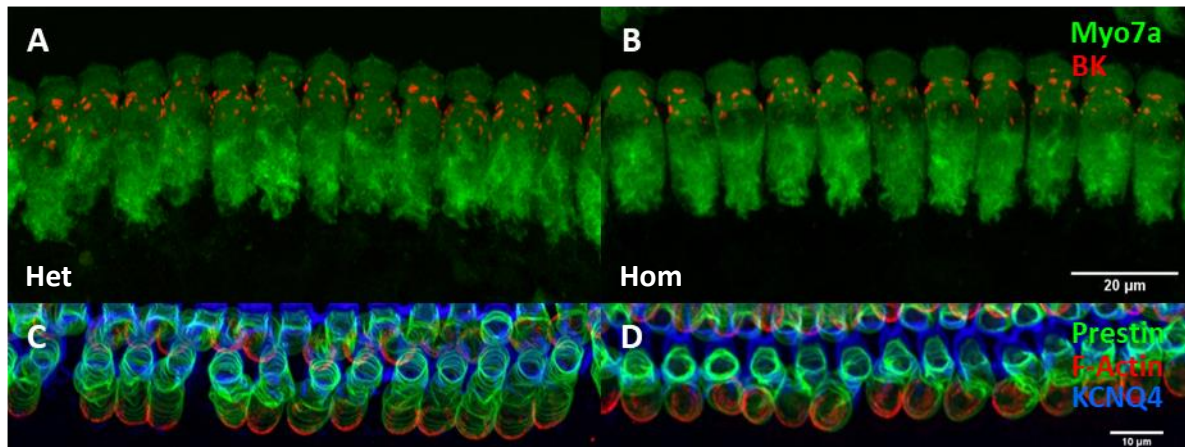


Figure 6.20 – Investigating the maturation of inner and outer hair cells in BAIAP2L2 knock-out animals – Inner hair cells of heterozygous (A) and homozygous (B) *BAIAP2L2^{tm1b}* mice in whole-mount sections labelled with Myo7a (1:500, green) and the BK potassium channel (1:200, red)(n=3 P32 animals per genotype, single representative maximal intensity projection shown). P32 outer hair cells of *BAIAP2L2^{tm1b}* heterozygous (C) and homozygous (D) mice immunolabelled for prestin (1:5000, green), KCNQ4 (1:100, blue) and F-actin (phalloidin, 1:1000, red)(n=3 animals per genotype, single representative maximal intensity projection shown).

6.2.4 – The impact of BAIAP2L2 knock-out on the morphology of the stereocilia bundle

The electrophysiological experiments indicate that the BAIAP2L2 mutation elicits the initial decrease in hearing sensitivity detected by the ABRs through the dysfunction of outer hair cell amplification. Fluid jet stimulation indicates that this appears to be caused by deficits in outer hair cell mechanotransduction, with no effect on the adaptation kinetics of the MET channel. Scanning electron microscopy (SEM) was thus used to determine whether this transduction deficit is caused by loss of stereocilia rows, similar to the EPS8L2 knock-out (Furness *et al.* 2013), or through a loss of the stereocilia staircase morphology as with the EPS8 knock-out (Zampini *et al.* 2011). Due to time constraints, these experiments were carried out solely by Anna Underhill (Another PhD student in Professor Marcotti's lab) and reproduced with permission. As seen in **Figure 6.21**, at P10 the morphology of the stereocilia is not severely affected by the BAIAP2L2 homozygous mutation. The wide field view of the whole cochlear sensory epithelia indicates that the gross morphology and polarity of the stereocilia is not obviously affected (**Figure 6.21A and B**). Furthermore, focusing on the inner hair cells indicates that the number of rows and the general staircase morphology is maintained in the knock-out animal (**Figure 6.21C and D**). Conversely, third row of stereocilia within the outer hair cells present early signs of degeneration in the BAIAP2L2 knock-out, with a few stereocilia missing from this row (**Figure 6.21E and F**). This aligns with the MET data, which indicates a significant loss of maximal mechanotransduction current at P11 (**Figure 6.10**).

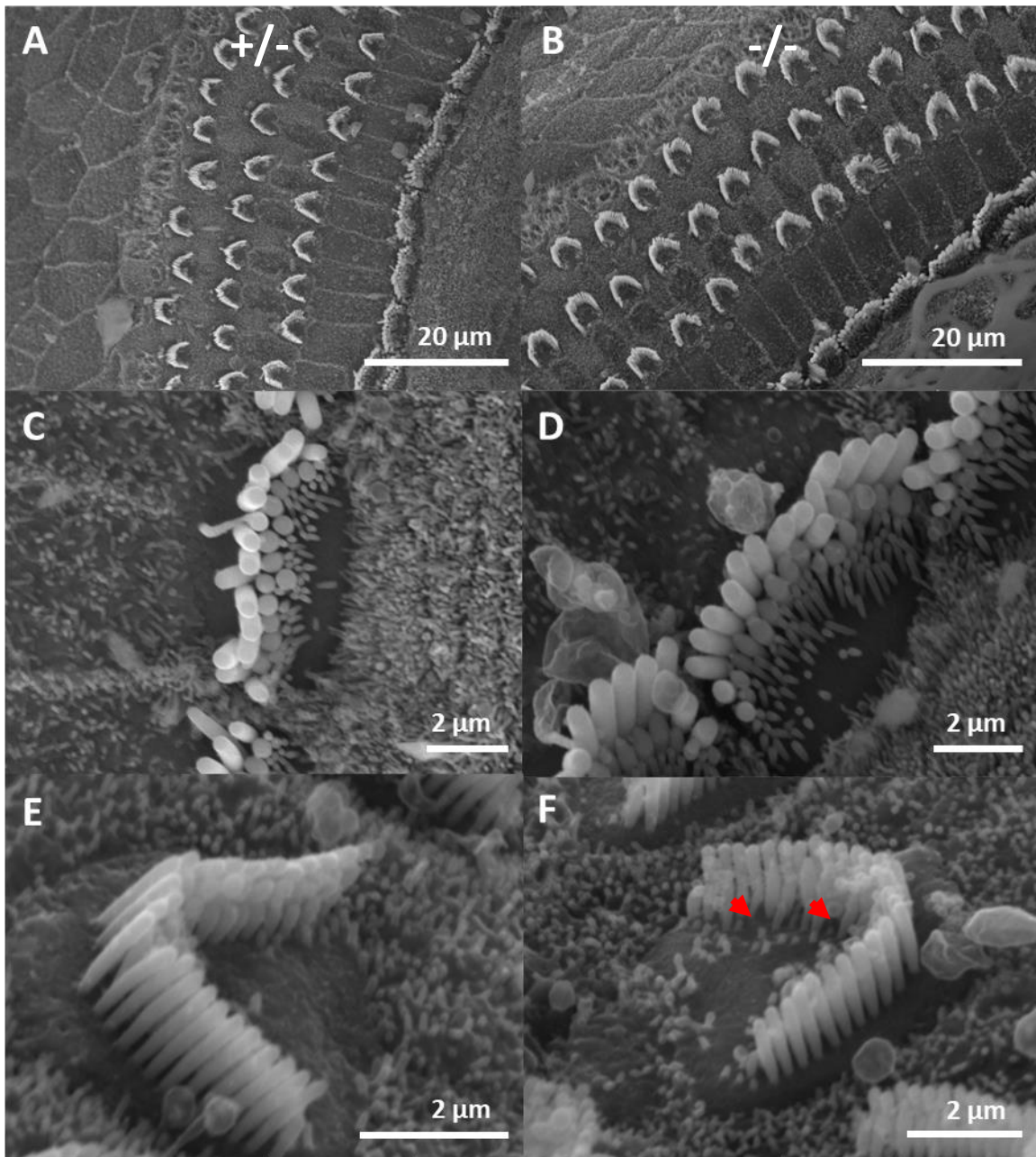


Figure 6.21 – Hair bundle morphology in heterozygous and homozygous P10 BAIAP2L2 mice – Representative scanning electron microscopy images of P10 heterozygous and homozygous mice. (A and B) wide field images of the cochlear sensory epithelia of heterozygous control (A) and homozygous BAIAP2L2 knock-out (B) animals. (C and D) Greater magnification focused on the hair bundles of the inner hair cells in for both genotypes. (E and F) High magnification images of the hair bundles of control and knock-out outer hair cells. Red arrows indicate missing stereocilia within the third row (n=3 mice per genotype). This data was collected by Anna Underhill (see main text), and reproduced with permission.

Further SEM experiments in older mice, between P49 and P54, indicated that the gross bundle morphology and orientation was not affected by the BAIAP2L2 knock-out in the older animals (**Figure 6.22A and B**). The inner hair cell morphology, similar to the younger P10 animals, indicated no apparent difference in row morphology between the two genotypes, though the view angle makes it difficult to view all three rows (**Figure 6.22C and D**). However, the BAIAP2L2 knock-out outer hair cells appeared to have an almost entirely degenerated row 3 relative to the heterozygous control animals (**Figure 6.22E and F**). Carrying out a similar experiment at the older age of P245, which is preliminary with one animal per genotype due to a limited number of available mice, shows that this degeneration of the hair bundle continues after P54. At P245 both inner and outer hair cell stereocilia show signs of degeneration, with inner hair cells lacking most of their third row and some of their second row, while outer hair cells have lost all their third row and most of their second row (**Figure 6.23**). Thus it seems as though the mutation induces hearing loss by the progressive degeneration of the shorter rows of stereocilia in both inner and outer hair cells, resulting in deficits in mechanotransduction leading to reduced hair cell sensitivity and ultimately deafness.

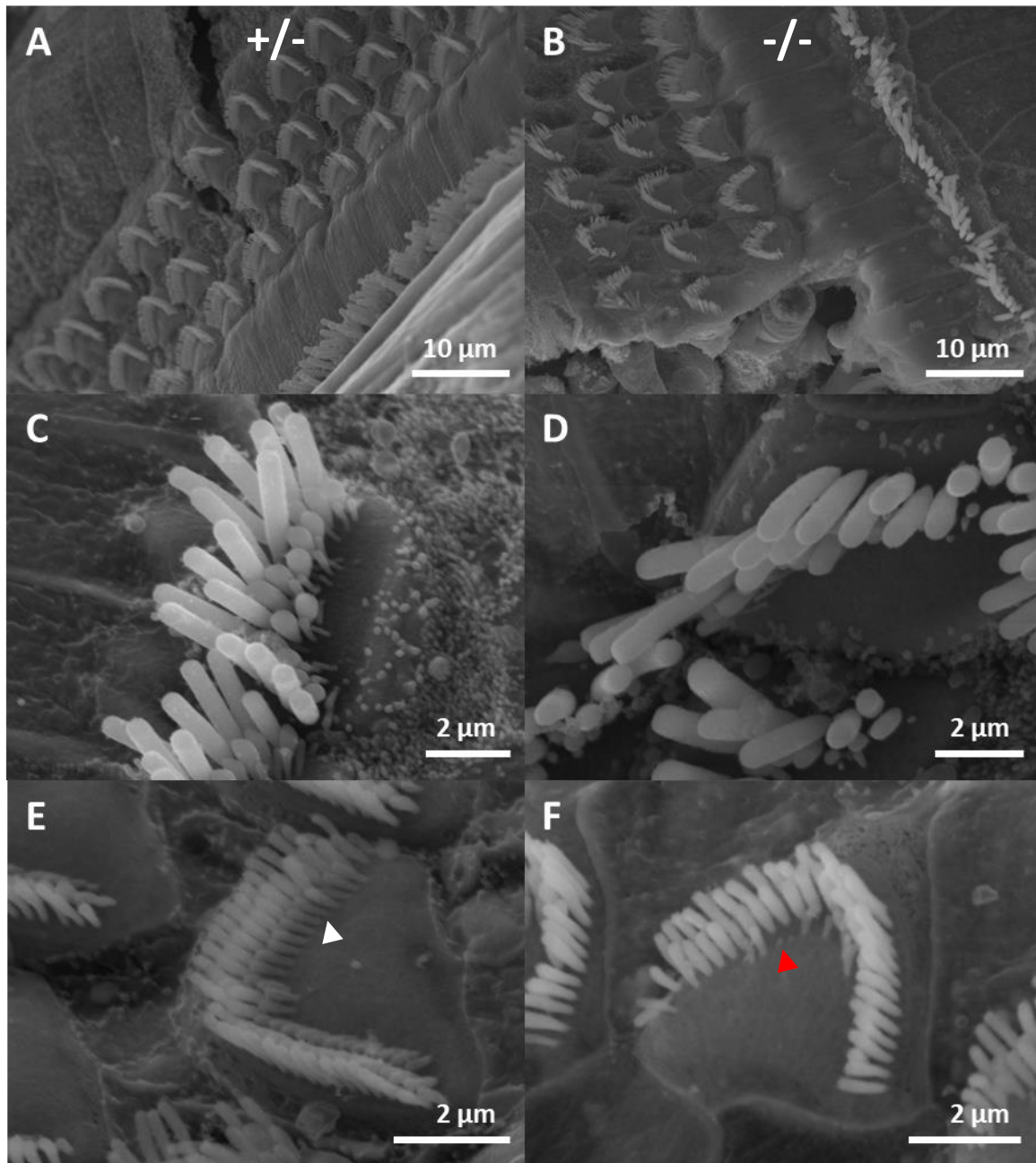


Figure 6.22 - Hair bundle morphology in heterozygous and homozygous P49-54 BAIAP2L2 mice – Representative low-magnification scanning electron microscopy images of the whole cochlear sensory epithelia of heterozygous (A) and homozygous (B) *BAIAP2L2^{tmlb}* animals. (C and D) Greater magnification images of the inner hair cell stereocilia for both genotype. (E and F) High-magnification images of the outer hair cell stereocilia in both control (E) and knock-out (F) mice. The red arrowhead indicates areas of missing third row stereocilia. The white arrowhead highlights the presence of the third row of stereocilia (n=4 animals per genotype). This data was collected by Anna Underhill and reproduced with permission.

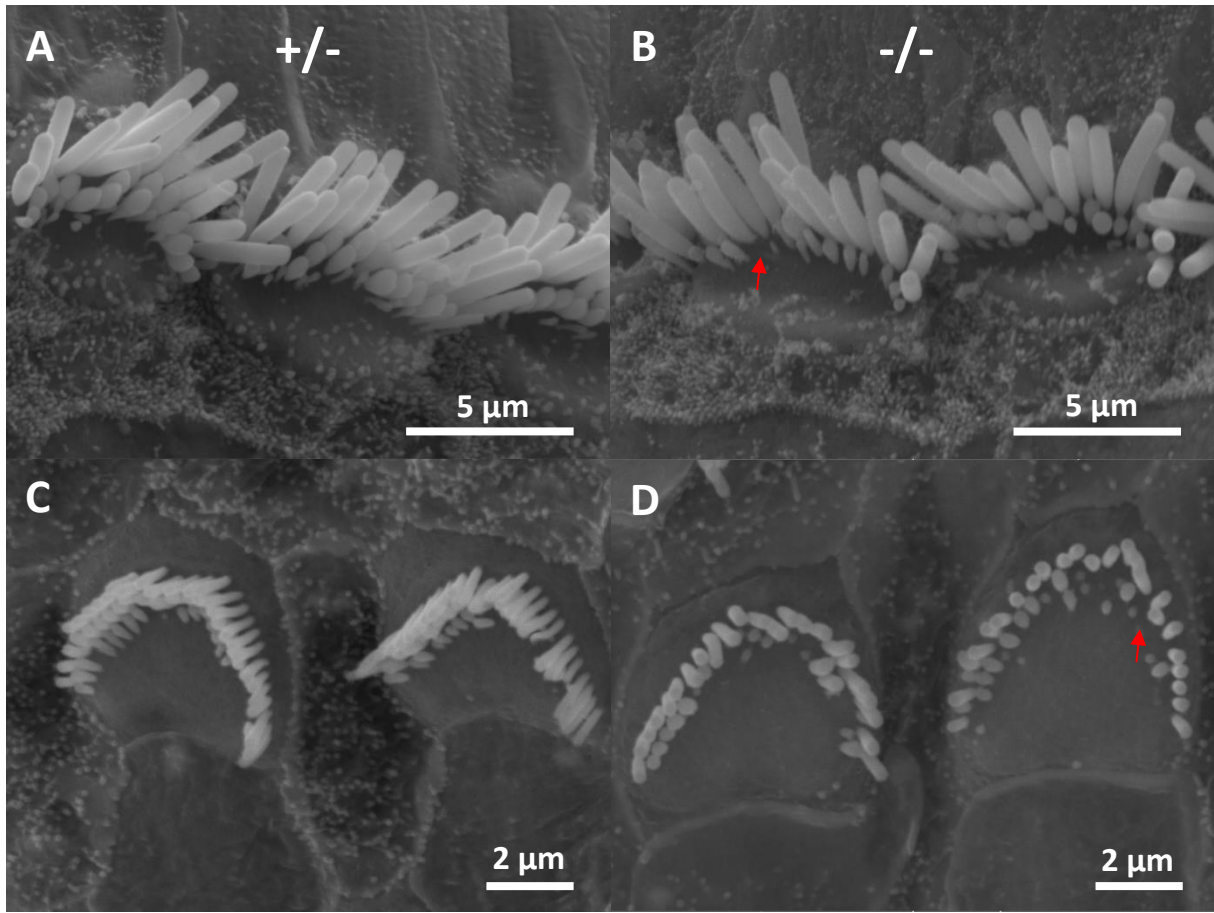


Figure 6.23 – Hair bundle morphology in heterozygous and homozygous P245 *BAIAP2L2* mice – Representative scanning electron microscopy images of P245 *BAIAP2L2*^{tm1b} control (A and C) and knock-out (B and D) mice focusing on both the inner (A and B) and outer (C and D) hair cells. Red arrows indicate areas missing stereocilia of the second row. This preliminary experiment possesses only one animal per genotype, and the data was collected by Anna Underhill and reproduced with permission.

6.2.5 – The subcellular localisation of BAIAP2L2 within the hair cells

Following the electrophysiology and SEM experiments we now understand the mechanism by which the *BAIAP2L2*^{tm1b} knock-out induces the quickly deteriorating increase in hearing threshold. We next wanted to investigate where in the hair cell BAIAP2L2 is localised. Based on the previous reports on the action of I-BAR proteins in the brush border of the gut, the hypothesis is that BAIAP2L2 is functioning to localise EPS8 to the tallest row of stereocilia, and thus should perfectly co-localise (Postema *et al.* 2018). Immunofluorescence experiments, which were carried out together with Dr Jing-Yi Jeng (Post-doc in Professor Marcotti's lab), indicate that BAIAP2L2 is present predominantly at the tips of the second row of stereocilia (**Figure 6.24**). The protein remains at this location in both inner and outer hair cells up until at least P113. The localisation at this site is unexpected, as EPS8 is primarily located at the tips of the tallest row, with only small amounts being detectable in row 2 (Zampini *et al.* 2011).

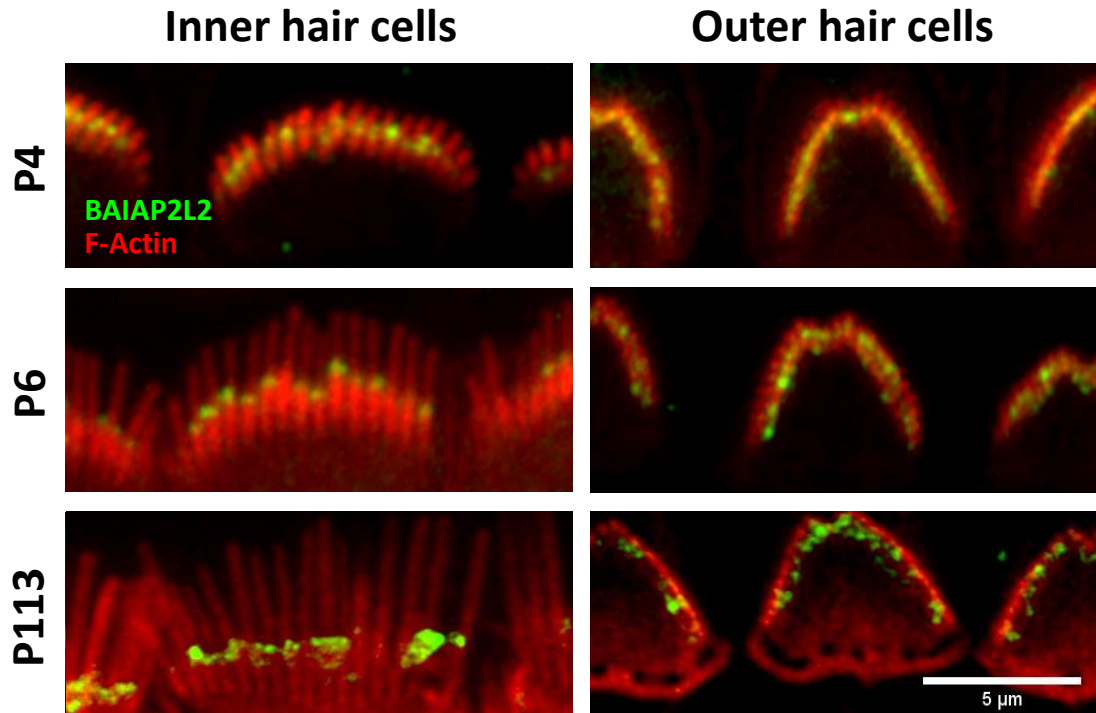


Figure 6.24 – The expression and localisation of BAIAP2L2 in P4-113 wild-type hair bundles – Representative maximal intensity projections of whole-mount cochlea sections of P4 (n=2), P6 (n=1) and P113 (n=2) wild-type mice immunolabelled for BAIAP2L2 (1:50, green) and F-actin (phalloidin, 1:1000, red). These confocal images were collected at the level of stereocilia focusing on both the inner and the outer hair cell hair bundles.

In order to deduce whether BAIAP2L2 is functioning to localise EPS8 to the tallest row of stereocilia, in line with the hypothesis, we investigated EPS8 immunostaining in BAIAP2L2 heterozygous and homozygous mice. As seen in **Figure 6.25**, the proper localisation of EPS8 to the tips of row 1 stereocilia is unaffected by the BAIAP2L2 knock-out, suggesting that the protein is not responsible for the proper localisation of EPS8. However, the localisation of BAIAP2L2 is entirely lost in the EPS8 homozygous knock-out animal (**Figure 6.25**). Thus, instead of mirroring the system in the brush border of the gut, the localisation appears to be inverted, and BAIAP2L2 fails to correctly localise in the absence of EPS8.

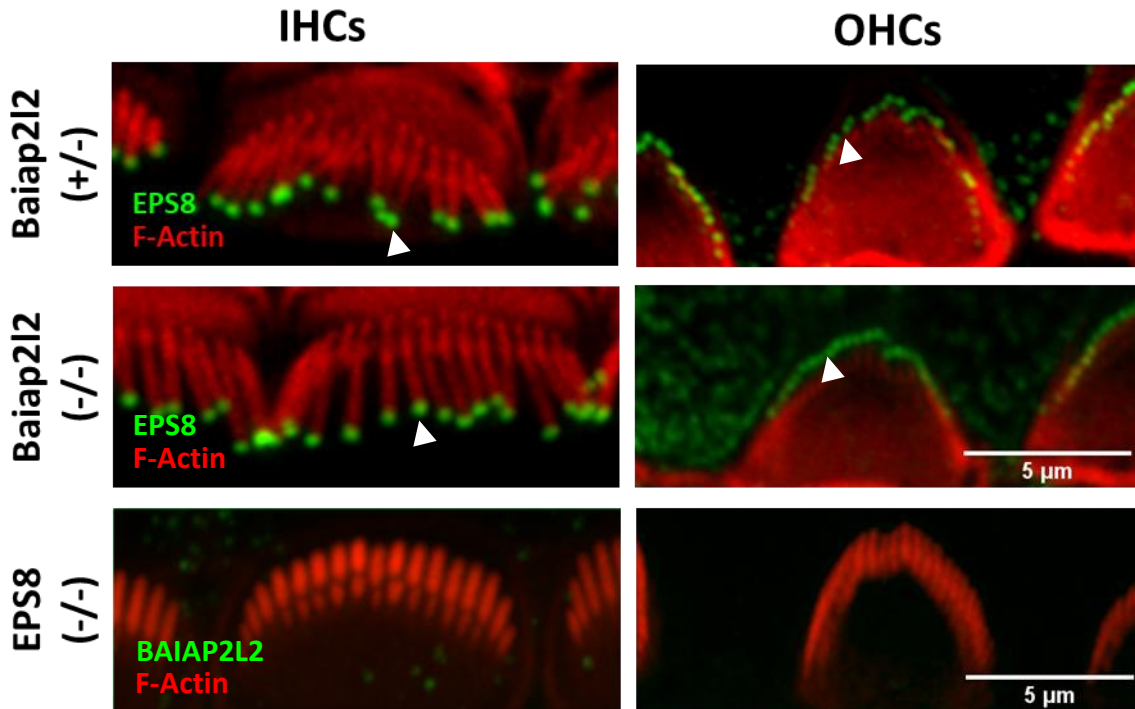


Figure 6.25 – Investigating whether BAIAP2L2 functions to localise EPS8 to the tallest row of stereocilia in outer hair cells – *BAIAP2L2^{tm1b}* heterozygous control and homozygous knock-out inner and outer hair cells immunolabelled for EPS8 (1:1000, green) and F-actin (phalloidin, 1:1000, red) (n=3 animals per genotype). The EPS8 homozygous knock-out inner and outer hair cells are immunolabelled for BAIAP2L2 (1:50, green) and F-actin (phalloidin, 1:1000, red). The white arrowheads indicate green signal at the tips of the tallest row of stereocilia.

6.3 – Discussion

The data presented on the *BAIAP2L2^{tm1b}* knock-out animal indicates that removal of the protein results in a rapidly progressing hearing loss beginning from as young as P14, only two days after the onset of hearing in mice (Mikaelian and Ruben 1965). Further analysis of the hearing thresholds via ABR experiments indicates that this loss of hearing sensitivity continues all the way up to the oldest age analysed at P166-245, at which stage the knock-out animals are profoundly deaf. The DPOAE thresholds, SEM data and MET patch clamp experiments suggest that hearing loss in the absence of BAIAP2L2 is

primarily caused, at least initially, by dysfunction of the outer hair cell amplification system due to deficits in mechanotransduction.

The MET experiments performed on homozygous and heterozygous BAIAP2L2 outer hair cells appear to indicate a rapid loss in the mechanotransduction of the mutant cells between P8 and P11. These experiments should yield relatively consistent MET amplitudes, as the number of MET channel per cell is similar between cells and the bundle is always subjected to a saturating stimulus. Though bundles can be damaged by repeated fluid jet stimulation, all cells were subjected to the same conditions and the bundle was exposed to stimulation for the minimum period possible prior to recording. Further analysis of the MET current in outer hair cells of older ages could provide a better insight into the hearing threshold degradation. P11 is the oldest age at which MET current recordings can be reliably performed due to the attachment of the tectorial membrane with the outer hair cell stereocilia in older animals (Verpy *et al.* 2011). However, if these animals were crossed with tectA/tectB knock-outs (Legan *et al.* 2000), resulting in a loss of this stereocilin based connection, we could analyse the MET current in much older animals and monitor how this progresses alongside the hearing loss (Jeng *et al.* 2020).

It would be informative to know whether the dimensions of the stereocilia are affected by the absence of BAIAP2L2. The most reliable method to measure stereocilia dimensions is transmission electron microscopy (TEM), which allows for an exact quantification of the height and width of stereocilia throughout the life-course, to determine whether the shorter stereocilia show the thinning seen in EPS8L2 knock-out animals prior to degeneration (Furness *et al.* 2013). It would also indicate if the stereocilia are significantly shorter in the knock-out, similar to the EPS8 phenotype (Zampini *et al.* 2011). However, given the original hypothesis and limited time due to the 6 months of lockdown we experienced at Sheffield, the SEM approach allowed for a good overview of the number of rows and any obvious degeneration. If given more time, it would be interesting to perform both SEM and TEM analysis on much older animals at around one year of age, to determine whether the second row remains unaffected or whether the shortest row is simply the first to degenerate.

The basolateral currents of the inner hair cells appear to be normal in the BAIAP2L2 knock-out, with the control and knock-out cells showing a very similar I/V curve, and thus possess a similar voltage dependence. In line with this, the resting membrane potential, $I_{K,f}$

current at -25 mV, sustained current at 0 mV and $I_{K,n}$ current at -124 mV are all statistically similar between the knock-out and control cells. This conclusion is also supported by the SEM data, which indicate little degeneration of the IHC hair bundles until very advanced ages in animals lacking BAIAP2L2. The BK immunostaining experiments, though low in sensitivity, also indicate that the expression of the BK potassium channel appears normal at P19. The basolateral properties of the outer hair cells, despite the preliminary nature of the data and the non-significant differences, appears to show some decrease in the outward potassium current and the mature negatively activating $I_{K,n}$ in BAIAP2L2 knock-out animals. Further experiments are required to determine if a significant difference is truly apparent between OHCs of the two genotypes at any age. In support of the non-significant difference in the OHC basolateral properties, staining experiments suggest that the mutation does not appear to have affected the expression of prestin and KCNQ4, consistent with the idea that the cells mature as normal.

Similar to the conclusions drawn from the ABR/DPOAE experiments, further staining to analyse ribbon synapses appears to indicate no obvious impairments in synapse formation or alignment in the mutant. Had a synaptic phenotype been expected based on the literature, the synaptic kinetics could have been further analysed via capacitance changes after a voltage step stimulus. By measuring the capacitance before and after the stimulus, we could obtain information on the release rate or size of the RRP or SRP of vesicle. However, these experiments are very difficult and time consuming, and thus would only have been performed if given sufficient indication of synaptic involvement.

Chapter 7 – General Discussion

The role of dystroglycan in cochlear hair cells

Hair cell development is an intricate process involving several physiological and morphological changes, which are required to generate the extremely specialized auditory IHCs and OHCs (Section 1.2.2 and section 1.4.2). Two key aspects of hair cell development are linked to changes at the mechano-electrical transducer apparatus and synaptic machinery (Section 1.2.2 and section 1.3.3). Although a lot of progress has been made in the past 10-20 years, we still do not have a full understanding of the complex molecular mechanisms driving these developmental processes. Here, we have investigated two molecules (DAG1 and BAIAP2L2) that we hypothesised are playing a crucial role in the acquisition of normal vesicle exocytosis and hair bundle morphology in the mouse cochlear hair cells. Specifically, preliminary data suggests both molecules may modulate the morphology of the stereocilia through regulation of the EPS8/EPS8L2 differential localisation axis.

Dystroglycan is a specialised transmembrane adhesion receptor best known for the role it possesses at the sarcolemma in preventing contraction induced muscle damage (Batchelor and Winder 2006). Preliminary data suggested that pY890 β DG is present within the organ of Corti, where it had previously been reported absent, and an SH3 interactome screen suggested that β DG interacts with EPS8L2 (Section 1.5.4, Thompson *et al.* 2008). DG also plays a critical role in retinal ribbon synapse development, opening up a possibility that it may be playing a similar role in the organ of Corti (Orlandi *et al.* 2018). However, the pY890 antibody staining in the cochlea proved to be an artefact, and the hair cell specific post-natal deletion of DG had no effect on mice hearing thresholds at any age tested.

The second molecule of interest, the I-BAR family member BAIAP2L2, was hypothesized to interact with and localise EPS8 in the organ of Corti. In the brush border of the gut, another I-BAR family member, BAIAP2L1, localises itself to the growing actin protrusions and recruits EPS8 to promote growth (Postema *et al.* 2018). Furthermore, an IMPC screen identified that BAIAP2L2 knock-out results in significantly elevated hearing thresholds (Dickinson *et al.* 2016). Thus, the hypothesis was that BAIAP2L2 localises itself to the stereocilia and recruits EPS8 to control growth as it does in the brush border, and thus the expectation was that the BAIAP2L2 knock-out would be similar to the EPS8 knock-out (Zampini *et al.* 2011). We found that the deletion of BAIAP2L2 resulted in

progressive hearing loss detectable in mice as young as P14, caused by the progressive loss of the shorter stereocilia rows. This resulted in a reduction in the size of the MET current in OHCs from just before the onset of hearing with no impact on the resting open probability of the MET channel. Therefore, while certain aspects of the phenotype are consistent with the original hypothesis, and BAIAP2L2 is involved in hearing via regulation of the stereocilia, the BAIAP2L2 knock-out appears more closely related to the EPS8L2 knock-out than the EPS8 phenotype (Furness *et al.* 2013, Zampini *et al.* 2011). This similarity is also reflected in the localisation of BAIAP2L2 to the shorter two rows and the characteristics of the MET responses, which will be discussed in greater detail below.

The role of dystroglycan in cochlear ribbon synapses

Based on the previously reported role of dystroglycan in the formation of ribbon synapses within the retina, we hypothesized that a similar mechanism may be at play in the organ of Corti (Sato *et al.* 2008, Omori *et al.* 2012). If this was the case, we would expect dystrophin, dystroglycan, pikachurin and GPR179 to cluster at the ribbon synapses in the cochlea forming a trans-synaptic connection (Orlandi *et al.* 2018). While pikachurin did appear to display particularly strong signal in the organ of Corti relative to the surrounding tissues (**Figure 4.5**), this signal did not show any localisation to ribbon synapses. Furthermore, the α DG signal showed no labelling at ribbon synapses, and appeared scattered and unreliable (**Figure 4.6**), indicating that dystroglycan is unlikely to be present at the basal pole of hair cells. This was in part confirmed by the lack of a hearing phenotype in the conditional DAG1 knock-out mice. Had a phenotype been present, we could have performed the analysis of the amplitude and latency of wave I analysis, similar to that used to analyse the BAIAP2L2 knock-out mouse (Section 6.2.1 and see below). Further immunofluorescent analysis of the DAG-1 knock-out indicates no impact on either the synapse count or the alignment of the CtBP2 synaptic puncta with the PSD95 labelled post-synaptic density. These results indicate that the original hypothesis was incorrect, and dystroglycan does not have a role in cochlear ribbon synapse formation through a pikachurin based interaction. Though given the apparent expression of pikachurin within the organ of Corti, investigating a pikachurin knock-out animal could be an interesting area of further study. Pikachurin could theoretically act in a similar manner in the cochlea

as it does in the retina, forming a trans-synaptic link to regulate ultrastructure (Sato *et al.* 2008) and synaptic kinetics (Orlandi *et al.* 2018). If so, these effects could be assessed in the cochlea via transmission electron microscopy, and deficits in synaptic transmission could be deduced from ABR and wave I analysis similar to the work performed here (Section 6.2.1).

The role of dystroglycan in stereocilia morphogenesis and maintenance

Preliminary data, in the form of an SH3 interactome screen (Thompson *et al.* 2008), indicated that β DG may interact with EPS8L2, suggesting that β DG may function to properly localise the actin effector in cochlear hair cells. In order to investigate whether the two interact, we first turned to *in vitro* techniques to compare this binding with the other members of the EPS8 family. Both peptide SPOT arrays and pull-downs of β DG purified from bacteria indicated direct binding with the EPS8L2 SH3 domain, but not SH3 domains from other members of the EPS8 family. However, pull-downs and co-immunoprecipitations using GST/Myc tagged SH3 domains of the EPS8 family, which were carried out in cell lysates containing the entire protein repertoire of the VOT-E36 cell line, indicated no evidence of any binding between β DG and EPS8L2. Exactly why the interaction between EPS8L2 and β DG appears present within the simpler biochemical conditions and not in the more complex milieu of a cell lysate is not clear. If the lack of β DG-EPS8L2 interaction is due to competition with another binding partner, this could potentially be identified via mass spectrometry experiments of the post pull-down beads to identify exactly what is out-competing β DG. These experiments were not performed not only because they normally require substantial amount of funding, which were not available for this project, it is rather the case that the additional work is unlikely to help understanding the role of dystroglycan in the cochlea. If the lack of binding between EPS8L2 and β DG is due to differences in the secondary structure of β DG, induced by either phosphorylation at Y890 (Abdullah *et al.* 2020) or another site, this could explain why the binding was evident only when using purified and un-modified peptides. Phosphorylation blocking binding with EPS8L2 would dispute the preliminary data, which suggested that β DG is only present within the organ of Corti in the Y890 phosphorylated state. Due to the position of the Y890 phosphorylation relative to the EPS8L2 binding consensus sequence (**Figure 3.1**), the SPOT arrays do not provide an indicator as to how

the phosphorylation affects EPS8L2 binding. Thus, assuming the hypothesis is correct, we would expect this binding to be viable even with phosphorylated β DG, or puncta of unphosphorylated β DG present only at the tips of the stereocilia in the following immunofluorescence data. The overall conclusion for this *in vitro* aspect of the project was that the data alone is inconclusive, and the interpretation was dependent on the super-resolution immunofluorescence experiments (Chapter 4) discussed below.

At the time of the immunofluorescence experiments, the only antibody at our disposal, which indicated any signal within the organ of Corti, was the pY890 Ab 1709 sera (Ilsley *et al.* 2001) created using an Y890 phosphopeptide of the intracellular domain of β DG. Even the pY890 Ab 1710 sera (Ilsley *et al.* 2001), created using the exact same immunizing peptide, did not display the organ of Corti signal of the 1709 antibody (data not shown). The initial conclusions regarding the absence of dystroglycan within the organ of Corti had previously been drawn from the use of antibodies with similar binding epitopes as Mandag2 (Heaney and Schulte 2003, **Figure 4.1**). This antibody is directed against the intracellular tail of β DG (Pereboev *et al.* 2001). The binding of Mandag2 to β DG, or indeed any antibodies which bind to a similar region, can be blocked by the Y890 phosphorylation, and thus the hypothesis based on our preliminary data was that β DG is present in the organ of Corti only in the phosphorylated state. Furthermore, any involvement of β DG in either stereocilia or ribbon synapses would be present as areas of particular signal localisation, and provide direction for the following *in vivo* work and patch clamping experiments. Indeed, super-resolution immunofluorescence microscopy using the 1709 sera on apical cochlea sections indicated that the 1709 signal was localised to the tips of all three rows of stereocilia in outer hair cells, but not inner hair cells. This outer hair cell specificity is unexpected, but not unreasonable given the morphologies of the cells; the inner and outer hair cells are physiologically and morphologically very different. This is particularly evident in the stereocilia, which are shorter in outer hair cells, with a less marked difference in height between the rows. The current understanding in the field is that the staircase morphology is solely established and maintained through the differential localisation of different actin effector proteins across the rows of stereocilia (Peng *et al.* 2009, Mburu *et al.* 2010, Manor *et al.* 2011, Zampini *et al.* 2011, Furness *et al.* 2013, Avenarius *et al.* 2014, Fang *et al.* 2015, Tadenev *et al.* 2019). Therefore it follows that the stereocilia tip content of outer hair cells must be partially independent from the inner hair cells to permit their differences in morphology.

Given the original hypothesis that β DG is functioning to properly localise EPS8L2 to the shorter rows of stereocilia via a direct interaction, the finding that 1709 signal was evident across all three rows was unexpected. Assuming the β DG was functioning to localise EPS8L2, this would suggest some unknown mechanism was in place preventing the build-up of EPS8L2 at the tallest row, the site of EPS8 specific localisation (Zampini *et al.* 2011). Again, if the β DG signal had proven specific, the impact of β DG deletion on the localisation of EPS8L2 could have been analysed in our conditional knock-out animal, and a further understanding of this localisation mechanism could have been established. However, the purification of the 1709 crude sera, with both protein A columns and an antigen affinity column, removed all of the antibodies specific to the stereocilia from the specific antibody fraction. The validation experiments carried out, primarily using SPOT arrays and immunofluorescence staining of sgRNA control and DAG1 CRIPSR knock-out KM155 cells, indicated that the specific fraction was still capable of specifically staining p β DG. Furthermore, immunolabelling whole mount sections of the cochlear apex with the affinity purified fraction indicated that the antibody is capable of staining the p β DG in the myelin of the afferent fibres. Taken together, this suggests that the stereocilia tip staining seen when using the crude sera was entirely an artefact of non-specific IgGs within the antibody mixture.

Given that the stereocilia tip signal was entirely lost from the affinity purified fraction, we would expect the flow through of the affinity column, termed the depleted IgG fraction, to be able to entirely recapitulate the original stereocilia signal. However, the purification process somehow resulted in the loss of the antibodies staining the tips of the tallest row of stereocilia from both fractions, leaving a depleted fraction which selectively stains tips of the shorter two rows. It is possible that the antibody weakly adhered to the affinity column during the initial serum flow-through, and was subsequently removed with the following wash steps. If the purified fraction indicated a complete loss of p β DG binding capacity in the validation experiments, a protein A resin column could have been used to recover the lost IgGs from the stored wash solution. However, as we had no reason to believe that the IgGs in any way correspond to p β DG, this was not carried out. Thus, at this stage, the signal from the purified 1709 antibody resembles that of Mandag2 in the preliminary data (**Figure 4.1**), and we now possess no antibodies that indicate the presence of β DG within the organ of Corti.

The staining of the shorter two rows of stereocilia in the outer hair cells by the non-specific IgG fraction raises an interesting question of what exactly is the identity of the protein that the antibody is binding to. To date, no known actin capping protein is specific to the outer hair cells shorter rows (Section 1.2.2), and thus classifying this protein may significantly further our understanding of how the different morphologies of inner and outer hair cells are established. Initially, we had hoped to identify this protein by creating a concentrated stereocilia lysate using a modified version of the “twist-off” method, originally used to isolate vestibular hair bundles of the bullfrog (Section 2.1.7, Gillespie and Hudspeth 1991). The depleted pY890 AB could then have been used in an immunoprecipitation experiment to selectively purify the protein of interest which could then be identified via mass spectrometry. Preliminary experiments had indicated that the stereocilia signal of the depleted antibody was also present in the vestibular utricle (data not shown), allowing us to employ the method for the harvesting of the long compact stereocilia present within the vestibular system. Initial experiments indicated that we could isolate vestibular hair cell stereocilia using this method (Gillespie and Hudspeth 1991), and an actin band could be obtained from such samples, but many utricles were needed to see even a faint actin band. As such, the collection of utricle stereocilia was time consuming, and due to limited time this aspect of the project was not pursued to completion. However, this remains an area for future investigation, as this could theoretically identify a novel stereocilia localised actin effector or a protein responsible for the localisation of actin effectors that helps establish the morphological difference between the hair bundle of inner and outer hair cells.

At this stage, without any staining to indicate the presence of dystroglycan at the stereocilia, the final experimentation to address whether β DG localises EPS8L2 was to analyse the hearing thresholds and outer hair cell amplification in the DAG1 conditional knock-out animal. The expectation, based on the original hypothesis that β DG localises EPS8L2, was for the conditional DAG-1 knock-out to have phenocopied the EPS8L2 knock-out animal, showing progressive hearing loss due to stereocilia degeneration evident from around 2 months of age (Furness et al 2013). However, the knock-out animal showed no significant increase in hearing or DPOAE thresholds at the ages tested between one month and six months. Thus our original hypothesis was incorrect, and dystroglycan does not function to localise EPS8L2 in the organ of Corti.

Dystroglycan appears not to play a role in the mammalian cochlea

Whilst the results have indicated that dystroglycan has no role in the development and function of cochlear hair cells, it is important to note that the knock-out has not been directly validated due to an inability to localise dystroglycan expression to hair cells using the available antibodies. The MYO15Cre line has been used extensively in the lab, in both published work (Caberlotto *et al.* 2011, Corns *et al.* 2018) and ongoing projects, and as such is not predicted to be non-functional in the DAG1 x MYO15Cre model. Conversely, while the DAG1 flox line has been successfully utilised in other labs (Cohn *et al.* 2002), it has not previously been proven effective in our hands. The plan to unequivocally demonstrate that the DAG1 flox line was functional was to cross these mice with a Sox2-Cre line in order to obtain embryonic Cre-deletion of DAG1 in a wide array of tissues (Hayashi *et al.* 2002). The knockdown of DAG1 mice could have then been validated by comparing the expression level between the Cre positive and negative animals in muscle tissue. However, due to unplanned delays associated with Covid-19, this part of the project remained unfinished. Additional work that could have been done during the last 7 months of my studentship was to optimise the use of hybridising fluorescent probes to compare DAG1 mRNA levels between the MYO15Cre positive and negative animal. Alternatively, single cell RT-PCR from individual hair cells could have been employed to allow detailed comparison of DAG1 mRNA expression. Attempts to validate the conditional knock-out of DAG1 mRNA via qPCR yielded no significant different difference between the control and knock-out animals. However this could be due to the large amount of tissue taken relative to the small number of hair cells. Optimising this technique by selectively using the cochlear sensory epithelia rather than the entire cochlea minus the vestibular system may provide a more successful validation, but due to time constraints this repeat was not possible. As alpha dystroglycan has been reported present within the hair cells of the organ of Corti before (Heaney and Schulte 2003) this optimised technique should be able to detect intact DAG1 mRNA within the control animal that is absent in the Cre positive knock-out. However, it is entirely possible that similar to the crude 1709 sera, the α DG signal reported previously could have been an unspecific or artefact of the antibody staining, and both subunits of DG are absent in cochlear hair cells.

Much still needs to be investigated to determine how mutations within Xp21.2, corresponding to dystrophin, are capable of inducing non-syndromic X-linked hearing loss (Lalwani *et al.* 1994). It is theoretically possible that the Cre driver we have chosen, based

on the EPS8L2 and pikachurin preliminary data, is knocking out DG expression too late at P3, and a phenotype would be detectable if the knock-out was earlier. Conversely, it may not be the timing of the mutation causing a lack of a detectable phenotype but rather the tissue specificity of the knock-out. As introduced in section 1.1, the presence of the inwardly rectifying potassium channel Kir4.1 within the intermediate cells of the stria vascularis is essential for the establishment and maintenance of the endocochlear potential (Marcus *et al.* 2002). Kir4.1 is also known to co-localise with aquaporin-4 (AQP4), a membrane channel protein involved in cellular water balance, which also results in hearing loss if mutated (Nielsen *et al.* 1997, Li and Verkman 2001, Nagelhus *et al.* 2004, Eckhard *et al.* 2012). Both of these proteins have been previously reported to interact with the DGC. The proper localisation of Kir4.1 has been shown to be dependent on the DGC, and it is known to interact with alpha syntrophin, a short dystrophin splice isoform (Dp71) and β DG (Connors and Kofuji 2002, Connors *et al.* 2004). Also, the localisation and expression of AQP4 has been shown to be dependent on the presence of alpha syntrophin (Neely *et al.* 2001, Saadoun *et al.* 2003, Amiry-Moghaddam *et al.* 2003). Thus, it is possible that the mutation in Xp21.2 induces hearing loss via disruption of the DGC, and therefore of the endocochlear potential due to mislocalization of the Kir4.1/AQP4 channel complex. Due to the diverse roles of dystroglycan, investigating this possible phenotype is difficult, and would possibly require a global dystroglycan knock-out, paired with measurements of the EP. Though this mechanism of hearing loss was not within the original scope of the project, and thus could be an area of future work.

Therefore, for the work on a hair cell specific knock-out of dystroglycan, we conclude no significant impact on hearing thresholds, hair cell maturation, stereocilia or ribbon synapses. Functions could exist for dystroglycan before P2 or in tissues not targeted by the MYO15Cre system, but these are outside of the scope of the project given the original hypotheses.

Investigating the role of BAIAP2L2 in stereocilia morphogenesis and maintenance

Based on the published data suggesting an interaction between EPS8 and BAIAP2L2, and the reported role of BAIAP2L1 in localising EPS8 to microvilli tips in the brush border of the gut (Postema *et al.* 2018), we hypothesized that BAIAP2L2 could function to properly localise EPS8 in the cochlea. Therefore, we expected the BAIAP2L2 phenotype to be very

similar to the EPS8 knock-out; with BAIAP2L2 knock-out animals showing extra rows of stereocilia with an overall shorter length in each row alongside an immature IHC basolateral profile (Zampini *et al.* 2011). While EPS8 knock-out mice are deaf, EPS8L2 knock-out animals showed a progressive hearing loss evident from around 2 months of age with the greatest impact at the higher frequencies (Zampini *et al.* 2011, Furness *et al.* 2013). Different from the above strains, BAIAP2L2 showed an early onset progressive hearing loss, which was already apparent two day after the onset of hearing (P14).. DPOAE experiments performed in slightly older animals at P19-22 suggest that the raised hearing threshold is caused, at least in part, by dysfunctional outer hair cell amplification. Similar to the ABRs, EPS8L2 knock-out animals only show deficits in outer hair cell amplification at only the highest stimulus frequencies at 2 months of age (Furness *et al.* 2013), whereas the BAIAP2L2 knock-out has the greatest effect relative to the control animals at the mid-range frequencies. Hearing thresholds continue to rise in the BAIAP2L2 homozygous animal relative to the heterozygous control until the latest age tested of around P166-245, at which point the knock-out animals are profoundly deaf. More detailed ABR wave I wave-form analysis indicates no apparent latency difference between the two genotypes, with the amplitude response difference again suggesting deficits in the amplification response in the knock-out animal. The phenotype associated with the BAIAP2L2 knock-out therefore appears unique, and between EPS8 and EPS8L2 in terms of severity. This already suggested that the phenotype associated with knocking out BAIAP2L2 may be unique, and was likely not be caused by lack of EPS8 localisation as we originally hypothesised.

Degeneration of the stereociliary bundle of hair cell hair in BAIAP2L2 knock-out animals

MET experiments, in which the outer hair cell (OHCs) stereocilia bundles are stimulated with saturating stimuli from a fluid jet, indicate that mechanotransduction is normal in the P8 knock-outs similar to the results seen in P7 EPS8L2 knock-out OHCs (Furness *et al.* 2013). However, by P11 the MET current in the OHCs of BAIAP2L2 knockout mice was already about half to that of the heterozygous control animal. Furthermore, the resting open probability and adaptation of the MET current appears normal, indicating that the observed phenotype was unlikely to be caused by defects on the biophysical properties of the MET channels. In contrast, in EPS8 knock-out animals the resting current of the MET

channel is entirely lost relative to control animals. The SEM images at P10 (**Figure 6.21**), showed that both IHCs and OHCs possess a normal gross morphology of the hair bundle. However, OHCs have some transducing stereocilia missing from the 3rd row of their hair bundles, explaining the reduced MET current apparent at this early age. At 2 months of age, the SEM data indicates that the third row of stereocilia was almost entirely absent (**Figure 6.22**), showing similar signs of degeneration to the EPS8L2 knock-out animal. The BAIAP2L2 animals however did not appear to show the thinning of the second row of stereocilia seen in the EPS8L2 model. At the oldest age checked at 8 months old, the second row of stereocilia is almost entirely degenerated in outer hair cells, with inner hair cells showing an almost entirely degenerated row 3 and signs of stereocilia loss in row 2. Again, this data indicates a phenotype which is distinct from the other two knock-out models, showing a more severe version of the progression seen in an EPS8L2 knock-out (Furness *et al.* 2013).

In contrast to the EPS8 knock-out, which impacts the current responses of IHCs but not OHCs, the BAIAP2L2 knock-out appears to have no effect on the basolateral membrane proteins in both IHCs and OHCs (Zampini *et al.* 2011). This difference may be caused by the manner with which these mutations impact the MET channel, as the loss of the resting MET in several mutations has been associated with an immature basolateral profile (Marcotti *et al.* 2006, Corns *et al.* 2018, Nakanishi *et al.* 2018), and the resting current in BAIAP2L2 homozygotes appears normal. Regarding the increased vulnerability of the OHCs, immunolabelling data indicated that BAIAP2L2 is present in both sets of hair cells well into adulthood, and thus the reason for the higher severity in OHCs seen in the SEM data is not known. Perhaps another SH3 containing I-BAR protein is present as a temporary compensatory mechanism in IHCs that is not present in OHCs, or perhaps OHCs due to a variety of factors are overall more vulnerable to stereocilia loss and thus are affected first in the BAIAP2L2 knock-out. In order to fully understand the mechanisms associated with the loss of BAIAP2L2 more work is needed to obtain a better picture of the molecular networks within the stereocilia, as the currently incomplete picture makes any theory purely speculative.

The localisation of BAIAP2L2 by EPS8

Given the original hypothesis, that BAIAP2L2 functions to recruit EPS8 to the tips of row 1 stereocilia, it was striking to discover that the recruitment of BAIAP2L2 is the opposite of what was originally hypothesized. Indeed, based on the data presented in this thesis it appears as though the localisation of BAIAP2L2 is dependent on the presence of EPS8, which is interesting given the localisation difference between the two proteins (Zampini *et al.* 2011). Based on the experiments carried out, it is difficult to determine whether this dependency on EPS8 is in fact due to a direct interaction between EPS8 and BAIAP2L2. Significant impairment of hair bundle mechanotransduction, such as that seen in the EPS8 knock-out (Zampini *et al.* 2011), can result in loss of row identity, and thus result in proteins such as EPS8 losing their row specificity while causing others such as GPSM2 to not accumulate at all (Krey *et al.* 2020). In order to investigate the significance of the BAIAP2L2-EPS8 interaction, the binding between the two proteins would need to be blocked without significantly impairing the resting MET current. As such, future work could perhaps be focused on selectively mutating the SH3 domain of BAIAP2L2 with CRISPR, as this domain is essential for the binding between BAIAP2L2 and EPS8 (**Figure 6.1**, Postema *et al.* 2018). This would allow for blocking the interaction with EPS8 while leaving the I-BAR domain intact, and make it easier to view the effect of the direct interaction with EPS8 without significantly disrupting the bundle. However, we can say that BAIAP2L2 is most likely not localising itself to the stereocilia tips through the detection of negative membrane curvature by the I-BAR domain, as BAIAP2L1 does in the brush border (Section 6.1, Postema *et al.* 2018). If this were indeed the case, the localisation of BAIAP2L2 would require only the presence of the stereocilia morphology, and not require interaction with any other protein. Also, further experimentation is required in order to determine exactly how BAIAP2L2 is maintaining row 3. At this stage, we cannot determine whether BAIAP2L2 affects the actin equilibrium directly, through the WH2 domain (Zhoa *et al.* 2011, Postema *et al.* 2018), whether it is acting indirectly by recruiting a currently unknown effector protein to the location, or both possible mechanisms work together.

Conclusions and future work

In summary, the work presented here is a detailed analysis of two proteins originally believed to modulate the EPS8-EPS8L2 differential localisation axis. Dystroglycan appears to possess no significant role in the hair cells of the cochlea, and without further evidence to better link dystroglycan or other DGC components in hearing loss, there is no compelling rationale to pursue this line of questioning further. In contrast, the investigation into the I-BAR protein BAIAP212 has revealed a new modulator of stereocilia maintenance and a key protein for normal mechano-electrical transduction at the stereociliary bundles. Furthermore, the I-BAR protein family contains two other members that contain an SH3 domain that allow for actin effector recruitment, including BAIAP211 which is known to localise EPS8 in the gut. The work presented in this thesis has revealed a whole family of proteins which may be involved in hearing loss, and provides avenues for a plethora of future work. Future projects can both further dissect the mechanism by which BAIAP2L2 induces hearing loss and investigate whether the other SH3 containing I-BAR proteins are at all involved in stereocilia morphogenesis and maintenance.

Bibliography

- Abcam. (2013). Stripping for reprobing. *ABCAM Technical*.
- Abdullah, M., Hassan, A., Rashid, S., & Naeem, M. (2020). Tyrosine phosphorylation as a regulator of dystrophin and beta-dystroglycan interaction: A molecular insight. *Journal of Molecular Graphics and Modelling*.
<https://doi.org/10.1016/j.jmgm.2020.107623>
- Abe, T., Kakehata, S., Kitani, R., Maruya, S. I., Navaratnam, D., Santos-Sacchi, J., & Shinkawa, H. (2007). Developmental expression of the outer hair cell motor prestin in the mouse. *Journal of Membrane Biology*. <https://doi.org/10.1007/s00232-007-9004-5>
- Acuna, C., Liu, X., Gonzalez, A., & Südhof, T. C. (2015). RIM-BPs Mediate Tight Coupling of Action Potentials to Ca²⁺-Triggered Neurotransmitter Release. *Neuron*.
<https://doi.org/10.1016/j.neuron.2015.08.027>
- Adams, M. E., Kramarcy, N., Krall, S. P., Rossi, S. G., Rotundo, R. L., Sealock, R., & Froehner, S. C. (2000). Absence of α -syntrophin leads to structurally aberrant neuromuscular synapses deficient in utrophin. *Journal of Cell Biology*.
<https://doi.org/10.1083/jcb.150.6.1385>
- Ahmed, S., Goh, W. I., & Bu, W. (2010). I-BAR domains, IRSp53 and filopodium formation. In *Seminars in Cell and Developmental Biology*.
<https://doi.org/10.1016/j.semcd.2009.11.008>
- Akhavan, A., Crivelli, S. N., Singh, M., Lingappa, V. R., & Muschler, J. L. (2008). SEA domain proteolysis determines the functional composition of dystroglycan. *The FASEB Journal*. <https://doi.org/10.1096/fj.07-8354com>
- Al Dhaibani, M. A., El-Hattab, A. W., Ismayl, O., & Suleiman, J. (2018). B3GALNT2 - Related Dystroglycanopathy: Expansion of the Phenotype with Novel Mutation Associated with Muscle-Eye-Brain Disease, Walker-Warburg Syndrome, Epileptic Encephalopathy-West Syndrome, and Sensorineural Hearing Loss. *Neuropediatrics*, 49(4), 289–295. <https://doi.org/10.1055/s-0038-1651519>
- Amiry-Moghaddam, M., Otsuka, T., Hurn, P. D., Traystman, R. J., Haug, F.-M., Froehner, S. C., Adams, M. E., Neely, J. D., Agre, P., Ottersen, O. P., & Bhardwaj, A. (2003). An α -syntrophin-dependent pool of AQP4 in astroglial end-feet confers bidirectional water flow between blood and brain. *Proceedings of the National Academy of Sciences*, 100(4), 2106–2111. <https://doi.org/10.1073/pnas.0437946100>
- Ashmore, J., Avan, P., Brownell, W. E., Dallos, P., Dierkes, K., Fettiplace, R., Grosh, K., Hackney, C. M., Hudspeth, A. J., Jülicher, F., Lindner, B., Martin, P., Meaud, J., Petit, C., Santos Sacchi, J. R., & Canlon, B. (2010). The remarkable cochlear amplifier. In *Hearing Research*. <https://doi.org/10.1016/j.heares.2010.05.001>
- Assad, J. A., Hacohen, N., & Corey, D. P. (1989). Voltage dependence of adaptation and active bundle movement in bullfrog saccular hair cells. *Proceedings of the National*

Academy of Sciences of the United States of America.

<https://doi.org/10.1073/pnas.86.8.2918>

Avenarius, M. R., Krey, J. F., Dumont, R. A., Morgan, C. P., Benson, C. B., Vijayakumar, S., Cunningham, C. L., Scheffer, D. I., Corey, D. P., Müller, U., Jones, S. M., & Barr-Gillespie, P. G. (2017). Heterodimeric capping protein is required for stereocilia length and width regulation. *Journal of Cell Biology*.
<https://doi.org/10.1083/jcb.201704171>

Avenarius, M. R., Saylor, K. W., Lundeberg, M. R., Wilmarth, P. A., Shin, J.-B., Spinelli, K. J., Pagana, J. M., Andrade, L., Kachar, B., Choi, D., David, L. L., & Barr-Gillespie, P. G. (2014). Correlation of Actin Crosslinker and Capper Expression Levels with Stereocilia Growth Phases. *Molecular & Cellular Proteomics*, 13(2), 606–620. <https://doi.org/10.1074/mcp.M113.033704>

Ayalon, G., Davis, J. Q., Scotland, P. B., & Bennett, V. (2008). An Ankyrin-Based Mechanism for Functional Organization of Dystrophin and Dystroglycan. *Cell*.
<https://doi.org/10.1016/j.cell.2008.10.018>

Babai, N., Bartoletti, T. M., & Thoreson, W. B. (2010). Calcium regulates vesicle replenishment at the cone ribbon synapse. *Journal of Neuroscience*.
<https://doi.org/10.1523/JNEUROSCI.2891-10.2010>

Baden, T., Euler, T., Weckström, M., & Lagnado, L. (2013). Spikes and ribbon synapses in early vision. In *Trends in Neurosciences*. <https://doi.org/10.1016/j.tins.2013.04.006>

Barclay, M., Ryan, A. F., & Housley, G. D. (2011). Type I vs type II spiral ganglion neurons exhibit differential survival and neuritogenesis during cochlear development. *Neural Development*. <https://doi.org/10.1186/1749-8104-6-33>

Bardhan, T., Jeng, J. Y., Waldmann, M., Ceriani, F., Johnson, S. L., Olt, J., Rüttiger, L., Marcotti, W., & Holley, M. C. (2019). Gata3 is required for the functional maturation of inner hair cells and their innervation in the mouse cochlea. *Journal of Physiology*.
<https://doi.org/10.1113/JP277997>

Barresi, R. (2006). Dystroglycan: from biosynthesis to pathogenesis of human disease. *Journal of Cell Science*, 119(2), 199–207. <https://doi.org/10.1242/jcs.02814>

Bassat, E., Mutlak, Y. E., Genzelinakh, A., Shadrin, I. Y., Baruch Umansky, K., Yifa, O., Kain, D., Rajchman, D., Leach, J., Riabov Bassat, D., Udi, Y., Sarig, R., Sagi, I., Martin, J. F., Bursac, N., Cohen, S., & Tzahor, E. (2017). The extracellular matrix protein agrin promotes heart regeneration in mice. *Nature*, 547(7662), 179–184.
<https://doi.org/10.1038/nature22978>

Batchelor, C. L., & Winder, S. J. (2006). Sparks, signals and shock absorbers: how dystrophin loss causes muscular dystrophy. In *Trends in Cell Biology* (Vol. 16, Issue 4, pp. 198–205). <https://doi.org/10.1016/j.tcb.2006.02.001>

Bateman, A. (2019). UniProt: A worldwide hub of protein knowledge. *Nucleic Acids Research*. <https://doi.org/10.1093/nar/gky1049>

- Becker, L., Schnee, M. E., Niwa, M., Sun, W., Maxeiner, S., Talaei, S., Kachar, B., Rutherford, M. A., & Ricci, A. J. (2018). The presynaptic ribbon maintains vesicle populations at the hair cell afferent fiber synapse. *ELife*. <https://doi.org/10.7554/eLife.30241>
- Beggs, A. H., Hoffman, E. P., Snyder, J. R., Arahata, K., Specht, L., Shapiro, F., Angelini, C., Sugita, H., & Kunkel, L. M. (1991). Exploring the molecular basis for variability among patients with Becker muscular dystrophy: Dystrophin gene and protein studies. *American Journal of Human Genetics*.
- Beltrán, D., Anderson, M. E., Bharathy, N., Settlemeyer, T. P., Svalina, M. N., Bajwa, Z., Shern, J. F., Gultekin, S. H., Cuellar, M. A., Yonekawa, T., Keller, C., & Campbell, K. P. (2019). Exogenous expression of the glycosyltransferase LARGE1 restores α -dystroglycan matriglycan and laminin binding in rhabdomyosarcoma. *Skeletal Muscle*. <https://doi.org/10.1186/s13395-019-0195-0>
- Belyantseva, I. A., Adler, H. J., Curi, R., Frolenkov, G. I., & Kachar, B. (2000). Expression and localization of prestin and the sugar transporter GLUT-5 during development of electromotility in cochlear outer hair cells. *The Journal of Neuroscience : The Official Journal of the Society for Neuroscience*. <https://doi.org/10.1523/jneurosci.20-24-j0002.2000>
- Belyantseva, I. A., Boger, E. T., & Friedman, T. B. (2003). Myosin XVa localizes to the tips of inner ear sensory cell stereocilia and is essential for staircase formation of the hair bundle. *Proceedings of the National Academy of Sciences of the United States of America*. <https://doi.org/10.1073/pnas.2334417100>
- Ben-Yosef, T., Belyantseva, I. A., Saunders, T. L., Hughes, E. D., Kawamoto, K., Van Itallie, C. M., Beyer, L. A., Halsey, K., Gardner, D. J., Wilcox, E. R., Rasmussen, J., Anderson, J. M., Dolan, D. F., Forge, A., Raphael, Y., Camper, S. A., & Friedman, T. B. (2003). Claudin 14 knockout mice, a model for autosomal recessive deafness DFNB29, are deaf due to cochlear hair cell degeneration. In *Human Molecular Genetics*. <https://doi.org/10.1093/hmg/ddg210>
- Berglund, A. M., & Ryugo, D. K. (1987). Hair cell innervation by spiral ganglion neurons in the mouse. *Journal of Comparative Neurology*. <https://doi.org/10.1002/cne.902550408>
- Beurg, M., Cui, R., Goldring, A. C., Ebrahim, S., Fettiplace, R., & Kachar, B. (2018). Variable number of TMC1-dependent mechanotransducer channels underlie tonotopic conductance gradients in the cochlea. *Nature Communications*, 9(1). <https://doi.org/10.1038/s41467-018-04589-8>
- Beurg, M., Fettiplace, R., Nam, J.-H., & Ricci, A. J. (2009). Localization of inner hair cell mechanotransducer channels using high-speed calcium imaging. *Nature Neuroscience*, 12(5), 553–558. <https://doi.org/10.1038/nn.2295>
- Beurg, M., Goldring, A. C., Ricci, A. J., & Fettiplace, R. (2016). Development and localization of reverse-polarity mechanotransducer channels in cochlear hair cells.

Proceedings of the National Academy of Sciences of the United States of America.
<https://doi.org/10.1073/pnas.1601067113>

Beurg, M., Michalski, N., Safieddine, S., Bouleau, Y., Schneggenburger, R., Chapman, E. R., Petit, C., & Dulon, D. (2010b). Control of exocytosis by synaptotagmins and otoferlin in auditory hair cells. *The Journal of Neuroscience*, *30*(40), 13281–13290. <https://doi.org/10.1523/JNEUROSCI.2528-10.2010>

Beurg, M., Nam, J. H., Chen, Q., & Fettiplace, R. (2010a). Calcium balance and mechanotransduction in rat cochlear hair cells. *Journal of Neurophysiology*. <https://doi.org/10.1152/jn.00019.2010>

Bewick, G. S., Nicholson, L. V., Young, C., Odonnell, E., & Slater, C. R. (1992). Different distributions of dystrophin and related proteins at nerve-muscle junctions. *NeuroReport*. <https://doi.org/10.1097/00001756-199210000-00009>

Bijata, M., Wlodarczyk, J., & Figiel, I. (2015). Dystroglycan controls dendritic morphogenesis of hippocampal neurons in vitro. *Frontiers in Cellular Neuroscience*, *9*. <https://doi.org/10.3389/fncel.2015.00199>

Biswas, S., Watters, J., Bachay, G., Varshney, S., Hunter, D. D., Hu, H., & Brunken, W. J. (2018). Laminin-dystroglycan signaling regulates retinal arteriogenesis. *FASEB Journal*. <https://doi.org/10.1096/fj.201800232R>

Blake, D. J., Nawrotzki, R., Peters, M. F., Froehner, S. C., & Davies, K. E. (1996). Isoform diversity of dystrobrevin, the murine 87-kDa postsynaptic protein. *Journal of Biological Chemistry*. <https://doi.org/10.1074/jbc.271.13.7802>

Bönnemann, C. G., Wang, C. H., Quijano-Roy, S., Deconinck, N., Bertini, E., Ferreira, A., Muntoni, F., Sewry, C., Bérout, C., Mathews, K. D., Moore, S. A., Bellini, J., Rutkowski, A., & North, K. N. (2014). Diagnostic approach to the congenital muscular dystrophies. *Neuromuscular Disorders*. <https://doi.org/10.1016/j.nmd.2013.12.011>

Booler, H. S., Pagalday-Vergara, V., Williams, J. L., Hopkinson, M., & Brown, S. C. (2017). Evidence of early defects in Cajal–Retzius cell localization during brain development in a mouse model of dystroglycanopathy. *Neuropathology and Applied Neurobiology*. <https://doi.org/10.1111/nan.12376>

Bowl, M. R., & Dawson, S. J. (2015). The mouse as a model for age-related hearing loss - A mini-review. *Gerontology*. <https://doi.org/10.1159/000368399>

Boyle, M. P., Bernard, A., Thompson, C. L., Ng, L., Boe, A., Mortrud, M., Hawrylycz, M. J., Jones, A. R., Hevner, R. F., & Lein, E. S. (2011). Cell-type-specific consequences of reelin deficiency in the mouse neocortex, hippocampus, and amygdala. *Journal of Comparative Neurology*. <https://doi.org/10.1002/cne.22655>

Brancaccio, A., Schulthess, T., Gesemann, M., & Engel, J. (1995). Electron microscopic evidence for a mucin-like region in chick muscle α -dystroglycan. *FEBS Letters*, *368*(1), 139–142. [https://doi.org/10.1016/0014-5793\(95\)00628-M](https://doi.org/10.1016/0014-5793(95)00628-M)

- Brancaccio, A., Schulthess, T., Gesemann, M., & Engel, J. (1997). The N-terminal region of α -dystroglycan is an autonomous globular domain. *European Journal of Biochemistry*. <https://doi.org/10.1111/j.1432-1033.1997.00166.x>
- Brandt, A., Striessnig, J., & Moser, T. (2003). Cav1.3 Channels Are Essential for Development and Presynaptic Activity of Cochlear Inner Hair Cells. *Journal of Neuroscience*. <https://doi.org/10.1523/JNEUROSCI.23-34-10832.2003>
- Briggs, D. C., Yoshida-Moriguchi, T., Zheng, T., Venzke, D., Anderson, M. E., Strazzulli, A., Moracci, M., Yu, L., Hohenester, E., & Campbell, K. P. (2016). Structural basis of laminin binding to the LARGE glycans on dystroglycan. *Nature Chemical Biology*. <https://doi.org/10.1038/nchembio.2146>
- Brockington, M., Blake, D. J., Prandini, P., Brown, S. C., Torelli, S., Benson, M. A., Ponting, C. P., Estournet, B., Romero, N. B., Mercuri, E., Voit, T., Sewry, C. A., Guicheney, P., & Muntoni, F. (2001). Mutations in the fukutin-related protein gene (FKRP) cause a form of congenital muscular dystrophy with secondary laminin α 2 deficiency and abnormal glycosylation of α -dystroglycan. *American Journal of Human Genetics*. <https://doi.org/10.1086/324412>
- Brown, M. C., Nuttall, A. L., Masta, R. I., & Lawrence, M. (1983). Cochlear inner hair cells: Effects of transient asphyxia on intracellular potentials. *Hearing Research*. [https://doi.org/10.1016/0378-5955\(83\)90023-0](https://doi.org/10.1016/0378-5955(83)90023-0)
- Brownell, W. E., Bader, C. R., Bertrand, D., & De Ribaupierre, Y. (1985). Evoked mechanical responses of isolated cochlear outer hair cells. *Science*. <https://doi.org/10.1126/science.3966153>
- Buran, B. N., Strenzke, N., Neef, A., Gundelfinger, E. D., Moser, T., & Liberman, M. C. (2010). Onset coding is degraded in auditory nerve fibers from mutant mice lacking synaptic ribbons. *Journal of Neuroscience*. <https://doi.org/10.1523/JNEUROSCI.0389-10.2010>
- Burda, H., & Branis, M. (1988). Postnatal development of the organ of Corti in the wild house mouse, laboratory mouse, and their hybrid. *Hearing Research*. [https://doi.org/10.1016/0378-5955\(88\)90140-2](https://doi.org/10.1016/0378-5955(88)90140-2)
- Buysse, K., Riemersma, M., Powell, G., Van reeuwijk, J., Chitayat, D., Roscioli, T., Kamsteeg, E. J., Van den elzen, C., Van beusekom, E., Blaser, S., Babul-Hirji, R., Halliday, W., Wright, G. J., Stemple, D. L., Lin, Y. Y., Lefeber, D. J., & Van bokhoven, H. (2013). Missense mutations in β -1,3-N-acetylglucosaminyltransferase 1 (B3GNT1) cause Walker-Warburg syndrome. *Human Molecular Genetics*. <https://doi.org/10.1093/hmg/ddt021>
- Caberlotto, E., Michel, V., Foucher, I., Bahloul, A., Goodyear, R. J., Pepermans, E., Michalski, N., Perfettini, I., Alegria-Prevot, O., Chardenoux, S., Do Cruzeiro, M., Hardelin, J.-P., Richardson, G. P., Avan, P., Weil, D., & Petit, C. (2011). Usher type 1G protein sans is a critical component of the tip-link complex, a structure controlling actin polymerization in stereocilia. *Proceedings of the National Academy of Sciences*, 108(14), 5825–5830. <https://doi.org/10.1073/pnas.1017114108>

- Campanelli, J. T., Roberds, S. L., Campbell, K. P., & Scheller, R. H. (1994). A role for dystrophin-associated glycoproteins and utrophin in agrin-induced AChR clustering. *Cell*, 77(5), 663–674. [https://doi.org/10.1016/0092-8674\(94\)90051-5](https://doi.org/10.1016/0092-8674(94)90051-5)
- Cao, L. H., Luo, D. G., & Yau, K. W. (2014). Light responses of primate and other mammalian cones. *Proceedings of the National Academy of Sciences of the United States of America*. <https://doi.org/10.1073/pnas.1400268111>
- Carrott, L., Bowl, M. R., Aguilar, C., Johnson, S. L., Chessum, L., West, M., Morse, S., Dorning, J., Smart, E., Hardisty-Hughes, R., Ball, G., Parker, A., Barnard, A. R., MacLaren, R. E., Wells, S., Marcotti, W., & Brown, S. D. M. (2016). Absence of neuroligin-3 affects synaptogenesis in mouse inner hair cells and causes profound hearing loss. *Journal of Neuroscience*. <https://doi.org/10.1523/JNEUROSCI.1808-15.2016>
- Cavaldesi, M., Macchia, G., Barca, S., Defilippi, P., Tarone, G., & Petrucci, T. C. (1999). Association of the dystroglycan complex isolated from bovine brain synaptosomes with proteins involved in signal transduction. *Journal of Neurochemistry*. <https://doi.org/10.1046/j.1471-4159.1999.721648.x>
- Ceriani, F., Hendry, A., Jeng, J., Johnson, S. L., Stephani, F., Olt, J., Holley, M. C., Mammano, F., Engel, J., Kros, C. J., Simmons, D. D., & Marcotti, W. (2019). Coordinated calcium signalling in cochlear sensory and non-sensory cells refines afferent innervation of outer hair cells. *The EMBO Journal*. <https://doi.org/10.15252/emj.201899839>
- Chakrabarti, R., Michanski, S., & Wichmann, C. (2018). Vesicle sub-pool organization at inner hair cell ribbon synapses. *EMBO Reports*. <https://doi.org/10.15252/embr.201744937>
- Chapman, E. R., Desai, R. C., Davis, A. F., & Tornehl, C. K. (1998). Delineation of the oligomerization, AP-2 binding, and synprint binding region of the C2B domain of synaptotagmin. *Journal of Biological Chemistry*. <https://doi.org/10.1074/jbc.273.49.32966>
- Chapochnikov, N. M., Takago, H., Huang, C. H., Pangršič, T., Khimich, D., Neef, J., Auge, E., Göttfert, F., Hell, S. W., Wichmann, C., Wolf, F., & Moser, T. (2014). Uniquantal release through a dynamic fusion pore is a candidate mechanism of hair cell exocytosis. *Neuron*. <https://doi.org/10.1016/j.neuron.2014.08.003>
- Chen, J., Johnson, S. L., Lewis, M. A., Hilton, J. M., Huma, A., Marcotti, W., & Steel, K. P. (2014). A reduction in Ptpaq1 associated with specific features of the deafness phenotype of the miR-96 mutant mouse *diminuendo*. *European Journal of Neuroscience*. <https://doi.org/10.1111/ejn.12484>
- Choquet, D., & Triller, A. (2003). The role of receptor diffusion in the organization of the postsynaptic membrane. *Nature Reviews Neuroscience*, 4(4), 251–265. <https://doi.org/10.1038/nrn1077>

- Chou, A. M., Sem, K. P., Wright, G. D., Sudhakaran, T., & Ahmed, S. (2014). Dynamin1 is a novel target for IRSp53 protein and works with mammalian enabled (Mena) protein and Eps8 to regulate filopodial dynamics. *Journal of Biological Chemistry*. <https://doi.org/10.1074/jbc.M114.553883>
- Chung, W., & Campanelli, J. T. (1999). WW and EF hand domains of dystrophin-family proteins mediate dystroglycan binding. *Molecular Cell Biology Research Communications*. <https://doi.org/10.1006/mcbr.1999.0168>
- Cirak, S., Foley, A. R., Herrmann, R., Willer, T., Yau, S., Stevens, E., Torelli, S., Brodd, L., Kamynina, A., Vondracek, P., Roper, H., Longman, C., Korinthenberg, R., Marrosu, G., Nürnberg, P., Michele, D. E., Plagnol, V., Hurler, M., Moore, S. A., ... Muntoni, F. (2013). ISPD gene mutations are a common cause of congenital and limb-girdle muscular dystrophies. *Brain*. <https://doi.org/10.1093/brain/aws312>
- Clements, R., Turk, R., Campbell, K. P., & Wright, K. M. (2017). Dystroglycan maintains inner limiting membrane integrity to coordinate retinal development. *Journal of Neuroscience*. <https://doi.org/10.1523/JNEUROSCI.0946-17.2017>
- Clements, R., & Wright, K. M. (2018). Retinal Ganglion Cell Axon Sorting at the Optic Chiasm Requires Dystroglycan. *Developmental Biology*, 442(August), 210–219. <https://doi.org/10.1016/j.ydbio.2018.08.010>
- Coate, T. M., Scott, M. K., & Gurjar, M. (2019). Current concepts in cochlear ribbon synapse formation. In *Synapse*. <https://doi.org/10.1002/syn.22087>
- Cohn, R. D., Henry, M. D., Michele, D. E., Barresi, R., Saito, F., Moore, S. A., Flanagan, J. D., Skwarchuk, M. W., Robbins, M. E., Mendell, J. R., Williamson, R. A., & Campbell, K. P. (2002). Disruption of DAG1 in differentiated skeletal muscle reveals a role for dystroglycan in muscle regeneration. *Cell*. [https://doi.org/10.1016/S0092-8674\(02\)00907-8](https://doi.org/10.1016/S0092-8674(02)00907-8)
- Colognato, H., Galvin, J., Wang, Z., Relucio, J., Nguyen, T., Harrison, D., Yurchenco, P. D., & Ffrench-Constant, C. (2007). Identification of dystroglycan as a second laminin receptor in oligodendrocytes, with a role in myelination. *Development*. <https://doi.org/10.1242/dev.02819>
- Connors, N. C., Adams, M. E., Froehner, S. C., & Kofuji, P. (2004). The potassium channel Kir4.1 associates with the dystrophin-glycoprotein complex via α -syntrophin in glia. *Journal of Biological Chemistry*, 279(27), 28387–28392. <https://doi.org/10.1074/jbc.M402604200>
- Connors, N. C., & Kofuji, P. (2002). Dystrophin Dp71 is critical for the clustered localization of potassium channels in retinal glial cells. *The Journal of Neuroscience: The Official Journal of the Society for Neuroscience*, 22(11), 4321–4327. <https://doi.org/20026510>
- Cooper, B., Hemmerlein, M., Ammermüller, J., Imig, C., Reim, K., Lipstein, N., Kalla, S., Kawabe, H., Brose, N., Brandstätter, J. H., & Varoqueaux, F. (2012). Munc13-

- independent vesicle priming at mouse photoreceptor ribbon synapses. *Journal of Neuroscience*. <https://doi.org/10.1523/JNEUROSCI.4240-11.2012>
- Corns, L. F., Bardhan, T., Houston, O., Olt, J., Holley, M. C., Masetto, S., Johnson, S. L., & Marcotti, W. (2014). Functional Development of Hair Cells in the Mammalian Inner Ear. In *Development of Auditory and Vestibular Systems: Fourth Edition*. <https://doi.org/10.1016/B978-0-12-408088-1.00006-3>
- Corns, L. F., Johnson, S. L., Kros, C. J., & Marcotti, W. (2016). Tmc1 point mutation affects Ca²⁺ sensitivity and block by dihydrostreptomycin of the mechano-electrical transducer current of mouse outer hair cells. *Journal of Neuroscience*. <https://doi.org/10.1523/JNEUROSCI.2439-15.2016>
- Corns, L. F., Johnson, S. L., Roberts, T., Ranatunga, K. M., Hendry, A., Ceriani, F., Safieddine, S., Steel, K. P., Forge, A., Petit, C., Furness, D. N., Kros, C. J., & Marcotti, W. (2018). Mechanotransduction is required for establishing and maintaining mature inner hair cells and regulating efferent innervation. *Nature Communications*. <https://doi.org/10.1038/s41467-018-06307-w>
- Cossu, G. (2004). Fusion of bone marrow-derived stem cells with striated muscle may not be sufficient to activate muscle genes. In *Journal of Clinical Investigation*. <https://doi.org/10.1172/JCI23733>
- Côté, P. D., Moukhles, H., Lindenbaum, M., & Carbonetto, S. (1999). Chimaeric mice deficient in dystroglycans develop muscular dystrophy and have disrupted myoneural synapses. *Nature Genetics*, 23(3), 338–342. <https://doi.org/10.1038/15519>
- Crawford, A. C., Evans, M. G., & Fettiplace, R. (1989). Activation and adaptation of transducer currents in turtle hair cells. *The Journal of Physiology*. <https://doi.org/10.1113/jphysiol.1989.sp017878>
- Croce, A., Cassata, G., Disanza, A., Gagliani, M. C., Tacchetti, C., Malabarba, M. G., Carlier, M. F., Scita, G., Baumeister, R., & Di Fiore, P. P. (2004). A novel actin barbed-end-capping activity in EPS-8 regulates apical morphogenesis in intestinal cells of *Caenorhabditis elegans*. *Nature Cell Biology*. <https://doi.org/10.1038/ncb1198>
- Dallos, P., Wu, X., Cheatham, M. A., Gao, J., Zheng, J., Anderson, C. T., Jia, S., Wang, X., Cheng, W. H. Y., Sengupta, S., He, D. Z. Z., & Zuo, J. (2008). Prestin-Based Outer Hair Cell Motility Is Necessary for Mammalian Cochlear Amplification. *Neuron*. <https://doi.org/10.1016/j.neuron.2008.02.028>
- Darrow, K. N., Maison, S. F., & Liberman, M. C. (2006). Cochlear efferent feedback balances interaural sensitivity. *Nature Neuroscience*. <https://doi.org/10.1038/nn1807>
- De Bernabé, D. B. V., Currier, S., Steinbrecher, A., Celli, J., Van Beusekom, E., Van der Zwaag, B., Kayserili, H., Merlini, L., Chitayat, D., Dobyns, W. B., Cormand, B., Lehesjoki, A. E., Cruces, J., Voit, T., Walsh, C. A., Van Bokhoven, H., & Brunner, H. G. (2002). Mutations in the O-mannosyltransferase gene POMT1 give rise to the severe neuronal migration disorder Walker-Warburg syndrome. *American Journal of Human Genetics*. <https://doi.org/10.1086/342975>

- Deconinck, A. E., Potter, A. C., Tinsley, J. M., Wood, S. J., Vater, R., Young, C., Metzinger, L., Vincent, A., Slater, C. R., & Davies, K. E. (1997a). Postsynaptic abnormalities at the neuromuscular junctions of utrophin-deficient mice. *Journal of Cell Biology*. <https://doi.org/10.1083/jcb.136.4.883>
- Deconinck, A. E., Rafael, J. A., Skinner, J. A., Brown, S. C., Potter, A. C., Metzinger, L., Watt, D. J., Dickson, J. G., Tinsley, J. M., & Davies, K. E. (1997b). Utrophin-dystrophin-deficient mice as a model for Duchenne muscular dystrophy. *Cell*. [https://doi.org/10.1016/S0092-8674\(00\)80532-2](https://doi.org/10.1016/S0092-8674(00)80532-2)
- DeRosier, D. J., & Tilney, L. G. (1989). The structure of the cuticular plate, an in vivo actin gel. *Journal of Cell Biology*. <https://doi.org/10.1083/jcb.109.6.2853>
- Di Blasi, C., Morandi, L., Barresi, R., Blasevich, F., Cornelio, F., & Mora, M. (1996). Dystrophin-associated protein abnormalities in dystrophin-deficient muscle fibers from symptomatic and asymptomatic Duchenne/Becker muscular dystrophy carriers. *Acta Neuropathologica*, 92(4), 369–377. <https://doi.org/10.1007/s004010050532>
- Dick, O., Tom Dieck, S., Altroch, W. D., Ammermüller, J., Weiler, R., Garner, C. C., Gundelfinger, E. D., & Brandstätter, J. H. (2003). The presynaptic active zone protein bassoon is essential for photoreceptor ribbon synapse formation in the retina. *Neuron*. [https://doi.org/10.1016/S0896-6273\(03\)00086-2](https://doi.org/10.1016/S0896-6273(03)00086-2)
- Dickinson, M. E., Flenniken, A. M., Ji, X., Teboul, L., Wong, M. D., White, J. K., Meehan, T. F., Weninger, W. J., Westerberg, H., Adissu, H., Baker, C. N., Bower, L., Brown, J. M., Brianna Caddle, L., Chiani, F., Clary, D., Cleak, J., Daly, M. J., Denegre, J. M., ... Murakami, A. (2016). High-throughput discovery of novel developmental phenotypes. *Nature*. <https://doi.org/10.1038/nature19356> - www.mousephenotype.org
- Di Rosa, G., Messina, S., D'Amico, A., Bertini, E., Pustorino, G., Spanò, M., & Tortorella, G. (2011). A new form of alpha-dystroglycanopathy associated with severe drug-resistant epilepsy and unusual EEG features. *Epileptic Disorders*. <https://doi.org/10.1684/epd.2011.0461>
- Dmytrenko, G. M., Pumplin, D. W., & Bloch, R. J. (1993). Dystrophin in a membrane skeletal network: Localization and comparison to other proteins. *Journal of Neuroscience*. <https://doi.org/10.1523/jneurosci.13-02-00547.1993>
- Dodson, H. C., Piper, T. A., Clarke, J. D. W., Quinlivan, R. M., & Dickson, G. (1995). Dystrophin expression in the hair cells of the cochlea. *Journal of Neurocytology*. <https://doi.org/10.1007/BF01257377>
- Douville, P. J., Harvey, W. J., & Carbonetto, S. (1988). Isolation and partial characterization of high affinity laminin receptors in neural cells. *Journal of Biological Chemistry*.
- Dubowitz, V. (2000). Congenital muscular dystrophy: An expanding clinical syndrome. In *Annals of Neurology*. [https://doi.org/10.1002/1531-8249\(200002\)47:2<143::AID-ANA2>3.0.CO;2-Y](https://doi.org/10.1002/1531-8249(200002)47:2<143::AID-ANA2>3.0.CO;2-Y)

- Duchenne, G.-B. (1868). De la paralysie musculaire pseudo-hypertrophique, ou paralysie myo-sclérosique. In *Archives Générales de Médecine*.
- Echteler, S. M. (1992). Developmental segregation in the afferent projections to mammalian auditory hair cells. *Proceedings of the National Academy of Sciences of the United States of America*. <https://doi.org/10.1073/pnas.89.14.6324>
- Echteler, S. M., & Nofsinger, Y. C. (2000). Development of ganglion cell topography in the postnatal cochlea. *Journal of Comparative Neurology*. [https://doi.org/10.1002/1096-9861\(20000925\)425:3<436::AID-CNE8>3.0.CO;2-1](https://doi.org/10.1002/1096-9861(20000925)425:3<436::AID-CNE8>3.0.CO;2-1)
- Eckhard, A., Gleiser, C., Rask-Andersen, H., Arnold, H., Liu, W., MacK, A., Müller, M., Löwenheim, H., & Hirt, B. (2012). Co-localisation of Kir4.1 and AQP4 in rat and human cochleae reveals a gap in water channel expression at the transduction sites of endocochlear K⁺ recycling routes. *Cell and Tissue Research*, 350(1), 27–43. <https://doi.org/10.1007/s00441-012-1456-y>
- Eckrich, T., Varakina, K., Johnson, S. L., Franz, C., Singer, W., Kuhn, S., Knipper, M., Holley, M. C., & Marcotti, W. (2012). Development and Function of the Voltage-Gated Sodium Current in Immature Mammalian Cochlear Inner Hair Cells. *PLoS ONE*. <https://doi.org/10.1371/journal.pone.0045732>
- Elgoyhen, A. B., Johnson, D. S., Boulter, J., Vetter, D. E., & Heinemann, S. (1994). $\alpha 9$: An acetylcholine receptor with novel pharmacological properties expressed in rat cochlear hair cells. *Cell*. [https://doi.org/10.1016/0092-8674\(94\)90555-X](https://doi.org/10.1016/0092-8674(94)90555-X)
- Elgoyhen, A. B., Vetter, D. E., Katz, E., Rothlin, C. V., Heinemann, S. F., & Boulter, J. (2001). $\alpha 10$: A determinant of nicotinic cholinergic receptor function in mammalian vestibular and cochlear mechanosensory hair cells. *Proceedings of the National Academy of Sciences of the United States of America*. <https://doi.org/10.1073/pnas.051622798>
- Ervasti, J. M., & Campbell, K. P. (1993). A role for the dystrophin-glycoprotein complex as a transmembrane linker between laminin and actin. *Journal of Cell Biology*, 122(4), 809–823. <https://doi.org/10.1083/jcb.122.4.809>
- Ervasti, J. M., Ohlendieck, K., Kahl, S. D., Gaver, M. G., & Campbell, K. P. (1990). Deficiency of glycoprotein component of the dystrophin complex in dystrophic muscle. *Nature*, 345(6273), 315–319. <https://doi.org/10.1038/345315a0>
- Esapa, C. T., Bentham, G. R. B., Schröder, J. E., Kröger, S., & Blake, D. J. (2003). The effects of post-translational processing on dystroglycan synthesis and trafficking. *FEBS Letters*, 555(2), 209–216. [https://doi.org/10.1016/S0014-5793\(03\)01230-4](https://doi.org/10.1016/S0014-5793(03)01230-4)
- Evans, E. F., & Klinke, R. (1982). The effects of intracochlear and systemic furosemide on the properties of single cochlear nerve fibres in the cat. *The Journal of Physiology*. <https://doi.org/10.1113/jphysiol.1982.sp014379>

- Eyermann, C., Czaplinski, K., & Colognato, H. (2012). Dystroglycan promotes filopodial formation and process branching in differentiating oligodendroglia. *Journal of Neurochemistry*. <https://doi.org/10.1111/j.1471-4159.2011.07600.x>
- Fang, Q., Indzhykulian, A. A., Mustapha, M., Riordan, G. P., Dolan, D. F., Friedman, T. B., Belyantseva, I. A., Frolenkov, G. I., Camper, S. A., & Bird, J. E. (2015). The 133-kDa N-terminal domain enables myosin 15 to maintain mechanotransducing stereocilia and is essential for hearing. *ELife*. <https://doi.org/10.7554/eLife.08627>
- Fariñas, I., Jones, K. R., Tessarollo, L., Vigers, A. J., Huang, E., Kirstein, M., De Caprona, D. C., Coppola, V., Backus, C., Reichardt, L. F., & Fritsch, B. (2001). Spatial shaping of cochlear innervation by temporally regulated neurotrophin expression. *Journal of Neuroscience*. <https://doi.org/10.1523/jneurosci.21-16-06170.2001>
- Farris, H. E., LeBlanc, C. L., Goswami, J., & Ricci, A. J. (2004). Probing the pore of the auditory hair cell mechanotransducer channel in turtle. *Journal of Physiology*. <https://doi.org/10.1113/jphysiol.2004.061267>
- Fenster, S. D., Chung, W. J., Zhai, R., Cases-Langhoff, C., Voss, B., Garner, A. M., Kaempf, U., Kindler, S., Gundelfinger, E. D., & Garner, C. C. (2000). Piccolo, a presynaptic zinc finger protein structurally related to Bassoon. *Neuron*. [https://doi.org/10.1016/S0896-6273\(00\)80883-1](https://doi.org/10.1016/S0896-6273(00)80883-1)
- Fettiplace, R. (2017). Hair Cell Transduction, Tuning, and Synaptic Transmission in the Mammalian Cochlea. *Comprehensive Physiology*, 7, 1197–1227.
- Fettiplace, R., & Hackney, C. M. (2006). The sensory and motor roles of auditory hair cells. In *Nature Reviews Neuroscience*. <https://doi.org/10.1038/nrn1828>
- Fitzgerald, K. M., Cibis, G. W., Giambrone, S. A., & Harris, D. J. (1994). Retinal signal transmission in Duchenne muscular dystrophy: Evidence for dysfunction in the photoreceptor/depolarizing bipolar cell pathway. *Journal of Clinical Investigation*. <https://doi.org/10.1172/JCI117250>
- Flagella, M., Clarke, L. L., Miller, M. L., Erway, L. C., Giannella, R. A., Andringa, A., Gawenis, L. R., Kramer, J., Duffy, J. J., Doetschman, T., Lorenz, J. N., Yamoah, E. N., Cardell, E. Lou, & Shull, G. E. (1999). Mice lacking the basolateral Na-K-2Cl cotransporter have impaired epithelial chloride secretion and are profoundly deaf. *Journal of Biological Chemistry*. <https://doi.org/10.1074/jbc.274.38.26946>
- Flock, Å., & Cheung, H. C. (1977). Actin filaments in sensory hairs of inner ear receptor cells. *Journal of Cell Biology*. <https://doi.org/10.1083/jcb.75.2.339>
- Frank, T., Rutherford, M. A., Strenzke, N., Neef, A., Pangršič, T., Khimich, D., Fetjova, A., Gundelfinger, E. D., Liberman, M. C., Harke, B., Bryan, K. E., Lee, A., Egner, A., Riedel, D., & Moser, T. (2010). Bassoon and the synaptic ribbon organize Ca²⁺ channels and vesicles to add release sites and promote refilling. *Neuron*. <https://doi.org/10.1016/j.neuron.2010.10.027>

- Fuchs, P. A. (2005). Time and intensity coding at the hair cell's ribbon synapse. *The Journal of Physiology*, 566(1), 7–12. <https://doi.org/10.1113/jphysiol.2004.082214>
- Furness, D. N., Johnson, S. L., Manor, U., Rüttiger, L., Tocchetti, A., Offenhauser, N., Olt, J., Goodyear, R. J., Vijayakumar, S., Dai, Y., Hackney, C. M., Franz, C., Di Fiore, P. P., Masetto, S., Jones, S. M., Knipper, M., Holley, M. C., Richardson, G. P., Kachar, B., & Marcotti, W. (2013). Progressive hearing loss and gradual deterioration of sensory hair bundles in the ears of mice lacking the actin-binding protein Eps8L2. *Proceedings of the National Academy of Sciences*, 110(34), 13898–13903. <https://doi.org/10.1073/pnas.1304644110>
- Garfinkle, T. J., & Saunders, J. C. (1983). Morphology of inner hair cell stereocilia in C57BL/6J mice as studied by scanning electron microscopy. *Otolaryngology-Head and Neck Surgery*. <https://doi.org/10.1177/019459988309100415>
- Gee, S. H., Montanaro, F., Lindenbaum, M. H., & Carbonetto, S. (1994). Dystroglycan- α , a dystrophin-associated glycoprotein, is a functional agrin receptor. *Cell*, 77(5), 675–686. [https://doi.org/10.1016/0092-8674\(94\)90052-3](https://doi.org/10.1016/0092-8674(94)90052-3)
- Gillespie, P. G., & Hudspeth, A. J. (1991). High-purity isolation of bullfrog hair bundles and subcellular and topological localization of constituent proteins. *Journal of Cell Biology*. <https://doi.org/10.1083/jcb.112.4.625>
- Glowatzki, E., & Fuchs, P. A. (2000). Cholinergic synaptic inhibition of inner hair cells in the neonatal mammalian cochlea. *Science*. <https://doi.org/10.1126/science.288.5475.2366>
- Glowatzki, E., & Fuchs, P. A. (2002). Transmitter release at the hair cell ribbon synapse. *Nature Neuroscience*. <https://doi.org/10.1038/nn796>
- Goh, W. I., Lim, K. B., Sudhaharan, T., Sem, K. P., Bu, W., Chou, A. M., & Ahmed, S. (2012). mDia1 and WAVE2 proteins interact directly with IRSp53 in filopodia and are involved in filopodium formation. *Journal of Biological Chemistry*. <https://doi.org/10.1074/jbc.M111.305102>
- Goldberg, J. M., Lysakowski, A., & Fernández, C. (1990). Morphophysiological and ultrastructural studies in the mammalian cristae ampullares. *Hearing Research*, 49(1–3), 89–102. [https://doi.org/10.1016/0378-5955\(90\)90097-9](https://doi.org/10.1016/0378-5955(90)90097-9)
- Goodyear, R. J., Marcotti, W., Kros, C. J., & Richardson, G. P. (2005). Development and properties of stereociliary link types in hair cells of the mouse cochlea. *Journal of Comparative Neurology*. <https://doi.org/10.1002/cne.20513>
- Grabner, C. P., Ratliff, C. P., Light, A. C., & DeVries, S. H. (2016). Mechanism of High-Frequency Signaling at a Depressing Ribbon Synapse. *Neuron*. <https://doi.org/10.1016/j.neuron.2016.05.019>
- Gracida-Jiménez, V., Mondragón-González, R., Vélez-Aguilera, G., Vásquez-Limeta, A., Laredo-Cisneros, M. S., Gómez-López, J. D. D., Vaca, L., Gourlay, S. C., Jacobs, L. A., Winder, S. J., & Cisneros, B. (2017). Retrograde trafficking of β -dystroglycan

from the plasma membrane to the nucleus. *Scientific Reports*.
<https://doi.org/10.1038/s41598-017-09972-x>

- Grady, R. M., Merlie, J. P., & Sanes, J. R. (1997a). Subtle neuromuscular defects in utrophin-deficient mice. *Journal of Cell Biology*.
<https://doi.org/10.1083/jcb.136.4.871>
- Grady, R. M., Teng, H., Nichol, M. C., Cunningham, J. C., Wilkinson, R. S., & Sanes, J. R. (1997b). Skeletal and cardiac myopathies in mice lacking utrophin and dystrophin: A model for Duchenne muscular dystrophy. *Cell*, *90*(4), 729–738.
[https://doi.org/10.1016/S0092-8674\(00\)80533-4](https://doi.org/10.1016/S0092-8674(00)80533-4)
- Grady, R. M., Zhou, H., Cunningham, J. M., Henry, M. D., Campbell, K. P., & Sanes, J. R. (2000). Maturation and maintenance of the neuromuscular synapse: Genetic evidence for roles of the dystrophin-glycoprotein complex. *Neuron*, *25*(2), 279–293.
[https://doi.org/10.1016/S0896-6273\(00\)80894-6](https://doi.org/10.1016/S0896-6273(00)80894-6)
- Grati, M., & Kachar, B. (2011). Myosin VIIa and sans localization at stereocilia upper tip-link density implicates these Usher syndrome proteins in mechanotransduction. *Proceedings of the National Academy of Sciences of the United States of America*.
<https://doi.org/10.1073/pnas.1104161108>
- Graydon, C. W., Cho, S., Li, G.-L., Kachar, B., & von Gersdorff, H. (2011). Sharp Ca²⁺ Nanodomains beneath the Ribbon Promote Highly Synchronous Multivesicular Release at Hair Cell Synapses. *Journal of Neuroscience*, *31*(46), 16637–16650.
<https://doi.org/10.1523/JNEUROSCI.1866-11.2011>
- Hackney, C. M., & Furness, D. N. (2013). The composition and role of cross links in mechano-electrical transduction in vertebrate sensory hair cells. *Journal of Cell Science*, *126*(Pt 8), 1721–1731. <https://doi.org/10.1242/jcs.106120>
- Hannaert, P., Alvarez-Guerra, M., Pirot, D., Nazaret, C., & Garay, R. (2002). Rat NKCC2/NKCC1 cotransporter selectivity for loop diuretic drugs. *Naunyn-Schmiedeberg's Archives of Pharmacology*. <https://doi.org/10.1007/s00210-001-0521-y>
- Harley, R. J., Murdy, J. P., Wang, Z., Kelly, M. C., Ropp, T. J. F., Park, S. H., Maness, P. F., Manis, P. B., & Coate, T. M. (2018). Neuronal cell adhesion molecule (NrCAM) is expressed by sensory cells in the cochlea and is necessary for proper cochlear innervation and sensory domain patterning during development. *Developmental Dynamics*. <https://doi.org/10.1002/dvdy.24629>
- Hayashi, S., Lewis, P., Pevny, L., & McMahon, A. P. (2002). Efficient gene modulation in mouse epiblast using a Sox2Cre transgenic mouse strain. *Gene Expression Patterns*.
[https://doi.org/10.1016/S0925-4773\(02\)00292-7](https://doi.org/10.1016/S0925-4773(02)00292-7)
- Heaney, D. L. M., & Schulte, B. A. (2003). Dystroglycan expression in the mouse cochlea. *Hearing Research*, *177*(1–2), 12–20. [https://doi.org/10.1016/S0378-5955\(02\)00769-4](https://doi.org/10.1016/S0378-5955(02)00769-4)

- Heffner, H. E., & Heffner, R. S. (2007). Hearing ranges of laboratory animals. In *Journal of the American Association for Laboratory Animal Science*.
- Hertzog, M., Milanesi, F., Hazelwood, L., Disanza, A., Liu, H., Perlade, E., Malabarba, M. G., Pasqualato, S., Maiolica, A., Confalonieri, S., Le Clainche, C., Offenhauser, N., Block, J., Rottner, K., Fiore, P. P. Di, Carlier, M. F., Volkmann, N., Hanein, D., & Scita, G. (2010). Molecular basis for the dual function of Eps8 on actin dynamics: Bundling and capping. *PLoS Biology*. <https://doi.org/10.1371/journal.pbio.1000387>
- Hino, N., Kobayashi, M., Shibata, N., Yamamoto, T., Saito, K., & Osawa, M. (2001). Clinicopathological study on eyes from cases of Fukuyama type congenital muscular dystrophy. *Brain and Development*. [https://doi.org/10.1016/S0387-7604\(01\)00189-9](https://doi.org/10.1016/S0387-7604(01)00189-9)
- Hoffman, E. P., Brown, R. H., & Kunkel, L. M. (1987). Dystrophin: The protein product of the duchenne muscular dystrophy locus. *Cell*. [https://doi.org/10.1016/0092-8674\(87\)90579-4](https://doi.org/10.1016/0092-8674(87)90579-4)
- Hollinger, S., & Hepler, J. R. (2002). Cellular regulation of RGS proteins: Modulators and integrators of G protein signaling. In *Pharmacological Reviews*. <https://doi.org/10.1124/pr.54.3.527>
- Holt, K. H., Crosbie, R. H., Venzke, D. P., & Campbell, K. P. (2000). Biosynthesis of dystroglycan: Processing of a precursor propeptide. *FEBS Letters*, 468(1), 79–83. [https://doi.org/10.1016/S0014-5793\(00\)01195-9](https://doi.org/10.1016/S0014-5793(00)01195-9)
- Hosoya, M., Fujioka, M., Ogawa, K., & Okano, H. (2016). Distinct Expression Patterns of Causative Genes Responsible for Hereditary Progressive Hearing Loss in Non-Human Primate Cochlea. *Scientific Reports*. <https://doi.org/10.1038/srep22250>
- Housley, G. D., & Ashmore, J. F. (1992). Ionic currents of outer hair cells isolated from the guinea-pig cochlea. *The Journal of Physiology*. <https://doi.org/10.1113/jphysiol.1992.sp019030>
- Howard, J., & Hudspeth, a J. (1987). Mechanical relaxation of the hair bundle mediates adaptation in mechano-electrical transduction by the bullfrog's saccular hair cell. *Proceedings of the National Academy of Sciences of the United States of America*, 84(9), 3064–3068. <https://doi.org/10.1073/pnas.84.9.3064>
- Huang, L. C., Barclay, M., Lee, K., Peter, S., Housley, G. D., Thorne, P. R., & Montgomery, J. M. (2012). Synaptic profiles during neurite extension, refinement and retraction in the developing cochlea. *Neural Development*. <https://doi.org/10.1186/1749-8104-7-38>
- Huang, L. C., Thorne, P. R., Housley, G. D., & Montgomery, J. M. (2007). Spatiotemporal definition of neurite outgrowth, refinement and retraction in the developing mouse cochlea. *Development*. <https://doi.org/10.1242/dev.001925>
- Hudspeth, A. J. (2000). Hearing and deafness. *Neurobiology of Disease*. <https://doi.org/10.1006/nbdi.2000.0343>

- Hudspeth, A. J., & Corey, D. P. (1977). Sensitivity, polarity, and conductance change in the response of vertebrate hair cells to controlled mechanical stimuli. *Proceedings of the National Academy of Sciences of the United States of America*. <https://doi.org/10.1073/pnas.74.6.2407>
- Ibraghimov-Beskrovnya, O., Ervasti, J. M., Leveille, C. J., Slaughter, C. A., Sernett, S. W., & Campbell, K. P. (1992). Primary structure of dystrophin-associated glycoproteins linking dystrophin to the extracellular matrix. *Nature*, 355(6362), 696–702. <https://doi.org/10.1038/355696a0>
- Ilsley, J. L., Sudol, M., & Winder, S. J. (2001). The interaction of dystrophin with beta-dystroglycan is regulated by tyrosine phosphorylation. *Cellular Signalling*, 13, 625–632.
- Indzhukulian, A. A., Stepanyan, R., Nelina, A., Spinelli, K. J., Ahmed, Z. M., Belyantseva, I. A., Friedman, T. B., Barr-Gillespie, P. G., & Frolenkov, G. I. (2013). Molecular Remodeling of Tip Links Underlies Mechanosensory Regeneration in Auditory Hair Cells. *PLoS Biology*. <https://doi.org/10.1371/journal.pbio.1001583>
- Ivanova, D., Dirks, A., Montenegro-Venegas, C., Schöne, C., Altmann, W. D., Marini, C., Frischknecht, R., Schanze, D., Zenker, M., Gundelfinger, E. D., & Fejtova, A. (2015). Synaptic activity controls localization and function of Ct BP 1 via binding to Bassoon and Piccolo. *The EMBO Journal*. <https://doi.org/10.15252/emboj.201488796>
- Jacobson, C., Côté, P. D., Rossi, S. G., Rotundo, R. L., & Carbonetto, S. (2001). The dystroglycan complex is necessary for stabilization of acetylcholine receptor clusters at neuromuscular junctions and formation of the synaptic basement membrane. *Journal of Cell Biology*. <https://doi.org/10.1083/jcb.152.3.435>
- Jagger, D. J., & Housley, G. D. (2003). Membrane properties of type II spiral ganglion neurones identified in a neonatal rat cochlear slice. *Journal of Physiology*. <https://doi.org/10.1111/j.1469-7793.2003.00525.x>
- James, M., Nuttall, A., Ilsley, J. L., Ottersbach, K., Tinsley, J. M., Sudol, M., & Winder, S. J. (2000). Adhesion-dependent tyrosine phosphorylation of β -dystroglycan regulates its interaction with utrophin. *Journal of Cell Science*.
- Jarsky, T., Cembrowski, M., Logan, S. M., Kath, W. L., Riecke, H., Demb, J. B., & Singer, J. H. (2011). A synaptic mechanism for retinal adaptation to luminance and contrast. *Journal of Neuroscience*. <https://doi.org/10.1523/JNEUROSCI.2631-11.2011>
- Jat, P. S., Noble, M. D., Ataliotis, P., Tanaka, Y., Yannoutsos, N., Larsen, L., & Kioussis, D. (1991). Direct derivation of conditionally immortal cell lines from an H-2Kb-tsA58 transgenic mouse. *Proceedings of the National Academy of Sciences of the United States of America*. <https://doi.org/10.1073/pnas.88.12.5096>
- Jean, P., de la Morena, D. L., Michanski, S., Tobón, L. M. J., Chakrabarti, R., Picher, M. M., Neef, J., Jung, S. Y., Gültas, M., Maxeiner, S., Neef, A., Wichmann, C., Strenzke, N., Grabner, C., & Moser, T. (2018). The synaptic ribbon is critical for sound

encoding at high rates and with temporal precision. *ELife*.
<https://doi.org/10.7554/eLife.29275>

- Jeng, J. Y., Johnson, S. L., Carlton, A. J., De Tomasi, L., Goodyear, R. J., De Faveri, F., Furness, D. N., Wells, S., Brown, S. D. M., Holley, M. C., Richardson, G. P., Mustapha, M., Bowl, M. R., & Marcotti, W. (2020). Age-related changes in the biophysical and morphological characteristics of mouse cochlear outer hair cells. *Journal of Physiology*. <https://doi.org/10.1113/JP279795>
- Johnson, C. P., & Chapman, E. R. (2010). Otoferlin is a calcium sensor that directly regulates SNARE-mediated membrane fusion. *Journal of Cell Biology*.
<https://doi.org/10.1083/jcb.201002089>
- Johnson, K. R., Erway, L. C., Cook, S. A., Willott, J. F., & Zheng, Q. Y. (1997). A major gene affecting age-related hearing loss in C57BL/6J mice. *Hearing Research*.
[https://doi.org/10.1016/S0378-5955\(97\)00155-X](https://doi.org/10.1016/S0378-5955(97)00155-X)
- Johnson, S. L., Adelman, J. P., & Marcotti, W. (2007). Genetic deletion of SK2 channels in mouse inner hair cells prevents the developmental linearization in the Ca²⁺ dependence of exocytosis. *Journal of Physiology*.
<https://doi.org/10.1113/jphysiol.2007.136630>
- Johnson, S. L., Forge, A., Knipper, M., Münkner, S., & Marcotti, W. (2008). Tonotopic variation in the calcium dependence of neurotransmitter release and vesicle pool replenishment at mammalian auditory ribbon synapses. *Journal of Neuroscience*.
<https://doi.org/10.1523/JNEUROSCI.0785-08.2008>
- Johnson, S. L., Franz, C., Knipper, M., & Marcotti, W. (2009). Functional maturation of the exocytotic machinery at gerbil hair cell ribbon synapses. *Journal of Physiology*.
<https://doi.org/10.1113/jphysiol.2009.168542>
- Johnson, S. L., Franz, C., Kuhn, S., Furness, D. N., Rüttiger, L., Münkner, S., Rivolta, M. N., Seward, E. P., Herschman, H. R., Engel, J., Knipper, M., & Marcotti, W. (2010). Synaptotagmin IV determines the linear Ca²⁺ dependence of vesicle fusion at auditory ribbon synapses. *Nature Neuroscience*. <https://doi.org/10.1038/nn.2456>
- Johnson, S. L., Kennedy, H. J., Holley, M. C., Fettiplace, R., & Marcotti, W. (2012). The resting transducer current drives spontaneous activity in prehearing mammalian cochlear inner hair cells. *Journal of Neuroscience*.
<https://doi.org/10.1523/JNEUROSCI.0803-12.2012>
- Johnson, S. L., Marcotti, W., & Kros, C. J. (2005). Increase in efficiency and reduction in Ca²⁺ dependence of exocytosis during development of mouse inner hair cells. *The Journal of Physiology*, 563, 177–191. <https://doi.org/10.1113/jphysiol.2004.074740>
- Johnson, S. L., Olt, J., Cho, S., von Gersdorff, H., & Marcotti, W. (2017). The coupling between Ca²⁺ channels and the exocytotic Ca²⁺ sensor at hair cell ribbon synapses varies tonotopically along the mature cochlea. *Journal of Neuroscience*.
<https://doi.org/10.1523/JNEUROSCI.2867-16.2017>

- Jones, C., Roper, V. C., Foucher, I., Qian, D., Banizs, B., Petit, C., Yoder, B. K., & Chen, P. (2008). Ciliary proteins link basal body polarization to planar cell polarity regulation. *Nature Genetics*. <https://doi.org/10.1038/ng.2007.54>
- Jung, D., Yang, B., Meyer, J., Chamberlain, J. S., & Campbell, K. P. (1995). Identification and characterization of the dystrophin anchoring site on β -dystroglycan. *Journal of Biological Chemistry*, 270(45), 27305–27310. <https://doi.org/10.1074/jbc.270.45.27305>
- Jung, S., Maritzen, T., Wichmann, C., Jing, Z., Neef, A., Revelo, N. H., Al-Moyed, H., Meese, S., Wojcik, S. M., Panou, I., Bulut, H., Schu, P., Ficner, R., Reisinger, E., Rizzoli, S. O., Neef, J., Strenzke, N., Haucke, V., & Moser, T. (2015a). Disruption of adaptor protein 2μ (AP-2 μ) in cochlear hair cells impairs vesicle reloading of synaptic release sites and hearing. *The EMBO Journal*. <https://doi.org/10.15252/emj.201591885>
- Jung, S., Oshima-Takago, T., Chakrabarti, R., Wong, A. B., Jing, Z., Yamanbaeva, G., Picher, M. M., Wojcik, S. M., Göttfert, F., Predoehl, F., Michel, K., Hell, S. W., Schoch, S., Strenzke, N., Wichmann, C., & Moser, T. (2015b). Rab3-interacting molecules 2α and 2β promote the abundance of voltage-gated CaV1.3 Ca²⁺ channels at hair cell active zones. *Proceedings of the National Academy of Sciences of the United States of America*. <https://doi.org/10.1073/pnas.1417207112>
- Kachar, B., Parakkal, M., Kurc, M., Zhao, Y. -d., & Gillespie, P. G. (2000). High-resolution structure of hair-cell tip links. *Proceedings of the National Academy of Sciences*, 97(24), 13336–13341. <https://doi.org/10.1073/pnas.97.24.13336>
- Kane, K. L., Longo-Guess, C. M., Gagnon, L. H., Ding, D., Salvi, R. J., & Johnson, K. R. (2012). Genetic background effects on age-related hearing loss associated with Cdh23 variants in mice. *Hearing Research*. <https://doi.org/10.1016/j.heares.2011.11.007>
- Kano, H., Kobayashi, K., Tachikawa, M., Toda, T., Kano, H., Yoshikawa, H., Herrmann, R., Straub, V., Voit, T., Manya, H., Endo, T., Nishino, I., Nonaka, I., Talim, B., & Topaloglu, H. (2002). Deficiency of α -dystroglycan in muscle-eye-brain disease. *Biochemical and Biophysical Research Communications*. <https://doi.org/10.1006/bbrc.2002.6608>
- Kärkkäinen, S., Hiipakka, M., Wang, J. H., Kleino, I., Vähä-Jaakkola, M., Renkema, G. H., Liss, M., Wagner, R., & Saksela, K. (2006). Identification of preferred protein interactions by phage-display of the human Src homology-3 proteome. *EMBO Reports*. <https://doi.org/10.1038/sj.embor.7400596>
- Kawashima, Y., Géléoc, G. S. G., Kurima, K., Labay, V., Lelli, A., Asai, Y., Makishima, T., Wu, D. K., Della Santina, C. C., Holt, J. R., & Griffith, A. J. (2011). Mechanotransduction in mouse inner ear hair cells requires transmembrane channel-like genes. *Journal of Clinical Investigation*. <https://doi.org/10.1172/JCI60405>
- Kazmierczak, P., Sakaguchi, H., Tokita, J., Wilson-Kubalek, E. M., Milligan, R. A., Müller, U., & Kachar, B. (2007). Cadherin 23 and protocadherin 15 interact to form

- tip-link filaments in sensory hair cells. *Nature*, 449(7158), 87–91.
<https://doi.org/10.1038/nature06091>
- Keen, E. C., & Hudspeth, A. J. (2006). Transfer characteristics of the hair cell's afferent synapse. *Proceedings of the National Academy of Sciences of the United States of America*. <https://doi.org/10.1073/pnas.0601103103>
- Keithley, E. M., & Feldman, M. L. (1982). Hair cell counts in an age-graded series of rat cochleas. *Hearing Research*. [https://doi.org/10.1016/0378-5955\(82\)90017-X](https://doi.org/10.1016/0378-5955(82)90017-X)
- Kemp, D. T. (2002). Otoacoustic emissions, their origin in cochlear function, and use. In *British Medical Bulletin*. <https://doi.org/10.1093/bmb/63.1.223>
- Kersigo, J., & Fritsch, B. (2015). Inner Ear hair cells deteriorate in mice engineered to have no or diminished innervation. *Frontiers in Aging Neuroscience*.
<https://doi.org/10.3389/fnagi.2015.00033>
- Khimich, D., Nouvtan, R., Pujol, R., Diesk, S. T., Egner, A., Gundelfinger, E. D., & Moser, T. (2005). Hair cell synaptic ribbons are essential for synchronous auditory signalling. *Nature*. <https://doi.org/10.1038/nature03418>
- Khurana, T. S., Hoffman, E. P., & Kunkel, L. M. (1990). Identification of a chromosome 6-encoded dystrophin-related protein. *Journal of Biological Chemistry*.
- Kikuchi, T., Adams, J. C., Miyabe, Y., So, E., & Kobayashi, T. (2000). Potassium ion recycling pathway via gap junction systems in the mammalian cochlea and its interruption in hereditary nonsyndromic deafness. In *Medical Electron Microscopy* (Vol. 33, Issue 2, pp. 51–56). <https://doi.org/10.1007/s007950070001>
- Kim, J., & Koo, M. (2015). Mass and stiffness impact on the middle ear and the cochlear partition. In *Korean Journal of Audiology*. <https://doi.org/10.7874/jao.2015.19.1.1>
- Kim, K. X., & Fettiplace, R. (2013). Developmental changes in the cochlear hair cell mechanotransducer channel and their regulation by transmembrane channel-like proteins. *Journal of General Physiology*. <https://doi.org/10.1085/jgp.201210913>
- Kim, M. H., Li, G. L., & von Gersdorff, H. (2013). Single Ca²⁺ channels and exocytosis at sensory synapses. *Journal of Physiology*.
<https://doi.org/10.1113/jphysiol.2012.249482>
- Kitajiri, S. I., Miyamoto, T., Mineharu, A., Sonoda, N., Furuse, K., Hata, M., Sasaki, H., Mori, Y., Kubota, T., Ito, J., Furuse, M., & Tsukita, S. (2004). Compartmentalization established by claudin-11-based tight junctions in stria vascularis is required for hearing through generation of endocochlear potential. *Journal of Cell Science*.
<https://doi.org/10.1242/jcs.01393>
- Kong, J., & Anderson, J. E. (1999). Dystrophin is required for organizing large acetylcholine receptor aggregates. *Brain Research*. [https://doi.org/10.1016/S0006-8993\(99\)01737-0](https://doi.org/10.1016/S0006-8993(99)01737-0)

- Koschak, A., Reimer, D., Huber, I., Grabner, M., Glossmann, H., Engel, J., & Striessnig, J. (2001). α 1D (Cav1.3) Subunits Can Form L-type Ca^{2+} Channels Activating at Negative Voltages. *Journal of Biological Chemistry*.
<https://doi.org/10.1074/jbc.M101469200>
- Krey, J. F., Chatterjee, P., Dumont, R. A., O'Sullivan, M., Choi, D., Bird, J. E., & Barr-Gillespie, P. G. (2020). Mechanotransduction-Dependent Control of Stereocilia Dimensions and Row Identity in Inner Hair Cells. *Current Biology*.
<https://doi.org/10.1016/j.cub.2019.11.076>
- Krinner, S., Butola, T., Jung, S., Wichmann, C., & Moser, T. (2017). Rim-binding protein 2 promotes a large number of Cav1.3 Ca^{2+} -channels and contributes to fast synaptic vesicle replenishment at hair cell active zones. *Frontiers in Cellular Neuroscience*.
<https://doi.org/10.3389/fncel.2017.00334>
- Kroll, J., Jaime Tobón, L. M., Vogl, C., Neef, J., Kondratiuk, I., König, M., Strenzke, N., Wichmann, C., Milosevic, I., & Moser, T. (2019). Endophilin-A regulates presynaptic Ca^{2+} influx and synaptic vesicle recycling in auditory hair cells. *The EMBO Journal*. <https://doi.org/10.15252/embj.2018100116>
- Kros, C. J., Marcotti, W., Van Netten, S. M., Self, T. J., Libby, R. T., Brown, S. D. M., Richardson, G. P., & Steel, K. P. (2002). Reduced climbing and increased slipping adaptation in cochlear hair cells of mice with Myo7a mutations. *Nature Neuroscience*.
<https://doi.org/10.1038/nn784>
- Kros, C. J., Ruppersberg, J. P., & Rüscher, A. (1998). Expression of a potassium current inner hair cells during development of hearing in mice. *Nature*.
<https://doi.org/10.1038/28401>
- Kubisch, C., Schroeder, B. C., Friedrich, T., Lütjohann, B., El-Amraoui, A., Marlin, S., Petit, C., & Jentsch, T. J. (1999). KCNQ4, a novel potassium channel expressed in sensory outer hair cells, is mutated in dominant deafness. *Cell*.
[https://doi.org/10.1016/S0092-8674\(00\)80556-5](https://doi.org/10.1016/S0092-8674(00)80556-5)
- Kulkarni, V. A., & Firestein, B. L. (2012). The dendritic tree and brain disorders. In *Molecular and Cellular Neuroscience* (Vol. 50, Issue 1, pp. 10–20).
<https://doi.org/10.1016/j.mcn.2012.03.005>
- Kurima, K., Ebrahim, S., Pan, B., Sedlacek, M., Sengupta, P., Millis, B. A., Cui, R., Nakanishi, H., Fujikawa, T., Kawashima, Y., Choi, B. Y., Monahan, K., Holt, J. R., Griffith, A. J., & Kachar, B. (2015). TMC1 and TMC2 Localize at the Site of Mechanotransduction in Mammalian Inner Ear Hair Cell Stereocilia. *Cell Reports*.
<https://doi.org/10.1016/j.celrep.2015.07.058>
- Lalwani, A. K., Brister, J. R., Fex, J., Grundfast, K. M., Pikus, A. T., Ploplis, B., San Agustin, T., Skarka, H., & Wilcox, E. R. (1994). A new nonsyndromic X-linked sensorineural hearing impairment linked to Xp21.2. *Am J Hum Genet*, 55(4), 685–694.

- Lara-Chacón, B., De León, M. B., Leocadio, D., Gómez, P., Fuentes-Mera, L., Martínez-Vieyra, I., Ortega, A., Jans, D. A., & Cisneros, B. (2010). Characterization of an importin in α/β -recognized nuclear localization signal in β -dystroglycan. *Journal of Cellular Biochemistry*. <https://doi.org/10.1002/jcb.22581>
- Latorre, R., & Brauchi, S. (2006). Large conductance Ca^{2+} -activated K^+ (BK) channel: Activation by Ca^{2+} and voltage. In *Biological Research*. <https://doi.org/10.4067/S0716-97602006000300003>
- Lawoko-Kerali, G., Milo, M., Davies, D., Halsall, A., Helyer, R., Johnson, C. M., Rivolta, M. N., Tones, M. A., & Holley, M. C. (2004). Ventral otic cell lines as developmental models of auditory epithelial and neural precursors. *Developmental Dynamics*, 231(4), 801–814. <https://doi.org/10.1002/dvdy.20187>
- Lee, S. H., Kerff, F., Chereau, D., Ferron, F., Klug, A., & Dominguez, R. (2007). Structural Basis for the Actin-Binding Function of Missing-in-Metastasis. *Structure*. <https://doi.org/10.1016/j.str.2006.12.005>
- Legan, P. K., Lukashkina, V. A., Goodyear, R. J., Kössl, M., Russell, I. J., & Richardson, G. P. (2000). A targeted deletion in α -tectorin reveals that the tectorial membrane is required for the gain and timing of cochlear feedback. *Neuron*. [https://doi.org/10.1016/S0896-6273\(00\)00102-1](https://doi.org/10.1016/S0896-6273(00)00102-1)
- Li, J., & Verkman, A. S. (2001). Impaired Hearing in Mice Lacking Aquaporin-4 Water Channels. *Journal of Biological Chemistry*, 276(33), 31233–31237. <https://doi.org/10.1074/jbc.M104368200>
- Liberman, M. C. (1982). Single-neuron labeling in the cat auditory nerve. *Science*. <https://doi.org/10.1126/science.7079757>
- Liberman, L. D., Wang, H., & Liberman, M. C. (2011). Opposing gradients of ribbon size and AMPA receptor expression underlie sensitivity differences among cochlear-nerve/hair-cell synapses. *Journal of Neuroscience*. <https://doi.org/10.1523/JNEUROSCI.3389-10.2011>
- Liberman, M. C., Dodds, L. W., & Pierce, S. (1990). Afferent and efferent innervation of the cat cochlea: Quantitative analysis with light and electron microscopy. *Journal of Comparative Neurology*. <https://doi.org/10.1002/cne.903010309>
- Liberman, M. C., & Kiang, N. Y. S. (1978). Acoustic trauma in cats. Cochlear pathology and auditory-nerve activity. *Acta Oto-Laryngologica Supplement*, 358, 1–63. <https://doi.org/10.3109/00016487809127889>
- Liberman, L. D., & Liberman, M. C. (2016). Postnatal maturation of auditory-nerve heterogeneity, as seen in spatial gradients of synapse morphology in the inner hair cell area. *Hearing Research*. <https://doi.org/10.1016/j.heares.2016.06.002>
- Liley, A. W., & North, K. A. (1953). An electrical investigation of effects of repetitive stimulation on mammalian neuromuscular junction. *Journal of Neurophysiology*. <https://doi.org/10.1152/jn.1953.16.5.509>

- Lim, D. J., & Anniko, M. (1985). Developmental morphology of the mouse inner ear: A scanning electron microscopic observation. *Acta Oto-Laryngologica*.
<https://doi.org/10.3109/00016488509121766>
- Liu, C., Glowatzki, E., & Fuchs, P. A. (2015). Unmyelinated type II afferent neurons report cochlear damage. *Proceedings of the National Academy of Sciences of the United States of America*. <https://doi.org/10.1073/pnas.1515228112>
- Liu, Y. P., & Zhao, H. B. (2008). Cellular characterization of Connexin26 and Connexin30 expression in the cochlear lateral wall. *Cell and Tissue Research*.
<https://doi.org/10.1007/s00441-008-0641-5>
- Livak, K. J., & Schmittgen, T. D. (2001). Analysis of relative gene expression data using real-time quantitative PCR and the 2- $\Delta\Delta$ CT method. *Methods*.
<https://doi.org/10.1006/meth.2001.1262>
- Longman, C., Brockington, M., Torelli, S., Jimenez-Mallebrera, C., Kennedy, C., Khalil, N., Feng, L., Saran, R. K., Voit, T., Merlini, L., Sewry, C. A., Brown, S. C., & Muntoni, F. (2003). Mutations in the human LARGE gene cause MDC1D, a novel form of congenital muscular dystrophy with severe mental retardation and abnormal glycosylation of α -dystroglycan. *Human Molecular Genetics*.
<https://doi.org/10.1093/hmg/ddg307>
- Lunardi, A., Cremisi, F., & Dente, L. (2006). Dystroglycan is required for proper retinal layering. *Developmental Biology*, 290(2), 411–420.
<https://doi.org/10.1016/j.ydbio.2005.11.044>
- Lv, C., Stewart, W. J., Akanyeti, O., Frederick, C., Zhu, J., Santos-Sacchi, J., Sheets, L., Liao, J. C., & Zenisek, D. (2016). Synaptic Ribbons Require Ribeye for Electron Density, Proper Synaptic Localization, and Recruitment of Calcium Channels. *Cell Reports*. <https://doi.org/10.1016/j.celrep.2016.05.045>
- Lyons, P. R., & Slater, C. R. (1991). Structure and function of the neuromuscular junction in young adult mdx mice. *Journal of Neurocytology*.
<https://doi.org/10.1007/BF01187915>
- Maeda, R., Kindt, K. S., Mo, W., Morgan, C. P., Erickson, T., Zhao, H., Clemens-Grisham, R., Barr-Gillespie, P. G., & Nicolson, T. (2014). Tip-link protein protocadherin 15 interacts with transmembrane channel-like proteins TMC1 and TMC2. *Proceedings of the National Academy of Sciences of the United States of America*. <https://doi.org/10.1073/pnas.1402152111>
- Magupalli, V. G., Schwarz, K., Alpadi, K., Natarajan, S., Seigel, G. M., & Schmitz, F. (2008). Multiple RIBEYE-RIBEYE interactions create a dynamic scaffold for the formation of synaptic ribbons. *Journal of Neuroscience*.
<https://doi.org/10.1523/JNEUROSCI.1964-08.2008>
- Mahendrasingam, S., Beurg, M., Fettiplace, R., & Hackney, C. M. (2010). The ultrastructural distribution of prestin in outer hair cells: A post-embedding immunogold investigation of low-frequency and high-frequency regions of the rat

cochlea. *European Journal of Neuroscience*. <https://doi.org/10.1111/j.1460-9568.2010.07182.x>

- Mamchaoui, K., Trollet, C., Bigot, A., Negroni, E., Chaouch, S., Wolff, A., Kandalla, P. K., Marie, S., Di Santo, J., St Guily, J. L., Muntoni, F., Kim, J., Philippi, S., Spuler, S., Levy, N., Blumen, S. C., Voit, T., Wright, W. E., Aamiri, A., ... Mouly, V. (2011). Immortalized pathological human myoblasts: Towards a universal tool for the study of neuromuscular disorders. *Skeletal Muscle*. <https://doi.org/10.1186/2044-5040-1-34>
- Mammano, F., & Ashmore, J. F. (1993). Reverse transduction measured in the isolated cochlea by laser Michelson interferometry. *Nature*. <https://doi.org/10.1038/365838a0>
- Manor, U., Disanza, A., Grati, M., Andrade, L., Lin, H., Di Fiore, P. P., Scita, G., & Kachar, B. (2011). Regulation of stereocilia length by myosin XVa and whirlin depends on the actin-regulatory protein Eps8. *Current Biology*, *21*(2), 167–172. <https://doi.org/10.1016/j.cub.2010.12.046>
- Marcotti, W. (2012). Functional assembly of mammalian cochlear hair cells. *Experimental Physiology*. <https://doi.org/10.1113/expphysiol.2011.059303>
- Marcotti, W., Erven, A., Johnson, S. L., Steel, K. P., & Kros, C. J. (2006). Tmc1 is necessary for normal functional maturation and survival of inner and outer hair cells in the mouse cochlea. *Journal of Physiology*. <https://doi.org/10.1113/jphysiol.2005.095661>
- Marcotti, W., Géléoc, G. S. G., Lennan, G. W. T., & Kros, C. J. (1999). Transient expression of an inwardly rectifying potassium conductance in developing inner and outer hair cells along the mouse cochlea. *Pflügers Archiv European Journal of Physiology*. <https://doi.org/10.1007/s004240051134>
- Marcotti, W., Johnson, S. L., Holley, M. C., & Kros, C. J. (2003a). Development of changes in the expression of potassium currents of embryonic, neonatal and mature mouse inner hair cells. *Journal of Physiology*. <https://doi.org/10.1113/jphysiol.2002.034801>
- Marcotti, W., Johnson, S. L., & Kros, C. J. (2004a). A transiently expressed SK current sustains and modulates action potential activity in immature mouse inner hair cells. *The Journal of Physiology*, *560*(3), 691–708. <https://doi.org/10.1113/jphysiol.2004.072868>
- Marcotti, W., Johnson, S. L., & Kros, C. J. (2004b). Effects of intracellular stores and extracellular Ca²⁺ on Ca²⁺-activated K⁺ currents in mature mouse inner hair cells. *Journal of Physiology*. <https://doi.org/10.1113/jphysiol.2003.060137>
- Marcotti, W., Johnson, S. L., Rüscher, A., & Kros, C. J. (2003b). Sodium and calcium currents shape action potentials in immature mouse inner hair cells. In *Journal of Physiology*. <https://doi.org/10.1113/jphysiol.2003.043612>

- Marcotti, W., & Kros, C. J. (1999). Developmental expression of the potassium current I(K,n) contributes to maturation of mouse outer hair cells. *Journal of Physiology*. <https://doi.org/10.1111/j.1469-7793.1999.00653.x>
- Marcus, D. C., Wu, T., Wangemann, P., & Kofuji, P. (2002). KCNJ10 (Kir4.1) potassium channel knockout abolishes endocochlear potential. *AJP: Cell Physiology*, 282(2), C403–C407. <https://doi.org/10.1152/ajpcell.00312.2001>
- Martínez-Vieyra, I. A., Vásquez-Limeta, A., González-Ramírez, R., Morales-Lázaro, S. L., Mondragón, M., Mondragón, R., Ortega, A., Winder, S. J., & Cisneros, B. (2013). A role for β -dystroglycan in the organization and structure of the nucleus in myoblasts. *Biochimica et Biophysica Acta - Molecular Cell Research*. <https://doi.org/10.1016/j.bbamcr.2012.11.019>
- Masaki, T., Matsumura, K., Saito, F., Sunada, Y., Shimizu, T., Yorifuji, H., Motoyoshi, K., & Kamakura, K. (2000). Expression of dystroglycan and laminin-2 in peripheral nerve under axonal degeneration and regeneration. *Acta Neuropathologica*. <https://doi.org/10.1007/PL00007440>
- Mason, M. J. (2016). Structure and function of the mammalian middle ear. II: Inferring function from structure. *Journal of Anatomy*. <https://doi.org/10.1111/joa.12316>
- Matsubara, A., Laake, J. H., Davanger, S., Usami, S. I., & Ottersen, O. P. (1996). Organization of AMPA receptor subunits at a glutamate synapse: A quantitative immunogold analysis of hair cell synapses in the rat organ of corti. *Journal of Neuroscience*. <https://doi.org/10.1523/jneurosci.16-14-04457.1996>
- Matsumura, K., Nonaka, I., Tomé, F. M., Arahata, K., Collin, H., Leturcq, F., Récan, D., Kaplan, J. C., Fardeau, M., & Campbell, K. P. (1993). Mild deficiency of dystrophin-associated proteins in Becker muscular dystrophy patients having in-frame deletions in the rod domain of dystrophin. *American Journal of Human Genetics*, 53(2), 409–416. <http://www.pubmedcentral.nih.gov/articlerender.fcgi?artid=1682334&tool=pmcentrez&rendertype=abstract>
- Mauro, V. P., Krushel, L. A., Cunningham, B. A., & Edelman, G. M. (1992). Homophilic and heterophilic binding activities of Nr-CAM, a nervous system cell adhesion molecule. *Journal of Cell Biology*. <https://doi.org/10.1083/jcb.119.1.191>
- Maxeiner, S., Luo, F., Tan, A., Schmitz, F., & Südhof, T. C. (2016). How to make a synaptic ribbon: RIBEYE deletion abolishes ribbons in retinal synapses and disrupts neurotransmitter release. *The EMBO Journal*. <https://doi.org/10.15252/emj.201592701>
- May-Simera, H. L., Petralia, R. S., Montcouquiol, M., Wang, Y. X., Szarama, K. B., Liu, Y., Lin, W., Deans, M. R., Pazour, G. J., & Kelley, M. W. (2015). Ciliary proteins bbs8 and ift20 promote planar cell polarity in the cochlea. *Development (Cambridge)*. <https://doi.org/10.1242/dev.113696>

- Mburu, P., Mustapha, M., Varela, A., Weil, D., El-Amraoui, A., Holme, R. H., Rump, A., Hardisty, R. E., Blanchard, S., Coimbra, R. S., Perfettini, I., Parkinson, N., Mallon, A. M., Glenister, P., Rogers, M. J., Paige, A. J., Moir, L., Clay, J., Rosenthal, A., ... Brown, S. D. M. (2003). Defects in whirlin, a PDZ domain molecule involved in stereocilia elongation, cause deafness in the whirler mouse and families with DFNB31. *Nature Genetics*. <https://doi.org/10.1038/ng1208>
- Mburu, P., Romero, M. R., Hilton, H., Parker, A., Townsend, S., Kikkawa, Y., & Brown, S. D. M. (2010). Gelsolin plays a role in the actin polymerization complex of hair cell stereocilia. *PLoS ONE*. <https://doi.org/10.1371/journal.pone.0011627>
- Menna, E., Zambetti, S., Morini, R., Donzelli, A., Disanza, A., Calvigioni, D., Braidà, D., Nicolini, C., Orlando, M., Fossati, G., Cristina Regondi, M., Pattini, L., Frassoni, C., Francolini, M., Scita, G., Sala, M., Fahnstock, M., & Matteoli, M. (2013). Eps8 controls dendritic spine density and synaptic plasticity through its actin-capping activity. *EMBO Journal*. <https://doi.org/10.1038/emboj.2013.107>
- Mennerick, S., & Matthews, G. (1996). Ultrafast exocytosis elicited by calcium current in synaptic terminals of retinal bipolar neurons. *Neuron*. [https://doi.org/10.1016/S0896-6273\(00\)80254-8](https://doi.org/10.1016/S0896-6273(00)80254-8)
- Merchan-Perez, A., & Liberman, M. C. (1996). Ultrastructural differences among afferent synapses on cochlear hair cells: Correlations with spontaneous discharge rate. *Journal of Comparative Neurology*. [https://doi.org/10.1002/\(SICI\)1096-9861\(19960722\)371:2<208::AID-CNE2>3.3.CO;2-P](https://doi.org/10.1002/(SICI)1096-9861(19960722)371:2<208::AID-CNE2>3.3.CO;2-P)
- Messina, S., Tortorella, G., Concolino, D., Spanò, M., D'Amico, A., Bruno, C., Santorelli, F. M., Mercuri, E., & Bertini, E. (2009). Congenital muscular dystrophy with defective α -dystroglycan, cerebellar hypoplasia, and epilepsy. *Neurology*. <https://doi.org/10.1212/WNL.0b013e3181c0d47a>
- Meyer, A. C., Frank, T., Khimich, D., Hoch, G., Riedel, D., Chapochnikov, N. M., Yarin, Y. M., Harke, B., Hell, S. W., Egner, A., & Moser, T. (2009). Tuning of synapse number, structure and function in the cochlea. *Nature Neuroscience*. <https://doi.org/10.1038/nn.2293>
- Meyer, A. C., & Moser, T. (2010). Structure and function of cochlear afferent innervation. In *Current Opinion in Otolaryngology and Head and Neck Surgery*. <https://doi.org/10.1097/MOO.0b013e32833e0586>
- Mianné, J., Chessum, L., Kumar, S., Aguilar, C., Codner, G., Hutchison, M., Parker, A., Mallon, A. M., Wells, S., Simon, M. M., Teboul, L., Brown, S. D. M., & Bowl, M. R. (2016). Correction of the auditory phenotype in C57BL/6N mice via CRISPR/Cas9-mediated homology directed repair. *Genome Medicine*. <https://doi.org/10.1186/s13073-016-0273-4>
- Michanski, S., Smaluch, K., Maria Steyer, A., Chakrabarti, R., Setz, C., Oestreicher, D., Fischer, C., Möbius, W., Moser, T., Vogl, C., & Wichmann, C. (2019). Mapping developmental maturation of inner hair cell ribbon synapses in the apical mouse

- cochlea. *Proceedings of the National Academy of Sciences of the United States of America*. <https://doi.org/10.1073/pnas.1812029116>
- Miike, T., Miyatake, M., Zhao, J., Yoshioka, K., & Uchino, M. (1989). Immunohistochemical dystrophin reaction in synaptic regions. *Brain and Development*. [https://doi.org/10.1016/S0387-7604\(89\)80067-1](https://doi.org/10.1016/S0387-7604(89)80067-1)
- Mikaelian, D., & Ruben, R. J. (1965). Development of hearing in the normal cba-j mouse: Correlation of physiological observations with behavioral responses and with cochlear anatomy. *Acta Oto-Laryngologica*. <https://doi.org/10.3109/00016486509124579>
- Moore, C. J., & Winder, S. J. (2010). Dystroglycan versatility in cell adhesion: a tale of multiple motifs. *Cell Communication and Signaling : CCS*, 8, 3. <https://doi.org/10.1186/1478-811X-8-3>
- Moser, T., & Beutner, D. (2000). Kinetics of exocytosis and endocytosis at the cochlear inner hair cell afferent synapse of the mouse. *Proceedings of the National Academy of Sciences*, 97(2), 883–888. <https://doi.org/10.1073/pnas.97.2.883>
- Moser, T., Grabner, C. P., & Schmitz, F. (2020). Sensory processing at ribbon synapses in the retina and the cochlea. *Physiological Reviews*. <https://doi.org/10.1152/physrev.00026.2018>
- Moser, T., Neef, A., & Khimich, D. (2006). Mechanisms underlying the temporal precision of sound coding at the inner hair cell ribbon synapse. In *Journal of Physiology*. <https://doi.org/10.1113/jphysiol.2006.114835>
- Müller, T. M., Gierke, K., Joachimsthaler, A., Sticht, H., Izsvák, Z., Hamra, F. K., Fejtová, A., Ackermann, F., Garner, C. C., Kremers, J., Brandstätter, J. H., & Regus-Leidig, H. (2019). A multiple piccolino-RIBEYE interaction supports plate-shaped synaptic ribbons in retinal neurons. *Journal of Neuroscience*. <https://doi.org/10.1523/JNEUROSCI.2038-18.2019>
- Müller, M., Klinke, R., Arnold, W., & Oestreicher, E. (2003). Auditory nerve fibre responses to salicylate revisited. *Hearing Research*. [https://doi.org/10.1016/S0378-5955\(03\)00217-X](https://doi.org/10.1016/S0378-5955(03)00217-X)
- Müller, M., Von Hünenbein, K., Hoidis, S., & Smolders, J. W. T. (2005). A physiological place-frequency map of the cochlea in the CBA/J mouse. *Hearing Research*. <https://doi.org/10.1016/j.heares.2004.08.011>
- Nagel, A., Lehmann-Horn, F., & Engel, A. G. (1990). Neuromuscular transmission in the mdx mouse. *Muscle & Nerve*. <https://doi.org/10.1002/mus.880130813>
- Nagelhus, E. A., Mathiisen, T. M., & Ottersen, O. P. (2004). Aquaporin-4 in the central nervous system: Cellular and subcellular distribution and coexpression with KIR4.1. *Neuroscience*. <https://doi.org/10.1016/j.neuroscience.2004.08.053>

- Nakanishi, H., Kurima, K., Pan, B., Wangemann, P., Fitzgerald, T. S., Géléoc, G. S., Holt, J. R., & Griffith, A. J. (2018). Tmc2 expression partially restores auditory function in a mouse model of DFNB7/B11 deafness caused by loss of Tmc1 function. *Scientific Reports*. <https://doi.org/10.1038/s41598-018-29709-8>
- Neely, S. T. (1998). *From Sound to Synapse: Physiology of the Mammalian Ear*. Ear and Hearing. <https://doi.org/10.1097/00003446-199812000-00011>
- Neely, J. D., Amiry-Moghaddam, M., Ottersen, O. P., Froehner, S. C., Agre, P., & Adams, M. E. (2001). Syntrophin-dependent expression and localization of Aquaporin-4 water channel protein. *Proceedings of the National Academy of Sciences*, 98(24), 14108–14113. <https://doi.org/10.1073/pnas.241508198>
- Neher, E. (1998). Vesicle pools and Ca²⁺ microdomains: New tools for understanding their roles in neurotransmitter release. In *Neuron*. [https://doi.org/10.1016/S0896-6273\(00\)80983-6](https://doi.org/10.1016/S0896-6273(00)80983-6)
- Nenov, A. P., Norris, C., & Bobbin, R. P. (1996). Acetylcholine response in guinea pig outer hair cells. II. Activation of a small conductance Ca²⁺-activated K⁺ channel. *Hearing Research*. [https://doi.org/10.1016/S0378-5955\(96\)00143-8](https://doi.org/10.1016/S0378-5955(96)00143-8)
- Neyroud, N., Tesson, F., Denjoy, I., Leibovici, M., Donger, C., Barhanin, J., Fauré, S., Gary, F., Coumel, P., Petit, C., Schwartz, K., & Guicheney, P. (1997). A novel mutation in the potassium channel gene KVLQT1 causes the Jervell and Lange-Nielsen cardioauditory syndrome. *Nature Genetics*. <https://doi.org/10.1038/ng0297-186>
- Nickolls, A. R., & Bönemann, C. G. (2018). The roles of dystroglycan in the nervous system: Insights from animal models of muscular dystrophy. In *DMM Disease Models and Mechanisms*. <https://doi.org/10.1242/dmm.035931>
- Nielsen, S., Nagelhus, E. A., Amiry-Moghaddam, M., Bourque, C., Agre, P., & Ottersen, O. R. (1997). Specialized membrane domains for water transport in glial cells: High-resolution immunogold cytochemistry of aquaporin-4 in rat brain. *Journal of Neuroscience*. <https://doi.org/10.1523/jneurosci.17-01-00171.1997>
- Nishida, Y., Rivolta, M. N., & Holley, M. C. (1998). Timed markers for the differentiation of the cuticular plate and stereocilia in hair cells from the mouse inner ear. *Journal of Comparative Neurology*. [https://doi.org/10.1002/\(SICI\)1096-9861\(19980525\)395:1<18::AID-CNE2>3.0.CO;2-K](https://doi.org/10.1002/(SICI)1096-9861(19980525)395:1<18::AID-CNE2>3.0.CO;2-K)
- Nin, F., Hibino, H., Doi, K., Suzuki, T., Hisa, Y., & Kurachi, Y. (2008). The endocochlear potential depends on two K⁺ diffusion potentials and an electrical barrier in the stria vascularis of the inner ear. *Proceedings of the National Academy of Sciences*, 105(5), 1751–1756. <https://doi.org/10.1073/pnas.0711463105>
- Nishida, Y., Rivolta, M. N., & Holley, M. C. (1998). Timed markers for the differentiation of the cuticular plate and stereocilia in hair cells from the mouse inner ear. *Journal of Comparative Neurology*. [https://doi.org/10.1002/\(SICI\)1096-9861\(19980525\)395:1<18::AID-CNE2>3.0.CO;2-K](https://doi.org/10.1002/(SICI)1096-9861(19980525)395:1<18::AID-CNE2>3.0.CO;2-K)

- Noben-Trauth, K., Zheng, Q. Y., & Johnson, K. R. (2003). Association of cadherin 23 with polygenic inheritance and genetic modification of sensorineural hearing loss. *Nature Genetics*. <https://doi.org/10.1038/ng1226>
- Nodari, A., Previtali, S. C., Dati, G., Occhi, S., Court, F. A., Colombelli, C., Zambroni, D., Dina, G., Del Carro, U., Campbell, K. P., Quattrini, A., Wrabetz, L., & Feltri, M. L. (2008). $\alpha\beta4$ integrin and dystroglycan cooperate to stabilize the myelin sheath. *Journal of Neuroscience*. <https://doi.org/10.1523/JNEUROSCI.0326-08.2008>
- Nouvian, R., Beutner, D., Parsons, T. D., & Moser, T. (2006). Structure and function of the hair cell ribbon synapse. In *Journal of Membrane Biology* (Vol. 209, Issues 2–3, pp. 153–165). <https://doi.org/10.1007/s00232-005-0854-4>
- Nouvian, R., Neef, J., Bulankina, A. V., Reisinger, E., Pangršić, T., Frank, T., Sikorra, S., Brose, N., Binz, T., & Moser, T. (2011). Exocytosis at the hair cell ribbon synapse apparently operates without neuronal SNARE proteins. *Nature Neuroscience*. <https://doi.org/10.1038/nn.2774>
- Oesch, N. W., & Diamond, J. S. (2011). Ribbon synapses compute temporal contrast and encode luminance in retinal rod bipolar cells. *Nature Neuroscience*. <https://doi.org/10.1038/nn.2945>
- Offenhäuser, N., Borgonovo, A., Disanza, A., Romano, P., Ponzanelli, I., Iannolo, G., Di Fiore, P. P., & Scita, G. (2004). The eps8 Family of Proteins Links Growth Factor Stimulation to Actin Reorganization Generating Functional Redundancy in the Ras/Rac Pathway. *Molecular Biology of the Cell*. <https://doi.org/10.1091/mbc.E03-06-0427>
- Offenhäuser, N., Castelletti, D., Mapelli, L., Soppo, B. E., Regondi, M. C., Rossi, P., D'Angelo, E., Frassoni, C., Amadeo, A., Tocchetti, A., Pozzi, B., Disanza, A., Guarnieri, D., Betsholtz, C., Scita, G., Heberlein, U., & Di Fiore, P. P. (2006). Increased Ethanol Resistance and Consumption in Eps8 Knockout Mice Correlates with Altered Actin Dynamics. *Cell*. <https://doi.org/10.1016/j.cell.2006.09.011>
- Oghalai, J. S., Patel, A. A., Nakagawa, T., & Brownell, W. E. (1998). Fluorescence-imaged microdeformation of the outer hair cell lateral wall. *Journal of Neuroscience*. <https://doi.org/10.1523/jneurosci.18-01-00048.1998>
- Ohlemiller, K. K. (2019). Mouse methods and models for studies in hearing. *The Journal of the Acoustical Society of America*. <https://doi.org/10.1121/1.5132550>
- Oliver, D., He, D. Z. Z., Klöcker, N., Ludwig, J., Schulte, U., Waldegger, S., Ruppertsberg, J. P., Dallos, P., & Fakler, B. (2001). Intracellular anions as the voltage sensor of prestin, the outer hair cell motor protein. *Science*. <https://doi.org/10.1126/science.1060939>
- Olson, E. S. (2004). Harmonic distortion in intracochlear pressure and its analysis to explore the cochlear amplifier. *The Journal of the Acoustical Society of America*. <https://doi.org/10.1121/1.1645611>

- Omori, Y., Araki, F., Chaya, T., Kajimura, N., Irie, S., Terada, K., Muranishi, Y., Tsujii, T., Ueno, S., Koyasu, T., Tamaki, Y., Kondo, M., Amano, S., & Furukawa, T. (2012). Presynaptic dystroglycan-pikachurin complex regulates the proper synaptic connection between retinal photoreceptor and bipolar cells. *Journal of Neuroscience*. <https://doi.org/10.1523/JNEUROSCI.0322-12.2012>
- Oppizzi, M. L., Akhavan, A., Singh, M., Fata, J. E., & Muschler, J. L. (2008). Nuclear translocation of β -dystroglycan reveals a distinctive trafficking pattern of autoproteolyzed mucins. *Traffic*. <https://doi.org/10.1111/j.1600-0854.2008.00822.x>
- Orlandi, C., Omori, Y., Wang, Y., Cao, Y., Ueno, A., Roux, M. J., Condomitti, G., de Wit, J., Kanagawa, M., Furukawa, T., & Martemyanov, K. A. (2018). Transsynaptic Binding of Orphan Receptor GPR179 to Dystroglycan-Pikachurin Complex Is Essential for the Synaptic Organization of Photoreceptors. *Cell Reports*, 25(1), 130-145.e5. <https://doi.org/10.1016/j.celrep.2018.08.068>
- Pahlberg, J., Frederiksen, R., Pollock, G. E., Miyagishima, K. J., Sampath, A. P., & Cornwall, M. C. (2017). Voltage-sensitive conductances increase the sensitivity of rod photoresponses following pigment bleaching. *Journal of Physiology*. <https://doi.org/10.1113/JP273398>
- Palmer, A. R., & Russell, I. J. (1986). Phase-locking in the cochlear nerve of the guinea-pig and its relation to the receptor potential of inner hair-cells. *Hearing Research*. [https://doi.org/10.1016/0378-5955\(86\)90002-X](https://doi.org/10.1016/0378-5955(86)90002-X)
- Pang, Z. P., & Südhof, T. C. (2010). Cell biology of Ca²⁺-triggered exocytosis. In *Current Opinion in Cell Biology*. <https://doi.org/10.1016/j.ceb.2010.05.001>
- Pangršič, T., Reisinger, E., & Moser, T. (2012). Otoferlin: A multi-C 2 domain protein essential for hearing. In *Trends in Neurosciences*. <https://doi.org/10.1016/j.tins.2012.08.002>
- Peachey, N. S., Ray, T. A., Florijn, R., Rowe, L. B., Sjoerdsma, T., Contreras-Alcantara, S., Baba, K., Tosini, G., Pozdeyev, N., Iuvone, P. M., Bojang, P., Pearing, J. N., Simonsz, H. J., Van Genderen, M., Birch, D. G., Traboulsi, E. I., Dorfman, A., Lopez, I., Ren, H., ... Gregg, R. G. (2012). GPR179 is required for depolarizing bipolar cell function and is mutated in autosomal-recessive complete congenital stationary night blindness. *American Journal of Human Genetics*. <https://doi.org/10.1016/j.ajhg.2011.12.006>
- Peng, A. W., Belyantseva, I. A., Hsu, P. D., Friedman, T. B., & Heller, S. (2009). Twinfilin 2 regulates actin filament lengths in cochlear stereocilia. *Journal of Neuroscience*. <https://doi.org/10.1523/JNEUROSCI.2782-09.2009>
- Pereboev, A. V., Ahmed, N., Man, N. T., & Morris, G. E. (2001). Epitopes in the interacting regions of β -dystroglycan (PPxY motif) and dystrophin (WW domain). *Biochimica et Biophysica Acta - General Subjects*. [https://doi.org/10.1016/S0304-4165\(01\)00147-7](https://doi.org/10.1016/S0304-4165(01)00147-7)

- Perkins, R. E., & Morest, D. K. (1975). A study of cochlear innervation patterns in cats and rats with the Golgi method and Nomarski optics. *Journal of Comparative Neurology*. <https://doi.org/10.1002/cne.901630202>
- Petit, C., & Richardson, G. P. (2009). Linking genes underlying deafness to hair-bundle development and function. In *Nature Neuroscience*. <https://doi.org/10.1038/nn.2330>
- Petros, T. J., Rebsam, A., & Mason, C. A. (2008). Retinal Axon Growth at the Optic Chiasm: To Cross or Not to Cross. *Annual Review of Neuroscience*. <https://doi.org/10.1146/annurev.neuro.31.060407.125609>
- Picher, M. M., Oprişoreanu, A. M., Jung, S. Y., Michel, K., Schoch, S., & Moser, T. (2017). Rab interacting molecules 2 and 3 directly interact with the pore-forming Cav 1.3 Ca²⁺ channel subunit and promote its membrane expression. *Frontiers in Cellular Neuroscience*. <https://doi.org/10.3389/fncel.2017.00160>
- Pickles, J. O., Comis, S. D., & Osborne, M. P. (1984). Cross-links between stereocilia in the guinea pig organ of Corti, and their possible relation to sensory transduction. *Hearing Research*, 15(2), 103–112. [https://doi.org/10.1016/0378-5955\(84\)90041-8](https://doi.org/10.1016/0378-5955(84)90041-8)
- Pihko, H., Lappi, M., Raitta, C., Sainio, K., Valanne, L., Somer, H., & Santavuori, P. (1995). Ocular findings in muscle-eye-brain (MEB) disease: a follow-up study. *Brain and Development*. [https://doi.org/10.1016/0387-7604\(94\)00101-3](https://doi.org/10.1016/0387-7604(94)00101-3)
- Pillers, D. A. M., Weleber, R. G., Green, D. G., Rash, S. M., Dally, G. Y., Howard, P. L., Powers, M. R., Hood, D. C., Chapman, V. M., Ray, P. N., & Woodward, W. R. (1999). Effects of dystrophin isoforms on signal transduction through neural retina: Genotype-phenotype analysis of Duchenne muscular dystrophy mouse mutants. *Molecular Genetics and Metabolism*. <https://doi.org/10.1006/mgme.1998.2784>
- Platzer, J., Engel, J., Schrott-Fischer, A., Stephan, K., Bova, S., Chen, H., Zheng, H., & Striessnig, J. (2000). Congenital deafness and sinoatrial node dysfunction in mice lacking class D L-type Ca²⁺ channels. *Cell*. [https://doi.org/10.1016/S0092-8674\(00\)00013-1](https://doi.org/10.1016/S0092-8674(00)00013-1)
- Porter, G. A., Dmytrenko, G. M., Winkelmann, J. C., & Bloch, R. J. (1992). Dystrophin colocalizes with β -spectrin in distinct subsarcolemmal domains in mammalian skeletal muscle. *Journal of Cell Biology*. <https://doi.org/10.1083/jcb.117.5.997>
- Postema, M. M., Grega-Larson, N. E., Neining, A. C., & Tyska, M. J. (2018). IRTKS (BAIAP2L1) Elongates Epithelial Microvilli Using EPS8-Dependent and Independent Mechanisms. *Current Biology*, 28(18), 2876-2888.e4. <https://doi.org/10.1016/j.cub.2018.07.022>
- Pujol, R., Lavigne-Rebillard, M., & Lenoir, M. (1998). *Development of Sensory and Neural Structures in the Mammalian Cochlea*. https://doi.org/10.1007/978-1-4612-2186-9_4
- Pykäläinen, A., Boczkowska, M., Zhao, H., Saarikangas, J., Rebowski, G., Jansen, M., Hakanen, J., Koskela, E. V., Peränen, J., Vihinen, H., Jokitalo, E., Salminen, M.,

- Ikonen, E., Dominguez, R., & Lappalainen, P. (2011). Pinkbar is an epithelial-specific BAR domain protein that generates planar membrane structures. *Nature Structural and Molecular Biology*. <https://doi.org/10.1038/nsmb.2079>
- Ramakrishnan, N. A., Drescher, M. J., & Drescher, D. G. (2009). Direct interaction of otoferlin with syntaxin 1A, SNAP-25, and the L-type voltage-gated calcium channel Ca v1.3. *Journal of Biological Chemistry*. <https://doi.org/10.1074/jbc.M803605200>
- Ramarao, M. K., & Cohen, J. B. (1998). Mechanism of nicotinic acetylcholine receptor cluster formation by rapsyn. *Proceedings of the National Academy of Sciences of the United States of America*. <https://doi.org/10.1073/pnas.95.7.4007>
- Raphael, Y., & Altschuler, R. A. (2003). Structure and innervation of the cochlea. In *Brain Research Bulletin*. [https://doi.org/10.1016/S0361-9230\(03\)00047-9](https://doi.org/10.1016/S0361-9230(03)00047-9)
- Rayleigh, Lord. (1907). On our perception of sound direction. *Philosophical Magazine Series 6*, 13(74), 214–232. <https://doi.org/10.1080/14786440709463595>
- Regus-Leidig, H., Fuchs, M., Löhner, M., Leist, S. R., Leal-Ortiz, S., Chiodo, V. A., Hauswirth, W. W., Garner, C. C., & Brandstätter, J. H. (2014). In vivo knockdown of Piccolino disrupts presynaptic ribbon morphology in mouse photoreceptor synapses. *Frontiers in Cellular Neuroscience*. <https://doi.org/10.3389/fncel.2014.00259>
- Regus-Leidig, H., Ott, C., Löhner, M., Atorf, J., Fuchs, M., Sedmak, T., Kremers, J., Fejtová, A., Gundelfinger, E. D., & Brandstätter, J. H. (2013). Identification and Immunocytochemical Characterization of Piccolino, a Novel Piccolo Splice Variant Selectively Expressed at Sensory Ribbon Synapses of the Eye and Ear. *PLoS ONE*. <https://doi.org/10.1371/journal.pone.0070373>
- Reisinger, E., Bresee, C., Neef, J., Nair, R., Reuter, K., Bulankina, A., Nouvian, R., Koch, M., Bückers, J., Kastrup, L., Roux, I., Petit, C., Hell, S. W., Brose, N., Rhee, J. S., Kügler, S., Brigande, J. V., & Moser, T. (2011). Probing the functional equivalence of otoferlin and synaptotagmin 1 in exocytosis. *Journal of Neuroscience*. <https://doi.org/10.1523/JNEUROSCI.5122-10.2011>
- Ren, T., He, W., & Porsov, E. (2011). Localization of the cochlear amplifier in living sensitive ears. *PLoS ONE*. <https://doi.org/10.1371/journal.pone.0020149>
- Rentschler, S., Linn, H., Deininger, K., Bedford, M. T., Espanel, X., & Sudol, M. (1999). The WW domain of dystrophin requires EF-hands region to interact with β -dystroglycan. *Biological Chemistry*. <https://doi.org/10.1515/BC.1999.057>
- Rhode, W., & Geisler, C. (1967). Model of the displacement between opposing points on the tectorial membrane and reticular lamina. *J. Acoust. Soc. Am*, 42, 185–190.
- Ricci, A. J., Crawford, A. C., & Fettiplace, R. (2003). Tonotopic Variation in the Conductance of the Hair Cell Mechanotransducer Channel. *Neuron*. [https://doi.org/10.1016/S0896-6273\(03\)00721-9](https://doi.org/10.1016/S0896-6273(03)00721-9)

- Ricci, A. J., & Fettiplace, R. (1998). Calcium permeation of the turtle hair cell mechanotransducer channel and its relation to the composition of endolymph. *Journal of Physiology*. <https://doi.org/10.1111/j.1469-7793.1998.159bx.x>
- Ricci, A. J., Wu, Y. C., & Fettiplace, R. (1998). The endogenous calcium buffer and the time course of transducer adaptation in auditory hair cells. *Journal of Neuroscience*. <https://doi.org/10.1523/jneurosci.18-20-08261.1998>
- Richardson, G. P., Lukashkin, A. N., & Russell, I. J. (2008). The tectorial membrane: One slice of a complex cochlear sandwich. In *Current Opinion in Otolaryngology and Head and Neck Surgery*. <https://doi.org/10.1097/MOO.0b013e32830e20c4>
- Riemersma, M., Mandel, H., Van Beusekom, E., Gazzoli, I., Roscioli, T., Eran, A., Gershoni-Baruch, R., Gershoni, M., Pietrokovski, S., Vissers, L. E., Lefeber, D. J., Willemsen, M. A., Wevers, R. A., & Van Bokhoven, H. (2015). Absence of α - and β -dystroglycan is associated with Walker-Warburg syndrome. *Neurology*. <https://doi.org/10.1212/WNL.0000000000001615>
- Rivolta, M. N., & Holley, M. C. (2002). Cell lines in inner ear research. In *Journal of Neurobiology*. <https://doi.org/10.1002/neu.10111>
- Roux, I., Safieddine, S., Nouvian, R., Grati, M., Simmler, M. C., Bahloul, A., Perfettini, I., Le Gall, M., Rostaing, P., Hamard, G., Triller, A., Avan, P., Moser, T., & Petit, C. (2006). Otoferlin, Defective in a Human Deafness Form, Is Essential for Exocytosis at the Auditory Ribbon Synapse. *Cell*. <https://doi.org/10.1016/j.cell.2006.08.040>
- Roux, I., Wersinger, E., McIntosh, J. M., Fuchs, P. A., & Glowatzki, E. (2011). Onset of cholinergic efferent synaptic function in sensory hair cells of the rat cochlea. *Journal of Neuroscience*. <https://doi.org/10.1523/JNEUROSCI.2743-11.2011>
- Rueda, J., De La Sen, C., Juiz, J. M., & Merchan, J. A. (1987). Neuronal loss in the spiral ganglion of Young rats. *Acta Oto-Laryngologica*. <https://doi.org/10.3109/00016488709128269>
- Russo, K., Di Stasio, E., Macchia, G., Rosa, G., Brancaccio, A., & Corinna Petrucci, T. (2000). Characterization of the β -dystroglycan-growth factor receptor 2 (Grb2) interaction. *Biochemical and Biophysical Research Communications*. <https://doi.org/10.1006/bbrc.2000.3103>
- Rutherford, M. A., & Moser, T. (2016). *The Ribbon Synapse Between Type I Spiral Ganglion Neurons and Inner Hair Cells*. https://doi.org/10.1007/978-1-4939-3031-9_5
- Saadoun, S., Papadopoulos, M. C., & Krishna, S. (2003). Water transport becomes uncoupled from K⁺ siphoning in brain contusion, bacterial meningitis, and brain tumours: immunohistochemical case review. *J Clin Pathol*, 56(12), 972–975. <https://doi.org/10.1136/jcp.56.12.972>

- Saarikangas, J., Hakanen, J., Mattila, P. K., Grumet, M., Salminen, M., & Lappalainen, P. (2008). ABBA regulates plasma-membrane and actin dynamics to promote radial glia extension. *Journal of Cell Science*. <https://doi.org/10.1242/jcs.027466>
- Sadanaga, M., & Morimitsu, T. (1995). Development of endocochlear potential and its negative component in mouse cochlea. *Hearing Research*. [https://doi.org/10.1016/0378-5955\(95\)00133-X](https://doi.org/10.1016/0378-5955(95)00133-X)
- Safari, F., & Suetsugu, S. (2012). The BAR domain superfamily proteins from subcellular structures to human diseases. In *Membranes*. <https://doi.org/10.3390/membranes2010091>
- Safieddine, S., & Wenthold, R. J. (1999). SNARE complex at the ribbon synapses of cochlear hair cells: Analysis of synaptic vesicle- and synaptic membrane-associated proteins. *European Journal of Neuroscience*. <https://doi.org/10.1046/j.1460-9568.1999.00487.x>
- Saito, F., Masaki, T., Kamakura, K., Anderson, L. V. B., Fujita, S., Fukuta-Ohi, H., Sunada, Y., Shimizu, T., & Matsumura, K. (1999). Characterization of the transmembrane molecular architecture of the dystroglycan complex in Schwann cells. *Journal of Biological Chemistry*. <https://doi.org/10.1074/jbc.274.12.8240>
- Saito, F., Saito-Arai, Y., Nakamura, A., Shimizu, T., & Matsumura, K. (2008). Processing and secretion of the N-terminal domain of α -dystroglycan in cell culture media. *FEBS Letters*. <https://doi.org/10.1016/j.febslet.2008.01.006>
- Salt, A. N., Melichar, I., & Thalmann, R. (1987). Mechanisms of Endocochlear Potential Generation by Stria Vascularis. *The Laryngoscope*, 97, 984–991. <https://doi.org/10.1121/1.2024413>
- Santarelli, R., del Castillo, I., Cama, E., Scimemi, P., & Starr, A. (2015). Audibility, speech perception and processing of temporal cues in ribbon synaptic disorders due to OTOF mutations. In *Hearing Research*. <https://doi.org/10.1016/j.heares.2015.07.007>
- Sato, S., Omori, Y., Katoh, K., Kondo, M., Kanagawa, M., Miyata, K., Funabiki, K., Koyasu, T., Kajimura, N., Miyoshi, T., Sawai, H., Kobayashi, K., Tani, A., Toda, T., Usukura, J., Tano, Y., Fujikado, T., & Furukawa, T. (2008). Pikachurin, a dystroglycan ligand, is essential for photoreceptor ribbon synapse formation. *Nature Neuroscience*. <https://doi.org/10.1038/nn.2160>
- Schindelin, J., Arganda-Carreras, I., Frise, E., Kaynig, V., Longair, M., Pietzsch, T., Preibisch, S., Rueden, C., Saalfeld, S., Schmid, B., Tinevez, J. Y., White, D. J., Hartenstein, V., Eliceiri, K., Tomancak, P., & Cardona, A. (2012). Fiji: An open-source platform for biological-image analysis. In *Nature Methods*. <https://doi.org/10.1038/nmeth.2019>
- Schmitz, F., Königstorfer, A., & Südhof, T. C. (2000). RIBEYE, a component of synaptic ribbons: A protein's journey through evolution provides insight into synaptic ribbon function. *Neuron*. [https://doi.org/10.1016/S0896-6273\(00\)00159-8](https://doi.org/10.1016/S0896-6273(00)00159-8)

- Schnee, M. E., Lawton, D. M., Furness, D. N., Benke, T. A., & Ricci, A. J. (2005). Auditory hair cell-afferent fiber synapses are specialized to operate at their best frequencies. *Neuron*. <https://doi.org/10.1016/j.neuron.2005.06.004>
- Schnee, M. E., & Ricci, A. J. (2003). Biophysical and pharmacological characterization of voltage-gated calcium currents in turtle auditory hair cells. In *Journal of Physiology*. <https://doi.org/10.1113/jphysiol.2002.037481>
- Schnee, M. E., Santos-Sacchi, J., Castellano-Muñoz, M., Kong, J. H., & Ricci, A. J. (2011). Calcium-Dependent Synaptic Vesicle Trafficking Underlies Indefatigable Release at the Hair Cell Afferent Fiber Synapse. *Neuron*, *70*(2), 326–338. <https://doi.org/10.1016/j.neuron.2011.01.031>
- Schneeweis, D. M., & Schnapf, J. L. (1995). Photovoltage of rods and cones in the macaque retina. *Science*. <https://doi.org/10.1126/science.7754386>
- Schwander, M., Kachar, B., & Müller, U. (2010). The cell biology of hearing. In *Journal of Cell Biology*. <https://doi.org/10.1083/jcb.201001138>
- Sciandra, F., Bozzi, M., Bigotti, M., & Brancaccio, A. (2013). The Multiple Affinities of Dystroglycan. *Current Protein & Peptide Science*. <https://doi.org/10.2174/1389203711209070644>
- Sciandra, F., Schneider, M., Giardina, B., Baumgartner, S., Petrucci, T. C., & Brancaccio, A. (2001). Identification of the β -dystroglycan binding epitope within the C-terminal region of α -dystroglycan. *European Journal of Biochemistry*. <https://doi.org/10.1046/j.1432-1327.2001.02386.x>
- Scita, G., Nordstrom, J., Carbone, R., Tenca, P., Giardina, G., Gutkind, S., Bjarnegård, M., Betsholtz, C., & Di Fiore, P. P. (1999). EPS8 and E3B1 transduce signals from Ras to Rac. *Nature*, *401*(6750), 290–293. <https://doi.org/10.1038/45822>
- Sekerková, G., Richter, C. P., & Bartles, J. R. (2011). Roles of the espin actin-bundling proteins in the morphogenesis and stabilization of hair cell stereocilia revealed in CBA/CaJ congenic jerker mice. *PLoS Genetics*. <https://doi.org/10.1371/journal.pgen.1002032>
- Shapira, M., Zhai, R. G., Dresbach, T., Bresler, T., Torres, V. I., Gundelfinger, E. D., Ziv, N. E., & Garner, C. C. (2003). Unitary assembly of presynaptic active zones from Piccolo-Bassoon transport vesicles. *Neuron*. [https://doi.org/10.1016/S0896-6273\(03\)00207-1](https://doi.org/10.1016/S0896-6273(03)00207-1)
- Sheets, L., Kindt, K. S., & Nicolson, T. (2012). Presynaptic cav1.3 channels regulate synaptic ribbon size and are required for synaptic maintenance in sensory hair cells. *Journal of Neuroscience*. <https://doi.org/10.1523/JNEUROSCI.3005-12.2012>
- Sheets, L., Trapani, J. G., Mo, W., Obholzer, N., & Nicolson, T. (2011). Ribeye is required for presynaptic CaV1.3a channel localization and afferent innervation of sensory hair cells. *Development*. <https://doi.org/10.1242/dev.059451>

- Sheikh, M. O., Halmo, S. M., & Wells, L. (2017). Recent advancements in understanding mammalian O-mannosylation. *Glycobiology*. <https://doi.org/10.1093/glycob/cwx062>
- Shotwell, S. L., Jacobs, R., & Hudspeth, A. J. (1981). Directional sensitivity of individual vertebrate hair cells to controlled deflection of their hair bundles. *Annals of the New York Academy of Sciences*. <https://doi.org/10.1111/j.1749-6632.1981.tb30854.x>
- Signorino, G., Covaceuszach, S., Bozzi, M., Hubner, W., Monkemoller, V., Konarev, P. V., Cassetta, A., Barnaccio, A., & Sciandra, F. (2017). A Dystroglycan Mutation (p.Cys667Phe) Associated to Muscle-Eye-Brain Disease with Multicystic Leucodystrophy Results in ER-Retention of the Mutant Protein. *Human Mutation, Epub*, 1–15.
- Simmons, D. D. (1994). A transient afferent innervation of outer hair cells in the postnatal cochlea. *NeuroReport*. <https://doi.org/10.1097/00001756-199406270-00003>
- Simmons, D. D., Mansdorf, N. B., & Kim, J. H. (1996). Olivocochlear innervation of inner and outer hair cells during postnatal maturation: Evidence for a waiting period. *Journal of Comparative Neurology*. [https://doi.org/10.1002/\(SICI\)1096-9861\(19960708\)370:4<551::AID-CNE10>3.0.CO;2-M](https://doi.org/10.1002/(SICI)1096-9861(19960708)370:4<551::AID-CNE10>3.0.CO;2-M)
- Simmons, P. J., & De Ruyter Van Steveninck, R. (2005). Reliability of signal transfer at a tonically transmitting, graded potential synapse of the locust ocellar pathway. *Journal of Neuroscience*. <https://doi.org/10.1523/JNEUROSCI.1119-05.2005>
- Singer, J. H. (2007). Multivesicular release and saturation of glutamatergic signalling at retinal ribbon synapses. In *Journal of Physiology*. <https://doi.org/10.1113/jphysiol.2006.125302>
- Singh, J., Itahana, Y., Knight-Krajewski, S., Kanagawa, M., Campbell, K. P., Bissell, M. J., & Muschler, J. (2004). Proteolytic enzymes and altered glycosylation modulate dystroglycan function in carcinoma cells. *Cancer Research*. <https://doi.org/10.1158/0008-5472.CAN-04-1638>
- Smalheiser, N. R., & Schwartz, N. B. (1987). Cranin: a laminin-binding protein of cell membranes. *Proceedings of the National Academy of Sciences of the United States of America*. <https://doi.org/10.1073/pnas.84.18.6457>
- Smith, C. A., & Sjöstrand, F. S. (1961). Structure of the nerve endings on the external hair cells of the guinea pig cochlea as studied by serial sections. *Journal of Ultrastructure Research*, 5(6), 523–556. [https://doi.org/10.1016/S0022-5320\(61\)80025-7](https://doi.org/10.1016/S0022-5320(61)80025-7)
- Sobkowicz, H. M., Rose, J. E., Scott, G. L., & Levenick, C. V. (1986). Distribution of synaptic ribbons in the developing organ of Corti. *Journal of Neurocytology*. <https://doi.org/10.1007/BF01625188>
- Sobkowicz, H. M., Rose, J. E., Scott, G. E., & Slapnick, S. M. (1982). Ribbon synapses in the developing intact and cultured organ of Corti in the mouse. *The Journal of Neuroscience : The Official Journal of the Society for Neuroscience*, 2(7), 942–957. <http://www.ncbi.nlm.nih.gov/pubmed/7097321>

- Song, L., McGee, J., & Walsh, E. J. (2006). Frequency- and level-dependent changes in auditory brainstem responses (ABRs) in developing mice. *The Journal of the Acoustical Society of America*. <https://doi.org/10.1121/1.2180533>
- Sotgia, F., Bonuccelli, G., Bedford, M., Brancaccio, A., Mayer, U., Wilson, M. T., Campos-Gonzalez, R., Brooks, J. W., Sudol, M., & Lisanti, M. P. (2003). Localization of phospho- β -dystroglycan (pY892) to an intracellular vesicular compartment in cultured cells and skeletal muscle fibers in vivo. *Biochemistry*, 42(23), 7110–7123. <https://doi.org/10.1021/bi0271289>
- Spassova, M. A., Avissar, M., Furman, A. C., Crumling, M. A., Saunders, J. C., & Parsons, T. D. (2004). Evidence that rapid vesicle replenishment of the synaptic ribbon mediates recovery from short-term adaptation at the hair cell afferent synapse. *JARO - Journal of the Association for Research in Otolaryngology*. <https://doi.org/10.1007/s10162-004-5003-8>
- Spence, H. J., Dhillon, A. S., James, M., & Winder, S. J. (2004). Dystroglycan, a scaffold for the ERK-MAP kinase cascade. *EMBO Reports*. <https://doi.org/10.1038/sj.embor.7400140>
- Spiwoeks-Becker, I., Glas, M., Lasarzik, I., & Vollrath, L. (2004). Mouse photoreceptor synaptic ribbons lose and regain material in response to illumination changes. *European Journal of Neuroscience*. <https://doi.org/10.1111/j.1460-9568.2004.03198.x>
- Spoendlin, H. (1975). Neuroanatomical basis of cochlear coding mechanisms. *International Journal of Audiology*. <https://doi.org/10.3109/00206097509071752>
- Steel, K. P. (2014). What's the Use of Genetics? https://doi.org/10.1007/978-1-4614-9102-6_30
- Strenzke, N., Chakrabarti, R., Al-Moyed, H., Müller, A., Hoch, G., Pangrsic, T., Yamanbaeva, G., Lenz, C., Pan, K., Auge, E., Geiss-Friedlander, R., Urlaub, H., Brose, N., Wichmann, C., & Reisinger, E. (2016). Hair cell synaptic dysfunction, auditory fatigue and thermal sensitivity in otoferlin Ile515Thr mutants. *The EMBO Journal*. <https://doi.org/10.15252/emj.201694564>
- Sudhaharan, T., Sem, K. P., Liew, H. F., Yu, Y. H., Goh, W. I., Chou, A. M., & Ahmed, S. (2016). The rho GTPase rif signals through IRTKS, EPS8 and WAVE2 to generate dorsal membrane ruffles and filopodia. *Journal of Cell Science*. <https://doi.org/10.1242/jcs.179655>
- Südhof, T. C. (2002). Synaptotagmins: Why so many? In *Journal of Biological Chemistry*. <https://doi.org/10.1074/jbc.R100052200>
- Sudo, A., Kanagawa, M., Kondo, M., Ito, C., Kobayashi, K., Endo, M., Minami, Y., Aiba, A., & Toda, T. (2018). Temporal requirement of dystroglycan glycosylation during brain development and rescue of severe cortical dysplasia via gene delivery in the fetal stage. *Human Molecular Genetics*. <https://doi.org/10.1093/hmg/ddy032>

- Sudol, M. (1996). Structure and function of the WW domain. In *Progress in Biophysics and Molecular Biology*. [https://doi.org/10.1016/S0079-6107\(96\)00008-9](https://doi.org/10.1016/S0079-6107(96)00008-9)
- Suetsugu, S., Kurisu, S., Oikawa, T., Yamazaki, D., Oda, A., & Takenawa, T. (2006). Optimization of WAVE2 complex-induced actin polymerization by membrane-bound IRSp53, PIP3, and Rac. *Journal of Cell Biology*. <https://doi.org/10.1083/jcb.200509067>
- Sugiyama, J., Bowen, D. C., & Hall, Z. W. (1994). Dystroglycan binds nerve and muscle agrin. *Neuron*, 13(1), 103–115. [https://doi.org/10.1016/0896-6273\(94\)90462-6](https://doi.org/10.1016/0896-6273(94)90462-6)
- Sugiyama, J. E., Glass, D. J., Yancopoulos, G. D., & Hall, Z. W. (1997). Laminin-induced acetylcholine receptor clustering: An alternative pathway. *Journal of Cell Biology*. <https://doi.org/10.1083/jcb.139.1.181>
- Tadenev, A. L. D., Akturk, A., Devanney, N., Mathur, P. D., Clark, A. M., Yang, J., & Tarchini, B. (2019). GPSM2-GNAI Specifies the Tallest Stereocilia and Defines Hair Bundle Row Identity. *Current Biology*. <https://doi.org/10.1016/j.cub.2019.01.051>
- Tarchini, B., Jolicoeur, C., & Cayouette, M. (2013). A Molecular Blueprint at the Apical Surface Establishes Planar Asymmetry in Cochlear Hair Cells. *Developmental Cell*. <https://doi.org/10.1016/j.devcel.2013.09.011>
- Tarchini, B., Tadenev, A. L. D., Devanney, N., & Cayouette, M. (2016). A link between planar polarity and staircase-like bundle architecture in hair cells. *Development*. <https://doi.org/10.1242/dev.139089>
- Tasaki, I., Davis, H., & Eldkedge, D. H. (1954). Exploration of Cochlear Potentials in Guinea Pig with a Microelectrode. *Journal of the Acoustical Society of America*. <https://doi.org/10.1121/1.1907415>
- Thompson, O., Moore, C. J., Hussain, S. A., Kleino, I., Peckham, M., Hohenester, E., Ayscough, K. R., Saksela, K., & Winder, S. J. (2010). Modulation of cell spreading and cell-substrate adhesion dynamics by dystroglycan. *Journal of Cell Science*. <https://doi.org/10.1242/jcs.047902>
- Thompson, O., Kleino, I., Crimaldi, L., Gimona, M., Saksela, K., & Winder, S. J. (2008). Dystroglycan, Tks5 and Src mediated assembly of podosomes in myoblasts. *PLoS ONE*, 3(11). <https://doi.org/10.1371/journal.pone.0003638>
- Thoreson, W. B. (2007). Kinetics of synaptic transmission at ribbon synapses of rods and cones. In *Molecular Neurobiology*. <https://doi.org/10.1007/s12035-007-0019-9>
- Tilney, L. G., Tilney, M. S., & DeRosier, D. J. (1992). Actin filaments, stereocilia, and hair cells: How cells count and measure. In *Annual Review of Cell Biology*. <https://doi.org/10.1146/annurev.cb.08.110192.001353>
- Tinsley, J. M., Blake, D. J., Roche, A., Fairbrother, U., Riss, J., Byth, B. C., Knight, A. E., Kendrick-Jones, J., Suthers, G. K., Love, D. R., Edwards, Y. H., & Davies, K. E.

- (1992). Primary structure of dystrophin-related protein. *Nature*.
<https://doi.org/10.1038/360591a0>
- Tocchetti, A., Soppo, C. B. E., Zani, F., Bianchi, F., Gagliani, M. C., Pozzi, B., Rozman, J., Elvert, R., Ehrhardt, N., Rathkolb, B., Moerth, C., Horsch, M., Fuchs, H., Gailus-Durner, V., Beckers, J., Klingenspor, M., Wolf, E., De Angelis, M. H., Scanziani, E., ... Offenhäuser, N. (2010). Loss of the actin remodeler Eps8 causes intestinal defects and improved metabolic status in mice. *PLoS ONE*.
<https://doi.org/10.1371/journal.pone.0009468>
- Toda, T., Kobayashi, K., Kondo-Iida, E., Sasaki, J., & Nakamura, Y. (2000). The Fukuyama congenital muscular dystrophy story. In *Neuromuscular Disorders*.
[https://doi.org/10.1016/S0960-8966\(99\)00109-1](https://doi.org/10.1016/S0960-8966(99)00109-1)
- Van Putten, M., Kumar, D., Hulsker, M., Hoogaars, W. M. H., Plomp, J. J., van Opstal, A., van Ierson, M., Admiraal, P., van Ommen, G. J. B., 't Hoen, P. A. C., & Aartsma-Rus, A. (2012). Comparison of skeletal muscle pathology and motor function of dystrophin and utrophin deficient mouse strains. *Neuromuscular Disorders*.
<https://doi.org/10.1016/j.nmd.2011.10.011>
- Van Reeuwijk, J., Janssen, M., Van Den Elzen, C., Beltran-Valero De Bernabé, D., Sabatelli, P., Merlini, L., Boon, M., Scheffer, H., Brockington, M., Muntoni, F., Huynen, M. A., Verrips, A., Walsh, C. A., Barth, P. G., Brunner, H. G., & Van Bokhoven, H. (2005). POMT2 mutations cause α -dystroglycan hypoglycosylation and Walker-Warburg syndrome. *Journal of Medical Genetics*.
<https://doi.org/10.1136/jmg.2005.031963>
- Verpy, E., Leibovici, M., Michalski, N., Goodyear, R. J., Houdon, C., Weil, D., Richardson, G. P., & Petit, C. (2011). Stereocilin connects outer hair cell stereocilia to one another and to the tectorial membrane. *Journal of Comparative Neurology*.
<https://doi.org/10.1002/cne.22509>
- Vierstra, J., Rynes, E., Sandstrom, R., Zhang, M., Canfield, T., Scott Hansen, R., Stehling-Sun, S., Sabo, P. J., Byron, R., Humbert, R., Thurman, R. E., Johnson, A. K., Vong, S., Lee, K., Bates, D., Neri, F., Diegel, M., Giste, E., Haugen, E., ... Stamatoyannopoulos, J. A. (2014). Mouse regulatory DNA landscapes reveal global principles of cis-regulatory evolution. *Science*.
<https://doi.org/10.1126/science.1246426>
- Vogl, C., Cooper, B. H., Neef, J., Wojcik, S. M., Reim, K., Reisinger, E., Brose, N., Rhee, J. S., Moser, T., & Wichmann, C. (2015). Unconventional molecular regulation of synaptic vesicle replenishment in cochlear inner hair cells. *Journal of Cell Science*.
<https://doi.org/10.1242/jcs.162099>
- Vollrath, M. A., & Eatock, R. A. (2003). Time course and extent of mechanotransducer adaptation in mouse utricular hair cells: Comparison with frog saccular hair cells. *Journal of Neurophysiology*. <https://doi.org/10.1152/jn.00893.2002>

- Von Békésy G (1960). Experiments in hearing. Acoustical Society of America through the American Institute of Physics by arrangement with McGraw-Hill Book Co, New York.
- Von Gersdorff, H., Vardi, E., Matthews, G., & Sterling, P. (1996). Evidence that vesicles on the synaptic ribbon of retinal bipolar neurons can be rapidly released. *Neuron*. [https://doi.org/10.1016/S0896-6273\(00\)80148-8](https://doi.org/10.1016/S0896-6273(00)80148-8)
- Vreugde, S., Erven, A., Kros, C. J., Marcotti, W., Fuchs, H., Kurima, K., Wilcox, E. R., Friedman, T. B., Griffith, A. J., Bailing, R., Hrabé de Angelis, M., Avraham, K. B., & Steel, K. P. (2002). Beethoven, a mouse model for dominant, progressive hearing loss DFNA36. *Nature Genetics*. <https://doi.org/10.1038/ng848>
- Wangemann, P. (2006). Supporting sensory transduction: Cochlear fluid homeostasis and the endocochlear potential. In *Journal of Physiology*. <https://doi.org/10.1113/jphysiol.2006.112888>
- Warr, W. B., & Guinan, J. J. (1979). Efferent innervation of the organ of corti: two separate systems. *Brain Research*. [https://doi.org/10.1016/0006-8993\(79\)91104-1](https://doi.org/10.1016/0006-8993(79)91104-1)
- Way, M., Pope, B., Cross, R. A., Kendrick-Jones, J., & Weeds, A. G. (1992). Expression of the N-terminal domain of dystrophin in E. coli and demonstration of binding to F-actin. *FEBS Letters*. [https://doi.org/10.1016/0014-5793\(92\)80249-G](https://doi.org/10.1016/0014-5793(92)80249-G)
- Wen, B., Wang, G. I., Dean, I., & Delgutte, B. (2012). Time course of dynamic range adaptation in the auditory nerve. *Journal of Neurophysiology*. <https://doi.org/10.1152/jn.00055.2012>
- Williamson, R. A., Henry, M. D., Daniels, K. J., Hrstka, R. F., Lee, J. C., Sunada, Y., Ibraghimov-Beskrovnaya, O., & Campbell, K. P. (1997). Dystroglycan is essential for early embryonic development: Disruption of Reichert's membrane in DAG1-null mice. *Human Molecular Genetics*, 6(6), 831–841. <https://doi.org/10.1093/hmg/6.6.831>
- Winder, S. J. (2001). The complexities of dystroglycan. *Trends in Biochemical Sciences*, 26(2), 118–124. [https://doi.org/10.1016/S0968-0004\(00\)01731-X](https://doi.org/10.1016/S0968-0004(00)01731-X)
- Wong, A. B., Rutherford, M. A., Gabrielaitis, M., Pangršič, T., Göttfert, F., Frank, T., Michanski, S., Hell, S., Wolf, F., Wichmann, C., & Moser, T. (2014). Developmental refinement of hair cell synapses tightens the coupling of Ca²⁺ influx to exocytosis. *EMBO Journal*. <https://doi.org/10.1002/embj.201387110>
- Wright, A. (1984). Dimensions of the cochlear stereocilia in man and the guinea pig. *Hearing Research*. [https://doi.org/10.1016/0378-5955\(84\)90099-6](https://doi.org/10.1016/0378-5955(84)90099-6)
- Wright, K. M., Lyon, K. A., Leung, H., Leahy, D. J., Ma, L., & Ginty, D. D. (2012). Dystroglycan Organizes Axon Guidance Cue Localization and Axonal Pathfinding. *Neuron*. <https://doi.org/10.1016/j.neuron.2012.10.009>

- Wu, Y. J., Krüttgen, A., Möller, J. C., Shine, D., Chan, J. R., Shooter, E. M., & Cosgaya, J. M. (2004). Nerve Growth Factor, Brain-Derived Neurotrophic Factor, and Neurotrophin-3 Are Sorted to Dense-Core Vesicles and Released Via the Regulated Pathway in Primary Rat Cortical Neurons. *Journal of Neuroscience Research*. <https://doi.org/10.1002/jnr.20048>
- Wu, Y. C., Ricci, A. J., & Fettiplace, R. (1999). Two components of transducer adaptation in auditory hair cells. *Journal of Neurophysiology*. <https://doi.org/10.1152/jn.1999.82.5.2171>
- Xin, H., Poy, F., Zhang, R., Joachimiak, A., Sudol, M., & Eck, M. J. (2000). Structure of a WW domain containing fragment of dystrophin in complex with B-dystroglycan. *Nature Structural Biology*, 7(8), 634–638. <https://doi.org/10.1038/77923>
- Xu, R., & Salpeter, M. M. (1997). Acetylcholine receptors in innervated muscles of dystrophic mdx mice degrade as after denervation. *Journal of Neuroscience*. <https://doi.org/10.1523/jneurosci.17-21-08194.1997>
- Yamamoto, T., Kato, Y., Kawaguchi-Niida, M., Shibata, N., Osawa, M., Saito, K., Kröger, S., & Kobayashi, M. (2008). Characteristics of neurons and glia in the brain of Fukuyama type congenital muscular dystrophy. *Acta Myologica*.
- Yamamoto, T., Toyoda, C., Kobayashi, M., Kondo, E., Saito, K., & Osawa, M. (1997). Pial-glial barrier abnormalities in fetuses with Fukuyama congenital muscular dystrophy. *Brain and Development*. [https://doi.org/10.1016/S0387-7604\(96\)00056-3](https://doi.org/10.1016/S0387-7604(96)00056-3)
- Yasunaga, S., Grati, M., Cohen-Salmon, M., El-Amraoui, A., Mustapha, M., Salem, N., El-Zir, E., Loiselet, J., & Petit, C. (1999). A mutation in OTOF, encoding otoferlin, a FER-1-like protein, causes DFNB9, a nonsyndromic form of deafness. *Nature Genetics*. <https://doi.org/10.1038/7693>
- Yoshida-Moriguchi, T., Yu, L., Stalnaker, S., Sarah Davis, S. H., Kunz, S., Madson, M., Oldstone, M. B. A., Schachter, H., Wells, L., & Campbell, K. P. (2010). O-Mannosyl phosphorylation of alpha-dystroglycan is required for laminin binding. *Science*. <https://doi.org/10.1126/science.1180512>
- Zaccaria, M. L., De Stefano, M. E., Gotti, C., Petrucci, T. C., & Paggi, P. (2000). Selective reduction in the nicotinic acetylcholine receptor and dystroglycan at the postsynaptic apparatus of mdx mouse superior cervical ganglion. *Journal of Neuropathology and Experimental Neurology*. <https://doi.org/10.1093/jnen/59.2.103>
- Zaccaria, M. L., Di Tommaso, F., Brancaccio, A., Paggi, P., & Petrucci, T. C. (2001). Dystroglycan distribution in adult mouse brain: A light and electron microscopy study. *Neuroscience*, 104(2), 311–324. [https://doi.org/10.1016/S0306-4522\(01\)00092-6](https://doi.org/10.1016/S0306-4522(01)00092-6)
- Zampighi, G. A., Schietroma, C., Zampighi, L. M., Woodruff, M., Wright, E. M., & Brecha, N. C. (2011). Conical tomography of a ribbon synapse: Structural evidence for vesicle fusion. *PLoS ONE*. <https://doi.org/10.1371/journal.pone.0016944>

- Zampini, V., Johnson, S. L., Franz, C., Knipper, M., Holley, M. C., Magistretti, J., Russo, G., Marcotti, W., & Masetto, S. (2014). Fine tuning of CaV1.3 Ca²⁺ channel properties in adult inner hair cells positioned in the most sensitive region of the gerbil cochlea. *PLoS ONE*. <https://doi.org/10.1371/journal.pone.0113750>
- Zampini, V., Johnson, S. L., Franz, C., Lawrence, N. D., Münkner, S., Engel, J., Knipper, M., Magistretti, J., Masetto, S., & Marcotti, W. (2010). Elementary properties of CaV1.3 Ca²⁺ channels expressed in mouse cochlear inner hair cells. *Journal of Physiology*. <https://doi.org/10.1113/jphysiol.2009.181917>
- Zampini, V., Ruttiger, L., Johnson, S. L., Franz, C., Furness, D. N., Waldhaus, J., Xiong, H., Hackney, C. M., Holley, M. C., Offenhauser, N., Fiore, P. P., Knipper, M., Masetto, S., & Marcotti, W. (2011). Eps8 regulates hair bundle length and functional maturation of mammalian auditory hair cells. *PLoS Biology*, 9(4). <https://doi.org/10.1371/journal.pbio.1001048>
- Zhai, R. G., Vardinon-Friedman, H., Cases-Langhoff, C., Becker, B., Gundelfinger, E. D., Ziv, N. E., & Garner, C. C. (2001). Assembling the presynaptic active zone: A characterization of an active zone precursor vesicle. *Neuron*. [https://doi.org/10.1016/S0896-6273\(01\)00185-4](https://doi.org/10.1016/S0896-6273(01)00185-4)
- Zhang, B., Luo, S., Wang, Q., Suzuki, T., Xiong, W. C., & Mei, L. (2008). LRP4 Serves as a Coreceptor of Agrin. *Neuron*. <https://doi.org/10.1016/j.neuron.2008.10.006>
- Zhao, B., Wu, Z., Grillet, N., Yan, L., Xiong, W., Harkins-Perry, S., & Müller, U. (2014). TMIE is an essential component of the mechanotransduction machinery of cochlear hair cells. *Neuron*. <https://doi.org/10.1016/j.neuron.2014.10.041>
- Zhao, H., Pykäläinen, A., & Lappalainen, P. (2011). I-BAR domain proteins: Linking actin and plasma membrane dynamics. In *Current Opinion in Cell Biology*. <https://doi.org/10.1016/j.ceb.2010.10.005>
- Zhao, K., Shen, C., Li, L., Wu, H., Xing, G., Dong, Z., Jing, H., Chen, W., Zhang, H., Tan, Z., Pan, J., Xiong, L., Wang, H., Cui, W., Sun, X. D., Li, S., Huang, X., Xiong, W. C., & Mei, L. (2018). Sarcoglycan alpha mitigates neuromuscular junction decline in aged mice by stabilizing LRP4. *Journal of Neuroscience*. <https://doi.org/10.1523/JNEUROSCI.0860-18.2018>
- Zhao, Y. D., Yamoah, E. N., & Gillespie, P. G. (1996). Regeneration of broken tip links and restoration of mechanical transduction in hair cells. *Proceedings of the National Academy of Sciences of the United States of America*. <https://doi.org/10.1073/pnas.93.26.15469>
- Zheng, J., Miller, K. K., Yang, T., Hildebrand, M. S., Shearer, A. E., DeLuca, A. P., Scheetz, T. E., Drummond, J., Scherer, S. E., Legan, P. K., Goodyear, R. J., Richardson, G. P., Cheatham, M. A., Smith, R. J., & Dallos, P. (2011). Carcinoembryonic antigen-related cell adhesion molecule 16 interacts with α -tectorin and is mutated in autosomal dominant hearing loss (DFNA4). *Proceedings of the National Academy of Sciences of the United States of America*. <https://doi.org/10.1073/pnas.1005842108>

Zheng, J., Shen, W., He, D. Z. Z., Long, K. B., Madison, L. D., & Dallos, P. (2000a). Prestin is the motor protein of cochlear outer hair cells. In *Nature*.
<https://doi.org/10.1038/35012009>

Zheng, L., Sekerková, G., Vranich, K., Tilney, L. G., Mugnaini, E., & Bartles, J. R. (2000b). The deaf jerker mouse has a mutation in the gene encoding the espin actin-bundling proteins of hair cell stereocilia and lacks espins. *Cell*.
[https://doi.org/10.1016/S0092-8674\(00\)00042-8](https://doi.org/10.1016/S0092-8674(00)00042-8)

Appendix 2.1 – Antibodies Used

Primary

<u>ID</u>	<u>Host/Isotype</u>	<u>Dilution</u>	<u>Supplier</u>
Anti-Alpha Dystroglycan (IIH6)	Mouse IgM	1:100 (IF)	Santa Cruz Biotechnology (sc-53987)
Anti-BAIAP2L2	Rabbit Polyclonal	1:50 (IF)	Atlas Antibodies (HPA003043)
Anti-Beta Dystroglycan (Mandag2)	Mouse IgG1	1:20 (WB + IF)	Pereboev <i>et al.</i> 2001
Anti-pY890 Beta Dystroglycan (1709)	Rabbit Polyclonal	1:500 (WB) 1:100 (IF)	Ilsley <i>et al.</i> 2001
Anti-BK	Mouse IgG1	1:200 (IF)	Antibodies Incorporated (75-408)
Anti-ChAT	Goat Polyclonal	1:500 (IF)	Merck (AB144P)
Anti-CtBP2	Mouse IgG1	1:500 (IF)	BD Biosciences (612044)
Anti-EPS8	Mouse IgG1	1:1000 (IF)	BD Biosciences, (610143)
Anti-GST	Mouse IgG1	1:1000 (WB)	Invitrogen (MA4-004)
Anti-KCNQ4	Mouse IgG1	1:100 (IF)	Biosciences (S43-6)
Anti-Myc (9E10)	Mouse IgG1	1:100 (IF + IP)	Invitrogen (13-2500)
Anti-Myo7a	Mouse IgG1	1:500 (IF)	DSHB (138-1-c)
Anti-Pikachurin	Rabbit Polyclonal	1:100 (IF)	ProteinTech (14578-1-AP)
Anti-Prestin	Rabbit Polyclonal	1:5000 (IF)	Gift from Robert Fettiplace
Anti-PSD95	Mouse IgG2a	1:1000 (IF)	Merck (MABN68)
Anti-SK2	Rabbit Polyclonal	1:200 (IF)	Merck (P0483)
Anti-Type III β -Tubulin	Mouse IgG2a	1:50 (IF)	Biologend (801201)

Secondary

<u>ID</u>	<u>Host/Isotype</u>	<u>Dilution</u>	<u>Supplier</u>
Anti-Mouse IgG HRP (H+L)	Goat Polyclonal	1:10,000	Invitrogen (62-6520)
Anti-Rabbit IgG HRP (H+L)	Goat Polyclonal	1:10,000	Invitrogen (65-6120)
Anti-Mouse IgG (H+L) Alexa Fluor 488	Goat Polyclonal	1:1,000	Invitrogen (A32723)
Anti-Mouse IgG1 Alexa Fluor 488	Goat Polyclonal	1:1,000	Invitrogen (A-21121)
Anti-Mouse IgG1 Alexa Fluor 568	Goat Polyclonal	1:1,000	Invitrogen (A-21124)
Anti-Mouse IgG1 Alexa Fluor 647	Goat Polyclonal	1:1,000	Invitrogen (A-21240)
Anti-Mouse IgG2a	Goat Polyclonal	1:1,000	Invitrogen (A-21131)

Alexa Fluor 488			
Anti-Mouse IgG2a Alexa Fluor 594	Goat Polyclonal	1:1,000	Invitrogen (A-21135)
Anti-Mouse IgM (Heavy Chain) Alexa Fluor 488	Goat Polyclonal	1:1000	Invitrogen (A-21042)
Anti-Rabbit IgG (H+L) Alexa Fluor 594	Goat Polyclonal	1:1,000	Invitrogen (A32740)
Anti-Rabbit IgG (H+L) Alexa Fluor 488	Goat Polyclonal	1:1,000	Invitrogen (A32731)

Other

<u>ID</u>	<u>Dilution/Working Concentration</u>	<u>Supplier</u>
DAPI	1 µg/ml	Roche (28718-90-3)
Phalloidin (Texas Red)	1:1000	Invitrogen (T7471)

Appendix 2.2 – PCR primers, reaction conditions and expected products

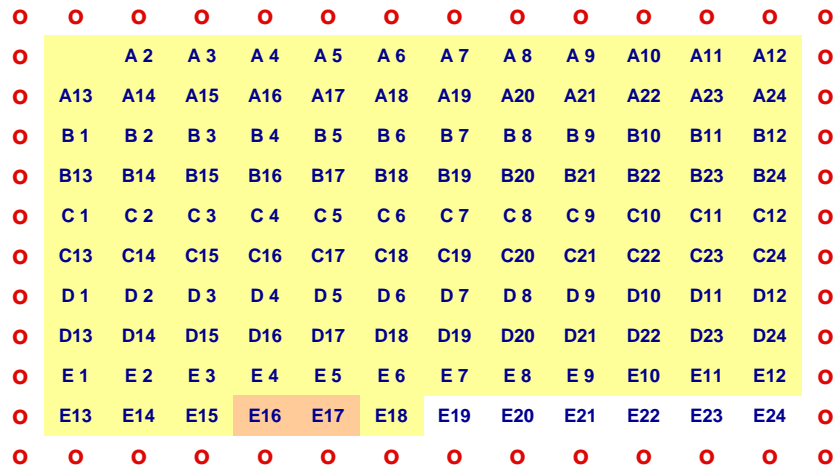
Experiment	Primer ID	Sequence	Conditions	Band(s)
L2 SH3 amplification	L2 Forward	CGCGGATCCATGAAATACGT- CAAAATTCTGTACGATTTACCG	1-98°C – 30sec 2-98°C – 10sec 3-63°C – 15sec 4-72°C – 15sec	200bp
	L2 Reverse	GCGAAGCTTGGACGTGCTTC- ACCCAGAATGTTACAC	(Repeat 2-4 10 times) 5-98°C – 10sec 6-65°C – 15sec 7-72°C – 15sec (Repeat 5-7 25 times) 8-72°C – 5min	
L3 SH3 amplification	L3 Forward	CGCGGATCCATGCTGAAAATGCAGG- TCCTGTATGAATTTGAAG	5-98°C – 10sec 6-65°C – 15sec 7-72°C – 15sec (Repeat 5-7 25 times) 8-72°C – 5min	200bp
	L3 Reverse	GCGAAGCTTGGTTGCAGTGGTTC- CAGAATGTTGG		
DAG1 flox genotype	Forward	GGAGAGGATCAATCATGG	1-94°C – 5min 2-94°C – 30sec 3-53°C – 30sec 4-72°C – 45sec (Repeat 2-4 29 times) 6-72°C – 5min	500bp – Wild Type 600bp – Flox Mutant
	Reverse	CAACTGCTGCATCTCTAC		
MYO15Cre genotype	P1	AGGGACCTGATCCACTTTGGG	1-94°C – 5min 2-94°C – 40sec 3-60°C – 40sec 4-72°C – 90sec (Repeat 2-4 30 times) 5-72°C – 5min	None – Wild Types 500bp – Cre Mutant
	P2	TGGTGCACAGTCAGCAGGTTTC		
DAG1xMYO15Cre validation qPCR	DAG1 Forward	CTGCATGCACTCAGTTCTCT	1-94°C – 5min 2-94°C – 1min 3-60°C – 30sec 4-72°C – 30sec (Repeat 2-4 40 times) 5-72°C – 5min	50bp – DAG1 mRNA present
	DAG1 Reverse	CAGTGTAGCCAAGACGGTAAG		
	HPRT Forward	GCTTGCTGGTGAAAAGGAC		50bp – HPRT mRNA present
	HPRT Reverse	AGATTCAACTTGCGTCATC		
<i>BAIAP2L2^{tm1b}</i> genotype	Crit-WTF Forward (Wild-Type primer)	CAGATCCTCAACACCAACGA	1-95°C – 5min 2-95°C – 30sec 3-60°C – 30sec 4-72°C – 45sec (Repeat 2-4 35	400bp – Wild Type 550bp

	LacZ Forward (Mutant primer)	CCAGTTGGTCTGGTGCA	times) 5-72°C – 5min	– Null Mutant
	3arm WTR Reverse	TCGGCTCCTTGATAAAAATGG		

Appendix 2.3 – Cell Lines Used

<u>ID</u>	<u>Maintenance conditions</u>	<u>References</u>
VOT-E36	33°C, 5% CO ₂ , Minimal Essential Media with 10% Foetal Calf Serum (FCS) and 50 units/ml of murine γ -Interferon (Peprotech).	<u>Lawoko-Kerali et al. 2004</u>
VOT-N33		
KM155 Human Muscle Myoblasts	37°C, 5% CO ₂ , Skeletal Muscle Growth Medium (With included supplement) with 10% FCS.	Mamchaoui et al. 2011 – Crispr DAG1 control and knock-out cells were created by Matthew Cook at the University of Sheffield
KM155 Human Muscle Myoblasts – DAG1 sgRNA Control		
KM155 Human Muscle Myoblasts – DAG1 Crispr mediated knock-out		

Appendix 2.4 – Celluspot array of the cytoplasmic domain of β DG



Spot ID	sequence	Spot ID	sequence	Spot ID	sequence
A 1	MICYRKKRKGKLTLE	B17	SSSMLPLIQEEKAPL	D 9	PLRDEDPNAPPYQPP
A 2	ICYRKKRKGKLTLED	B18	SSMPLILQEEKAPLP	D10	LRDEDPNAPPYQPPP
A 3	CYRKKRKGKLTLEDQ	B19	SMLILQEEKAPLPP	D11	RDEDPNAPPYQPPPP
A 4	YRKKRKGKLTLEDQA	B20	MPLILQEEKAPLPPP	D12	DEDPNAPPYQPPPPF
A 5	RKKRKGKLTLEDQAT	B21	PLILQEEKAPLPPPE	D13	EDPNAPPYQPPPPFT
A 6	KKRKGKLTLEDQATF	B22	LILQEEKAPLPPPEY	D14	DPNAPPYQPPPPFTV
A 7	KRKGKLTLEDQATFI	B23	ILQEEKAPLPPPEYP	D15	PNAPPYQPPPPFTVP
A 8	RKGKLTLEDQATFIK	B24	LQEEKAPLPPPEYPN	D16	NAPPYQPPPPFTVPM
A 9	KGKLTLEDQATFIKK	C 1	QEEKAPLPPPEYPNQ	D17	APPYQPPPPFTVPM
A10	GKLTLEDQATFIKKG	C 2	EKAPLPPPEYPNQS	D18	PPYQPPPPFTVPM
A11	KLTLEDQATFIKKG	C 3	EKAPLPPPEYPNQSV	D19	PYQPPPPFTVPM
A12	LTLEDQATFIKKG	C 4	KAPLPPPEYPNQSV	D20	YQPPPPFTVPM
A13	TLEDQATFIKKG	C 5	APLPPPEYPNQSV	D21	QPPPPFTVPM
A14	LEDQATFIKKG	C 6	PLPPPEYPNQSV	D22	PPPPFTVPM
A15	EDQATFIKKG	C 7	LPPPEYPNQSV	D23	PPPFTVPM
A16	DQATFIKKG	C 8	PPPEYPNQSV	D24	PPFTVPM
A17	QATFIKKG	C 9	PPEYPNQSV	E 1	PFTVPM
A18	ATFIKKG	C10	PEYPNQSV	E 2	FTVPM
A19	TFIKKG	C11	EYPNQSV	E 3	TVPM
A20	FIKKG	C12	YPNQSV	E 4	VPMEG
A21	IKKG	C13	PNQSV	E 5	PMEG
A22	KKG	C14	NQSV	E 6	MEG
A23	KG	C15	QSV	E 7	EG
A24	G	C16	SV	E 8	GK
B 1	VPIIFADELDDSKPP	C17	VPETTPLNQDTMGEY	E 9	KGSRPKNMTPYRSP
B 2	PIIFADELDDSKPPP	C18	PETTPLNQDTMGEYT	E10	GSRPKNMTPYRSP
B 3	IIFADELDDSKPPPS	C19	ETTPLNQDTMGEYTP	E11	SRPKNMTPYRSP
B 4	IFADELDDSKPPSS	C20	TTPLNQDTMGEYTPL	E12	RPKNMTPYRSP
B 5	FADELDDSKPPSSS	C21	TPLNQDTMGEYTPLR	E13	PKNMTPYRSP
B 6	ADELDDSKPPSSSM	C22	PLNQDTMGEYTPLRD	E14	KNMTPYRSP
B 7	DELDDSKPPSSSMP	C23	LNQDTMGEYTPLRDE	E15	KNMTPYRSP
B 8	ELDDSKPPSSSMPL	C24	NQDTMGEYTPLRDED	E16	Bio-AEEQKLISEEDLLR
B 9	LDDSKPPSSSMPLI	D 1	QDTMGEYTPLRDEDP	E17	Acetylated -ve ctrl
B10	DDSKPPSSSMPLIL	D 2	DTMGEYTPLRDEDPN	E18	KNMTPYRSP

B11	DSKPPSSSMPLILQ	D 3	TMGEYTPLRDEDPNA	E19	
B12	SKPPSSSMPLILQE	D 4	MGEYTPLRDEDPNAP	E20	
B13	KPPSSSMPLILQEE	D 5	GEYTPLRDEDPNAPP	E21	
B14	PPSSSMPLILQEEK	D 6	EYTPLRDEDPNAPPY	E22	
B15	PPSSSMPLILQEEKA	D 7	YTPLRDEDPNAPPYQ	E23	
B16	PSSSMPLILQEEKAP	D 8	TPLRDEDPNAPPYQP	E24	